IMMUNE AND HUNTINGTIN BIOLOGY IN HUNTINGTON'S DISEASE

James R C Miller

University College London

A thesis submitted in partial fulfilment of the requirements for the degree of

Doctor of Philosophy from University College London

2016

Declaration

I, James Miller, confirm that the work presented in this thesis is my original research work. Where others have contributed, this has been clearly indicated in the text.

Acknowledgements

I would firstly like to thank my primary supervisor, Professor Sarah Tabrizi, for her advice, support and encouragement over the last three and a half years. I would also like to thank my secondary supervisor, Dr Adrian Isaacs, as well as the UCL MBPhD programme and everyone who has helped guide me through the laboratory metamorphosis from rote-learning medical student to (hopefully) free-thinking scientist; for this special thanks must go to Dr Ralph Andre and Dr Ulrike Träger. This was made considerably easier by the excellent company provided by the Tabrizi group past and present, as well as everyone who has inhabited the student office during my time here (Xun, Luci, Rhia, Justin, Billy and Laura to name but a few…).

This project would not have been possible without the help of the patients and controls who were kind enough to donate samples, as well as the staff of the HD clinic at the NHNN (and Nicci Robertson in particular!). A special mention should also go to Kevin Williams, whose endless willingness to donate blood allowed me to optimise almost every experiment in this thesis.

I am constantly grateful for the support, both emotional and financial, provided by my long-suffering parents (who surely didn't anticipate it would take me 27 years to get a real job), as well as my brother Tom. I would also like to thank Vernon, Tom, Matt, Muska and anyone else who has voluntarily put up with me for as long as they have, as well as everyone I have been lucky enough to play live music or do business with over the course of the last few years. Finally, to Blastoise, Magnus and Fulgrim for keeping me company during the writing process. It's been a good few years. Thanks all!

Abstract

Huntington's disease (HD) is a fatal, autosomal dominant neurodegenerative disorder caused by a CAG repeat expansion in the huntingtin (*HTT*) gene. Expression of the mutant (m)HTT protein is the primary cause of disease pathology, so lowering intracellular levels of mHTT is a promising therapeutic strategy. The aim of this thesis was to achieve allele-selective suppression of mHTT using siRNA targeted to single nucleotide polymorphisms (SNPs) in the *HTT* gene. HD patients were genotyped for three SNPs before the mRNA and protein knockdown efficacy of a panel of siRNAs was tested in primary human myeloid cells. Functional validation was carried out by characterising the effects of selective siRNAs on the cells' hyper-reactive cytokine profile.

In parallel, RNA sequencing was used to carry out the first whole transcriptome analysis of primary human HD myeloid cells. HD myeloid cells are functionally abnormal, and there is mounting interest in the peripheral immune system as a modifier of HD progression. In contrast with previous studies that have required stimulation to elicit phenotypic abnormalities, this thesis demonstrates significant transcriptional changes in unstimulated HD monocytes, including increased resting expression of proinflammatory cytokines. Pathway analysis revealed enrichment of gene sets relating to innate immunity and inflammation, while upstream regulator analysis suggests this transcriptional dysregulation is mediated by abnormal basal activation of the NFκB intracellular signalling pathway; this was later confirmed by western blotting. These data are consistent with a priming

effect of mHTT, whereby resting dysfunction leads to an exaggerated response once a stimulus is encountered.

Finally, the contribution of adaptive immunity to HD peripheral immune dysfunction is yet to be satisfactorily investigated. This thesis demonstrates that mHTT expression does not affect the intrinsic phenotype of human HD T lymphocytes, suggesting that HD peripheral immune disturbance is not universal but is primarily the result of altered innate immunity.

Table of contents

List of figures

List of tables

Abbreviations

AAO	age at onset
AMPA	α-amino-3-hydroxy-5-methyl-4-isoxazolepropionic acid
ANOVA	analysis of variance
AP-1	activator protein 1
APC	allophycocyanin
ASO	antisense oligonucleotide
ATP	adenosine 5’-triphosphate
BCA	bicinchoninic acid
BCR	B cell receptor
BDNF	brain-derived neurotrophic factor
bp	base pair
BSA	bovine serum albumin
C	Celsius
CAG	glutamine
CB2	cannabinoid receptor type 2
CBP	cAMP response element-binding protein-binding protein
CCR	C-C chemokine receptor
CD	cluster of differentiation
cDNA	complementary deoxyribonucleic acid
CFSE	carboxyfluorescein succinimidyl ester
CNS	central nervous system
CSF	cerebrospinal fluid

Ct	threshold cycle
CXCR	C-X-C chemokine receptor
Cy	cyanine
ddH_2O	deionised distilled water
DNA	deoxyribonucleic acid
DNase	deoxyribonuclease
dNTP	deoxyribonucleotide triphosphate
DTT	dithiothreitol
EDTA	ethylenediaminetetraacetic acid
e.g.	for example
EP	Endo-Porter
ERK	extracellular signal-regulated kinase
FACS	fluorescence-activated cell sorting
FBS	foetal bovine serum
FDR	false discovery rate
FITC	fluorescein isothiocyanate
FOXP3	forkhead box P3
FSC	forward scatter
g	gram
GeRP	beta-1,3-D-glucan-encapsulated siRNA particle
GM-CSF	granulocyte-macrophage colony-stimulating factor
GO	Gene Ontology
GSEA	Gene Set Enrichment Analysis
h	hour

HD	Huntington's disease
HEAT	huntingtin, elongation factor 3, the PR65/A subunit of protein phosphatase 2A and the lipid kinase Tor
HEPES	4-(2-hydroxyethyl)-1-piperazineethanesulfonic acid
HTT	human huntingtin gene
HTT	human huntingtin protein
Htt	murine huntingtin gene
i.e.	id est
IFNγ	interferon gamma
IκB	inhibitor of kappa B
IKK	IκB kinase
IL	interleukin
IPA®	Ingenuity® Pathway Analysis
iPSC	induced pluripotent stem cell
IRAK	interleukin-1 receptor-associated kinase
IT15	interesting transcript 15
JAK	janus kinase
kb	kilo base pair
kDa	kilodalton
KEGG	Kyoto Encyclopedia of Genes and Genomes
KMO	kynurenine 3-monooxygenase
L	litre
LPS	lipopolysaccharide
M	molar
m	mutant

MACS	magnetic-activated cell sorting
MAPK	mitogen-activated protein kinase
MCP-1	monocyte chemoattractant protein-1
MGI	Mouse Genome Informatics
MHC	major histocompatibility complex
min	minutes
miRNA	micro-ribonucleic acid
ml	millilitre
mRNA	messenger ribonucleic acid
MSD	Meso Scale Discovery
MSN	media spiny neurons
mTOR	mechanistic target of rapamycin
MYC	v-myc avian myelocytomatosis viral oncogene homolog
MyD88	myeloid differentiation primary response gene 88
N	amino
n	number
NES	normalized enrichment score
NFAT	nuclear factor of activated T cells
NFκB	nuclear factor kappa-light-chain-enhancer of activated B cells
NK	natural killer
NKT	natural killer T
NMDA	N-methyl-D-aspartate
PAGE	polyacrylamide gel electrophoresis
PAMP	pathogen-associated molecular pattern

PBMC	peripheral blood mononuclear cell
PBS	phosphate-buffered saline
PCR	polymerase chain reaction
PE	phycoerythrin
PerCP	peridinin chlorophyll
PFA	paraformaldehyde
PHA	phytohaemagglutinin
PMSF	phenylmethane sulfonyl fluoride
PRR	pattern recognition receptor
PTGS	post-transcriptional gene silencing
Q	glutamine
QC	quality control
qPCR	quantitative polymerase chain reaction
REL	v-rel avian reticuloendotheliosis viral oncogene homolog
REST	RE1-silencing transcription factor
RIN	RNA integrity number
RIPA	radioimmunoprecipitation assay
RISC	RNA-induced silencing complex
RNA	ribonucleic acid
RNAi	RNA interference
RNase	ribonuclease
RNA-Seq	RNA sequencing
RPKM	reads per kilobase of transcript per million mapped reads
RPMI	Roswell Park Memorial Institute

rRNA	ribosomal ribonucleic acid
rs	reference SNP
s	seconds
SCR	scrambled
SD	standard deviation
SDS	sodium dodecyl sulfate
SEM	standard error of the mean
siRNA	small interfering ribonucleic acid
SLiC	SNP linkage by circularization
SNP	single nucleotide polymorphism
Sp1	specificity protein 1
SSC	side scatter
ssRNA	single-stranded ribonucleic acid
STAT	signal transducers and activators of transcription
TAE	tris-acetate-EDTA
Tb	terbium cryptate
TBP	TATA-binding protein
TCR	T cell receptor
TE	tris-EDTA
TFC	total functional capacity
TGF	transforming growth factor
T_h	T helper cell
TLR	toll-like receptor
TNF	tumour necrosis factor

TRAF	TNF receptor-associated factor
T_{reg}	regulatory T cell
TR-FRET	time-resolved Förster energy transfer
UCL	University College London
UHDRS	unified Huntington's disease rating scale
UPS	ubiquitin-proteasome system
UTR	untranslated region
V	volt
vs.	versus
×g	gravitational acceleration
YAC	yeast artificial chromosome

1 Introduction

1.1 Huntington's disease

Huntington's disease (HD) is an autosomal dominant neurodegenerative disorder caused by a CAG repeat expansion in exon 1 of the huntingtin (*HTT*) gene on chromosome 4 (The Huntington's Disease Collaborative Research Group, 1993). Patients are affected by a combination of symptoms ranging from movement disorders to psychiatric disturbances, with death occurring 15-20 years after symptom onset (Ross and Tabrizi, 2011). The disease affects approximately 10.6-13.7 individuals per 100,000 in Western populations (Bates et al., 2015); however, there is considerable variability between different regions and ethnic groups, (Warby et al., 2011).

1.1.1 The genetics of HD

While the clinical features of HD were first comprehensively described by George Huntington in 1872 (Huntington, 1872), the genetic cause was not mapped to chromosome 4 until 1983 (Gusella et al., 1983). The *IT15* region at 4p16.3 was then found to contain an expanded CAG repeat in HD patients (The Huntington's Disease Collaborative Research Group, 1993); this gene was later renamed *HTT*. Further study revealed that *HTT* is a large gene of 180 kb containing sixty-seven exons; these are alternatively spliced to form two mRNA transcripts of ten and twelve kb respectively (Ross and Tabrizi, 2011). Surprisingly for a neurodegenerative disease-causing gene, *HTT* is controlled by a housekeeping promoter, with relatively consistent expression in all cells and tissues that have been studied to date (Li et al., 1993).

The length of the CAG repeat is highly heterogeneous in the general population, with a healthy normal range of approximately ten to twenty-six. A repeat length of forty or more causes HD with complete penetrance, (Ross and Tabrizi, 2011), although shorter repeats between thirty-five and thirty-nine also cause HD with reduced penetrance. There have even been reports of subtle abnormalities with repeats ranging from twenty-seven to thirty-five CAGs (Squitieri and Jankovic, 2012). Onset itself occurs at a mean of 45 years of age, although this is highly variable (Bates et al., 2015). The length of the CAG repeat is strongly associated with age at onset (AAO), with longer repeats resulting in progressively earlier disease onset (Bates et al., 2014). Repeat lengths greater than sixty result in juvenile HD, which produces a more aggressive phenotype with onset in young adulthood or even childhood (Squitieri et al., 2006). The CAG repeat is subject to meiotic instability, with increasing CAG repeat length between generations leading to earlier onset; this phenomenon is known as anticipation, and is particularly common on paternal inheritance (Trottier et al., 1994). The existence of a defined mutation allows individuals to undergo predictive genetic testing.

Indeed, the length of the CAG repeat is the most important factor for determining AAO in HD. This occurs dominantly with no contribution from the shorter allele, regardless of its length (Lee et al., 2012). Studies on Venezuelan cohorts determined that genetic and environmental factors account for 59 % of AAO variability (Wexler et al., 2004), while a study of siblings found that 65-71 % of AAO variation was due to the length of the CAG repeat expansion (Rosenblatt et al., 2001). However, CAG repeat length correlates poorly with disease progression (Rosenblatt et al., 2006).

1.1.2 Clinical features of HD

The main clinical features of HD are caused by central nervous system (CNS) degeneration, resulting in a range of symptoms including motor abnormalities, cognitive impairment and psychiatric disturbances (Ross and Tabrizi, 2011). The degree to which patients are affected by each symptom type is highly variable; however, most will experience each aspect to at least some extent. A formal clinical diagnosis of HD is made when an otherwise unexplained extrapyramidal movement disorder (e.g. chorea or dystonia) develops in an individual with a genetically diagnosed CAG repeat expansion (Ross et al., 2014). However, the cognitive and psychiatric aspects of HD may develop many years before this.

The motor abnormalities caused by HD may be broadly divided between worsening involuntary movements and impairment of voluntary movements (Ross et al., 2014). Restlessness and loss of fine motor control occur early, before later progression to chorea (Wild and Tabrizi, 2007). Finally, advanced HD takes on a more Parkinsonian character, with increased rigidity and reduced chorea. The cognitive symptoms are highly variable, but include inhibition of executive function and impulsive behaviour (Novak and Tabrizi, 2010). Psychiatric disturbances are one of the most common features of HD, with approximately 40-50 % of HD patients experiencing depression (Paulsen et al., 2005). Suicide attempts have been found to be four times more likely in HD patients (Farrer, 1986), while apathy, aggression and psychosis have also been reported (Novak and Tabrizi, 2010).

The clinical course of HD may be divided between pre-manifest and manifest disease, with the pre-manifest phase containing an additional prodromal period of subtle abnormalities (Ross et al., 2014); this may precede formal diagnosis by up to fifteen years (Bates et al., 2015). While the disease course is highly variable, death occurs at a median of eighteen years from motor onset. Clinical characterisation may be carried out using the Unified Huntington's Disease Rating Scale (UHDRS) (Huntington Study Group, 1996) and Total Functional Capacity (TFC) (Shoulson, 1981) scores. However, it is important to recognise that motor onset is not a dichotomous state, but occurs insidiously over long periods. Concerted efforts have been made to characterise HD progression (Tabrizi et al., 2013), leading to the development of detailed predictive models (Langbehn et al., 2010).

1.1.3 CNS pathology in HD

The CNS degeneration caused by HD is widespread, with a reduction in total post-mortem brain volume of 19 % (Halliday et al., 1998). The most prominently affected site is the striatum in the basal ganglia, where 95 % of GABAergic medium spiny neurons (MSNs) are lost (Vonsattel and DiFiglia, 1998). This results in a total striatal volume loss of approximately 50 % (Vonsattel et al., 1985; Rosas et al., 2001). Striatal pathology is crucial for the HD phenotype, and has been shown to correlate with motor impairment (Guo et al., 2012). Other prominently affected sites include the cerebral cortex (Halliday et al., 1998) and hypothalamus (Politis et al., 2008). CNS atrophy occurs before symptom onset (Rosas et al., 2005; Tabrizi et al., 2009), suggesting that some degree of neuronal compensation exists. However, it is important to note that while neuronal death is the hallmark of

HD, dysfunction probably occurs earlier (Ross et al., 2014). CNS pathology in HD is not merely neuronal, as the mutant protein is also expressed in glial cells (Li et al., 1993). Indeed, the targeted astrocytic expression of mHTT is sufficient to produce a neurological phenotype in mice (Bradford et al., 2009).

1.1.4 Peripheral pathology in HD

While HD pathology was traditionally regarded as being confined to the CNS, in recent years it has emerged that HD is in fact a disease of the whole body (Fig. 1.1). The mHTT protein is expressed in all cells and tissues (Li et al., 1993), resulting in a range of pathologies as diverse as the tissues affected (van der Burg et al., 2009). This should perhaps not be surprising, given that wild-type HTT has important roles in non-neuronal cells (see Section 1.2.2). This suggests that the peripheral pathology seen in HD is not just a response to CNS pathology, but is instead a relevant disease process in its own right.

For example, prominent skeletal muscle wasting occurs in both patients and mouse models of HD (van der Burg et al., 2009), while cardiac muscle has also been shown to be atrophic in HD mice (Mihm et al., 2007). This is particularly relevant as heart failure is second only to pneumonia as the most common cause of death in HD patients (Lanska et al., 1988). Muscle wasting also plays a role in the profound weight loss seen in the latter stages of disease (Goodman et al., 2008). While such changes have a substantial effect on quality of life, they are also thought to affect disease progression, as patients with increased body weights show a slower rate of decline (van der Burg et al., 2009).

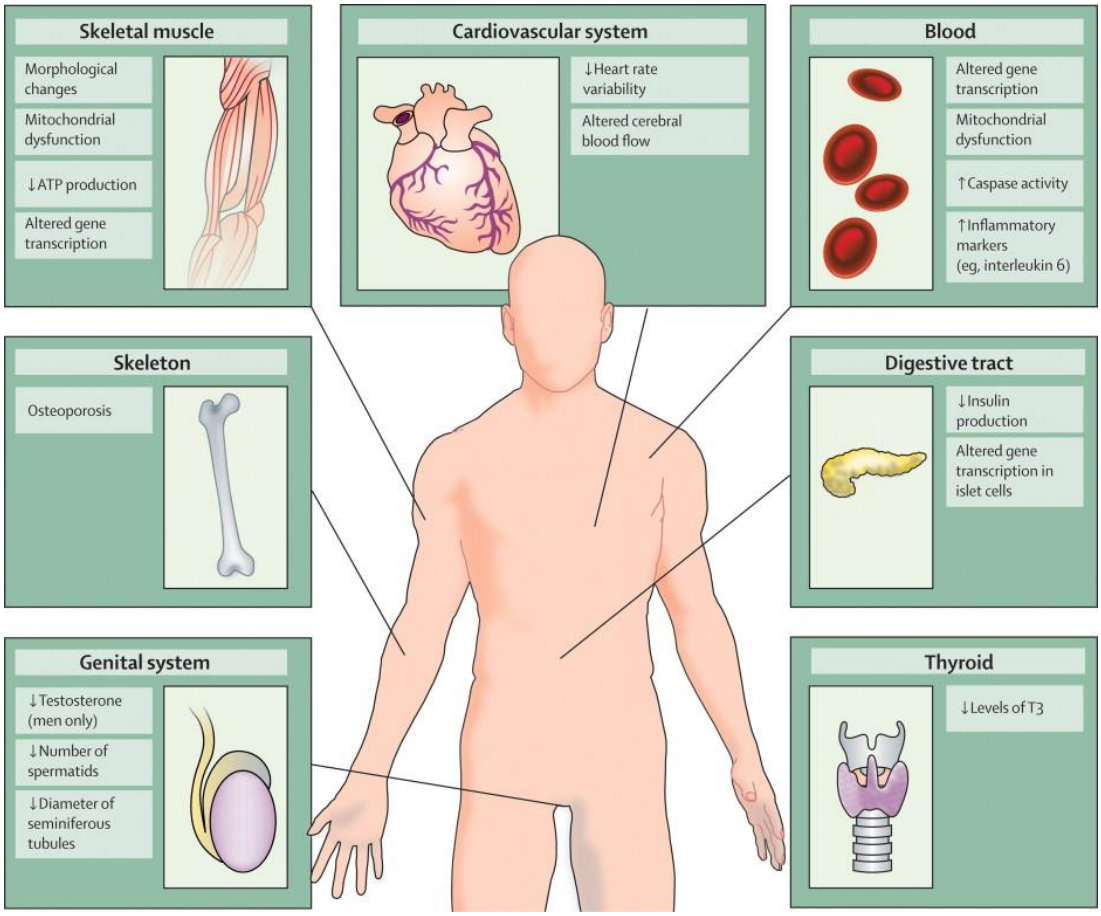

Figure 1.1. Peripheral pathology in HD. Mutant HTT is expressed throughout the body, leading to a wide range of abnormalities in the peripheral tissues of HD patients. Reprinted from The Lancet Neurology, Vol. 8, "*Beyond the brain: widespread pathology in Huntington's disease*", 765-74, van der Burg et al., ©2009, with permission from Elsevier.

One of the most important aspects of peripheral pathology relates to abnormal immune system function (see Section 1.7), with HD patients of all disease stages showing elevated levels of circulating proinflammatory cytokines and chemokines in their peripheral blood (Björkqvist et al., 2008; Wild et al., 2011). Further peripheral changes include endocrine dysfunction, osteoporosis and testicular atrophy (van der Burg et al., 2009). These data reinforce the conclusion that the ubiquitous expression of mHTT has cell-intrinsic negative effects on tissues far beyond the CNS.

1.1.5 Disease modifiers

While the length of the CAG repeat expansion is thought to be the single most important factor in determining AAO (Wexler et al., 2004; Rosenblatt et al., 2001), the other factors involved remain the subject of investigation. One key area has focused on the identification of disease-modifying genes other than m*HTT*; numerous candidates such as *GRIK2*, *PPARGC1A* and *TP53* have been suggested, although it has largely not been possible to replicate positive findings between studies (Gusella et al., 2014). However, a recent study identified a single nucleotide polymorphism (SNP) in the *HTT* promoter that acts as a bidirectional modifier of HD (Bečanović et al., 2015). The non-coding variant of the SNP was found to impair NFκB binding, resulting in reduced *HTT* transcription and delayed AAO in familial HD cases when it was located on the disease allele. In contrast, when the non-coding variant was located on the wild-type allele it was associated with earlier AAO. Furthermore, a large scale genome-wide association study identified genetic loci on chromosomes 8 and 15 that may modify AAO (Genetic Modifiers of Huntington's Disease (GeM-HD) Consortium, 2015). Pathway analysis implicated the *MLH1* gene as a potential modifier of disease progression, suggesting that DNA repair mechanisms are involved in determining AAO. Indeed, DNA repair pathways are a common genetic mechanism affecting AAO in multiple polyglutamine (polyQ) diseases (Bettencourt et al., 2016). Somatic instability of the CAG repeat in post-mitotic neurons has also been suggested as an important modifier of AAO (Swami et al., 2009).

Environmental and lifestyle factors are also thought to play an important role, as sedentary lifestyles lacking significant physical or intellectual exertion are

associated with earlier AAO (Trembath et al., 2010). This may be part of a more general phenomenon, as the risk of dementia has been found to decrease with increasing physical exercise (Hamer and Chida, 2009).

Identifying robust modifiers of HD progression has proved to be even more difficult than for AAO. Numerous candidates have been suggested, from the CAG repeat to modifying genes and the peripheral immune system (see section 1.7.2). However, the majority of current studies have been inconclusive, and considerable further study is needed to provide a comprehensive profile of the factors involved in modifying HD progression.

1.1.6 Biomarkers of HD

The advent of clinical trials for HD has necessitated the search for robust biomarkers to monitor disease progression. A biomarker is a quantifiable measure by which a biological or pathological process can be identified or assessed for severity or response to treatment (Andre et al., 2014). The nature of HD as a predominantly CNS disorder presents challenges for the reliable monitoring of disease progression, as access to the main tissue of interest is largely restricted to post-mortem analyses.

Potential HD biomarkers may be broadly divided into clinical, neuroimaging and biochemical measures (Andre et al., 2014). Clinical measures such as the UHDRS and quantitative motor tests are relatively easy to carry out, however they have limited sensitivity and are subject to significant inter-rater variability. Neuroimaging measures have the significant advantage of providing an accurate assessment of structural CNS changes; however, high quality neuroimaging assessments are both expensive and time consuming.

Biochemical measures would provide the ideal biomarker, as they are cheaper and easier than neuroimaging and more robust than clinical measures. The collection of blood and cerebrospinal fluid (CSF) is also significantly less invasive than direct sampling of the CNS. However, no biochemical measures have withstood longitudinal analysis as a biomarker of HD (Weir et al., 2011). While HD patients have been shown to have increased circulating levels of proinflammatory cytokines in their peripheral blood (Björkqvist et al., 2008), what is less clear is how these measurements are linked to progression. Measurement of mHTT protein levels has shown some promise, with a recent study demonstrating a significant increase in mHTT levels in patient CSF with advancing disease stage (Wild et al., 2015). Furthermore, mHTT levels in peripheral blood cells correlate with disease burden scores (Weiss et al., 2012). These measures are likely to be vital for clinical trials to lower cellular levels of mHTT, but further validation is needed.

1.1.7 Cell and animal models of HD

Numerous cell models exist to study HD in the lab, from *ex vivo* patient cells to neuronal cell lines with CAG repeat knock-ins, with a recent avenue of investigation focusing on the development of induced pluripotent stem cells (iPSCs) (Park et al., 2008). However, it is important to remember that HD pathogenesis is complex, and studying individual cell lines in isolation is therefore unlikely to provide a complete picture of the disease.

Animal models of HD range from Drosophila to mammals such as primates, sheep and rats (Pouladi et al., 2013). Murine models of HD are the most commonly used, and come in a variety of different types. Fragment models

contain an N-terminal fragment of the human *HTT* gene, and display an aggressive phenotype with late stage disease occurring between 12-15 weeks in the R6/2 mouse (Mangiarini et al., 1996). In contrast, full-length and knock-in models both contain an entire mutant gene; full-length models such as the YAC mouse express the entire human m*HTT* gene in addition to the normal mouse genes (Slow et al., 2003), whereas knock-in models such as the $Hdh^{150Q/150Q}$ have an artificial CAG repeat expansion inserted into both alleles of the mouse *Htt* gene (Lin et al., 2001). These models have a substantially longer disease course measured in months or even years.

1.2 The HTT protein

1.2.1 Wild-type HTT structure

Wild-type HTT is a 348 kDa protein that is expressed ubiquitously in all cells and tissues, although the highest expression is found in the CNS and testes (Li et al., 1993). While the size of the protein prohibits structural analysis by spectroscopy, substantial information has been discovered using alternative techniques (Fig. 1.2). The CAG repeat found in exon 1 of the *HTT* gene encodes an N-terminal polyQ sequence with a largely helical secondary structure (Kim et al., 2009), although the conformation of the polyQ tract is influenced by the surrounding protein regions. Wild-type HTT also contains a number of HEAT repeats, which are sequences of approximately fifty amino acids in anti-parallel α-helices (Li et al., 2006); these are interspersed with disordered regions and are thought to mediate protein-protein interactions (Bates et al., 2015). Indeed, the many interaction partners described for HTT suggests it acts as a molecular scaffold.

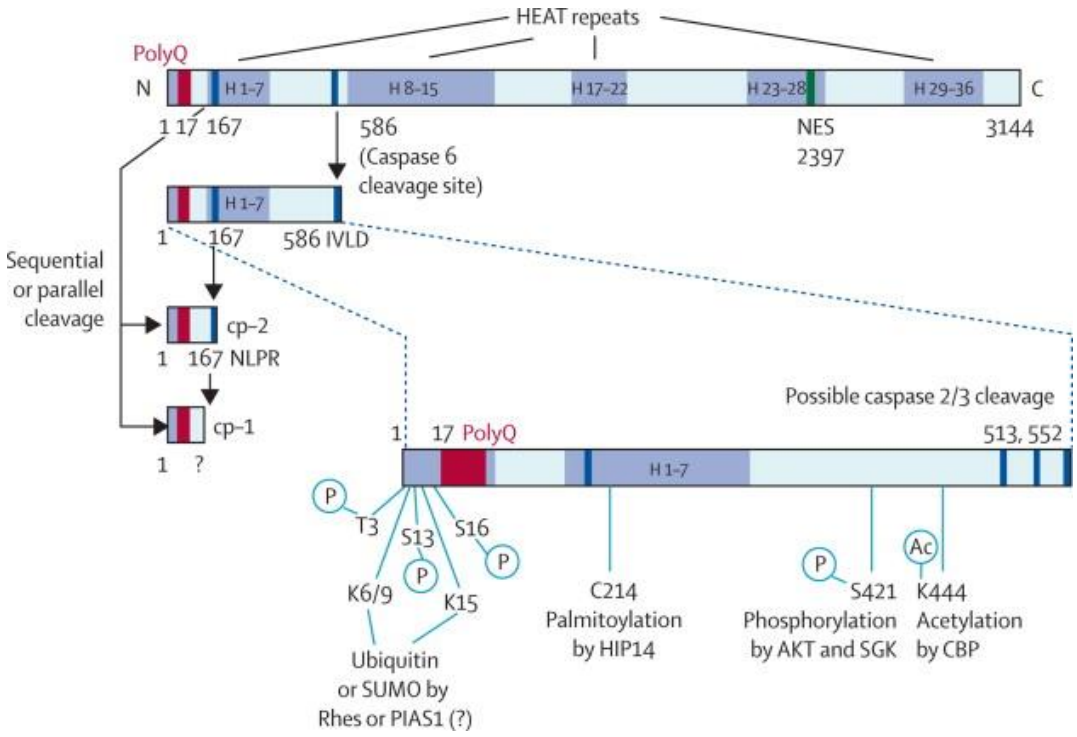

Figure 1.2. **The HTT protein.** HTT is a large, 348 kDa protein that contains a wide range of functional domains, in addition to sites for post-translational modification. Reprinted from The Lancet Neurology, Vol. 10, "*Huntington's disease: from molecular pathogenesis to clinical treatment*", 83-98, Ross and Tabrizi, ©2011, with permission from Elsevier.

Huntingtin undergoes extensive post-translational modification, including phosphorylation, ubiquitination, SUMOylation, acetylation and palmitoylation (Steffan et al., 2004; Thompson et al., 2009; Cong et al., 2011; Yanai et al., 2006). These modifications often occur in the disordered segments between HEAT repeats, and affect characteristics including half-life and aggregation, and can even modulate toxicity by increasing HTT clearance through the ubiquitin-proteasome system (UPS). Huntingtin also undergoes cleavage by numerous proteolytic enzymes (Ross and Tabrizi, 2011), although the physiological function of this is incompletely understood. However, an N-terminal fragment of approximately one hundred amino acids is thought to be particularly important for pathogenesis (Bates et al., 2015).

1.2.2 Wild-type HTT function

The exact functions of wild-type HTT remain similarly elusive, although much has been learned since the identification of mHTT as the disease-causing factor in HD. Huntingtin knockout mice are embryonic lethal prior to the period of nervous system development (Nasir et al., 1995; Zeitlin et al., 1995), suggesting that the wild-type protein has key roles in embryogenesis beyond the CNS. Huntingtin knockout mice also exhibit increased apoptosis (Zeitlin et al., 1995), while *Htt* overexpression has a protective, anti-apoptotic effect on striatal neurons in HD mice (Leavitt et al., 2006). Indeed, HTT is involved in the maintenance of tissues beyond the CNS, as conditional *Htt* knockout in mice leads to death from acute pancreatitis (Wang et al., 2016)

Wild-type HTT is thought to play a role in vesicular trafficking through the secretory and endocytic pathways (Velier et al., 1998), and has additional functions in cellular trafficking including brain-derived neurotrophic factor (BDNF) transport along microtubules (Gauthier et al., 2004). Huntingtin also affects gene transcription, for example by sequestering REST to indirectly increase the expression of BDNF (Zuccato et al., 2003). The localisation of HTT to the mitochondrial membrane further suggests that HTT is involved in the regulation of energy metabolism (Damiano et al., 2010). Intriguingly, a recent study suggested that wild-type HTT may have a novel role in immune cell function, as HTT-lowering was found to significantly reduce cytokine production by control cells following stimulation with lipopolysaccharide (LPS) and interferon-gamma (IFNγ) (Träger et al., 2014). These studies demonstrate that wild-type HTT is a multi-functional protein with diverse effects in both neuronal and non-neuronal cells.

1.2.3 Mutant HTT

The presence of an expanded polyQ tract brings about a number of structural and conformational changes in the mHTT protein that are key for HD pathogenesis (Ross and Tabrizi, 2011). Although the exact toxic mHTT species remain elusive, N-terminal fragments containing the polyQ tract have been shown to be necessary for pathology (Graham et al., 2006). While wild-type HTT is largely α-helical, toxic mHTT fragments form a compact β-sheet secondary structure (Ross and Tabrizi, 2011); this is able to form aggregates that are homologous to species seen in other protein misfolding diseases. The efficiency of this aggregation process is highly dependent on the length of the CAG repeat (Chen et al., 2001). The cellular localisation of mHTT also differs from that of the wild-type; whereas wild-type HTT is primarily cytoplasmic, mHTT forms inclusions in the nucleus (DiFiglia et al., 1997); these inclusions are largely formed from N-terminal fragments.

The prevailing hypothesis is that a toxic gain of mHTT function, rather than a loss of wild-type HTT function, is the principle cause of HD pathogenesis. HD mouse models expressing two copies of the mutant allele, for example the $Hdh^{150Q/150Q}$ mouse, are viable (Lin et al., 2001); this contrasts with the embryonic lethality displayed by *Htt* knockout mice (Nasir et al., 1995). These studies suggest that mHTT is able to substitute for wild-type HTT function, an observation supported by the fact that homozygous mutant HD patients do not display a more severe disease phenotype than heterozygotes (Wexler et al., 1987). Regardless, mHTT-related pathogenesis occurs early in the disease course, with functional deficits being detectable in cultured cells from HD patients up to fifteen years before onset (Paulsen et al., 2008).

1.3 Pathogenic mechanisms of mHTT

1.3.1 Cell-autonomous pathogenesis

The formation of large intracellular aggregates containing mHTT is pathognomonic for HD, however there is debate concerning their contribution to pathogenesis (Fig. 1.3). Aggregates sequester cellular proteins including transcription factors, ubiquitin and molecular chaperones (Steffan et al., 2000; Hay et al., 2004; Bennett et al., 2007), and reduced aggregation is associated with improved disease progression (Mielcarek et al., 2011). However, aggregate density does not correlate well with cell death in HD post-mortem brain (Vonsattel, 2008), and intranuclear inclusions of mHTT do not produce pathology in isolation (Gu et al., 2005; Gu et al., 2007). This suggests that aggregate formation is a protective response; this is supported by the association of intranuclear inclusion formation with neuronal survival (Arrasate et al., 2004). The primary toxic species in HD are therefore likely to be monomeric and oligomeric mHTT fragments (Miller et al., 2011). Aberrant splicing of *HTT* exon 1 mRNA has been shown to occur in a CAG-repeat dependent manner, resulting in the production of a HTT exon 1 protein (Sathasivam et al., 2013). This is likely to be highly pathogenic given the toxicity of similar species in fragment mouse models such as the R6/2.

Cellular pathways responsible for protein degradation are adversely affected by mHTT, and disruption of the UPS and autophagy is a consistent feature of HD (Ortega and Lucas, 2014; Martin et al., 2015). Examination of HD post-mortem brain tissue found evidence of residual autophagosomes containing mHTT (Sapp et al., 1997), suggesting there is a general inability of HD cells

to clear mHTT species, a phenomenon which is worsened by the inhibitory effects of mHTT on protein degradation pathways. Abnormal mitochondrial function is caused by the direct binding of mHTT to the outer mitochondrial membrane (Damiano et al., 2010), resulting in a lower calcium threshold to open the mitochondrial pores (Choo et al., 2004). Mitochondrial membrane potential regulates the release of apoptotic factors including cytochrome c, which along with apoptosis is upregulated in HD myoblast cultures. (Ciammola et al., 2006). The response to stressors is also diminished by progressive dysfunction in the vital heat shock response pathway (Labbadia et al., 2011), while neuronal metabolism is further impaired by the blocking of mitochondrial transport by mHTT aggregates (Chang et al., 2006).

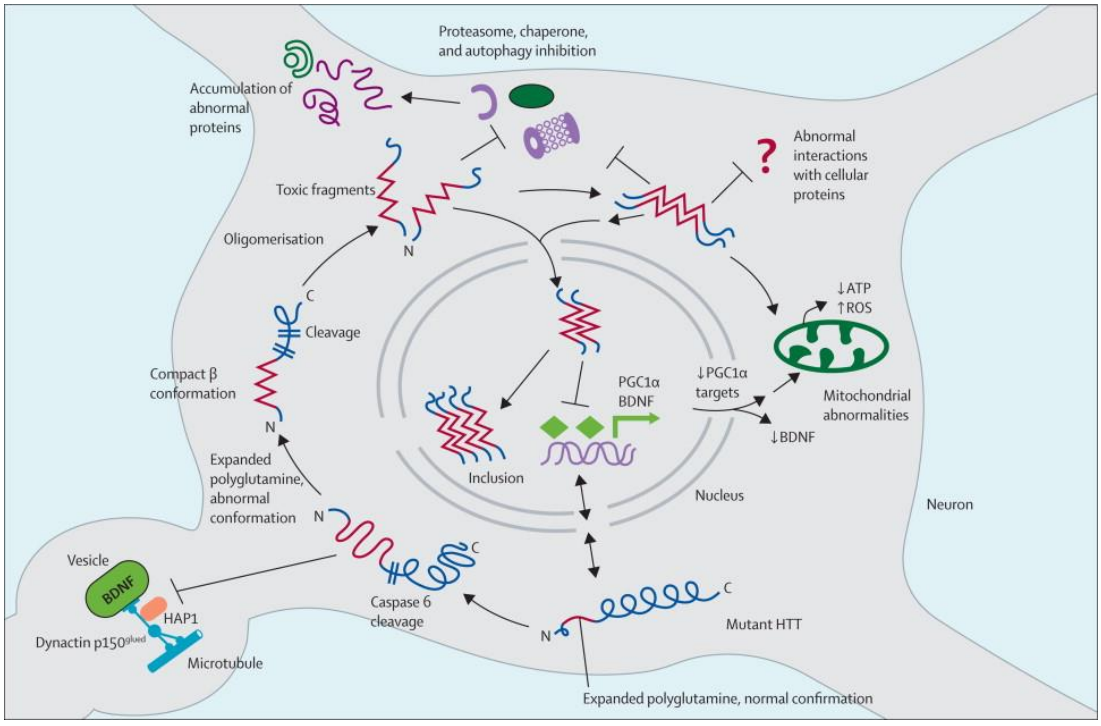

Figure 1.3. Cell-autonomous pathogenesis in HD. Mutant HTT has been shown to cause pathology by a wide range of cell-autonomous mechanisms, including the formation of toxic oligomeric fragments and the impairment of cellular energy metabolism. Reprinted from The Lancet Neurology, Vol. 10, "*Huntington's disease: from molecular pathogenesis to clinical treatment*", 83-98, Ross and Tabrizi, ©2011, with permission from Elsevier.

1.3.2 Non-cell-autonomous pathogenesis

While cell-autonomous pathogenesis is a central feature of HD, non-cell-autonomous pathogenesis is becoming increasingly recognised (Fig. 1.4). Glial cells play a key role in this process, as directed astrocytic expression of mHTT produces a neurological phenotype in mice (Bradford et al., 2009). Furthermore, glial expression of mHTT causes the death of neurons which do not express mHTT in co-culture (Shin et al., 2005). Mutant HTT aggregates may also spread from cell to cell in a prion-like manner (Brundin et al., 2010), and neural transplants into HD brain have been found to suffer from disease-like degeneration (Cicchetti et al., 2014). However, while mechanistically interesting, the ubiquitous expression of mHTT likely limits the pathogenic relevance of this phenomenon (Li et al., 1993).

Further possible mechanisms include impaired neuronal trafficking of BDNF (Gauthier et al., 2004), while reduced BDNF expression has also been found in HD patient brain (Zuccato et al., 2003). This may contribute to increased striatal vulnerability in HD, as MSNs are dependent on a cortical supply of BDNF (Ross and Tabrizi, 2011). Excitotoxicity is apoptosis occurring due to excessive activation of AMPA and NMDA glutamate receptors, high levels of which are expressed on MSNs (Nicholls, 2009). *In vivo* stimulation of striatal NMDA receptors gives an HD-like phenotype in rats (Beal et al., 1991), while levels of excitotoxic kynurenine 3-monooxygenase (KMO) metabolites are increased in HD brain (Guidetti et al., 2006). Potential excitotoxicity is likely worsened by impaired synaptic glutamate clearance (Liévens et al., 2001), while peripheral inhibition of the KMO pathway also has disease-modifying effects (see Section 1.7.2).

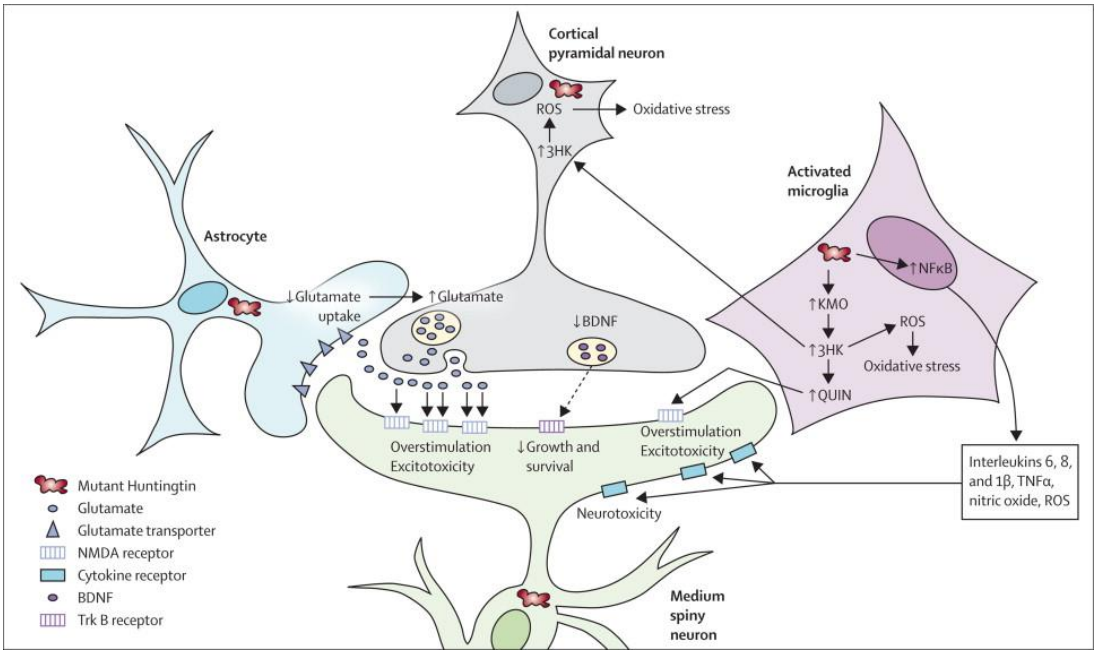

Figure 1.4. Non-cell-autonomous pathogenesis in HD. Mutant HTT has also been shown to cause pathology via alterations in cell-cell interactions. Reprinted from The Lancet Neurology, Vol. 10, "*Huntington's disease: from molecular pathogenesis to clinical treatment*", 83-98, Ross and Tabrizi, ©2011, with permission from Elsevier.

1.3.3 Transcriptional dysregulation in HD

Transcriptional dysregulation is a central feature of HD pathogenesis (Fig. 1.5) (Hodges et al., 2006), and has been demonstrated in a wide range of tissues in both HD patients and animal models (Seredenina and Luthi-Carter, 2012). Indeed, experiments in primary striatal neurons have shown that transcriptional dysregulation is caused by a cell-intrinsic effect of mHTT expression (Runne et al., 2008). Transcription factors including CBP, SP1, TBP and p53 are sequestered by mHTT aggregates, causing reduced binding to DNA (Seredenina and Luthi-Carter, 2012; Chen-Plotkin et al., 2006). The impaired protein degradation seen in HD is also likely to play a role in altering transcription factor processing by the UPS, while mHTT itself influences transcription by binding directly to DNA (Benn et al., 2008).

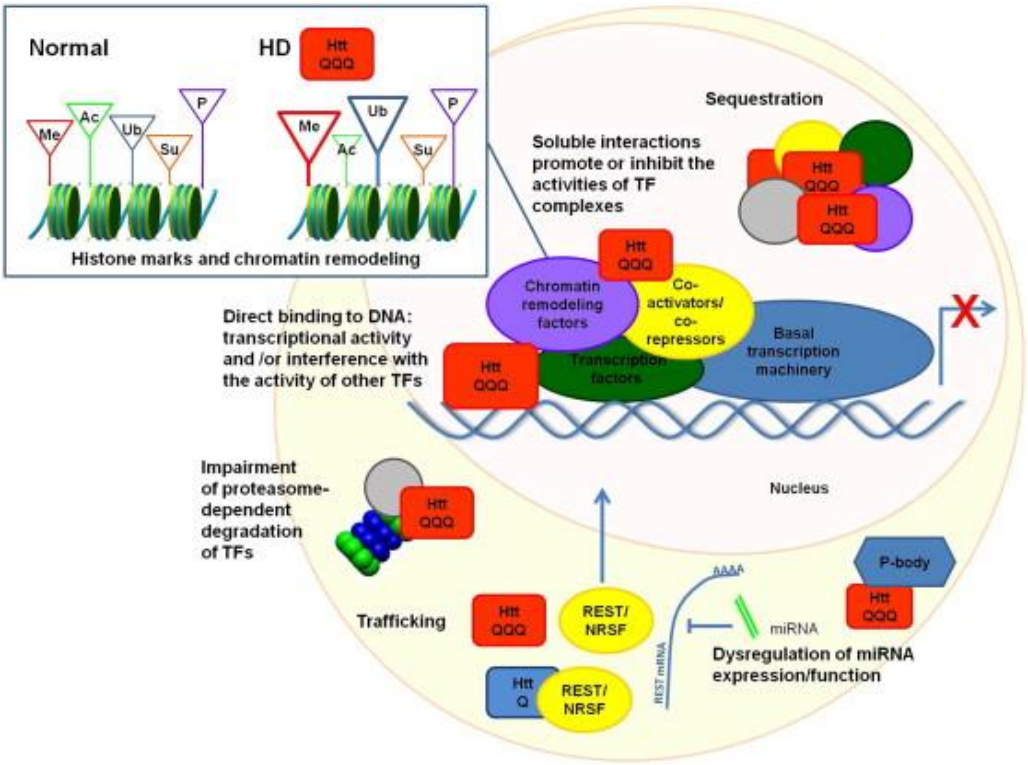

Figure 1.5. Transcriptional dysregulation in HD. Mutant *HTT* expression affects gene expression via a wide range of mechanisms, including the sequestration of transcription factors and the direct binding of mHTT to DNA. Reprinted from Neurobiology of Disease, Vol. 45, "*What have we learned from gene expression profiles in Huntington's disease?*", 83-98, Seredenina and Luthi-Carter, ©2012, with permission from Elsevier.

The activity of intracellular signalling pathways involved in regulating gene expression is similarly affected by mHTT. Mitogen-activated protein kinases (MAPKs) such as ERK show increased activity in HD (Apostol et al., 2006), while mHTT has a profound effect on NFκB signalling through a direct interaction with the IKK complex (Khoshnan et al., 2004). IKK phosphorylates IκB, one of the key cytoplasmic inhibitors of NFκB; this results in the dissociation of IκB from NFκB, which is then free to translocate to the nucleus and influence gene expression. Mutant HTT has been shown to increase IκB phosphorylation through its interaction with IKK, resulting in a decrease in NFκB inhibition and an upregulation in gene transcription.

Mutant HTT further affects gene expression through its influences on chromatin structure. Hyper-methylation of the H3K9 histone is associated with transcriptional repression, and occurs at increased rates in HD post-mortem brain (Ryu et al., 2006). Similar effects have been demonstrated for hypo-acetylation of H3 and H4 in HD (Labbadia et al., 2011; Sadri-Vakili et al., 2007), suggesting that the chromatin structure of HD cells may have more a repressive effect on transcription than in healthy controls.

It is important to note that transcriptional dysregulation may affect or be affected by the additional mechanisms of HD pathogenesis described above. For example, expression of BDNF promoters has been found to be reduced in a neuronal model of HD (Gambazzi et al., 2010); this is likely to worsen the lack of neurotrophic support seen in HD. Individual mechanisms should therefore be viewed within the whole spectrum of mHTT-related pathogenesis, instead of being considered purely in isolation.

1.4 HD therapeutics

1.4.1 Current therapeutics for HD

There are currently no therapeutics available to slow HD progression, with management instead focussing on symptomatic relief (Novak and Tabrizi, 2010). Tetrabenazine is the first drug specifically licensed for the treatment of HD-related chorea, although chorea may also be treated with neuroleptics such as haloperidol; these drugs are further useful for the management of non-motor symptoms including psychosis and irritability. Psychiatric manifestations are treated conventionally, for example with selective serotonin reuptake inhibitors for depression. Further treatment strategies

include the use of dietary supplements and physiotherapy for cachexia, while social care is often more effective than pharmacological intervention for improving behavioural issues (Ross et al., 2014). Recent clinical trials have largely yielded disappointing results (Bates et al., 2015).

1.4.2 Experimental therapeutics for HD

Substantial research into experimental therapeutics for HD has involved targeting a specific pathogenic mechanism, with the aim of ameliorating the relevant cellular deficit. It has been suggested that increasing the rate at which cells degrade proteins may aid in the clearance of mHTT (Ross and Tabrizi, 2011). Consistent with this hypothesis, the induction of mTOR-dependent autophagy protected against polyQ toxicity in fly and mouse models of HD (Martinez-Vicente et al., 2010). Further attempts to modulate cellular processing of mHTT have included the overexpression of molecular chaperones and administration of small molecule aggregation inhibitors (Vacher et al., 2005; Chopra et al., 2007). While promising, the off-target effects of such broad manipulation of cellular function may limit clinical utility.

Experimental therapeutics aimed at supporting or improving neuronal function have included overexpression of the *BDNF* gene in the forebrain of the R6/1 mouse; this improved motor performance and reduced brain weight loss (Gharami et al., 2008), while the pharmacological upregulation of BDNF using an ampakine was able to rescue synaptic plasticity and memory in an HD knock-in mouse model (Simmons et al., 2009). Further strategies have attempted to block the neuronal damage caused by excitotoxicity, however riluzole was not found to have a disease-modifying on HD in human clinical

trials (Landwehrmeyer et al., 2007). This strategy will therefore likely depend on the development of more robust pharmacological agents.

One interesting therapeutic strategy involves the use of grafts to directly replace neurons in the adult brain. This technique showed promise in rodent and primate models of HD (Hurelbrink et al., 2002; Palfi et al., 1998), however clinical trials in patients were inconclusive at best (Benraiss and Goldman, 2011). In addition, the worrying possibility remains that mHTT is able to spread in a prion-like manner, and disease-like degeneration of grafted tissue has been reported in post-mortem brain (Cicchetti et al., 2014). Further experimental therapeutics for HD have involved the targeting of transcriptional dysregulation, with both the inhibition and genetic knockdown of histone deacetylases improving motor function in HD mice (Labbadia et al., 2011; Mielcarek et al., 2011). However, the pathogenesis of mHTT is multi-factorial, and each of the experimental therapeutics outlined above is limited by the fact that it only targets a single mechanism.

1.4.3 Post-transcriptional gene silencing

In recent years there has been substantial interest in the use of post-transcriptional gene silencing (PTGS) to treat genetic disorders. This strategy works by preventing the translation of mRNA, thereby cutting off the pathogenic cascade at its source (Fig. 1.6). Initial clinical trials have shown promising results in diseases such as Duchenne's muscular dystrophy (Goemans et al., 2011). There are a number of ways in which PTGS may be achieved, the majority of which either physically block translation or harness cellular RNA interference (RNAi) pathways (Sah and Aronin, 2011).

One of the most commonly used methods of PTGS involves the administration of small interfering RNA (siRNA) molecules. These are double-stranded oligonucleotides of approximately 20-25 bp that hijack the endogenous miRNA system of post-transcriptional gene expression regulation (Sah and Aronin, 2011). Each siRNA molecule is made up of a guide strand and a passenger strand. Following delivery into the cytoplasm, the two strands separate and the guide strand joins with the multiprotein RNA-induced silencing complex (RISC), where it binds to complementary mRNA sequences to target them for degradation (Rand et al., 2005). This is typically carried out by the Argonaute enzyme family. In contrast, antisense oligonucleotides (ASOs) are single-stranded molecules of approximately 15-25 bp that mediate PTGS by either directing target mRNA for degradation by the ribonuclease H (RNase H) enzyme, or physically blocking translation by the ribosome (Bennett and Swayze, 2010).

Further differences between siRNAs and ASOs include their delivery mechanisms, as ASOs do not require a delivery vehicle and can be directly taken up by cells, including neurons (Kay et al., 2014). In contrast, siRNAs require a reliable transfection protocol to be delivered to a target cell. Furthermore, siRNAs are only able to target mRNA in the cytoplasm, and as such are limited to silencing exonic sequences, while ASOs can also enter the nucleus to target nuclear pre-mRNA (Sah and Aronin, 2011). However, siRNAs are generally thought to be more robust, and do not need to undergo the substantial chemical modifications often required to achieve potency with ASOs (Watts and Corey, 2012). They are also likely to be more stable than ASOs given the fact that they are double instead of single-stranded.

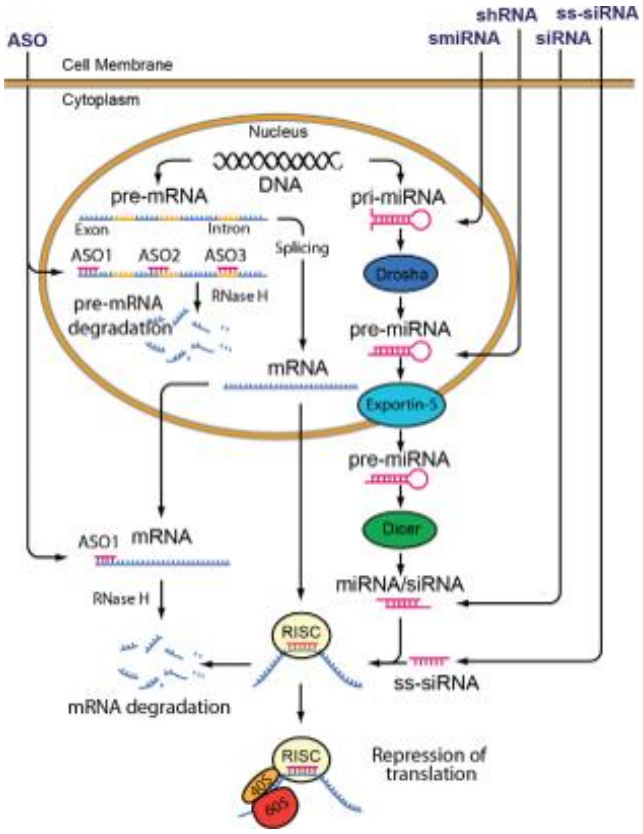

Figure 1.6. Post-transcriptional gene silencing techniques. After entering the cytoplasm, siRNAs harness the endogenous miRNA system to target complementary nucleotide sequences to the RISC. In contrast, ASOs mediate gene silencing by directing their target transcript for degradation by RNase H, or by physically blocking translation. Reprinted from Clinical Genetics, Vol. 86, "*Personalized gene silencing therapeutics for Huntington disease*", 29-36, Kay et al., ©2014, with permission from John Wiley and Sons.

1.4.4 HTT-lowering in HD

As a monogenic disorder, HD is a prime target for treatment by PTGS. An initial proof of concept study using doxycycline-mediated conditional knockout of m*HTT* demonstrated a reduction in brain pathology in an HD mouse model (Yamamoto et al., 2000), proving the hypothesis that a reduction in cellular mHTT levels has a beneficial effect on survival. More recent studies have made use of both siRNAs and ASOs with considerable success. Administration of anti-*HTT* siRNA using a lentiviral vector reduced

neuropathology in a mouse model of HD (Drouet et al., 2009), while the infusion of ASOs into the CSF of HD mice was shown to delay disease progression (Kordasiewicz et al., 2012). Interestingly, the improvement in symptoms was found to last longer than the reduction in *HTT* mRNA levels, suggesting that even occasional HTT-lowering treatment may be sufficient to provide an improvement in disease progression. These findings were also extended to *HTT* mRNA levels in the primate cortex.

These studies provide great promise for HTT-lowering as a future therapeutic for HD, although reliable delivery presents a significant hurdle. Traditional peripheral administration is likely to be futile, as the drugs will not cross the blood-brain barrier in sufficient quantities to have an appreciable therapeutic effect. Methods to directly deliver into the brain, for example implantable infusion systems, would bypass this issue. However, they are highly invasive and the extent to which they would be tolerated long-term is uncertain. One promising approach is the direct infusion of ASOs into the CSF, and initial studies of this method are currently underway (Ionis Pharmaceuticals, 2015).

1.4.5 Allele-selective HTT-lowering

One of the most important distinctions to draw is between those therapies that will non-selectively lower both wild-type and mutant *HTT* mRNA, and those that will selectively lower the mutant allele while sparing the wild-type. The majority of studies to date have made use of siRNAs and ASOs which do not discriminate between alleles, and for the purposes of this thesis will be referred to as ‘total’ *HTT*-lowering. This occurs because the target nucleotide sequence is present on both alleles (Sah and Aronin, 2011).

However, wild-type HTT has a number of important cellular roles (see Section 1.2.2), and it is not known what degree of wild-type HTT knockdown will be tolerated over extended periods. Although initial studies suggested that *Htt* knockout in the adult mouse brain causes neurodegeneration (Dragatsis et al., 2000), it has since been shown that non-specific HTT-lowering is tolerated for at least nine months in HD mice (Kordasiewicz et al., 2012; Stanek et al., 2014), while a six month reduction in *HTT* expression has no adverse effects in the rhesus putamen (Grondin et al., 2012). Surprisingly, death from ubiquitous *Htt* knockout in mice is caused by acute pancreatitis (Wang et al., 2016), and is therefore unlikely to be due to neuronal *Htt* depletion. Despite this, there is no information available on the long-term consequences of wild-type HTT suppression in the human brain, where therapies will necessarily be administered over the course of several decades. The ideal therapeutic strategy would therefore selectively lower mHTT while preserving wild-type. The allele-selective suppression of m*HTT* relies on the existence of polymorphisms between the two alleles, with the two most obvious targets being the expanded CAG repeat and SNPs. SNPs are genomic variants that result in a single nucleotide change between alleles; the *HTT* gene contains many such variants (Pfister et al., 2009).

A therapeutic strategy that targets the expanded CAG repeat would be applicable to all HD patients, and has shown some promise in *in vitro* testing. Patient-derived fibroblasts with mutant and wild-type CAG repeats of sixty-nine and seventeen respectively were treated with an ASO targeted to the CAG repeat expansion, achieving > 3.7 fold selectivity of inhibition (Gagnon et al., 2010). This was advanced using ssRNA molecules in place of ASOs,

achieving allele-selectivity > 100 fold (Yu et al., 2012). However, the selectivity of knockdown is markedly reduced when targeting expanded CAG repeats in the normal human range (forty-four vs. fifteen), with approximately 50 % off-target knockdown (Fiszer et al., 2013). Furthermore, there is the possibility that these therapeutics will have off-target effects on other CAG repeat-containing genes. These factors mean that SNP-targeted knockdown may provide a more promising alternative.

The SNP-targeted strategy involves genotyping HD patients for heterozygosity at specific SNP sites, before linking each SNP allele to either wild-type or m*HTT* (Sah and Aronin, 2011). The relevant SNP may then be targeted for knockdown using either siRNA or ASOs. While this strategy may allow more selective knockdown of mHTT, it is only applicable to patients who are heterozygous for SNPs of interest (Kay et al., 2014). The prevalence of heterozygosity at individual SNP sites varies between different ethnic groups (Lombardi et al., 2009; Warby et al., 2009), however it is estimated that two thirds of HD patients may be treated by targeting just two SNPs, rising to 75 % when three SNPs are utilised (Pfister et al., 2009). Furthermore, the T allele of the most prevalent SNP (rs362307 in the 3'-untranslated region (UTR)) has been shown to be linked to the mutant allele, raising the possibility that these 75 % of HD patients could be treated with five siRNAs targeting just three SNPs. Expanding SNP coverage beyond this point is not expected to provide much additional benefit, as approximately 25 % of patients do not have a heterozygous SNP associated with m*HTT* (Pfister et al., 2009). However, an alternative possibility would be to use two allele-selective siRNAs or ASOs to target a single SNP in both homozygous

and heterozygous patients; this would provide allele-selective knockdown in approximately half of cases and non-selective knockdown in the remainder, while limiting the need for an exhaustive clinical trial process for multiple SNP-targeted therapeutics (Skotte et al., 2014).

SNP-targeted allele-selective suppression was first achieved using human HD fibroblasts heterozygous for rs363125 in exon 39 of the *HTT* transcript (van Bilsen et al., 2008), with siRNA targeted to the mutant C allele generating approximately 80 % mRNA knockdown. Further work has been done by screening a large panel of ASOs targeting fifty SNPs in human HD fibroblasts, mouse neurons and an HD mouse model (Carroll et al., 2011). The best results were seen with an ASO targeted to rs7685686 in intron 42, with approximately five-fold selectivity being achieved. However, it is important to note that the fibroblasts were all either homozygous 'on-target' or homozygous 'off-target' for the SNPs of interest, and that for reasons of convenience the ASOs were not tested in heterozygous cell lines. Indeed, the expression of each *HTT* allele was not quantified separately.

This work was recently advanced by a study incorporating positional chemical modifications into an ASO targeting rs7685686, resulting in > 100 fold selectivity for a single SNP allele in human HD fibroblasts (Østergaard et al., 2013). This improved allele-selectivity was also found to translate to the brain of a humanised HD mouse model, and an additional panel of allele-selective ASOs has since been screened *in vivo* (Southwell et al., 2014). Interestingly, the latter study found that targeting a single SNP provided greater silencing than combinatorial targeting of multiple SNPs, although this may have been due to the potency of the ASOs in question. In this case HTT

quantification was also carried out using relatively insensitive immunoblotting techniques, with no analysis of allele-specific mRNA expression by qPCR; the use of certain chemical modifications was also found to produce toxicity. Further demonstrations of allele-selective suppression have been provided using adenoviral and lentiviral delivery of RNAi in mouse models and human stem cells (Drouet et al., 2014; Stanek et al., 2014), although in both cases the mouse models in question only possessed one copy of the human *HTT* gene. The extent to which selectivity is achieved in the presence of both alleles is therefore yet to be established. Indeed, allele-selective suppression is yet to be demonstrated in living *ex vivo* primary human HD cells.

1.5 The innate immune system

The immune system is responsible for the body's response to external pathogens and tissue injury, and is divided into two main arms. The innate immune system provides an immediate, generic response to a wide range of pathogens, the strength of which does not vary with multiple exposures (Owen et al., 2013). In contrast, the adaptive immune system generates a highly specific secondary response. While there is substantial interplay between the two arms of the immune system (Iwasaki and Medzhitov, 2015; Shanker, 2010), they are mediated by highly varied cells and mechanisms.

1.5.1 Cells of the innate immune system

Microglia are the primary immunocompetent cells of the CNS, and make up approximately 10 % of all brain cells (Ransohoff and Perry, 2009). During development microglia migrate into the nascent CNS from the embryonic yolk sac (Kierdorf et al., 2013), however in adulthood they form a self-

renewing population. (Ajami et al., 2007). Microglia are largely anti-inflammatory at rest, and are kept so by direct interactions with neurons (for example via CD200) (Hoek et al., 2000). However, in response to tissue injury they rapidly expand by microgliosis before directing neuroinflammation (Owen et al., 2013). While peripheral immune cells are able to cross the blood-brain barrier into the CNS in response to pathology, this does not happen under normal conditions (Ajami et al., 2007).

In contrast, peripheral immune cells are replenished by haematopoietic stem cells located in the bone marrow (Fig. 1.7); these differentiate into common myeloid progenitor or common lymphoid progenitor cells (Owen et al., 2013). Common myeloid progenitor cells may then undergo further differentiation to produce a range of cell types including monocytes, dendritic cells, neutrophils and megakaryocytes, while common lymphoid progenitors give rise to cell types including T and B lymphocytes and natural killer (NK) cells.

Monocytes are one of the most important cell types of the peripheral immune system, and account for approximately 10 % of circulating white blood cells in humans (Auffray et al., 2009). While all monocytes express the CD14 cell surface molecule, they may be divided into two broad populations depending on the degree to which they also express CD16 (Passlick et al., 1989). Classical monocytes ($CD14^{++}$ $CD16^{-}$) primarily circulate in the bloodstream responding to inflammatory mediators, and are thought to be largely phagocytic in function with limited inflammatory properties (Mukherjee et al., 2015). In contrast, alternative monocytes ($CD14^{+}$ $CD16^{+}$) are thought to represent a more mature phenotype which localise to a specific tissue and carry out the process of cytokine production (Ziegler-Heitbrock, 2007).

On encountering a stimulus, monocytes migrate into a specific tissue or site of injury and differentiate into macrophages (although some may also differentiate into dendritic cells) (Owen et al., 2013). Macrophages are the primary effector cells of the peripheral innate immune system, and form highly diverse populations depending on their location within the body (Geissmann et al., 2010). While macrophages were traditionally thought to be either broadly proinflammatory (M1 sub-type) or anti-inflammatory (M2 sub-type), in recent years it has been suggested that macrophage phenotypes form more of a flexible continuum (Martinez and Gordon, 2014).

Additional cell types involved in innate immune function include dendritic cells and granulocytes. Dendritic cells form a diverse group of cells which are involved in mediating the interactions between the innate and adaptive immune systems by the process of antigen presentation to lymphocytes (Owen et al., 2013). The granulocyte population is made up of a range of different cell types including neutrophils, eosinophils and basophils; these have diverse functions ranging from the phagocytosis of external pathogens to the release of inflammatory mediators (Owen et al., 2013).

1.5.2 Functions of the innate immune system

The functions of the innate immune system are as diverse as the cells which mediate them; however, as monocytes and macrophages form the main immunological focus of this thesis, this section will concentrate on describing their primary functions at the expense of those of alternative cell types. These primarily consist of immune surveillance, phagocytosis and the generation of inflammation through the process of cytokine production.

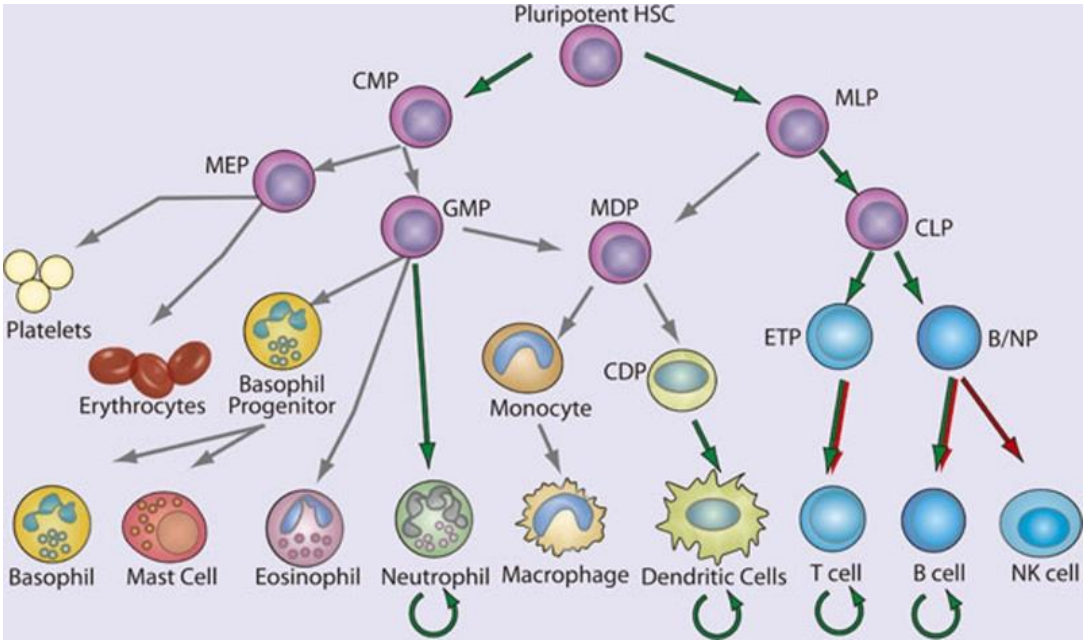

Figure 1.7. Haematopoiesis of immune cells. The cells of the immune system are produced by haematopoiesis, whereby stem cells located in the bone marrow go through a series of differentiation steps until mature cells are produced. HSC: haematopoietic stem cell, CMP: common myeloid progenitor, MLP: myeloid/lymphoid progenitor, MEP: megakaryocyte erythrocyte progenitor, GMP: granulocyte monocyte progenitor, MDP: macrophage dendritic cell progenitor, CDP: common dendritic cell progenitor, CLP: common lymphoid progenitor, ETP: early thymic precursor, B/NP: B-cell natural killer cell progenitor. Reprinted from Cell Research, Vol. 21, "*NF-κB in immunobiology*", 223-244, Hayden and Ghosh, ©2011, with permission from Nature Publishing Group.

Once they have been released from the bone marrow, monocytes circulate in the bloodstream until they encounter a chemotactic stimulus, the most common of which is MCP-1 (Deshmane et al., 2009). Monocytes then migrate into a tissue along the chemotactic gradient formed by the chemokine. At this point the monocyte differentiates into a mature macrophage phenotype and releases a range of cytokines to direct the immune response (Owen et al., 2013). The traditional view refers to either classical activation, involving pathogen associated molecules such as LPS,

or alternative activation, involving cytokines such as IL-4 and IL-10 (Owen et al., 2013). While the reality of this dichotomy is likely more complex, it is a useful paradigm for the limited discussion of macrophage function presented here. Classically activated macrophages largely produce proinflammatory cytokines such as IL-6 and TNFα, while alternatively activated macrophages primarily produce anti-inflammatory cytokines such IL-10 and TGF-β.

Cytokine release itself is a diverse process, and occurs in response to activation of the cellular signalling pathways described in Section 1.5.3. The classical method of cytokine release takes place via secretory granules or vesicles, although some cytokines are released via alternative methods (Lacy and Stow, 2011). For example, TNFα is synthesised as a membrane-bound precursor that is cleaved in response to cellular activation (Black et al., 1997). The specific mechanism of release for an individual cytokine may even vary between cell types, with IL-1β having been found to be secreted in numerous different ways including exocytosis and cell lysis (Eder, 2009).

A further essential macrophage function is that of phagocytosis (although this is a function shared by additional innate immune cell types including dendritic cells and neutrophils). Once a pathogen is recognised by a phagocytic cell, it is engulfed by a change in morphology of the cell membrane; this forms a phagosome, which is then internalised and fused with a lysosome containing enzymes capable of degrading the pathogen (Owen et al., 2013). Additional innate immune cell killing is carried out by NK cells, which insert granules containing cytotoxic substances into the cytoplasm of a target cell.

Macrophages and dendritic cells of the innate immune system, in addition to B lymphocytes of the adaptive immune system, also carry out an essential role as professional antigen presenting cells. Following internalisation of a specific antigen, these cells process a specific epitope of the antigen before presenting it to T lymphocytes in combination with the major histocompatibility complex (MHC) class II molecule (Owen et al., 2013) This allows T lymphocytes to begin directing the highly specific secondary immune response mediated by the adaptive immune system.

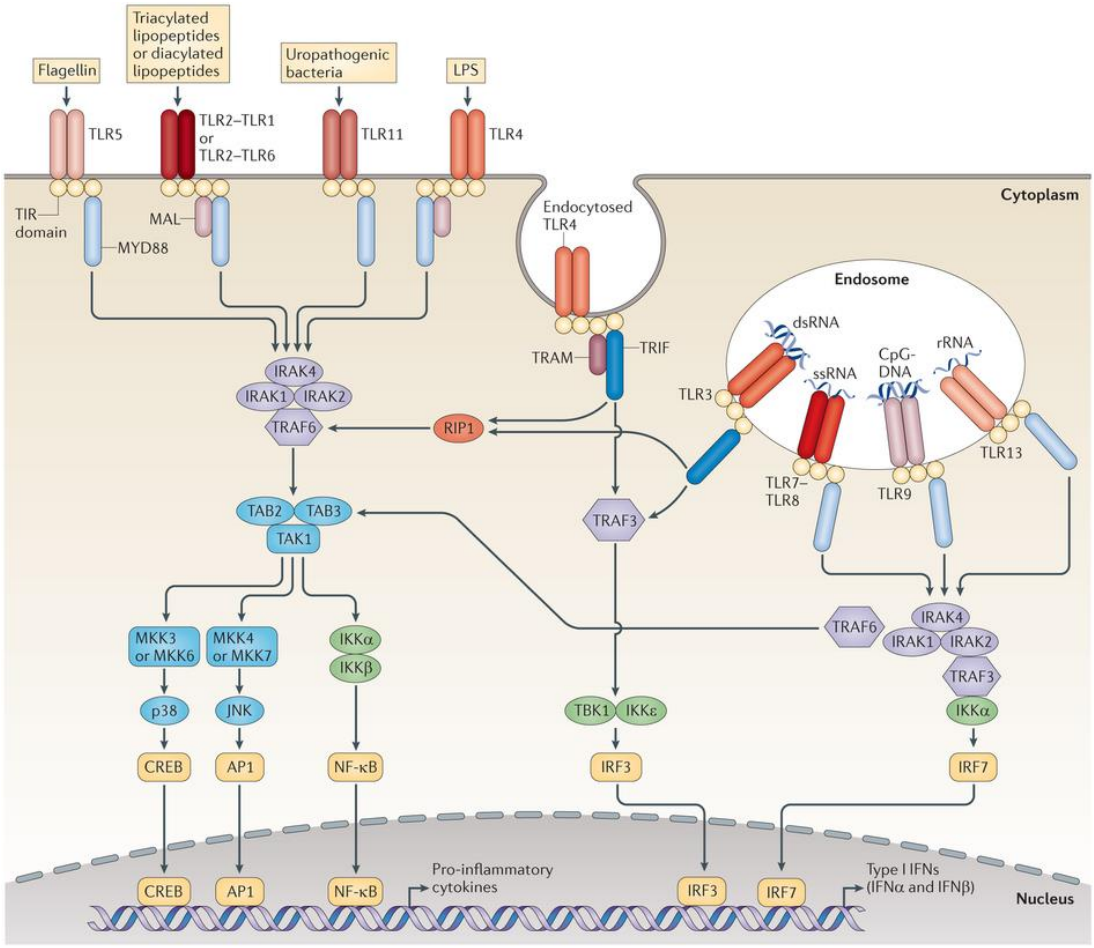

Figure 1.8. **TLR signalling cascades.** Following activation by LPS, TLR4 activates numerous intracellular signalling cascades, resulting in an increase in the transcription of proinflammatory genes. Reprinted from Nature Reviews Immunology, Vol. 13, "*The history of Toll-like receptors — redefining innate immunity*", 453-460, O'Neill et al., ©2013, with permission from with permission from Nature Publishing Group.

1.5.3 Innate immune signalling pathways

Activation of innate immune cells typically occurs in response to pathogen-associated molecular patterns (PAMPs), for example on LPS (Owen et al., 2013). LPS is a component of the outer membrane of Gram-negative bacteria that is frequently used as an artificial experimental stimulus (Okun et al., 2009). PAMPs are identified by pathogen recognition receptors (PRRs) located on the cell membrane. One of the most important classes of PRRs is the toll-like receptors (TLRs), which form homo or heterodimers that are highly specific for particular PAMPs (Kumar et al., 2009). For example, LPS is detected by homodimers of TLR4. The end result of TLR activation is an upregulation in the expression of proinflammatory genes; this reaches a peak after approximately 4 h, although depending on the gene peak expression may occur anywhere from 2-8 h (Aung et al., 2006; Yamamoto et al., 2004).

Once TLRs have bound their ligands, intracellular signalling cascades are activated via the cytoplasmic adaptor protein MyD88 (although MyD88-independent cascades are also present) (Yamamoto et al., 2003). MyD88 interacts with numerous signalling pathways (Fig. 1.8), including NFκB and the ERK and p38 MAPKs (Akira and Takeda, 2004). Briefly, NFκB signalling is activated by an interaction of MyD88 with IRAK, which activates the IκB kinase (IKK) complex by phosphorylation. IKK then phosphorylates IκB, the main cytoplasmic inhibitor of NFκB; this causes IκB to dissociate from NFκB, which then translocates to the nucleus (Owen et al., 2013). The NFκB family is made up of five members which form homo or heterodimeric transcription factors; RelA (p65), RelB, NFκB1 (p50), NFκB2 (p52) and c-Rel. They then regulate the expression of over 150 target genes (Akira and Takeda, 2004)

Additional signalling pathways are also activated through phosphorylation cascades, with an interaction of MyD88 with the TRAF6 protein causing an upregulation in MAPK signalling (Barton and Medzhitov, 2003). This leads to the induction of transcription factors including AP-1 and MYC, both of which contribute to the proinflammatory cellular response to LPS. It is important to note that these signalling pathways should not be viewed in isolation, as there is a great deal of crosstalk whereby one is able to influence the activity of the others (Hoesel and Schmid, 2013). There is also considerable overlap in the target genes that are regulated by each signalling pathway.

1.6 The adaptive immune system

1.6.1 Cells of the adaptive immune system

The primary cell types of the adaptive immune system are T and B lymphocytes, which make up approximately 20-40 % of circulating white blood cells (Owen et al., 2013). They are so named because T lymphocytes mature in the thymus, while B lymphocytes mature in the bone marrow. While morphologically similar, T and B lymphocytes may be reliably distinguished by specific cell surface proteins; T lymphocytes express CD3, while B lymphocytes express CD19. Furthermore, they are distinct in their expression of either the T cell receptor (TCR) or the B cell receptor (BCR). These are highly antigen specific, and receptors with affinity for over a billion antigens are present in the normal lymphocyte population (Owen et al., 2013). However, each individual lymphocyte will only express receptors for a single antigen; this is passed on to the daughter cells produced by division.

T lymphocytes subsets may be distinguished by their expression of additional cell surface proteins to the pan T cell marker CD3. The two most common subsets are $CD4^+$ helper T (T_h) lymphocytes, and $CD8^+$ cytotoxic T lymphocytes (Owen et al., 2013). The T_h lymphocyte population may be further divided up in a number of additional subsets, including T_h1, T_h2 and T_h17 lymphocytes. Regulatory T lymphocytes (T_{reg}) form an additional $CD4^+$ population, although they are distinct from helper T lymphocytes.

1.6.2 Functions of the adaptive immune system

In contrast to the immediate action of the innate immune system, responses generated by the adaptive immune system often take up to five or six days to reach their peak (Owen et al., 2013). T lymphocytes are only able to recognise antigens that have been processed and presented in combination with an MHC molecule. Helper T lymphocytes primarily recognise antigens presented in combination with MHC class II, which is expressed on the surface of professional antigen-presenting cells (Owen et al., 2013). Once naïve $CD4^+$ T lymphocytes have been presented with an antigen, they differentiate into one of a number of subsets. T_h1 cells are primarily involved in the response to intracellular pathogens, and secrete a range of cytokines including IFNγ and IL-2; the main target cells of T_h1 lymphocytes are macrophages and cytotoxic T lymphocytes (Owen et al., 2013). T_h2 lymphocytes primarily direct the immune response to extracellular pathogens via the release of cytokines including IL-4, IL-5 and IL-10, the main targets of which are B lymphocytes and granulocytes.

In contrast, naïve $CD8^+$ T lymphocytes primarily recognise antigens presented in combination with MHC class I, which is expressed on all nucleated cells. Following antigen presentation, they differentiate into mature cytotoxic T lymphocytes. Cytotoxic T lymphocytes act by inducing cell lysis through the release of cytotoxins such as granzymes; the simultaneous release of the pore-forming protein perforin allows these cytotoxins to enter the cytoplasm of the target cell (Owen et al., 2013). Further mechanisms include direct cell-cell interactions, including binding of Fas ligand to Fas.

Additional effector functions are carried out by T_h17 lymphocytes, which are characterised by their secretion of the proinflammatory cytokine IL-17, and are thought to play a key role in the immune response at mucosal surfaces (Owen et al., 2013). T_{reg} lymphocytes are characterised by expression of the cell surface protein CD25, in addition to the transcription factor FoxP3. They are primarily anti-inflammatory in function, and are involved in the inhibition of immune activity, in addition to the avoidance of autoimmune responses that have not been prevented by alternative processes.

B lymphocytes are responsible for antibody production, and express surface immunoglobulin (Ig) in the form of the BCR. Once the BCR has bound an antigen, it is internalised and presented to T lymphocytes in combination with MHC class II (Owen et al., 2013). Helper T lymphocytes then provide co-stimulation with cytokines including IL-4, in addition to cell-cell interactions mediated via the B lymphocyte surface protein CD40. Some antigens are also able to induce T cell independent activation. After activation, B lymphocytes proliferate and differentiate into plasma cells, which produce

vast quantities of antibody; these molecules direct pathogens for degradation by other immune cells, in addition to neutralising pathogens by direct binding.

Both T and B lymphocytes are responsible for immunological memory. Following clearance of a pathogen, a proportion of T and B lymphocytes will become memory cells; these retain their specificity for a particular antigen, and are able to rapidly proliferate in response to it being encountered a second time (Owen et al., 2013). This results in a greatly enhanced secondary immune response and more rapid clearance of the pathogen.

1.6.3 Adaptive immune signalling pathways

There is considerable overlap between the pathways involved in innate and adaptive immune signalling, with the NFκB and MAPK pathways also known to play an important role in T lymphocytes (Owen et al., 2013). However, the mechanisms by which these signalling pathways are activated, and the effect they have on cellular function, may vary considerably. For example, NFκB activation in T lymphocytes primarily takes place in response to TCR instead of TLR signalling (Brownlie and Zamoyska, 2013). While TLR4 is expressed by T lymphocytes, its function is not fully understood, and it has even been suggested to have a repressive effect (González-Navajas et al., 2010). Furthermore, while NFκB is almost exclusively proinflammatory in myeloid cells, it has been suggested to have anti-inflammatory effects in T lymphocytes, with overexpression of NFκB1 in naïve $CD4^+$ T lymphocytes leading to reduced expression of IL-2 (Kang et al., 1992). Additional signalling molecules such as the NFAT family of transcription factors are also heavily involved (Macian, 2005).

1.7 Immune dysfunction in HD

1.7.1 Central immune dysfunction

Inflammatory changes in the CNS, commonly referred to as neuroinflammation, have recently emerged as a crucial component in the pathogenesis of neurodegenerative diseases including Alzheimer's disease and Parkinson's disease (Björkqvist et al., 2009). Activated microglia accumulate in the post-mortem brains of HD patients of all disease stages (Sapp et al., 2001), while functional imaging studies have shown that microglia are abnormally activated even in the brains of premanifest HD gene carriers (Tai et al., 2007; Pavese et al., 2006); this activation correlates with neuronal loss, striatal dysfunction and disease severity. Abnormal microglial activation has also been demonstrated in the brains of R6/2 mice, demonstrating a common feature between species (Simmons et al., 2007).

One of the key areas of debate has centred on whether this abnormal microglial activation is harmful or protective. While microglia are considered to be largely neuroprotective, it has been suggested that an increase in their activation could result in healthy neurons being removed accidentally as part of a 'bystander effect' (Brown and Neher, 2010). Production of inflammatory complement components has been found to be upregulated in striatal HD microglia (Singhrao et al., 1999), with significantly increased levels of striatal *IL6*, *IL8*, and *TNF* mRNA being demonstrated in HD post-mortem brain tissue (Björkqvist et al., 2008). Furthermore, wild-type glia have a protective effect on mHTT-expressing neurons in co-culture, while mHTT-expressing glial cells only serve to increase neuronal vulnerability (Shin et al., 2005).

The expression of mHTT in glial cells also exacerbates neurological symptoms in HD mice (Bradford et al., 2010).

However, it must still be determined whether neuroinflammation is primarily a secondary response to neuronal pathology, or if mHTT has a cell-autonomous effect on microglial function. A recent study using a murine HD microglial cell line has shown that mHTT directly promotes autonomous microglial activation, likely via a priming effect that increases proinflammatory gene expression (Crotti et al., 2014). This suggests that central inflammatory changes are likely to occur both in response to and independently of neuronal death and dysfunction. It is also important to consider the possibility of peripheral changes contributing to central pathology, as proinflammatory cytokines such as IL-6 have been shown to cross the blood-brain barrier. Indeed, peripheral immune cells may also infiltrate the CNS, although no changes in the HD blood-brain barrier have been described to date.

1.7.2 Peripheral immune dysfunction

Immune-related pathology in HD is not merely restricted to the CNS (Fig. 1.9), and a wide range of peripheral immune abnormalities have been described in both HD patients and animal models of the disease (Ellrichmann et al., 2013). Proteomic profiling of HD patient plasma revealed a significant increase in the levels of proinflammatory mediators including IL-6 and complement components (Dalrymple et al., 2007), while further work showed that HD patients of all disease stages exhibit increased plasma levels of proinflammatory cytokines and chemokines (Björkqvist et al., 2008; Wild et al., 2011). Indeed, significant increases in IL-6 levels were detected up to

sixteen years before the predicted onset of motor symptoms. Interestingly, CSF levels of IL-6 and IL-8 were found to correlate strongly with these peripheral changes, while microglial activation has been shown to correlate with increased peripheral cytokine levels (Politis et al., 2015).

Myeloid cells from HD patients of all disease stages express mHTT, the levels of which correlate with disease burden scores and caudate atrophy (Weiss et al., 2012). Functional investigation has revealed that they are hyper-reactive, producing significantly increased levels of proinflammatory cytokines including IL-8 and TNFα following stimulation with LPS (Träger et al., 2014). This effect was found to be reversible following HTT-lowering, suggesting it is due to a direct effect of mHTT expression. This hypothesis was confirmed by knocking an expanded CAG repeat into a monocyte cell line, as the transfected cells also produced significantly increased levels of IL-6 and TNFα following stimulation. Myeloid cells from HD mouse models further show increased cytokine production (Träger et al., 2015), suggesting a common HD immune signature even between species. Further functional investigation of HD patient myeloid cells revealed functional deficits when migrating to chemotactic stimuli and phagocytosing fluorescent beads (Träger et al., 2015; Kwan et al., 2012b). However, it is important to note that the majority of studies to date have only demonstrated phenotypic abnormalities in response to stimulation, and it remains unclear if HD myeloid cells are also abnormal in their basal, resting state.

Furthermore, the vast majority of work to date has focused on the cells of the innate immune system, with very little information available on the adaptive immune system. T and B lymphocytes from HD patients express mHTT, the

levels of which correlate with disease burden scores (Weiss et al., 2012). Levels of the signature T_h2 cytokine IL-4 are also increased in the plasma of manifest HD patients (Björkqvist et al., 2008). However, the same study found no difference in the levels of circulating Ig between HD patients and controls, arguing against any substantial dysregulation of the HD adaptive immune response. This is supported by a study finding no enrichment of T lymphocytes in post-mortem HD brain tissue (Silvestroni et al., 2009). In either case this evidence is largely circumstantial, and further investigation is required to characterise HD adaptive immunity.

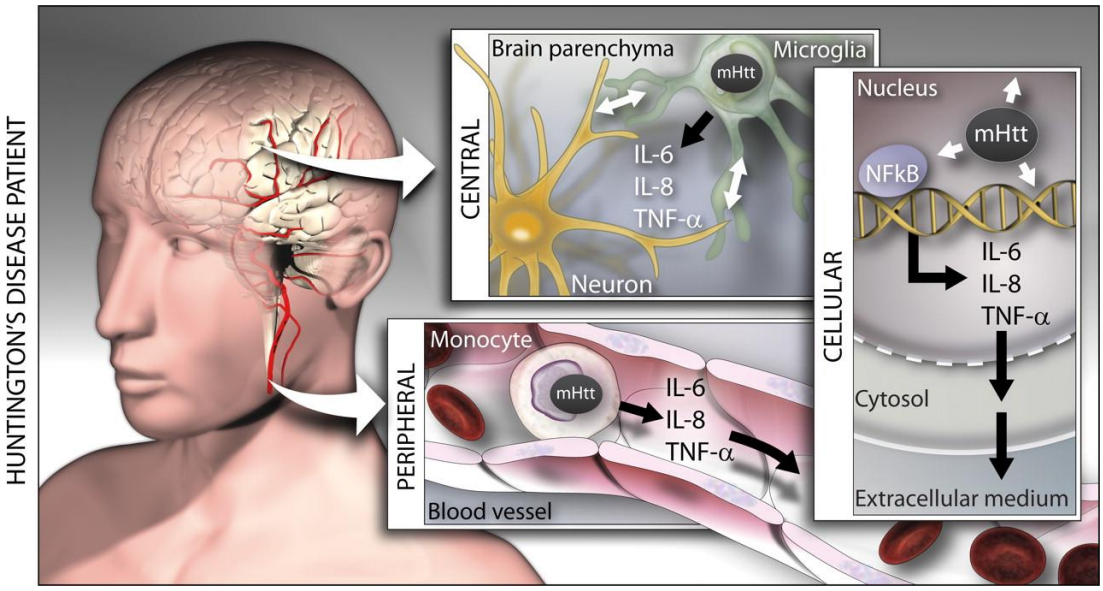

Figure 1.9. Central and peripheral immune dysfunction in HD. Elevated levels of proinflammatory cytokines are detectable in both the CNS and peripheral blood of HD patients of all disease stages. This is likely related to a direct mHTT effect causing abnormal activation of the NFκB pathway in HD immune cells. Reprinted from The Journal of Experimental Medicine, Vol. 205, "*A novel pathogenic pathway of immune activation detectable before clinical onset in Huntington's disease*", 1869-1877, Bjorkqvist et al., ©2008, with permission from The Rockefeller University Press.

One of the most intriguing possibilities relates to the peripheral immune system as a potential modifier of HD progression. The CB2 receptor acts to suppress immune cell cytokine production by inhibiting NFκB signalling, and genetic knockout of the CB2 receptor was found to produce earlier onset while worsening behavioural deficits in an HD mouse model (Palazuelos et al., 2009). Conversely, the administration of a CB2 agonist ameliorated motor deficits and CNS inflammation, in addition to extending the lifespan of HD mice (Bouchard et al., 2012). Interestingly, this effect was found to be ablated by the administration of a peripherally-restricted antagonist, suggesting that the improvements in disease phenotype were largely due to peripheral anti-inflammatory effects. Consistent with this hypothesis, the administration of an anti-inflammatory KMO inhibitor that does not cross the blood-brain barrier was found to extend life span, prevent synaptic loss and reduce microglial activation in HD mice (Zwilling et al., 2011). A further study found that inhibition of soluble TNFα is therapeutic in HD mice (Hsiao et al., 2014), while bone marrow transplantation also offers modest benefits (Kwan et al., 2012a). These studies demonstrate that abnormal peripheral inflammatory processes have a disease-modifying effect on the CNS.

1.7.3 Mechanisms of immune dysfunction

As the study of peripheral immunity in HD is a relatively recent development, the majority of studies to date have focused on characterising phenotypic abnormalities at the expense of obtaining mechanistic insight (Träger et al., 2014; Kwan et al., 2012b). There has been some progress in uncovering the mechanisms responsible, with gene expression profiling revealing a range of transcriptional changes in HD blood cells (Borovecki et al., 2005; Runne et

al., 2007; Mastrokolias et al., 2015). However, these studies have largely been done on heterogeneous cell populations and have rarely been validated between studies.

Mutant HTT has been shown to have a profound effect on NFκB signalling via a direct interaction with IKK (Khoshnan et al., 2004). HD myeloid cells exhibit an abnormal NFκB signalling response to LPS, both in the magnitude of the initial response and in the time taken for activation to return to baseline (Träger et al., 2014). This effect is associated with their hyper-reactive cytokine phenotype (Fig. 1.10). However, it is unclear whether HD myeloid cells also display abnormal NFκB signalling in their basal, resting state. While some changes in unstimulated NFκB related gene expression have been demonstrated using polymerase chain reaction (PCR) arrays (Träger et al., 2014), the small number of genes studied and lack of available mechanistic data means it is not yet possible to draw any firm conclusions.

Furthermore, signalling downstream of the LPS receptor TLR4 is complex, and includes activation of numerous signalling pathways such as those involving the ERK and p38 MAPKs (Akira and Takeda, 2004). The involvement of these alternative signalling pathways in HD myeloid cell dysfunction is yet to be fully explored. One signalling mechanism which seems unlikely to be involved in mediating HD myeloid cell dysfunction is the JAK/STAT pathway, as a study found that JAK/STAT signalling is not significantly altered in human HD monocytes (Träger et al., 2013).

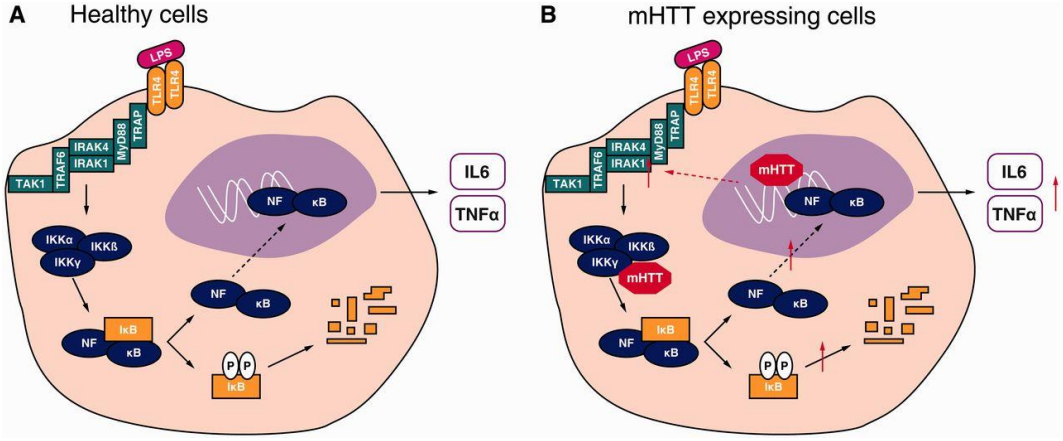

Figure 1.10. Mechanisms of immune dysfunction in HD. Mutant HTT has been shown to interact with IKK, a key regulator of the NFκB family of transcription factors. This leads to increased nuclear translocation of NFκB and upregulated expression of proinflammatory genes. Mutant HTT has also been shown to bind directly to DNA, and these mechanisms are associated by hyper-reactivity in HD myeloid cells. Reprinted from Brain, Vol. 137, "*HTT-lowering reverses Huntington's disease immune dysfunction caused by NFκB pathway dysregulation*", 819-833, Träger et al., ©2014, with permission from Oxford University Press.

One of the key outstanding questions surrounding HD myeloid cell dysfunction centres around whether these cells are only abnormal in response to stimulation, or if they are also abnormal in their basal, resting state. Experiments on an HD murine microglial cell line found evidence of increased proinflammatory gene expression in the absence of stimulation (Crotti et al., 2014). This is likely mediated by a 'priming' effect of mHTT, whereby basal dysfunction leads to an exaggerated inflammatory response when a stimulus is encountered. This effect was found to be mediated by a cell-autonomous increase in the expression of myeloid lineage-determining factors such as PU.1. Perhaps surprisingly, the PU.1 effect was not replicated in patient monocytes (Crotti et al., 2014); this was suggested to be due to their different developmental origins. However, NFκB binding motifs

were also found to be enriched in the murine microglial cell line, suggesting there is at least some overlap with peripheral HD myeloid cells.

Regardless of the mechanisms involved, it remains to be seen if mHTT has a similar priming effect on peripheral myeloid cells; this is likely key to determining whether HD myeloid cells are also abnormal in their basal, resting state. This has important implications for targeting the peripheral immune system as a therapeutic for HD, as intrinsic pathology is more likely to be treatable without the need to time intervention to coincide with specific infective or inflammatory events.

1.8 Thesis aims

1. To carry out the allele-selective suppression of mHTT in primary human myeloid cells, using siRNA targeted to three SNPs in the *HTT* transcript.

2. To determine the effects of selectively suppressing wild-type and mHTT on the hyper-reactive cytokine phenotype of HD myeloid cells.

3. To characterise the whole transcriptome of unstimulated and stimulated HD monocytes, in order to determine whether HD myeloid cells are also abnormal in the resting state.

4. To identify intracellular signalling pathways that may be involved in mediating transcriptional dysregulation in HD myeloid cells.

5. To determine whether the frequencies of immune cell subsets are altered between HD and control peripheral blood.

6. To characterise the phenotype of human HD T lymphocytes, in order to determine whether HD immune dysfunction is universal or restricted to specific cell types.

2 Materials and methods

2.1 Materials

Primary human monocytes and monocyte-derived macrophages were cultured in Primaria™ cell culture plates and dishes (Thermo Fisher Scientific), while all other immune cell types were cultured in Corning Cell Culture plates (Sigma-Aldrich) unless stated otherwise. All other consumables used for tissue culture were bought from Thermo Fisher Scientific, including phosphate-buffered saline (PBS), RPMI 1640 media, foetal bovine serum (FBS), L-glutamine and penicillin/streptomycin. All laboratory chemicals were bought from Sigma-Aldrich unless stated otherwise. Recombinant granulocyte macrophage-colony stimulating factor (GM-CSF) and IFNγ were bought from R&D systems, while LPS was bought from Sigma-Aldrich. The same batch of LPS was used for all replicates within experiments to eliminate batch variability. All magnetic-activated cell sorting (MACS) components were bought from Miltenyi Biotec. Centrifuge tubes and 96-well plates for adenosine 5'-triphosphate (ATP) and protein assays were bought from Greiner Bio-One.

2.2 Human subjects

2.2.1 Subject recruitment and classification

All human experiments were performed in accordance with the Declaration of Helsinki and approved by the University College London (UCL)/UCL Hospitals Joint Research Ethics Committee (REC 03/N008). All subjects

provided informed written consent prior to sample donation. Blood samples were donated by genetically-diagnosed HD patients and age-matched control subjects, primarily recruited from the HD clinic at the National Hospital for Neurology and Neurosurgery, London. Additional blood samples were obtained through designated research study visits that were carried out at the Royal London Hospital for Integrated Medicine, or at Huntington's Disease Association meetings in the community. Where necessary, further control subjects were recruited from staff and students at the UCL Institute of Neurology, in accordance with the study's ethics approval.

The UHDRS (Huntington Study Group, 1996) was used to classify premanifest HD mutation carriers by the absence of diagnostic motor abnormalities. The UHDRS comprises motor, cognitive, behavioural and functional assessments, with patients being rated from 0 (normal) to 4 (severe dysfunction) for each category. Where motor abnormalities were present, manifest HD patients were classified by their TFC score (Shoulson, 1981). The TFC scale is used to assess the ability of a patient to perform everyday tasks, working on a reducing score ranging from 13 (normal) to 0 (severe disability). All manifest HD subjects who donated samples for the experiments presented in this thesis had a TFC of 13-3, corresponding to early (13-7) or moderate (6-3) stage disease. Potential subjects with inflammatory or infective conditions were excluded for all studies, as were subjects on immunomodulatory medications. Current smokers were also excluded for the RNA sequencing (RNA-Seq) experiments contained in Chapter 4, due to the profound effects of smoking on the monocyte transcriptome (Zeller et al., 2010).

2.2.2 SNP genotyping of human subjects

Genotyping of human HD subjects for the *HTT* SNPs rs362331 (exon 50), rs362273 (exon 57) and rs362307 (3'-UTR) was carried out using FlashTaq 2X Master Mix (Empirical Bioscience). Twenty-five µl FlashTaq 2X Master Mix, 2 µl 10 µM primers (final concentration 400 nM; Table 2.1) and 1-5 µl DNA template (total DNA < 250 ng) were combined and the reaction mix was made up to 50 µl with H_2O. The thermal cycling conditions for the PCR were as follows: 95 °C for 15 min, followed by thirty-five cycles of 95 °C for 30 s, 60 °C for 30 s and 72 °C for 30 s, followed by incubation at 72 °C for 5 min before quickly chilling on ice. 10 µl of the PCR reaction mix was then run on a 1.5 % agarose, 1X Tris-acetate-EDTA (TAE) gel at 100 V for 1 h to confirm the presence of a single specific band. The remaining 40 µl was sent for sequencing by GeneWiz, Inc. (South Plainfield, NJ) to determine SNP genotype. Separate PCR reactions were carried out in order to genotype each subject for the three SNPs of interest. Subjects who were heterozygous for at least one SNP were recruited for the allele-selective suppression experiments described in Chapter 3.

Table 2.1. Primers used for SNP genotyping of human subjects.

Primer		Sequence
rs362331	Forward	GGG CAT TCT GTG ACT CGG TA
	Reverse	GAT AGG AAC CCA CCG TTC AT
rs362273	Forward	AGT GAC AAA TCC CCA AGA CC
	Reverse	GAG CTT TTC TCC TGG GTG TG
rs362307	Forward	GCT CTG CTC GCT CTC CAG
	Reverse	GCA GAG ACA CGC ACG TTG

2.3 SNP linkage by circularization

2.3.1 Sample preparation

Heterozygous SNPs were linked to the wild-type and mutant *HTT* alleles using the SNP linkage by circularization (SLiC) technique (Fig. 2.1) (Liu et al., 2008). All PCR reactions in this protocol were carried out using TaKaRa LA *Taq* DNA Polymerase with GC Buffer (Clontech). RNA was extracted from peripheral blood mononuclear cell (PBMC) samples (Section 2.7.2) before cDNA was synthesised using the Transcriptor First Strand cDNA Synthesis Kit (Roche). One µg RNA was mixed with 2 µl of 10 µM Oligo(dT) 15 Primer (Promega), before the sample volume was made up to 13 µl with RNase-free H_2O and the sample was incubated at 65 °C for 15 min. The sample was then mixed with 4 µl 5X First Strand Buffer, 2 µl dNTPs (10 mM of each), 0.5 µl Protector RNase Inhibitor and 0.5 µl Transcriptor Reverse Transcriptase before incubating at 55 °C for 90 min. Synthesis of full-length *HTT* cDNA was confirmed by amplifying a section of exon 1 containing the expanded CAG repeat, using the primers Exon 1 Forward and Exon 1 Reverse (Table 2.2). One µl cDNA was mixed with 25 µl GC Buffer I, 2 µl of each 10 µM primer solution (final concentration 400 nM), 8 µl dNTPs, 0.5 µl LA *Taq* DNA Polymerase and 11.5 µl H_2O. The following thermal cycling conditions were used: 98 °C for 3 min followed by thirty-two cycles of 98 °C for 30 s, 55 °C for 30 s and 72 °C for 2 min, followed by 72 °C for 5 min.

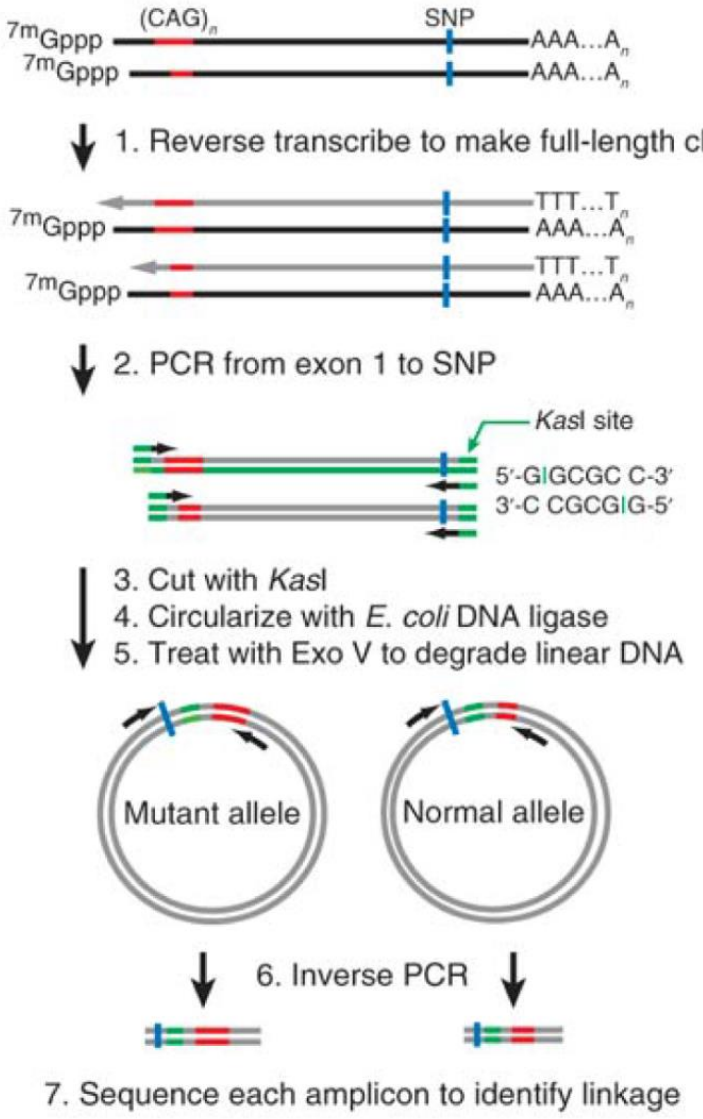

Figure 2.1. Summary of the SLiC protocol. Circularization of cDNA is used to bring the target SNP into close proximity with the CAG repeat in exon 1 of the *HTT* gene. This allows a relatively short section of cDNA to be sequenced to determine SNP linkage with the wild-type and mutant *HTT* alleles. Reprinted from Nature Methods, Vol. 5, "*Linking SNPs to CAG repeat length in Huntington's disease patients*", 951-953, Liu et al., ©2008, with permission from Nature Publishing Group.

Table 2.2. Primers used for SNP linkage by circularization.

Primer		Sequence
Exon 1	Forward	AAG GCC TTC GAG TCC CTC AAG TC
	Reverse	CGG CTG AGG CAG CAG CGG CT
	Long Forward	AGC TGA TGG GCG CCT TCG AGT CCC TCA AGT C
	Inverse Reverse	CGG CTG AGG CAG CAG CGG CT
Exon 50	Long Reverse	TGC ACT GCA GGC GCC TCC AGG ATG AAG TGC ACA C
	Inverse Forward	CAG ATC CCG CTG AGT CTG GAT CTC C

2.3.2 Long-range PCR

Long-range PCR was performed using the primers Exon 1 Long Forward and Exon 50 Long Reverse (Table 2.2); each contained a KasI restriction site. One µl cDNA was mixed with 25 µl GC Buffer I, 2 µl of each 10 µM primer solution (final concentration 400 nM), 8 µl dNTPs, 0.5 µl LA *Taq* DNA Polymerase and 11.5 µl H_2O. The following thermal cycling conditions were used: 98 °C for 3 min followed by thirty-eight cycles of 98 °C for 25 s, 55 °C for 15 s and 68 °C for 15 min, followed by 68 °C for 30 min. PCR products were analysed using a TAE 0.9 % agarose gel containing 0.3 µg/ml ethidium bromide at 150 V for 2 h. Bands of the expected molecular weight were excised and purified using the QIAquick® Gel Extraction Kit (QIAGEN).

To purify the RNA, the gel slice was weighed in a microcentrifuge tube before 300 µl Buffer QG was added for every 100 mg of gel. The sample was incubated at 50 °C for 10 min, vortexing every 2 min to dissolve the gel. If the solution was orange or violet in colour after dissolving, 10 µl of 3 M sodium acetate (pH 5.0) was added; this turned the mixture yellow. One gel volume

of 100 % isopropanol was then added before transferring the sample to a QIAquick® spin column and centrifuging at 17,900 ×g for 1 min to bind the DNA sample to the membrane. The membrane was first washed with 500 µl Buffer QG by centrifuging at 17,900 ×g for 1 min, before a further wash with 750 µl Buffer PE. The QIAquick® column was placed in a fresh 2 ml microcentrifuge tube before centrifuging at 17,900 ×g for 2 min to remove any residual wash buffer. The QIAquick® column was then transferred to a new 1.5 ml microcentrifuge tube and DNA was eluted by adding 30-50 µl Buffer EB to the membrane and centrifuging at 17,900 ×g for 1 min.

2.3.3 KasI digestion and DNA ligation

The gel-purified PCR products were digested using 10 U KasI in NEBuffer 2 (New England Biolabs) by incubating at 37°C for 2 h (reaction volume 40 µl). The enzyme was inactivated by incubating at 65 °C for 20 min, before NEBuffer 2 was exchanged for H_2O using the QIAquick® PCR Purification Kit. This was done by adding five volumes of Buffer PB to the reaction; if the solution was orange or violet in colour, 10 µl of 3 M sodium acetate (pH 5.0) was added to turn the mixture yellow. The sample was then transferred to a QIAquick® spin column and centrifuged at 17,900 ×g for 1 min to bind the DNA sample to the membrane. The membrane was washed with 750 µl Buffer PE by centrifuging at 17,900 ×g for 1 min, before the column was placed in a fresh 2 ml microcentrifuge tube and centrifuged at 17,900 ×g for 2 min to remove any residual wash buffer. The column was then transferred to a new 1.5 ml microcentrifuge tube before the DNA was eluted by adding 50 µl H_2O directly to the membrane and centrifuging at 17,900 ×g for 1 min.

The KasI-digested DNA was then circularised using *E. coli* DNA Ligase in 1X *E. coli* DNA Ligase Reaction Buffer (New England Biolabs) by incubating at 16 °C for 30 min (reaction volume 20 µl). The enzyme was inactivated by incubating at 65 °C for 20 min, before again exchanging the buffer for H_2O using the QIAquick® PCR Purification Kit as described above. The ligated product was then digested using Exonuclease V in NEBuffer 4 (New England Biolabs) with 50 µM ATP by incubating at 37 °C for 3 h (reaction volume 20 µl). The enzyme was inactivated by incubating at 65 °C for 20 min, before the product was used directly for inverse PCR.

2.3.4 Inverse PCR and sequencing

Inverse PCR to bring the SNP into close proximity with the CAG repeat was performed using the primers Exon 1 Inverse Reverse and Exon 50 Inverse Forward (Table 2.2). One µl circularised cDNA was mixed with 25 µl GC Buffer I, 2 µl of each 10 µM primer solution (final concentration 400 nM), 8 µl dNTPs, 0.5 µl LA *Taq* DNA Polymerase and 11.5 µl H_2O. The following thermal cycling conditions were used: 98 °C for 3 min followed by thirty-two cycles of 98 °C for 30 s, 55 °C for 30 s and 72 °C for 2 min, followed by 72 °C for 5 min. PCR products were analysed by gel electrophoresis using a TAE 1.8 % agarose gel containing 0.3 µg/ml ethidium bromide at 150 V for 80 min. Bands corresponding to the correct alleles were then excised using a scalpel and purified using the QIAquick® Gel Extraction Kit as described above. DNA was eluted in RNase-free water before being sent for sequencing by GeneWiz, Inc. (South Plainfield, NJ) to determine SNP heterozygosity using the relevant Inverse Forward primer.

2.4 Tissue culture

Culture of primary human immune cells was carried out in a Containment Level 2 laboratory using strict aseptic technique. A tissue culture hood with a laminar flow unit was used for all procedures, including preparation of culture media and reconstitution of reagents. All reagents and plasticware used for tissue culture were bought pre-sterilised and only opened once in the tissue culture hood. A water bath was used to warm media to 37 °C before use, while an incubator set to 37 °C with 5 % CO_2 was used to culture all cells.

2.4.1 Isolation of peripheral blood mononuclear cells

PBMCs were isolated from human peripheral blood samples by density centrifugation. Twenty-five ml of blood was carefully layered on top of 20 ml sterile 100 % Histopaque-1077 solution (Sigma-Aldrich) in a 50 ml centrifuge tube. Where larger blood samples were taken this process was repeated until the entire sample was layered on top of Histopaque-1077 in separate centrifuge tubes. The samples were centrifuged at 400 ×g for 30 min with no brake on deceleration. The middle PBMC layer was then transferred into a fresh 50 ml tube using a sterile Pasteur pipette (Biosigma), before washing with PBS by centrifuging at 400 ×g for 15 min. After washing, the cells were resuspended in sterile MACS buffer (PBS with 1 % bovine serum albumin (BSA) and 2 mM EDTA) and counted using a Neubauer counting chamber.

2.4.2 Magnetic-activated cell sorting

For experiments where a specific cell type was required, magnetic cell sorting was used to isolate the cells from among the PBMC population. After counting, the cells were pelleted at 400 ×g for 15 min before the supernatant was removed and the cells were resuspended in 10 µl microbeads (Miltenyi Biotec) and 40 µl MACS buffer per 10^7 cells. Anti-human CD14 microbeads were used to isolate monocytes, while anti-human CD4 microbeads were used to isolate helper T lymphocytes. After incubating for 15 min at 4 °C, the samples were centrifuged at 400 ×g for 5 min and resuspended in 500 µl MACS buffer. Magnetic cell sorting was carried out by placing MACS columns (Miltenyi Biotec) in a magnetic field and pre-washing with 500 µl MACS buffer, before adding each cell suspension to an individual column. Once the cell suspension had passed through, the columns were washed twice with 2 ml MACS buffer. Magnetically labelled cells were collected by removing the columns from the magnetic field and plunging 2 ml MACS buffer through the column twice using a plunger. Isolated monocytes and helper T lymphocytes were then counted using a Neubauer counting chamber before being seeded for downstream experiments. After sorting an aliquot of the isolated cell suspension was taken to check the purity of the sorted cell population by flow cytometry. On average, the sorted cell populations contained 85-95 % positively labelled cells (Fig. 2.2).

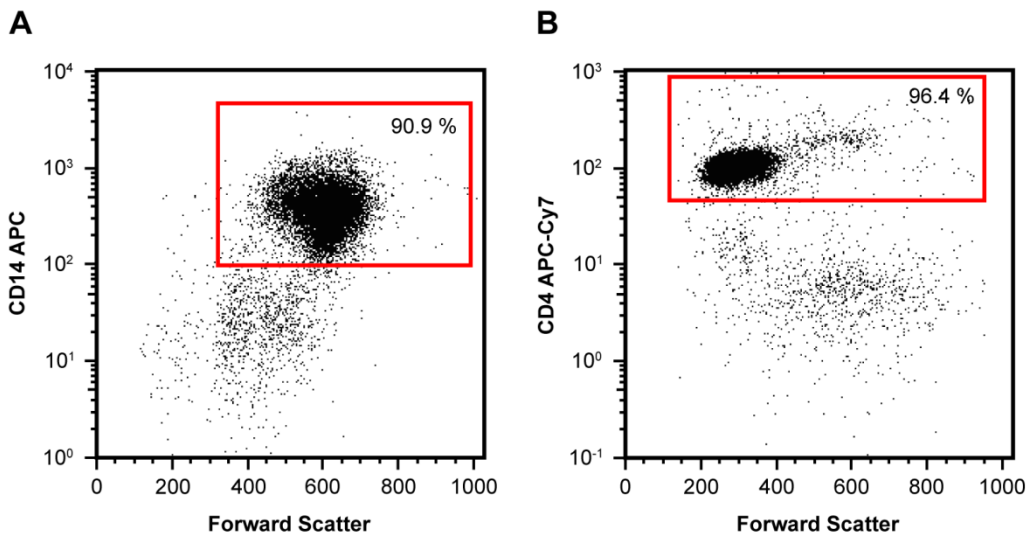

Figure 2.2. Analysis of MACS sorting by flow cytometry. (A) $CD14^+$ monocytes and (B) $CD4^+$ helper T lymphocytes were isolated from peripheral blood by MACS before the purity of the sorted cell populations was measured by flow cytometry. On average, the sorted cell populations contained 85-95 % positively labelled cells.

2.4.3 Culture of primary human immune cells

Primary human immune cells were cultured in R10 media (RPMI 1640 supplemented with 10 % FBS, 2 mM L-glutamine, 50 units/ml penicillin and 50 µg/ml streptomycin). Monocyte-derived macrophages were obtained by adding 20 ng/ml GM-CSF to the monocyte culture media for six days to induce differentiation prior to experimental use. The media was changed after three days to provide the cells with fresh media and GM-CSF for the final three days of the differentiation process. Monocytes treated with GM-CSF exhibited a macrophage phenotype after six days in culture.

2.4.4 Stimulation of primary human T lymphocytes

Stimulation of primary human T lymphocytes was carried out using plate-bound functional grade anti-human CD3 antibody (eBioscience). Five µg/ml antibody diluted in sterile PBS was added to each culture well the day before sample collection and incubated at 4 °C for 24 h. Immediately prior to seeding the wells were washed with PBS to remove any unbound antibody. Two µg/ml functional grade anti-human CD28 antibody (eBioscience) was also added to the culture media on seeding to provide appropriate co-stimulation. Alternative T lymphocyte stimulation using PHA-P was carried out by adding PHA-P (Sigma-Aldrich) directly to the culture media for a final concentration of 10 µg/ml when the cells were seeded.

2.5 HTT-lowering in primary human myeloid cells

2.5.1 Synthesis of glucan-encapsulated siRNA particles

β-1,3-D-glucan-encapsulated siRNA particles (GeRPs) were synthesised according to previously published methodology (Soto et al., 2012). *Saccharomyces cerevisiae* (100 g of SAF-Mannan; SAF Agri) was added to 1 L of 0.5 M NaOH and incubated at 80 °C for 1 h before the mixture was centrifuged at 5000 ×g for 20 min to collect the insoluble material containing the cell walls. The incubation and centrifugation steps were then repeated using this insoluble pellet, before washing three times each with 1 L H_2O, then 200 ml 100 % propan-2-ol, then 200 ml 100 % acetone. The slurry was dried at room temperature to produce 16.2 g of fine, off-white powder.

Loading of siRNA into 10^7 glucan particles was performed by mixing the appropriate siRNA (Dharmacon; Table 2.3) with 40 µl sterile saline (Sigma-Aldrich), 30 µl HEPES buffer (0.1 M, pH 7.5 in saline; Thermo Fisher Scientific) and 10 µl glucan particles (10^9 particles/ml in saline). This mixture was incubated for 2 h at room temperature in the dark. After incubation, 10 µl Endo-Porter (EP; diluted appropriately with saline; Gene Tools) was added and the mixture was incubated for 15 min at room temperature to trap the siRNA inside the glucan particles by complex formation (Tesz et al., 2011). The amount of siRNA and EP used for the loading reactions was varied depending on the concentration required in each GeRP. After loading, the GeRPs were added to single use aliquots and frozen at -80 °C. The loading reaction was scaled up proportionately if more GeRPs were required.

2.5.2 Transfection of primary human myeloid cell cultures

Primary human myeloid cells were isolated from peripheral blood samples by density centrifugation (Section 2.4.1) and MACS (Section 2.4.2), before seeding in Primaria™ plates and dishes at an experiment-dependent density. Monocytes were rested for 16 h after isolation before transfection with GeRP particles, while macrophages were transfected on day 3 of the differentiation protocol (when fresh GM-CSF was added by media change). GeRPs containing the appropriate siRNA were added to the cells at a 10:1 particle to cell ratio, before being removed after 24 h by a complete media change. Analysis of huntingtin mRNA and protein levels was carried out by harvesting the cells 72 h after GeRP treatment, while ATP assays (Section 2.6.1) took place 24 h after the GeRPs were added.

Table 2.3. siRNA sequences used in HTT-lowering experiments.

siRNA	Strand	Sequence
SCR	Guide	5'-pUUUCGAAGUACUCAGCGUGAG-3'
	Passenger	5'-CACGCUGAGUACUUCGAACUU-3'
Anti-total *HTT*	Guide	5'-pUUCAUCAGCUUUUCCAGGGUC-3'
	Passenger	5'-CCCUGGAAAAGCUGAUGACGG-3'
rs362331 anti-C	Guide	5'-pUUACACAGUGGAUGAGGGAGC-3'
	Passenger	5'-UCCCUCAUCCACUGUGUACAC-3'
rs362331 anti-U	Guide	5'-pGUACACAGUAGAUGAGGGAGC-3'
	Passenger	5'-UCCCUCAUCUACUGUGUAAAC-3'
rs362273 anti-A	Guide	5'-pUUUGAUUUGUAGCAGCAGCUU-3'
	Passenger	5'-GCUGCUGCUACAAAUCAACCC-3'
rs362273 anti-G	Guide	5'-pUUUGCUCUGCAGCAGCAGCUU-3'
	Passenger	5'-GCUGCUGCUGCAGAGCAACCC-3'
rs362307 anti-U (1)	Guide	5'-pCACACGGGCACAGACUUCCAA-3'
	Passenger	5'-GGAAGUCUGCGCCCGUGUUCC-3'
rs362307 anti-U (2)	Guide	5'-pCACAAUGGCACAGACUUCCAA-3'
	Passenger	5'-GGAAGUCUGUGCCAUUGUUCC-3'

2.6 Analysis of immune cell function

2.6.1 ATP assays

Cellular ATP levels were analysed using the CellTiter-Glo® Luminescent Cell Viability Assay (Promega). Prior to use the CellTiter-Glo® Buffer and Substrate were thawed and equilibrated to room temperature. After the Cell-Titer-Glo® Buffer had thawed it was transferred into the Substrate bottle to reconstitute the lyophilised enzyme/substrate mixture; this forms the CellTiter-Glo® Reagent, which was mixed to obtain a homogenous solution. Cells populations to be analysed were cultured at 1×10^5 cells per well in 96-

well plates; experimental cultures were changed to 100 µl fresh R10 media prior to analysis, while control wells containing media without cells were also prepared to obtain a measurement for background luminescence. After culture the plate and its contents were equilibrated at room temperature for 30 min, before 100 µl CellTiter-Glo® Reagent was added to each well. The plate was placed on a shaker for 2 min to induce cell lysis, after which it was incubated at room temperature for 10 min to stabilise the luminescent signal. The contents of the plate were then transferred to a fresh opaque-walled white 96-well plate (Greiner Bio-One), before luminescence was measured using an Infinite® 200 PRO microplate reader (Tecan). The results were analysed by setting one condition as standard and converting the sample readings to a percentage of its ATP levels using Excel (Microsoft).

2.6.2 Myeloid cell cytokine profiling

Primary human monocytes were isolated from peripheral blood samples and seeded at 1×10^5 cells per well in 96-well plates, before being differentiated into macrophages (Section 2.4.3) and treated with GeRPs (Section 2.5.2). On day 6 of the differentiation protocol (72 hours after GeRP treatment), stimulation was carried out by media changing to fresh media containing 2 µg/ml LPS and 10 ng/ml IFNγ. After 24 h the supernatants were collected and frozen at -80 °C, before the cells were washed once with sterile PBS and lysed in 60 µl radioimmunoprecipitation assay (RIPA) buffer (Section 2.11.1) to provide protein values for cytokine normalisation using bicinchoninic acid (BCA) assays (Section 2.11.2). The supernatants were then analysed using multiplex Meso Scale Discovery (MSD) cytokine assays (Section 2.12.2).

2.6.3 T lymphocyte cytokine profiling

Primary human helper T lymphocytes were isolated from peripheral blood samples and seeded at 1 × 10^5 cells per well in 96 well plates pre-treated with anti-human CD3 functional grade antibody (Section 2.4.4). Unstimulated samples were collected by seeding T lymphocytes in wells that were not pre-treated with antibody. After 48 h the supernatants were collected and frozen at -80 °C, before the cells were washed once with sterile PBS and lysed in 60 µl RIPA buffer (Section 2.11.1) to provide protein values for cytokine normalisation using BCA assays (Section 2.11.2). The supernatants were analysed using multiplex MSD cytokine assays (Section 2.12.2).

2.6.4 T lymphocyte proliferation assays

T lymphocyte proliferation assays were carried out using the intracellular dye carboxyfluorescein succinimidyl ester (CFSE). CFSE binds covalently to intracellular molecules, producing a highly stable fluorescent signal that is split equally between the daughter cells produced when a cell divides (Quah et al., 2007). This allows the profiling of cell division as a sequential halving of fluorescence intensity on flow cytometry, up to a maximum of approximately seven divisions. PBMCs were isolated from peripheral blood samples (Section 2.4.1), before being counted using a Neubauer counting chamber and resuspended at 1 × 10^7 cells per ml of PBS with 5 % FBS to buffer against the toxic effects of CFSE. CFSE (eBioscience) was added to the cell suspension for a final concentration of 5 µM, before the sample was mixed vigorously and incubated for 10 min at room temperature in the dark.

Labelling was stopped by adding four volumes of cold RPMI media with 10 % FBS and incubating for 5 min on ice.

After labelling the PBMCs were seeded at 5×10^5 cells per well in 48 well plates, and were either left unstimulated, stimulated with anti-human CD3 and anti-human CD28 antibodies, or stimulated with PHA-P (Section 2.4.4). Unstained cells were also seeded to provide appropriate compensation controls for flow cytometry. Cell cultures were harvested after 72, 96 and 120 h and transferred to 1.5 ml Eppendorf tubes. The cells were then washed twice with PBS by centrifuging at 400 ×g for 5 min before resuspending in 1 ml PBS containing 1 µl Fixable Viability Dye 660 (eBioscience) to label non-viable cells. This suspension was vortexed briefly before incubating for 30 min at 4 °C in the dark. The cells were then washed twice with FACS buffer (PBS with 1 % BSA and 0.02 % sodium azide) before being fixed with 200 µl PBS containing 4 % paraformaldehyde (PFA) for 10 min, stained with antibodies to the appropriate cell surface markers (Section 2.13.1) and analysed by flow cytometry (Section 2.13.3).

2.7 Quantitative polymerase chain reaction

2.7.1 RNeasy Mini Kit RNA isolation

RNA for all experiments except SLiC (Section 2.3) was isolated using the RNeasy Mini Kit (QIAGEN). Cells were lysed in Buffer RLT (350 µl for $< 5 \times 10^6$ cells, 600 µl for $\leq 1 \times 10^7$ cells) before an equal volume of 70 % ethanol (diluted in ddH_2O) was added to precipitate the RNA. Samples were then added to RNeasy spin columns and centrifuged at 8,000 ×g for 15 s to bind

the RNA to the column membrane. The columns were washed once with 350 µl Buffer RW1 by centrifuging at 8,000 ×g for 15 s, before RNase-free DNase solution (QIAGEN) was made up by adding 70 µl Buffer RDD to 10 µl DNase I stock solution (reconstituted in ddH_2O). 80 µl of this solution was added directly to the column membrane and the samples were incubated for 15 min at room temperature to digest genomic DNA. The columns were then washed again with 350 µl Buffer RW1, before being washed twice with 500 µl Buffer RPE by centrifuging at 8,000 ×g for 15 s and 2 min respectively. The columns were then dried by centrifuging at 8,000 ×g for 1 min, before the RNA was eluted by adding 15-50 µl RNase-free water directly to the column membrane and centrifuging at 8,000 ×g for 1 min. If higher concentrations of RNA were required, the RNA elution was re-added to the column membrane and centrifuged again. The RNA concentration in each sample was measured using an ND-1000 Spectrophotometer (NanoDrop). RNA was stored at -80 °C.

2.7.2 TRIzol® RNA isolation

RNA for SLiC (Section 2.3) was isolated using the TRIzol® (Thermo Fisher Scientific) method. PBMC pellets were isolated from peripheral blood samples (Section 2.4.1) and lysed in 1 ml TRIzol® Reagent by vortexing briefly. The sample was incubated at room temperature for 10 min before transferring to a microcentrifuge tube and adding 200 µl chloroform. The tube was then shaken vigorously by hand for 15 s before incubating at room temperature for 2 min and centrifuging at 12,000 ×g for 15 min at 4 °C. After centrifuging, the upper aqueous phase of the sample was removed by

angling the tube to 45 ° and pipetting the solution out. The aqueous phase was then added to a fresh microcentrifuge tube and mixed with 0.5 ml 100 % isopropanol per 1 ml TRIzol® Reagent used for cell lysis. After incubating at room temperature for 10 min this mixture was centrifuged at 12,000 ×g for 10 min at 4 °C; the supernatant was then removed, leaving only the RNA pellet. The pellet was washed with 1 ml 75 % ethanol before vortexing briefly, centrifuging at 7,500 ×g for 5 min and discarding the wash. After washing, the microcentrifuge tube was left with the lid open for 5-10 min to allow the pellet to dry. The pellet was then resuspended in 20-50 µl Tris-EDTA (TE) Buffer by pipetting up and down and incubating in a heat block set at 55 °C for 10-15 min. Finally, the RNA concentration was measured using an ND-1000 Spectrophotometer. RNA was stored at -80 °C.

2.7.3 RNA quality control

Confirmation of RNA integrity prior to RNA-Seq (Section 2.8) and PCR arrays (Section 2.9) was carried out using the 2100 Bioanalyzer system with the RNA 6000 Nano Kit (Agilent). This uses electrophoresis to analyse the integrity of the ribosomal S18 and S28 RNA molecules; samples with non-degraded RNA will give a separate, clear band for each RNA molecule (Fig. 2.3). This effect is quantified using the RNA Integrity Number (RIN).

RNA analysis was carried out by adding 550 µl RNA 6000 Nano Gel Matrix (Agilent) to a Safe-Lock Eppendorf Tube with a Spin Filter and centrifuging at 1,500 ×g for 10 min. After centrifuging, 1 µl of RNA Nano Dye Concentrate was added to 65 µl of the filtered gel. This mixture was vortexed thoroughly before centrifuging at 13,000 ×g for 10 min. An RNA 6000 Nano chip was

then placed on the chip priming station of the 2100 Bioanalyzer system and 9 µl of the gel-dye mix was added to well G of the chip. The system was pressurised using a syringe, before waiting for exactly 30 s and releasing the pressure; 9 µl of gel-dye mix was then added to the two wells directly above well G. Next, 5 µl of RNA 6000 Nano Marker was added to the well labelled with the ladder marker, in addition to all twelve of the sample wells. As each well of the chip is read separately, the RNA 6000 Nano Marker allows all of the electrophoresis reactions to be aligned correctly. Finally, 1 µl of sample was added to each of the twelve sample wells, while 1 µl of Agilent RNA 6000 Ladder was added to the well with the ladder marker. The chip was mixed by vortexing for 1 min before running on the Agilent 2100 Bioanalyzer system with 2100 Expert Software (Agilent). Each trace was inspected individually to confirm RNA integrity prior to use in downstream applications.

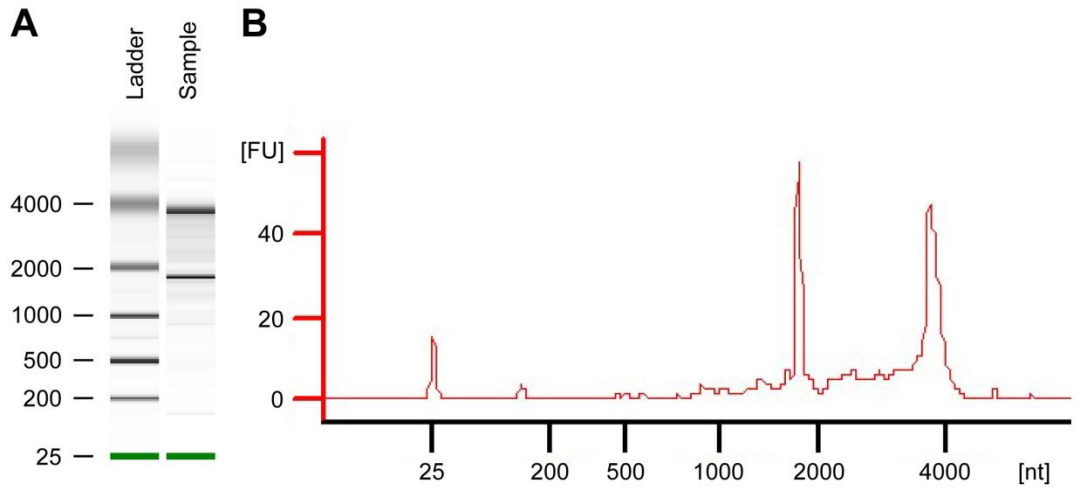

Figure 2.3. Example of RNA analysis using the Bioanalyzer system. RNA integrity was assessed using the 2100 Bioanalyzer system with the RNA 6000 Nano Kit. High quality RNA produces (A) two clear bands on the electrophoresis gel and (B) two clear peaks on flow cytometry for each of the ribosomal S18 and S28 RNA molecules. FU = fluorescent units. Nt = nucleotides.

2.7.4 Reverse transcription of RNA to cDNA

SuperScript II Reverse Transcriptase (Thermo Fisher Scientific) was used to reverse transcribe RNA to cDNA. 100-200 ng RNA was diluted in 10 µl RNase-free water before 1 µl random primers (3 µg/µl) and 1 µl dNTPs (10 mM of each) (both Thermo Fisher Scientific) were added. The mix was heated to 65 °C for 5 min and briefly incubated on ice before adding 4 µl 5X First-Strand Buffer, 2 µl 0.1 M DTT and 1 µl RNaseOUT Recombinant Ribonuclease Inhibitor (40 units/µl) (all Thermo Fisher Scientific). One µl (200 units) SuperScript II Reverse Transcriptase was then added after incubating at room temperature for 2 min. Reverse transcription was carried out by incubating the reaction mix at 25 °C for 10 min, followed by 42 °C for 50 min. The reaction was terminated by incubating at 70 °C for 15 min, before cDNA was diluted to a concentration of 5 ng/µl and stored at -20 °C.

2.7.5 SYBR® Green quantitative PCR

SYBR® Green PCR Master Mix (Thermo Fisher Scientific) was used for quantitative PCR (qPCR) analysis of mRNA expression. First, 12.5 µl SYBR® Green PCR Master Mix, 10.75 µl H_2O, 0.75 µl of 10 µM primers solution (final concentration 300 nM; Table 2.4) and 1 µl (5 ng) cDNA were mixed in MicroAmp Fast Optical 96-Well Reaction Plates (Thermo Fisher Scientific) to give a final reaction volume of 25 µl. The plates were covered with MicroAmp Optical Adhesive Film (Thermo Fisher Scientific) and centrifuged at 300 ×g for 10 s to collect the reaction mix at the bottom of each well, before being run on a 7500 Fast Real-Time PCR System (Thermo Fisher Scientific) using 7500 software. The following PCR cycling conditions

were used: 95 °C for 10 min, followed by forty cycles of 95 °C for 15 s and 60 °C for 1 min. A melting curve of 60-95 °C was also run when new primers were tested to exclude the possibility of primer-dimer formation. All reactions were run in either duplicate or triplicate and outliers were excluded were appropriate. Endogenous reference genes (*ACTB*, *B2M* and *GAPDH*) were also run in order to normalise the cycle threshold (Ct) values of genes of interest between samples.

Table 2.4. Primers used for SYBR® green qPCR experiments.

Primer		Sequence
ACTB	Forward	AAG GCC AAC CGT GAA AAG AT
	Reverse	GTG GTA CGA CCA GAG GCA TAC
B2M	Forward	GAA TTC ACC CCC ACT GAA AA
	Reverse	CCT CCA TGA TGC TGC TTA CA
CSF2	Forward	GCG TCT CCT GAA CCT GAG TA
	Reverse	CCT GGA GGT CAA ACA TTT CTG A
GAPDH	Forward	AAC AGC GAC ACC CAC TCC T
	Reverse	CAT ACC AGG AAA TGA GCT TGA CAA
HTT	Forward	AGT GAT TGT TGC TAT GGA GCG G
	Reverse	GCT GCT GGT TGG ACA GAA ACT C
IL19	Forward	TCT ACG TGG ACA GGG TGT TC
	Reverse	CTG ACA TTG CCG CAG AGT TT
IL23A	Forward	CCA AGG ACT CAG GGA CAA CA
	Reverse	CCG ATC CTA GCA GCT TCT CA
IL6	Forward	TAC CCC CAG GAG AAG ATT CC
	Reverse	AGT GCC TCT TTG CTG CTT TC
TYRO3	Forward	CCC CTT TAA CCT ACC CCT CC
	Reverse	CAG GTC TCG GTG GAT GAA GT
VEGFA	Forward	CAG ATT ATG CGG ATC AAA CCT C
	Reverse	CCT TTC CCT TTC CTC GAA CTG

2.7.6 TaqMan® quantitative PCR

TaqMan® Gene Expression Master Mix (Thermo Fisher Scientific) was used for the analysis of allele-specific *HTT* expression. Custom TaqMan® probes (Thermo Fisher Scientific) were designed for each allele of the *HTT* SNPs rs362331 (exon 50), rs362273 (exon 57) and rs362307 (3'-UTR). First, 12.5 µl TaqMan® Gene Expression Master Mix, 0.75 µl of 5 µM probe solution for each SNP allele (final concentration 150 nM; Table 2.5), 1.25 µl of 10 µM primers solution (final concentration 500 nM; Table 2.6), 8.75 µl H_20 and 1 µl (5 ng) cDNA were mixed in MicroAmp Fast Optical 96-Well Reaction Plates (Thermo Fisher Scientific) to give a final reaction volume of 25 µl. The plates were covered with MicroAmp Optical Adhesive Film (Thermo Fisher Scientific) and centrifuged at 300 ×g for 10 s to collect the reaction mix at the bottom of each well, before being run on a 7500 Fast Real-Time PCR System (Thermo Fisher Scientific) using 7500 software. The following PCR cycling conditions were used: 50 °C for 2 min and 95 °C for 10 min followed by forty cycles of 95 °C for 15 s and either 65 °C (for rs362331 and rs362273) or 67.5 °C (for rs362307) for 1 min. All reactions were run in either duplicate or triplicate and outliers were excluded where appropriate. Each sample was also analysed using Human ACTB (Beta Actin) Endogenous Control (FAM/MGB probe, non-primer limited) and Human GAPD (GAPDH) Endogenous Control (FAM/MGB probe, non-primer limited) mixes (Thermo Fisher Scientific) in order to normalise the Ct values of the SNP alleles between samples.

Table 2.5. Probes used for TaqMan® qPCR experiments.

Probe	5'-Dye	3'-Quencher	Sequence
rs362331 C	6-FAM	MGBNFQ	TCC CTC ATC CAC TGT GTG C
rs362331 T	6-FAM	MGBNFQ	TCC CTC ATC TAC TGT GTG C
rs362331 T	VIC	MGBNFQ	TCC CTC ATC TAC TGT GTG C
rs362273 A	6-FAM	MGBNFQ	GCT GCT GCT ACA GAT CAA C
rs362273 G	VIC	MGBNFQ	GCT GCT GCT GCA GAT CAA C
rs362307 C	6-FAM	MGBNFQ	TGG AAG TCT GCG CCC TTG TG
rs362307 T	VIC	MGBNFQ	TGG AAG TCT GTG CCC TTG TG

Table 2.6. Primers used for TaqMan® qPCR experiments.

Primer		Sequence
rs362331	Forward	CTG GAG CGT GGT CTC CTC CAC A
	Reverse	GTG TGT TTG GAT CTA CTT CCT CC
rs362273	Forward	CTA CTA CAG GTG CCC TCA TCA G
	Reverse	GTG ACG AAG GTG CAG GGG CG TC
rs362307	Forward	ATG GTG GGA GAG ACT GTG AGG C
	Reverse	ATG GCA GAG ACA CGC ACG TTG C

2.7.7 Analysis of quantitative PCR data

Quantitative PCR data was analysed using 7500 software. The 7500 software was used to determine the baseline and Ct values of each sample, before the Ct value of each gene of interest was normalised by subtracting the mean Ct value of the reference genes for the same sample. Relative gene expression was then calculated by setting one condition as standard and using the following formula:

Relative gene expression = $2^{\text{delta Ct (sample 1 – sample 2)}}$

Delta Ct is defined as the expression of the gene of interest, normalised to that of the mean of the reference genes. When analysing allele-specific qPCR each SNP allele was analysed independently.

2.8 RNA sequencing

Primary human monocytes were isolated from peripheral blood and seeded at 5.0 × 10^6 cells per dish in two 60 mm Primaria™ dishes (Section 2.4). After resting for 16 h the cells were either left unstimulated or stimulated with 2 µg/ml LPS and 10 ng/ml IFNγ. Stimulation was carried out for 4 h, as this has previously been shown to be the peak time point for TLR4-mediated gene activation following LPS stimulation (Aung et al., 2006; Yamamoto et al., 2004). The cells were then harvested before RNA was extracted (Section 2.7.1) and its integrity was assessed by 2100 Bioanalyzer (Section 2.7.3); only samples with non-degraded RNA were used for sequencing.

Sequencing of RNA samples was performed by deCODE Genetics, Iceland. Preparation of indexed cDNA sequencing libraries was carried out using the TruSeq™ poly-A mRNA method (Illumina). Briefly, poly-A mRNA transcripts were captured from total RNA using poly-T beads, before cDNA was generated using random hexamer priming. Paired-end sequencing (2 × 100 cycles) of indexed cDNA libraries was then carried out on a HiSeq 2500 Sequencing System (Illumina), generating at least 50 million reads (101 base pairs) per sample. Sequencing was performed using v4 SBS and Cluster Kits (Illumina). One sample failed the library generation step and was excluded from the study. After sequencing the indexed samples were demultiplexed before generation of FASTQ files for analysis. Raw data files are available

from the European Nucleotide Archive (http://www.ebi.ac.uk/ena) under the study accession number PRJEB12995.

2.9 Human T_h1 & T_h2 Responses RT^2 PCR Arrays

2.9.1 Sample collection

PCR arrays were carried out on primary human $CD4^+$ helper T lymphocytes that were isolated from peripheral blood samples and seeded at 3×10^6 cells per well in Primaria™ 6 well plates (Section 2.4). Cells were either left unstimulated or stimulated with functional grade anti-human CD3 antibodies for 8 h (Section 2.4.4), before the cells were harvested and RNA was extracted (Section 2.7.1). RNA integrity was assessed using the 2100 Bioanalyser (Section 2.7.3); only samples with non-degraded RNA were used for PCR arrays.

2.9.2 Reverse transcription

Reverse transcription for PCR arrays was carried out using the RT^2 First Strand Kit (QIAGEN). Six hundred ng RNA was diluted in 8 µl RNase-free water, before 2 µl GE buffer was added and the mixture was incubated at 42 °C for 5 min. After incubation the reaction mix was quickly chilled on ice before 4 µl 5X Buffer BC3, 3 µl RNase-free water, 2 µl RE3 Reverse Transcriptase Mix and 1 µl Control P2 were added. The mixture was then incubated at 42 °C for 15 min before the reaction was terminated by incubating at 95 °C for 5 min. Ninety-one µl RNase-free water was then added to the cDNA solution, which was frozen at -20 °C prior to analysis.

2.9.3 PCR arrays

The PCR reaction mix was made by adding 1350 µl 2X RT^2 SYBR® Green PCR Master Mix (QIAGEN) and 1248 µl RNase-free water to each cDNA sample and mixing thoroughly. The reaction mix was then transferred to a sterile reservoir and 25 µl was added to each well of the primer coated PCR array plates using a multichannel pipette. Reverse pipetting was used to ensure a consistent volume of reaction mix was added to each well. The plates were covered with MicroAmp Optical Adhesive Film (Thermo Fisher Scientific) before centrifuging at 300 ×g for 10 s to collect the reaction mix at the bottom of each well. The plates were then run on a 7500 Fast Real-Time PCR System (Thermo Fisher Scientific) using 7500 software. The following PCR cycling conditions were used: 95 °C for 10 min followed by forty cycles of 95 °C for 15 s and 60 °C for 1 min. Each plate was also analysed using a melting curve of 60-95 °C to exclude primer-dimer formation.

The Human T_h1 & T_h2 Responses RT^2 Profiler PCR Array plate (QIAGEN) contained wells for eighty-four genes of interest and five reference genes (*ACTB*, *B2M*, *GAPDH*, *HRPT1* and *RPLP0*), in addition to seven quality control (QC) wells (one for human genomic DNA contamination, three reverse transcription controls and three positive PCR controls). Plates were excluded from the final analysis if the Ct value for genomic DNA was < 35.

2.9.4 Data analysis

PCR array data was analysed using 7500 software. Prior to analysis a consistent threshold value was set for each gene to ensure consistency between plates, before the Ct and baseline values for each sample were

determined by the 7500 software. Data analysis was carried out using the online data analysis tool provided by the manufacturer (http://pcrdataanalysis.sabiosciences.com/pcr/arrayanalysis.php). This was done to calculate relative gene expression by setting one condition as standard and using the following formula:

Relative gene expression = $2^{\text{delta Ct (sample 1 – sample 2)}}$

Delta Ct is defined as the expression of the gene of interest, normalised to that of the mean of the five reference genes. Genes with an average Ct value of > 35 were excluded from the final results. Fold changes were then calculated by dividing the mean relative gene expression of the HD samples by the mean relative gene expression of the control samples.

2.10 Bioinformatic analysis

2.10.1 RNA-Seq data processing and expression analysis

Data QC was performed using the java program RNA-SeQC (DeLuca et al., 2012). Metrics including mapping rate, concordance mapping rate, uniqueness rate and rRNA rate were determined to confirm that they were within acceptable parameters. Four samples failed QC and were removed from further analysis. After QC the remaining samples were aligned using TopHat2 software (Kim et al., 2013), before the read counts were summarised using HTSeq (keeping any read duplicates). Differential expression analysis was then carried out using the R package DESeq2 (Love et al., 2014). Outlier counts were removed using a Cooks distance cut-off of 5 in DESeq2 packages. Gender was also included as a covariate in the

analysis. Differential splicing analysis was carried out on the aligned datasets using the R package Ballgown (Frazee et al., 2015); this was done to analyse differential exon, intron and transcript expression.

2.10.2 Gene Set Enrichment Analysis

Enrichment of differential expression among functional gene sets corresponding to biological hypotheses (pathways) was tested using the Gene Set Enrichment Analysis (GSEA) method (Subramanian et al., 2005). Rather than defining a list of significant genes, GSEA ranks all genes included in a sequencing experiment in order of their differential expression statistic, before testing whether the genes in a particular gene set or pathway have a higher rank overall than would be expected by chance (i.e. whether a functional gene set is significantly enriched in the dataset). The analysis is weighted by the differential expression statistic, thus giving more weight to more significant genes. Significance of enrichment was obtained by randomly permuting gene-wide association statistics among genes; this is quantified by the normalised enrichment score (NES). One-sided *p*-values were calculated separately for differential upregulation and downregulation of expression in HD, and these were then converted into the corresponding chi-square statistic for use in the GSEA analysis. To avoid making *a priori* assumptions, a large pathway set comprising Gene Ontology (GO) (Harris et al., 2004), Kyoto Encyclopedia of Genes and Genomes (KEGG) (Kanehisa et al., 2012), Mouse Genome Informatics (MGI) (Bult et al., 2008), Reactome (Croft et al., 2014), PANTHER v8.1 (Mi et al., 2013), Biocarta and NCIpathway interaction database (Schaefer et al., 2009) pathways was

used. This resulted in a total of 14,243 functional gene sets, many with overlapping members, containing between 3 and 500 genes. To correct for multiple testing, the GSEA *p*-values were converted into *q*-values (Storey and Tibshirani, 2003), which can be interpreted as the minimum false discovery rate (FDR) at which that *q*-value would be counted as significant.

2.10.3 Upstream regulator analysis

Upstream regulator analysis was carried out using Ingenuity Pathway Analysis® (IPA®) software (QIAGEN). IPA® is used to identify potential upstream regulators of transcriptional change in an expression dataset; an upstream regulator is defined as any molecule that has a downstream effect on gene expression. This analysis is quantified using the *p*-value of overlap and activation z-score statistics. The p-value of overlap statistic uses Fisher's exact test to determine whether there is statistically significant overlap between gene expression changes in a dataset and the genes that are affected by a specific transcriptional regulator; significance is attributed to regulators with a *p*-value of overlap of < 0.01. However, this does not take the direction of the expression changes into account (i.e. whether the relevant genes are upregulated or downregulated), so the activation z-score is used to predict whether potential upstream regulators are likely to be abnormally activated or inhibited in the dataset. An activation z-score of ≥ 2 or ≤ -2 is generally considered to be significant. Further information on the activation z-score statistic is available at http://www.ingenuity.com/. A p-value cut-off of 0.01 was used to determine which differentially expressed genes from the RNA-Seq dataset were included in the analysis.

2.11 Protein analysis

2.11.1 Protein isolation

RIPA buffer (25 mM Tris-HCl (pH 7.6), 150 mM NaCl, 1 % NP-40, 1 % sodium deoxycholate, 0.1 % sodium dodecyl sulfate (SDS)) containing one cOmplete™, Mini, EDTA-free Protease Inhibitor Cocktail Tablet (Roche) per 10 ml buffer was used to lyse cells for protein isolation. The culture media was removed and the cells were washed once with sterile PBS to remove exogenous protein, before adding the appropriate volume of RIPA buffer directly to the culture well. Lysis was then induced by shaking the cell culture plate for 10 min at 4 °C. Lysates were stored at -80 °C.

2.11.2 BCA protein assay

The Pierce BCA Protein Assay Kit (Thermo Fisher Scientific) was used to quantify the amount of protein in a sample. Prior to analysis the cell lysates were diluted appropriately with RIPA buffer depending on total cell number, while BSA standards were diluted in RIPA buffer according to the manufacturer's instructions. Twenty-five µl of each standard and lysate was added to separate wells of a clear 96-well plate (Greiner Bio-One), before 200 µl of working solution (made up of a fifty to one ratio of BCA Reagent A and BCA Reagent B) was added to each well. Each sample was analysed in duplicate. The plate was then incubated at 37 °C for 30 min, after which a Tecan Sunrise Reader (Tecan) was used to measure the absorbance signal intensity at 562 nm using XFluor™ software (Tecan). Analysis was carried out by using the BSA standards to create a standard curve for comparison.

2.11.3 Time-resolved Förster resonance energy transfer assay

Cellular levels of total and mHTT protein were analysed using a Time-resolved Förster resonance energy transfer (TR-FRET) assay. To perform the assay, cells were lysed in PBS with 1 % Triton X-100 and a cOmplete™, Mini, EDTA-free Protease Inhibitor Cocktail Tablet; 100 µl lysis buffer was used per 10^6 cells. Next, 5 µl of lysate was added to a white 384-well microtiter plate (Greiner) and mixed with 1 µl detection buffer (50 mM NaH_2PO_4, 400 mM NaF, 0.1 % BSA and 0.05 % Tween with antibody). Soluble total HTT was detected using 1 ng 2B7-Tb and 10 ng 2166-Alexa Fluor® 488 antibodies, while soluble mHTT was detected using 0.25 ng 2B7-Tb and 20 ng MW1-D2 antibodies. The microtiter plate was then centrifuged at 1,000 ×g for 30 s before incubating for 1 h at room temperature. The plate was analysed using an EnVision® Mulitilabel Plate Reader (PerkinElmer). The donor Tb fluorophore (CisBio) was excited at 320nm before a time delay of 100 ms, after which the donor Tb and acceptor Alexa Fluor® 488 (Thermo Fisher Scientific) or D2 (CisBio) emission signals were read at 620, 520 or 665 nm respectively. Total and mHTT levels corresponded to the ratios of the 520/620 and 665/620 nm emission spectra measured by the plate reader. Total and mHTT protein levels are presented as a percentage of the signal intensity measured over the background signal generated by the lysis buffer; protein levels were normalised to the total protein content of the lysate, which was measured using a BCA assay (Section 2.11.2).

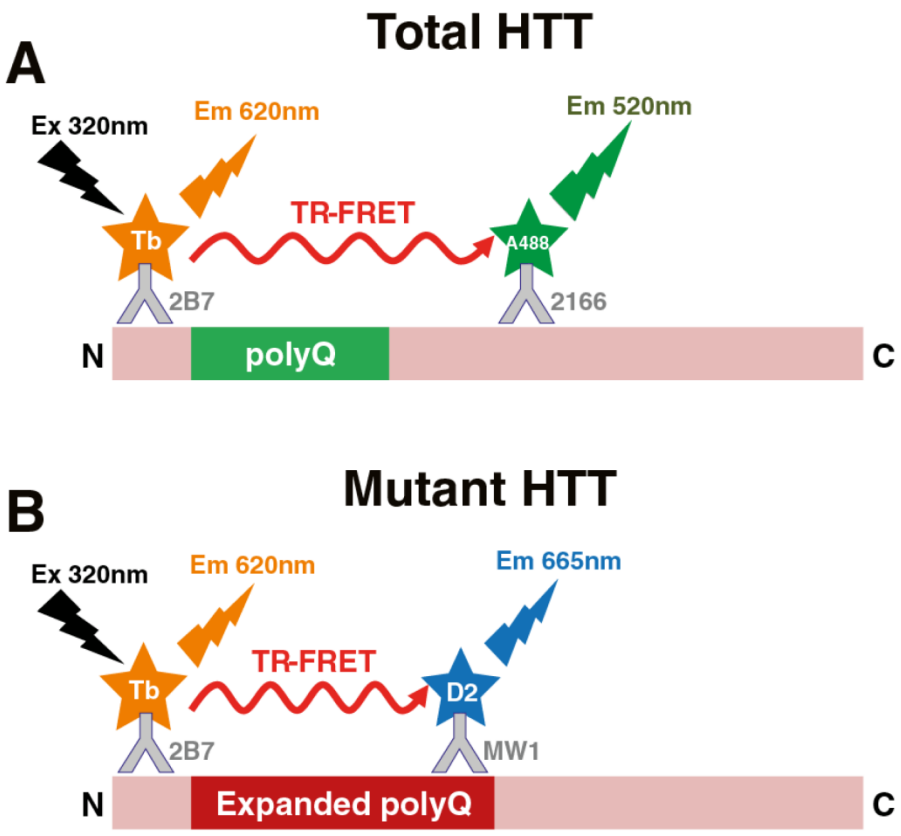

Figure 2.4. Schematic representation of the TR-FRET assay. (A) Total HTT protein levels were measured using the 2B7-Tb and 2166-Alexa Fluor® 488 antibodies, while (B) mHTT protein levels were measured using the 2B7-Tb and MW1-D2 antibodies. Reprinted and adapted from The Journal of Clinical Investigation, Vol. 122, "*Mutant huntingtin fragmentation in immune cells tracks Huntington's disease progression*", 3731-3736, Weiss et al., ©2012, with permission from The American Society for Clinical Investigation.

2.11.4 Western blotting

Primary human monocytes were isolated from peripheral blood samples, seeded at 2 × 10^6 cells per well in five wells of a 6 well plate and differentiated into macrophages (Section 2.4). On the final day of the differentiation protocol the macrophage cultures were stimulated with 1 µg/ml LPS and 10 ng/ml IFNγ for either 15, 30, 60 or 120 min, or left unstimulated. Following stimulation, the macrophages were lysed in RIPA buffer (Section

2.11.1) before mixing with 3X SDS-PAGE Loading Buffer (BioVision) and denaturing at 95 °C for 10 min. Protein samples were stored at -20 °C.

Western blotting was carried out using Novex™ 12 % Tris-Glycine Mini Protein Gels (1.5 mm, 15-well; Thermo Fisher Scientific). An HD and a control sample was always run on each gel. Fifteen µl of experimental sample was loaded per well, while 12 µl of normaliser sample was added to a separate well in order to allow comparison between blots. Eight µl of Precision Plus Protein™ All Blue Prestained Protein Standards (Bio-Rad) was also run on each gel to confirm protein size. Gels were run at 70 V for 30 min, followed by 120 V for 1.5-2.5 h using the XCell SureLock® Mini-Cell Electrophoresis System (Thermo Fisher Scientific) filled with 1X Tris-Glycine-SDS PAGE Buffer (National Diagnostics). Samples were transferred onto 0.2 µm nitrocellulose membranes at 35 V for 2 h, using the XCell II™ Blot Module (Thermo Fisher Scientific) filled with 1X Tris-Glycine Electroblotting Buffer (National Diagnostics) with 20 % methanol. Following transfer, the membranes were blocked with 1:1 PBS/Odyssey Blocking Buffer (LI-COR) at room temperature for 1 h with shaking, before incubation with primary antibody (Table 2.7) diluted in 1:1 PBS/Odyssey Blocking Buffer at 4 °C overnight with shaking. The following day the membranes were washed three times with PBS for 5 min, before incubating with secondary antibody (Table 2.8) diluted in 1:1 PBS/Odyssey Blocking Buffer for 1 h. After a further washing step, the signal was visualised using an Odyssey Infrared Imager (LI-COR) and quantified using TL100 software (TotalLab). When comparing between blots the signal from each sample was normalised to that of the normaliser sample run on the same gel prior to statistical analysis.

Table 2.7. Primary antibodies used for Western blotting.

Antibody	Source	Dilution	Company
Anti-human p44/42 MAPK (ERK1/2)	Rabbit	1:1000	Cell Signaling Technology
Anti-human phospho-p44/42 MAPK (ERK1/2)	Rabbit	1:1000	Cell Signaling Technology
Anti-human p38 MAPK	Rabbit	1:1000	Cell Signaling Technology
Anti-human phospho-p38 MAPK	Mouse	1:1000	Cell Signaling Technology
Anti-human β-actin	Mouse	1:10000	Abcam

Table 2.8. Secondary antibodies used for Western blotting.

Antibody	Source	Dilution	Company
IRDye® 680RD Anti-Mouse IgG	Goat	1:5000	LI-COR
IRDye® 800CW Goat Anti-Rabbit IgG	Goat	1:5000	LI-COR

2.12 Immunoassays

2.12.1 MSD HTT assays

While initial measurements of total and mHTT protein levels were carried out using TR-FRET (Section 2.11.3), later experiments were carried out using more sensitive MSD assays. Cell pellets were lysed in 100 µl MSD lysis buffer 3 (1 mM PMSF, 1 mm EDTA, 0.05 % SDS in wash buffer (0.2 % Tween in PBS) containing one cOmplete™, Mini, EDTA-free Protease Inhibitor Cocktail Tablet per 10 ml buffer) by pipetting gently, before the lysates were transferred to a V-bottom microtitre plate and incubated on ice for 15 min. During incubation, further mixing was carried out by pipetting up and down ten times every five minutes. The lysates were then cleared by centrifuging at 3220 ×g for 10 min at 4 °C, before the supernatants were

removed and divided into three aliquots. Two aliquots were used for MSD analysis of total and mHTT levels, while the third was used for BCA analysis of total protein levels in the cell pellet (Section 2.11.2). The aliquots were frozen at -80 °C until analysis.

To run the MSD assays, the coating antibody 2B7 (CHDI; Table 2.9) was diluted in coating buffer (15 mM Na_2CO_3, 35 mM $NaHCO_3$, pH 9.6) to a concentration of 1.5 µg/ml and added to an MA6000 96-well plate (MSD) at 50 µl per well. The plate was centrifuged at 100 ×g for 1 min to cover the entire bottom surface of the well, before the plate was sealed and incubated overnight at 4 °C. The following day the plate was washed three times with 100 µl wash buffer per well, with the solution being removed by inverting the plate. 150 µl blocking buffer (2 % Probumin® (Millipore) in wash buffer) was added to each well and the plate was incubated on a shaker for 1 h at room temperature before removing the blocking buffer. The cell lysates were then diluted at least five-fold in blocking buffer and 25 µl of each dilution was added to the appropriate wells of the MSD plate. The plate was sealed and incubated on a shaker for 1 h at room temperature, then washed four times with 100 µl wash buffer per well. After washing, the biotinylated detection antibodies MW1 (mHTT) and 4C9 (total HTT) (CHDI) were diluted in blocking buffer to final concentrations of 0.625 µg/ml and 0.5 µg/ml respectively. The diluted antibody was then added to the plate, which was sealed and incubated on a shaker for 1 h at room temperature. The antibody solution was removed by washing three times with 100 µl wash buffer per well.

To read the plate, streptavidin SULFO-TAG detection antibody (MSD) was diluted 1:12000 in blocking buffer and added to the plate at 25 µl per well.

The plate was sealed and incubated on a shaker for 1 h at room temperature, then washed three times with 100 µl wash buffer per well. After removing the wash buffer, 150 µl read buffer (MSD) was added to each well and the plate was analysed immediately using a Meso Sector S 600 (MSD). Total and mHTT levels were then normalised to the total protein content of each sample as measured by BCA assays.

Table 2.9. Antibodies used for MSD HTT assays.

Antibody	Assay	Purpose	Description	Concentration
2B7	Total and mHTT	Coating	Mouse monoclonal antibody raised against amino acids 1-17 of human HTT	1.5 µg/ml
MW1 (biotinylated)	mHTT	Detection	Mouse monoclonal antibody specific to the human polyQ region	0.625 µg/ml
4C9 (biotinylated)	Total HTT	Detection	Mouse monoclonal antibody raised against amino acids 51-71 of human HTT	0.5 µg/ml

2.12.2 MSD cytokine assays

Cytokine profiling was carried out using V-PLEX Assay Kits from MSD. Myeloid cell cytokine production was analysed using the V-PLEX Human Proinflammatory Panel II (4-Plex) Kit (IL-1β, IL-6, IL-8, TNFα), while helper T lymphocyte cytokine production was analysed using the V-PLEX Proinflammatory Panel 1 (Human) Kit (IFNγ, IL-10, IL-12p70, IL-13, IL-1β, IL-2, IL-4, IL-6, IL-8, TNFα) and the V-PLEX Human IL-5 Kit. Depending on the cell type and experimental condition, 50 µl of undiluted or 1:150, 1:500 or 1:600 diluted cell culture supernatants were added to the MSD plate and incubated with vigorous shaking for 2 h at room temperature. MSD Diluent 2

was used to dilute samples for the two multiplex assays, while MSD Diluent 43 was used to dilute samples for the IL-5 assay. Eight standards of known concentration were also added to the plates by carrying out serial fourfold dilutions of the Calibrator Blend included in each kit, according to the manufacturer's instructions. After incubation the plate was washed three times with PBS containing 0.05 % Tween before the detection antibody solution was made up by combining 60 µl of each detection antibody and making the final volume up to 3000 µl with MSD Diluent 3. Twenty-five µl of this solution was then added to each well before incubating with vigorous shaking for 2 h at room temperature. The plate was washed three times in PBS containing 0.05 % Tween before 150 µl 2X Read Buffer T was added to each well. After the Read Buffer was added the plate was analysed immediately using a Sector Imager 6000 with Discovery Workbench 4.0 software (MSD). Cytokine concentrations were calculated by comparing the samples to a standard curve made from the eight calibrators, before normalising to the total protein measured by BCA assays (Section 2.11.2).

2.13 Flow cytometry

2.13.1 Staining of cell surface markers

Cell surface marker staining was carried out by transferring a maximum of 1 × 10^6 cells into a V-bottom 96 well plate and centrifuging at 400 ×g for 5 min to collect the cells at the bottom of the well. The supernatant was removed by flicking the plate before the samples were washed once with 200 µl FACS buffer. The relevant panel of antibodies (Table 2.10) was then diluted in FACS buffer (to a final volume of 50 µl per well) and added to each well. The

samples were mixed by pipetting up and down before incubating for 60 min on a shaker at 4 °C. Samples were protected from light for the duration of the staining process. After incubation the samples were washed twice in 200 µl FACS buffer by centrifuging at 400 ×g for 5 min, before being fixed in 200 µl PBS containing 4 % PFA for 10 min. After fixation the samples were washed three times in 200 µl FACS buffer and kept at 4 °C in the dark until analysis.

2.13.2 Staining of intracellular markers

Staining of intracellular markers was carried out using the FOXP3 / Transcription Factor Staining Buffer Set (eBioscience). After cell surface marker staining (but before fixation), the cells were resuspended in 100 µl Fixation/Permeabilization Buffer (one part Fixation/Permeabilization Concentrate to three parts Fixation/Permeabilization Diluent) before incubating for 40 min on a shaker at 4 °C in the dark. The samples were then centrifuged at 400 ×g for 5 min before washing twice with 200 µl 1X Permeabilization Buffer. Staining was carried out by diluting the relevant panel of antibodies (Table 2.11) in 1X Permeabilization Buffer (to a final volume of 200 µl per well) and adding to each well. The samples were mixed by pipetting before incubating for 60 min on a shaker at 4 °C in the dark. After incubation the samples were washed twice in 200 µl FACS buffer by centrifuging at 400 ×g for 5 min and kept at 4 °C in the dark until analysis.

2.13.3 Data analysis

All flow cytometry samples were run on a MACSQuant with MACSQuantify software (Miltenyi Biotec). Unstained and single colour-stained controls were always analysed prior to the experimental samples in order to set

compensation values between antibodies with overlapping emission spectra. Data analysis was performed using FlowJo 7.2.5 (Tree Star).

Table 2.10. Antibodies used for staining of cell surface markers.

Antibody	Dilution	Company
Anti-human CCR2 PerCP-Cy5.5	2 µl per test	BioLegend
Anti-human CCR4/CD194 PE	5 µl per test	BD Biosciences
Anti-human CCR5 PE	2 µl per test	eBioscience
Anti-human CD3 eFluor450	2 µl per test	eBioscience
Anti-human CD4 APC-Cy7	2 µl per test	BD Biosciences
Anti-human CD8 VioGreen	4.5 µl per test	Miltenyi Biotec
Anti-human CD14 APC	2 µl per test	eBioscience
Anti-human CD16 FITC	2 µl per test	eBioscience
Anti-human CD19 APC	5 µl per test	eBioscience
Anti-human CD25 PE	10 µl per test	BD Biosciences
Anti-human CD56 FITC	2 µl per test	eBioscience
Anti-human CD62L PeCy5	5 µl per test	eBioscience
Anti-human CD138 FITC	5 µl per test	eBioscience
Anti-human CXCR3 APC	5 µl per test	BioLegend

Table 2.11. Antibodies used for staining of intracellular markers.

Antibody	Dilution	Company
Anti-human Il-17 PeCy7	4.5 µl per test	eBioscience
Anti-human FOXP3	5 µl per test	eBioscience

2.14 Statistical analysis

2.14.1 Chapter 3

Statistical analysis of all experiments contained in this chapter was carried out using GraphPad Prism 6 (GraphPad). Optimisation of GeRP transfection

was analysed using two-way ANOVAs with Bonferroni post-hoc multiple comparison testing, as was initial testing and dose-response profiling of allele-selective siRNAs. Cytokine profiling following allele-selective HTT-lowering was analysed using one-way ANOVAs with Tukey post-hoc multiple comparison testing. All error bars represent standard error of the mean.

2.14.2 Chapter 4

Statistical analysis of differential expression, splicing, GSEA and IPA® data was carried out using the software packages and analysis tools outlined above. Further statistical analysis was carried out using GraphPad Prism 6. IκBα western blotting experiments were analysed using unpaired two-tailed Student's *t*-tests. MAPK western blotting experiments were analysed by two-way ANOVAs with Bonferroni post-hoc multiple comparison testing. Quantitative PCR analysis of gene expression changes following HTT-lowering was carried out using unpaired two-tailed Student's *t*-tests. All error bars represent standard error of the mean.

2.14.3 Chapter 5

Statistical analysis of immune cell subset, proliferation and cytokine profiling data was carried out using GraphPad Prism 6, while PCR array data was analysed using the manufacturer's online data analysis tool (Section 2.9.4). All experiments were analysed using unpaired two-tailed Student's *t*-tests. Where appropriate, post-hoc analysis of multiple *t*-tests was carried out using a Holm-Šídák correction (alpha = 0.05) for multiple comparisons. All error bars represent standard error of the mean.

3 Allele-selective suppression of mHTT in HD myeloid cells

3.1 Background

Substantial research into HD therapeutics has focused on alleviating specific pathogenic mechanisms, for example via the upregulation of BDNF or the enhancement of autophagy (Simmons et al., 2009; Martinez-Vicente et al., 2010). Although these approaches have yielded promising results in animal models, they are limited by the fact that HD pathogenesis is multi-factorial; while targeting a single mechanism may improve disease progression, it is unlikely to prevent it completely. As a monogenic disorder, HD is an ideal candidate for treatment by PTGS, as lowering cellular mHTT levels will stop the pathogenic cascade at its source. The most commonly used therapeutics for PTGS are siRNAs and ASOs; these are short oligonucleotide molecules that bind to complementary sequences on an mRNA transcript to target it for degradation by endogenous cellular mechanisms (Sah and Aronin, 2011).

Numerous studies have demonstrated that lowering cellular mHTT levels is beneficial in animal models of HD (Drouet et al., 2009; Boudreau et al., 2009), with the therapeutic effects persisting longer than suppression of the *HTT* transcript (Kordasiewicz et al., 2012). This suggests that even occasional HTT-lowering may be sufficient to alleviate HD pathology, and the first human studies of intrathecal ASO delivery are currently underway (Ionis Pharmaceuticals, 2015). However, the majority of therapeutics tested have

provided suppression of both wild-type and mHTT; this occurs because the target sequence is present on both alleles (Sah and Aronin, 2011).

While this offers obvious therapeutic benefits, wild-type HTT has important roles in cellular function, and is key for neuronal development during embryogenesis (Godin et al., 2010; Tong et al., 2011). Furthermore, initial studies suggested that *Htt* knockout in the adult mouse brain causes neurodegeneration (Dragatsis et al., 2000), leading to fears about whether wild-type HTT suppression will be safe in patients. However, it has since been shown that non-specific HTT-lowering is tolerated for at least nine months in HD mice (Kordasiewicz et al., 2012; Stanek et al., 2014), while a six month reduction in *HTT* expression has no adverse effects in the rhesus putamen (Grondin et al., 2012). Indeed, a recent study found that neuronal *Htt* deletion is not deleterious in the adult mouse, with death from ubiquitous *Htt* knockout in early life instead being caused by acute pancreatitis (Wang et al., 2016). While this is promising, it is uncertain what percentage of wild-type HTT suppression would be tolerated in the adult human brain, where therapeutics will need to be administered over several decades. The ideal strategy would therefore selectively lower mHTT while sparing wild-type.

Allele-selective suppression of mHTT relies on polymorphisms between the wild-type and mutant alleles which may be exploited to provide differential knockdown. The CAG repeat is the most obvious target; however, it has proved to be technically challenging to reliably discriminate between alleles with CAG repeats in the normal patient range (Fiszer et al., 2013). There is also the potential for off-target knockdown of other CAG repeat-containing transcripts. An alternative strategy relies on genotyping HD patients to

identify heterozygous SNPs in the *HTT* gene. Each SNP allele may then be linked to either wild-type or m*HTT*, before delivering an siRNA or ASO that is specific for the SNP allele located on m*HTT* (Sah and Aronin, 2011).

SNP-targeted ASOs and siRNAs have been used successfully in a range of cell and animal models of HD, including human HD fibroblasts and mouse neurons (Carroll et al., 2011; Østergaard et al., 2013; Drouet et al., 2014). While they have been shown to be capable of providing increased allele-selectivity compared to CAG repeat-targeted therapeutics, it is important to note that this approach will only be applicable to HD patients who are heterozygous for specific SNPs. Although the prevalence of SNP heterozygosities varies between ethnic groups, genotyping of large cohorts has suggested that 75 % of HD patients would be treatable with five siRNAs targeting just three SNPs (Pfister et al., 2009). This provides a promising alternative should total HTT-lowering prove to have deleterious effects.

However, allele-selective suppression of mHTT is yet to be achieved in primary *ex vivo* HD patient cells. This is a key step in determining whether this therapeutic approach will have clinical relevance. Previous work has made use of GeRPs to transfect HD myeloid cells with anti-total *HTT* siRNA (Träger et al., 2014); these are yeast-derived sugar particles that are taken up by phagocytosis before delivering their siRNA cargo into the cytoplasm of the target cell (Aouadi et al., 2009). This study will use the same technology to deliver allele-selective siRNAs to HD patient myeloid cells, in addition to characterising the effect that allele-selective HTT-lowering has on the cells' hyper-reactive cytokine phenotype. This will allow the relative contributions of wild-type and mHTT to immune cell function to be further investigated.

3.2 Aims

1. To determine the optimal GeRP formulation for the transfection of primary human myeloid cells.

2. To characterise the selectivity and potency of *HTT* mRNA knockdown provided by a panel of siRNAs targeted to three of the most prevalent SNPs in the *HTT* gene.

3. To validate selective siRNAs with total and mHTT protein analysis.

4. To characterise the effects of allele-selective HTT-lowering on the hyper-reactive cytokine phenotype of HD myeloid cells.

3.3 Methods

HD subjects were genotyped for SNP heterozygosity (Section 2.2.2), before the SNP alleles were linked to either wild-type or m*HTT* by SLiC (Section 2.3). PBMCs were isolated using density centrifugation (Section 2.4.1), before $CD14^+$ monocytes were isolated by magnetic cell sorting (Section 2.4.2) and differentiated into macrophages (Section 2.4.3). Macrophages were treated with GeRPs containing siRNA (Section 2.5.2) and harvested 72 h after transfection. RNA was isolated using the RNeasy Mini Kit (Section 2.7.1) and cDNA was synthesised according to Section 2.7.4. Analysis of *HTT* expression was carried out using SYBR® Green (Section 2.7.5) and TaqMan® qPCR (Section 2.7.6), while analysis of total and mHTT protein levels was carried out using TR-FRET (Section 2.11.3) and MSD HTT assays (Section 2.12.1). Cytokine levels were quantified using MSD cytokine assays (Section 2.12.2) with normalisation to total protein using BCA assays (Section 2.11.2). Cell viability was assessed using ATP assays (Section 2.6.1). Statistical analysis was carried out according to Section 2.14.1.

3.4 Contributions

Work presented in this chapter was carried out in collaboration with University of Massachusetts Medical School. SNP genotyping was carried out by Lori Kennington, before SLiC was carried out by Dr Wanzhao Liu. siRNA molecules were synthesised by Dr Edith Pfister and Professor Neil Aronin, and loaded into GeRPs by Professor Gary Ostroff. Analysis of HTT protein levels was carried out by Promidis and BioFocus (assisted by CHDI). All remaining experiments and analyses were carried out by James Miller.

3.5 Results

3.5.1 Optimisation of GeRP transfection

Previous studies have made use of GeRP technology to transfect HD patient and control myeloid cells with anti-total *HTT* siRNA (Träger et al., 2014). This approach was used to demonstrate the reversibility of HD myeloid cell hyper-reactivity to LPS following HTT-lowering. Prior to investigating the effects of allele-selective siRNA on HD myeloid cells, a range of GeRP formulations were tested in order to determine the optimal conditions for achieving maximal knockdown while limiting cellular toxicity. Endo-Porter (EP) is a key factor in the GeRP particle that acts to permeabilise the endosome following phagocytosis, allowing the siRNA molecules contained within the GeRP to be released into the cytoplasm (Summerton, 2005). However, it is possible that the membrane permeabilisation process has an adverse effect on cellular function that may be limited by using less EP. The EP concentration is defined as its dilution by saline during the GeRP synthesis process, with previous work carried out using exclusively 1.0 EP GeRPs; experiments carried out as part of the initial study demonstrated that these have no significant effect on cell death (Träger et al., 2014). However, a detailed assessment of their effects on the more sensitive measure of cellular viability is yet to be performed.

GeRPs containing 1.0, 0.25, 0.1 and 0.05 EP were synthesised in order to determine whether lower EP concentrations have a beneficial effect on cellular viability. All GeRPs used for these experiments were synthesised as part of the same batch and were identical apart from the concentration of EP.

Monocyte-derived macrophages were isolated from peripheral blood samples donated by HD patient and control subjects and treated with GeRPs containing each concentration of EP on day three of the differentiation protocol; cellular viability was then assessed using ATP assays 24 h after transfection. Both scrambled (SCR) and anti-total *HTT* siRNA-containing GeRPs were tested in order to determine whether the siRNA used has any effect on cellular viability. As it has previously been shown that GeRP-mediated HTT knockdown does not vary between HD and control myeloid cells (Träger et al., 2014), the samples were pooled for analysis.

Treatment with GeRPs of all EP concentrations resulted in a decrease in cellular ATP levels compared to untreated control. However, GeRPs containing 0.25, 0.1 and 0.05 EP all provided a statistically significant rescue of cellular ATP levels compared to 1.0 EP GeRPs (Fig. 3.1). This demonstrates that using lower EP concentrations during transfection has a beneficial effect on cellular viability. A further significant increase in cellular ATP levels was seen for 0.05 EP compared to 0.25 EP GeRPs, however this was only the case for the anti-total *HTT* siRNA-containing GeRPs, with no difference seen for SCR. Despite this, no significant differences were seen between the SCR and anti-total *HTT* GeRPs at any of the EP concentrations tested, suggesting that the siRNA being delivered does not have a meaningful effect on cellular viability.

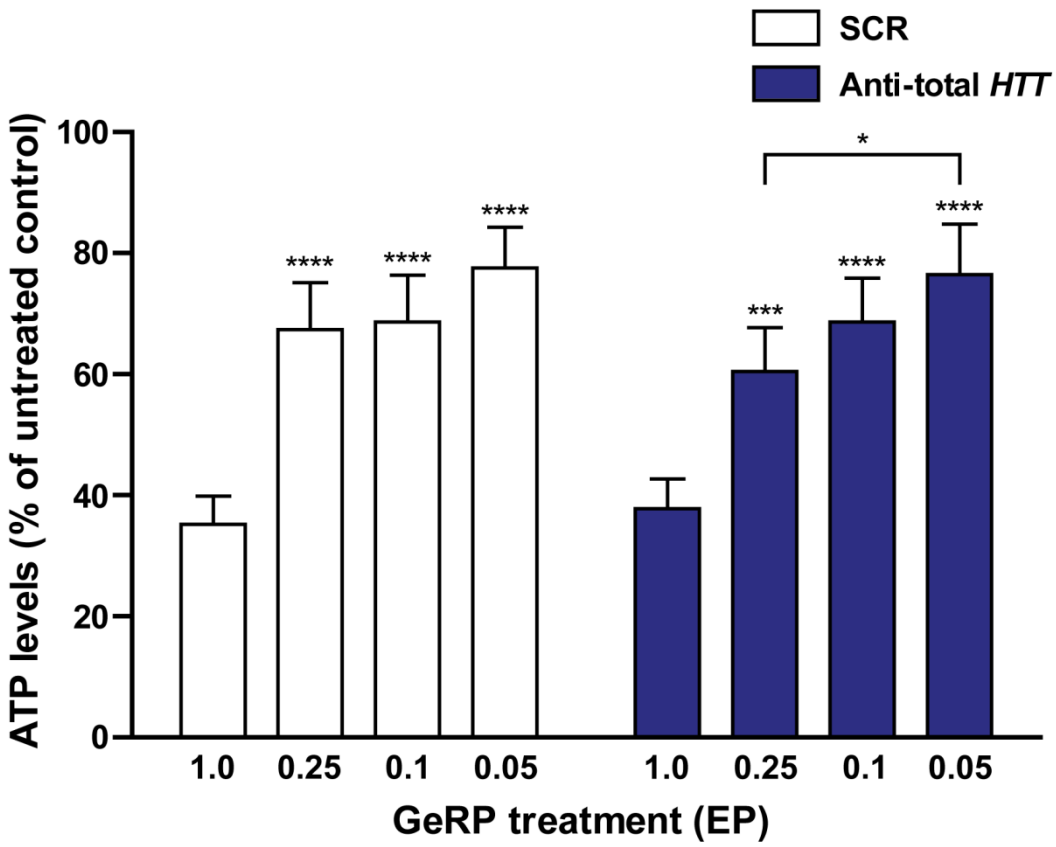

Figure 3.1. Lower EP doses ameliorate the cellular ATP deficit associated with GeRP transfection. Monocyte-derived macrophages were isolated from HD and control peripheral blood samples and treated with GeRPs containing variable concentrations of EP. ATP assays were then carried out 24 h after transfection. Lower EP doses were found to provide significant rescue of the cellular ATP deficit caused by 1.0 EP GeRPs, with no difference seen between SCR and anti-total *HTT* siRNA-containing GeRPs at any of the EP doses tested. Data show mean ATP levels ± SEM (n = 7 (2 controls and 5 HD), samples pooled for analysis), statistical analysis carried out using two-way ANOVA with Bonferroni post-hoc testing. Asterisks above bars show post-test significance compared to 1.0 EP GeRPs containing the same siRNA. *P < 0.05, **P < 0.01, ***P < 0.001, ****P < 0.0001.

While these data show that lowering the concentration of EP used during GeRP synthesis has a beneficial effect on cellular viability, it is likely that too much of a reduction will result in less siRNA being released into the cytoplasm, and therefore a reduction in the efficiency of knockdown. To address this, monocyte-derived macrophages were obtained from peripheral blood samples donated by HD patients and transfected with the GeRPs described above. Suppression of cellular *HTT* levels was then measured by qPCR 72 h after transfection; the anti-*HTT* GeRPs were each normalised to a SCR control of the same EP concentration to ensure consistency. As expected, significant knockdown of *HTT* mRNA was seen for all anti-*HTT* GeRP formulations compared to the equivalent SCR control (Fig. 3.2). However, the amount of knockdown was significantly reduced in the 0.05 EP GeRPs compared to the 1.0 EP GeRPs used for previous experiments. This confirms the hypothesis that lowering the EP concentration past a certain point will reduce transfection efficacy due to a decreased amount of siRNA entering the cytoplasm. However, no significant difference was seen in the knockdown provided by either the 0.25 or 0.1 EP GeRPs compared to 1.0 EP. This demonstrates that it is possible to limit adverse effects on cellular viability while still maintaining adequate *HTT* knockdown.

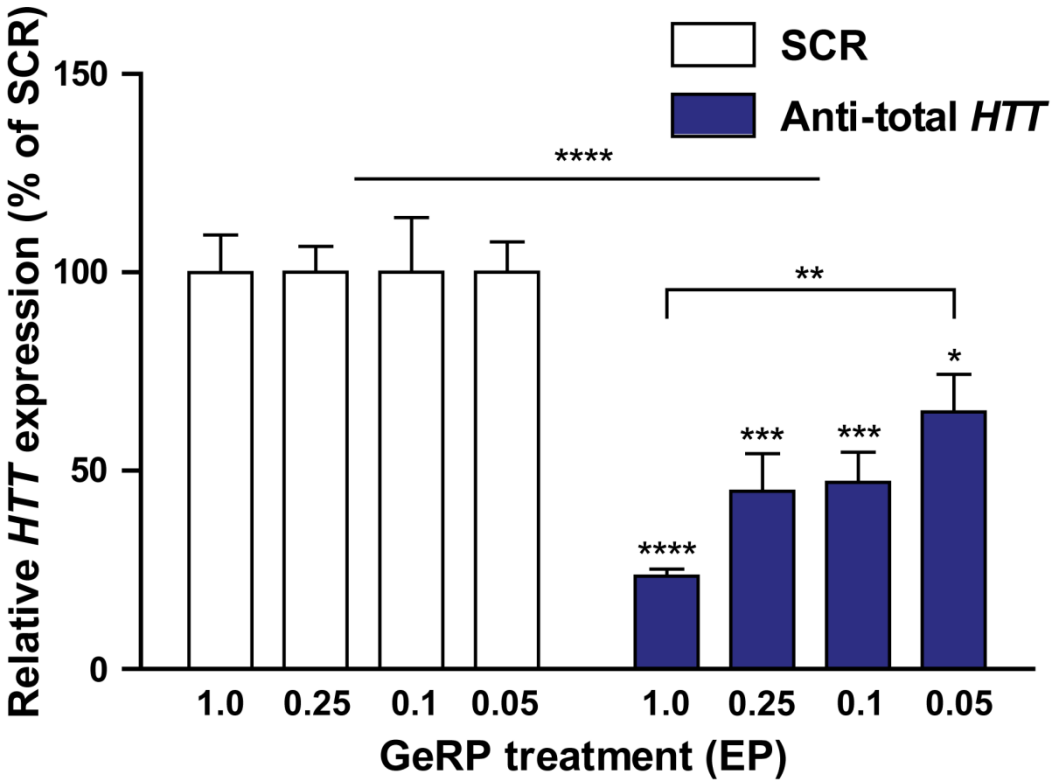

Figure 3.2. Characterisation of *HTT* mRNA suppression using lower EP GeRPs. Monocyte-derived macrophages were isolated from HD peripheral blood samples and treated with GeRPs containing variable concentrations of EP. *HTT* mRNA expression was then measured after 72 h by qPCR. Anti-*HTT* GeRPs of all EP concentrations suppressed cellular *HTT* levels, however the suppression provided by 0.05 EP GeRPs was significantly reduced compared to that provided by 1.0 EP GeRPs. Data show mean *HTT* levels ± SEM (n = 5), statistical analysis carried out using two-way ANOVA with Bonferroni post-hoc testing. Asterisks above bars show post-test significance compared to SCR GeRPs containing the same EP concentration. *P < 0.05, **P < 0.01, ***P < 0.001, ****P < 0.0001.

While promising, it is essential to validate such mRNA data with protein analysis, as the mHTT protein is the primary pathogenic species in HD. Further monocyte-derived macrophage cultures were obtained from peripheral blood samples donated by HD patients and transfected with SCR and anti-total *HTT* GeRPs containing either 0.25, 0.1 or 0.05 EP. Analysis of total and mHTT protein levels was then carried out 72 h after transfection using TR-FRET. A statistically significant reduction in both total and mHTT levels was seen for the anti-total *HTT*-treated samples compared to the SCR-treated samples. The overall knockdown provided was comparable to the approximately 50 % reduction in total HTT previously published using 1.0 EP GeRPs (Träger et al., 2014). Post-hoc analysis revealed a significant reduction in mHTT for all three anti-total *HTT* formulations compared to the equivalent SCR control (Fig. 3.3), however on total HTT analysis only the knockdown provided by the 0.1 EP GeRPs was found to be significant (Fig. 3.4). When combined with the ATP assay and qPCR data, this shows that 0.1 EP GeRPs are able to alleviate the reduction in cellular ATP levels caused by 1.0 EP GeRPs while still retaining adequate mRNA and protein knockdown. 0.1 EP GeRPs will therefore be used for all experiments contained in the remainder of this thesis.

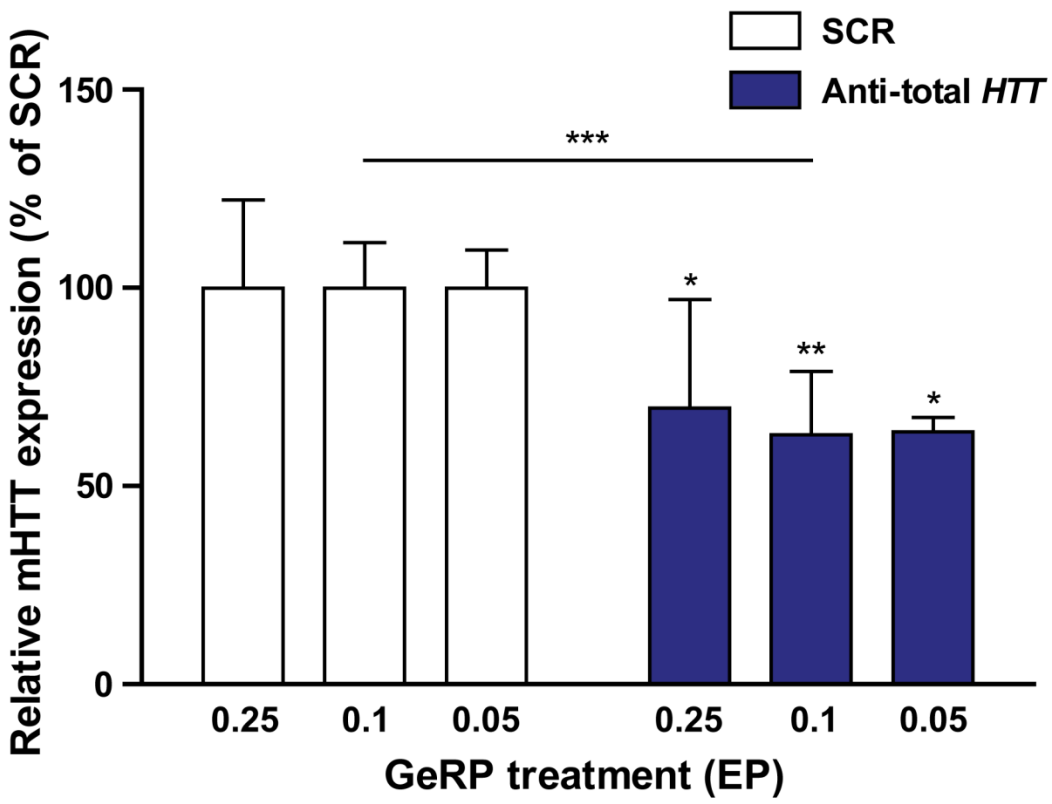

Figure 3.3. Characterisation of mHTT protein suppression using lower EP GeRPs. Monocyte-derived macrophages were isolated from HD peripheral blood samples and treated with GeRPs containing variable concentrations of EP. Mutant HTT protein expression was then measured after 72 h by TR-FRET. Anti-*HTT* GeRPs of all EP concentrations suppressed cellular mHTT levels, however the suppression provided by 0.1 EP GeRPs was more significant than that provided by 0.25 and 0.05 EP GeRPs. Data show mean mHTT levels ± SEM (n = 3), statistical analysis carried out using two-way ANOVA with Bonferroni post-hoc testing. Asterisks above bars show post-test significance compared to SCR GeRPs containing the same EP concentration. *P < 0.05, **P < 0.01, ***P < 0.001.

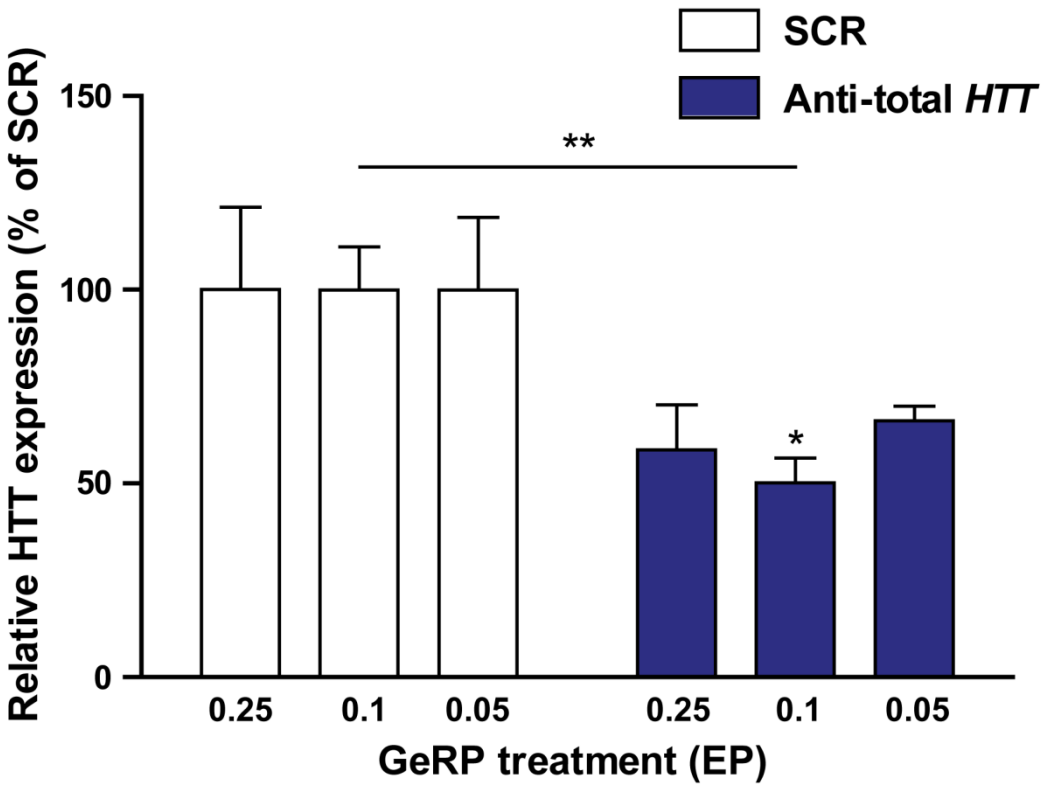

Figure 3.4. Characterisation of total HTT protein suppression using lower EP GeRPs. Monocyte-derived macrophages were isolated from HD peripheral blood samples and treated with GeRPs containing variable concentrations of EP. Total HTT protein expression was then measured after 72 h by TR-FRET. Of the GeRP formulations tested, only the 0.1 EP GeRPs provided significant suppression of total HTT on post-hoc testing. Data show mean HTT levels ± SEM (n = 3), statistical analysis carried out using two-way ANOVA with Bonferroni post-hoc testing. Asterisks above bars show post-test significance compared to SCR GeRPs containing the same EP concentration. *P < 0.05, **P < 0.01.

3.5.2 SNP genotyping of HD patients

Following GeRP optimisation it was necessary to genotype HD patients for SNP heterozygosity, in order to identify individuals who were suitable subjects for allele-selective silencing. Three SNPs in the *HTT* gene were selected for targeting on the basis of their high prevalence of heterozygosity among the HD patient population (Pfister et al., 2009); rs362331 in exon 50 (39.4 % C/T), rs362273 in exon 57 (35.2 % A/G) and rs362307 in the 3'-UTR (48.6 % C/T). Allele-selective siRNAs to target these SNPs were previously developed by collaborators at University of Massachusetts Medical School, with initial testing carried out in HeLa cells (Pfister et al., 2009).

Diagnostic DNA samples collected from HD patients from the NHNN cohort were genotyped for heterozygosity at each of the above SNP sites. This identified fifty-seven individuals who were heterozygous for rs362331, thirty-eight who were heterozygous for rs362273 and fifty-four who were heterozygous for rs362307. All following experiments described in this chapter were carried out using peripheral blood samples collected from this cohort of genotyped HD patients. As initial experiments focused exclusively on achieving optimal allele-selectivity at each SNP site, it was not yet necessary to carry out SLiC for m*HTT* linkage (this was performed in a subset of patients for later protein and cytokine experiments).

3.5.3 Characterisation of a panel of SNP-targeted siRNAs

Initial characterisation of allele-selective siRNA was carried out using GeRPs containing 36 nM siRNA, as this was the concentration of anti-total *HTT* siRNA used in previous studies of HD myeloid cells (Träger et al., 2014). Peripheral blood samples were collected from genotyped HD patients, before monocyte-derived macrophages were isolated and treated with GeRPs containing either SCR or allele-selective anti-*HTT* siRNA; an anti-total *HTT* control was also included in each experiment to allow comparison with previous work. Cultures were harvested after 72 h and the expression of each SNP allele was analysed using allele-specific qPCR.

The first SNP investigated was rs362331 in exon 50 of the *HTT* transcript; heterozygous subjects have a C allele and a T allele. Consistent with previous work, treatment with anti-total *HTT* siRNA resulted in approximately 75 % suppression of *HTT* mRNA levels (Träger et al., 2014), the degree of which did not differ between the C and T alleles of rs362331 (Fig. 3.5). This was expected as the nucleotide sequence targeted by the anti-total *HTT* siRNA is present on both *HTT* alleles. In contrast, treatment with siRNA selective for the U allele of rs362331 resulted in 74 % suppression of the on-target U allele (equivalent to that provided by anti-total *HTT* siRNA), with only 17 % suppression of the off-target C allele compared to SCR control; this off-target knockdown was not found to be statistically significant. Perhaps unsurprisingly, post-hoc testing following ANOVA revealed the selectivity offered by the anti-U siRNA to be highly statistically significant ($p < 0.001$).

Similarly, treatment with siRNA selective for the C allele of rs362331 resulted in 63 % suppression of the on-target C allele, with only 30 % knockdown of the off-target U allele compared to SCR control. The on-target knockdown was again found to be statistically equivalent to that provided by anti-total *HTT* siRNA, while post-hoc testing revealed significant discrimination between alleles ($p < 0.05$). Although no statistically significant differences were found for off-target allele expression for either siRNA compared to SCR control, it is clear from the data that some off-target effects exist. However, these data demonstrate that such effects are minor, and that it is possible to achieve highly significant allele selectivity using siRNA targeted to rs362331.

Next, the allele-selectivity of siRNAs targeting rs362273 in exon 57 of the *HTT* transcript was investigated; heterozygous subjects have an A allele and a G allele. As expected, treatment with anti-total *HTT* siRNA again resulted in equal SNP knockdown (Fig. 3.6). However, treatment with allele-selective siRNA provided greatly reduced selectivity compared to rs362331, with 77 % on-target and 63 % off-target suppression for the anti-A siRNA, and 78 % on-target and 58 % off-target suppression for the anti-G siRNA. Promisingly, post-hoc testing demonstrated significant allelic discrimination following treatment with the anti-G siRNA. However, no such significant discrimination was seen following treatment with the anti-A siRNA. It is also important to note that statistical significance does not always translate to biological relevance; clearly, mean off-target knockdown of this degree is far too great for either siRNA to be considered truly selective. While the potency of the knockdown provided by these siRNAs is promising, their selectivity will need to be significantly improved for future use.

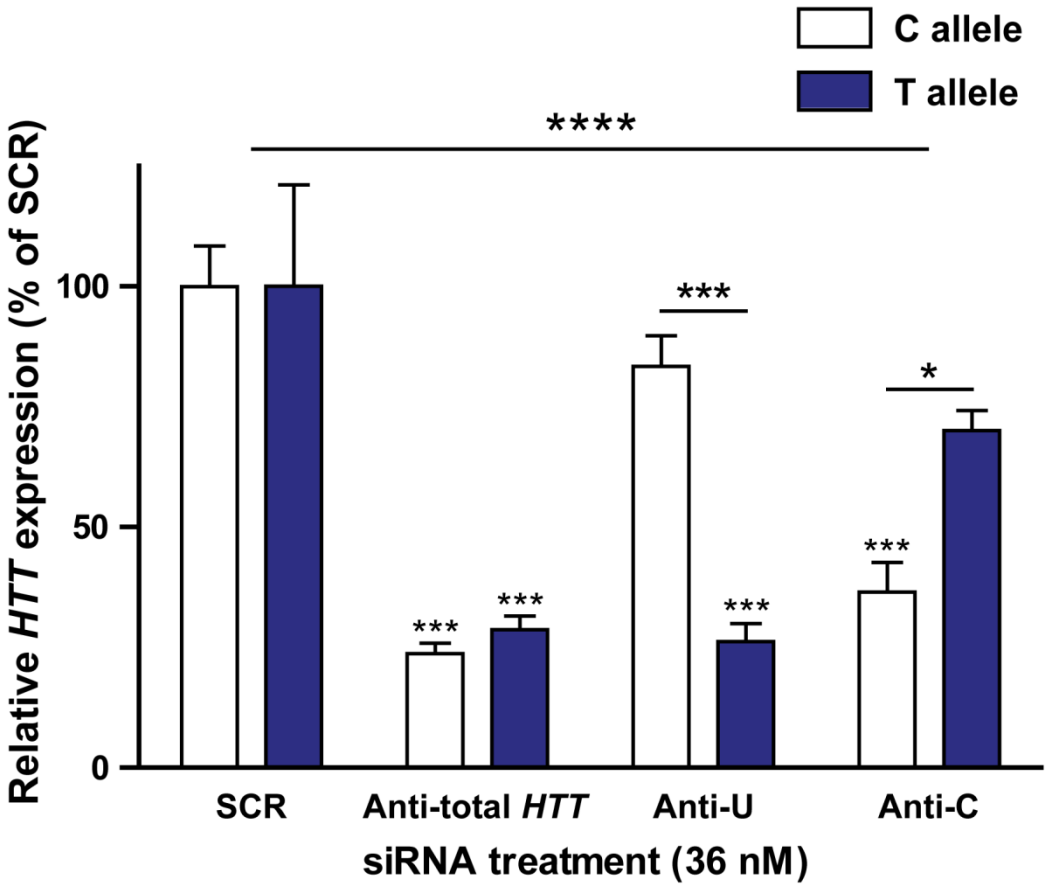

Figure 3.5. Characterisation of allele-selective siRNA targeting rs362331 in exon 50 of *HTT*. Monocyte-derived macrophages were isolated from SNP-genotyped HD patients and treated with GeRPs containing either SCR, anti-total *HTT* or allele-selective siRNA targeted to each allele of rs362331 in exon 50 of the *HTT* transcript. Expression of each SNP allele was then measured after 72 h by qPCR. Treatment with allele-selective GeRPs provided potent suppression of the on-target allele in each case, with no significant suppression of the off-target allele. The allelic discrimination provided by each allele-selective siRNA was further found to be statistically significant. Data show mean expression of each SNP allele ± SEM (n = 3), statistical analysis carried out using two-way ANOVA with Bonferroni post-hoc testing. Asterisks above bars show post-test significance compared to the same allele in SCR-treated samples. Asterisks between bars denote within treatment allele expression differences. *P < 0.05, **P < 0.01, ***P < 0.001, ****P < 0.0001.

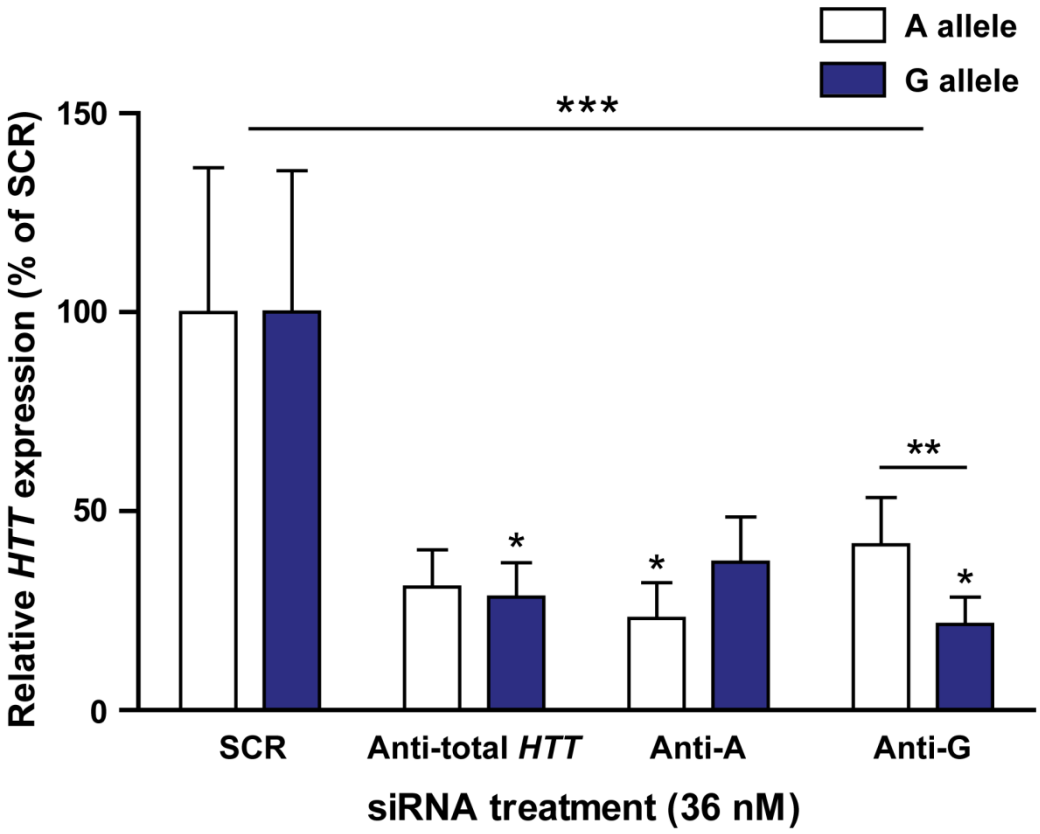

Figure 3.6. Characterisation of allele-selective siRNA targeting rs362273 in exon 57 of *HTT*. Monocyte-derived macrophages were isolated from SNP-genotyped HD patients and treated with GeRPs containing either SCR, anti-total *HTT* or allele-selective siRNA targeted to each allele of rs362273 in exon 57 of the *HTT* transcript. Expression of each SNP allele was then measured after 72 h by qPCR. Treatment with allele-selective GeRPs provided potent suppression of each SNP allele, with anti-G siRNA providing significantly increased suppression of the G allele compared to the C allele. However, substantial off-target suppression was observed for both of the allele-selective siRNAs. Data show mean expression of each SNP allele ± SEM (n = 4), statistical analysis carried out using two-way ANOVA with Bonferroni post-hoc testing. Asterisks above bars show post-test significance compared to the same allele in SCR-treated samples. Asterisks between bars denote within treatment allele expression differences. *P < 0.05, **P < 0.01, ***P < 0.001.

Finally, allele-selective suppression targeting rs362307 in the 3'-UTR of the *HTT* transcript was investigated; heterozygous subjects have a C allele and a T allele. However, the T allele has previously been shown to be linked to m*HTT*, eliminating the need to target the C allele as a potential therapeutic for HD (Pfister et al., 2009). This SNP is also known to be the most prevalent among Caucasian HD patients, with approximately 48.6 % heterozygosity; this makes it an attractive target for potential clinical trials. Two separate anti-U siRNAs were therefore tested for this SNP in order to maximise the potential for achieving selective knockdown. Again, significant non-selective knockdown of each allele was seen following treatment with anti-total *HTT* siRNA (Fig. 3.7). However, neither anti-U siRNA was found to provide any allelic discrimination, with equivalent expression of each allele being seen on qPCR in both cases. Furthermore, only anti-U (1) demonstrated any potency, achieving a 65-70 % reduction in mean *HTT* expression. In contrast, almost no change in mean *HTT* expression was seen following treatment with anti-U (2). While the lack of allelic discrimination seen with a 36 nM dose of anti-U (1) is disappointing, the potency of knockdown combined with the high SNP prevalence and observed selectivity in previous *in vitro* experiments suggests that further optimisation attempts are worthwhile.

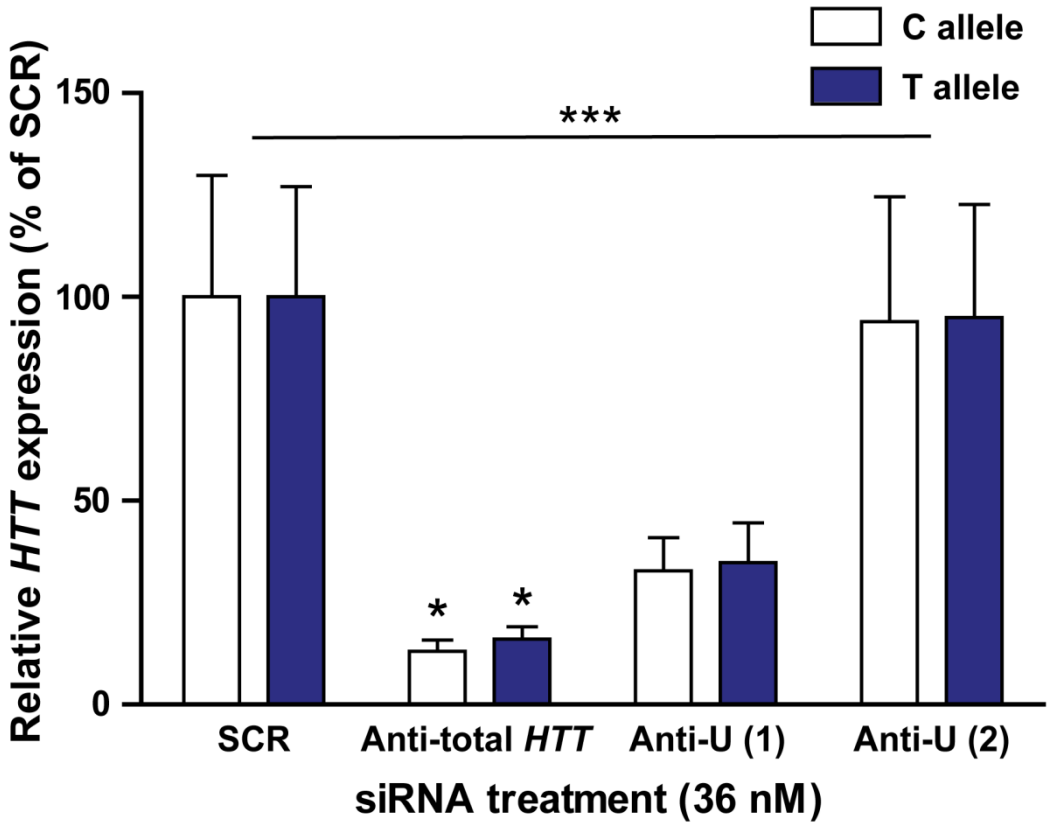

Figure 3.7. Characterisation of allele-selective siRNAs targeting rs362307 in the 3'-UTR of *HTT*. Monocyte-derived macrophages were isolated from SNP-genotyped HD patients and treated with GeRPs containing either SCR, anti-total *HTT* or allele-selective siRNA targeted to each allele of rs362307 in the 3'-UTR of the *HTT* transcript. Expression of each SNP allele was then measured after 72 h by qPCR. Treatment with anti-U (1) provided potent *HTT* mRNA suppression, however this was not selective between alleles. Treatment with anti-U (2) did not provide adequate suppression of either SNP allele. Data show mean expression of each SNP allele ± SEM (n = 4), statistical analysis carried out using two-way ANOVA with Bonferroni post-hoc testing. Asterisks above bars show post-test significance compared to the same allele in SCR-treated samples. *P < 0.05, **P < 0.01, ***P < 0.001.

3.5.4 Effects of siRNA dose-ranging on allele-selectivity

Previous studies have demonstrated that lowering the dose of the siRNAs used in this project is able to improve selectivity (Pfister et al., 2009). It is therefore possible that the lack of selectivity seen for rs362273 and rs362307 was due to using too high a dose of siRNA. The optimal dosage was an unknown factor at the start of these experiments, as these siRNAs have not previously been tested in primary human cells and converting doses between different cell models is challenging. Using a lower dose may therefore reduce off-target effects while retaining potent suppression of the on-target allele. To investigate this hypothesis, GeRPs were prepared to carry out a dose-ranging analysis of each siRNA. However, as the rs362307 anti-U (2) siRNA did not display potent knockdown at a dose of 36 nM, it was decided not to use it for further testing. Monocyte-derived macrophages were isolated from genotyped HD patients and transfected with GeRPs containing a range of concentrations of each SNP-targeted siRNA. After 72 h the expression of each SNP allele was measured by allele-specific qPCR, with each siRNA being compared to a SCR control of the same siRNA concentration.

First, the two allele-selective siRNAs targeting rs362331 were packaged into GeRPs at concentrations of 36 nM, 24 nM, 12 nM and 3.6 nM, before being used for transfection. Consistent with the initial suppression experiments, reduced expression of the on-target allele was seen relative to the off-target allele for both siRNAs at all of the doses that were tested (Figs. 3.8 and 3.9). However, no significant increase in selectivity was seen with the lower siRNA doses, and the most selective results were again seen using the anti-U siRNA at a dose of 36 nM. Although this contrasts with previous *in vitro*

experiments, the highly significant selectivity seen during the initial testing of these siRNAs shows that they are both suitable for the allele-selective suppression of m*HTT* in HD myeloid cells at a dose of 36 nM.

Next, the siRNAs targeting rs362273 were tested at concentrations of 36 nM, 24 nM, 12 nM and 3.6 nM. Consistent with the initial experiments, both the anti-A and anti-G siRNAs achieved potent *HTT* knockdown at a dose of 36 nM, although there was again considerable off-target suppression (Figs. 3.10 and 3.11). Disappointingly, reduced doses of each siRNA resulted in an almost complete loss of potency, with no appreciable improvement in the selectivity provided between the on-target and off-target alleles. Furthermore, the significant discrimination seen on initial testing of the anti-G siRNA was not replicated during these experiments. This suggests that rs362273 is unlikely to serve as a reliable target for allele-selective suppression of mHTT.

Finally, the anti-U (1) siRNA targeting rs362307 was packaged into GeRPs at concentrations 36 nM, 28.8 nM, 21.6 nM, 14.4 nM and 7.2 nM, before being used for transfection. Again, treatment with anti-U (1) resulted in a decrease in *HTT* mRNA expression; however, this was markedly reduced at doses of 14.4 nM and 7.2 nM (Fig. 3.12). Furthermore, none of the doses tested offered significant discrimination between the C and T alleles. This suggests that, as with rs362273, lowering the dose of siRNA packaged into each GeRP is not sufficient to achieve substantial allele-selectivity while retaining potency when targeting rs362307 with anti-U (1). Indeed, the loss of potency seen at the lower doses suggests that further reductions are unlikely to be beneficial, as even if selectivity is achieved the limited suppression of the on-target allele will be insufficient to have any real therapeutic benefit.

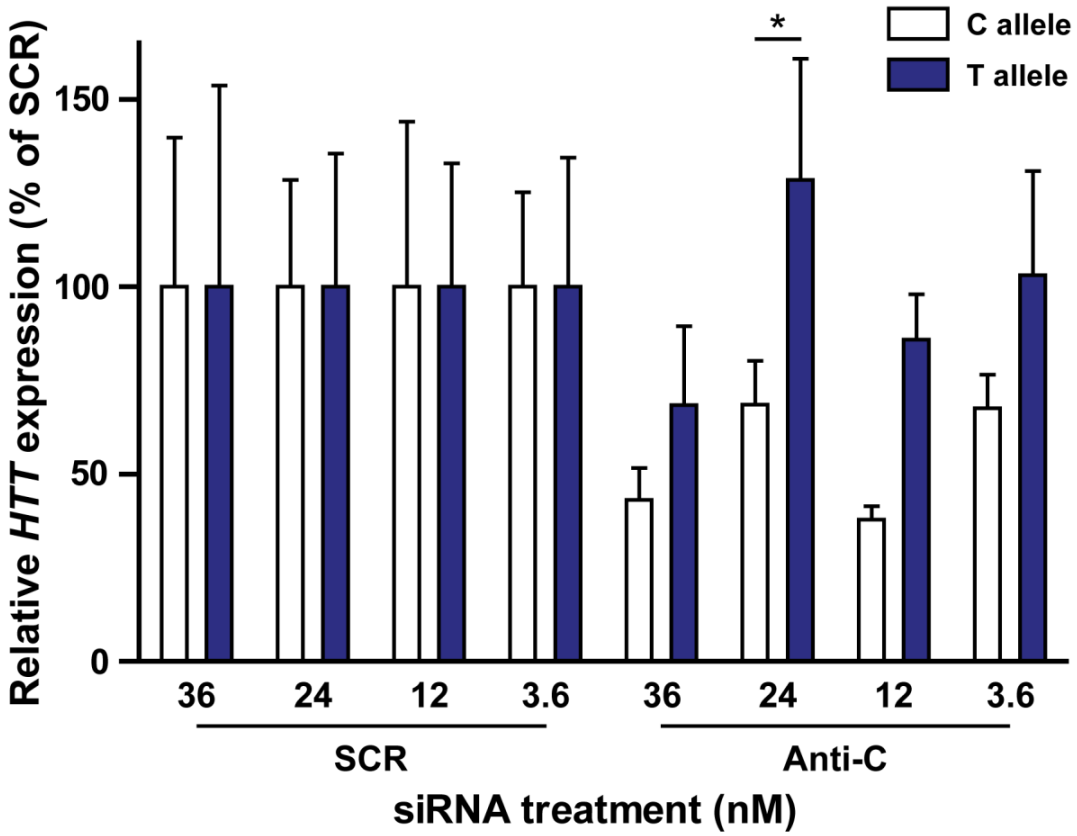

Figure 3.8. Dose-ranging analysis of siRNA targeting the C allele of rs362331. Monocyte-derived macrophages were isolated from SNP-genotyped HD patients and treated with GeRPs containing varying concentrations of siRNA targeted to the C allele of rs362331 in exon 50 of the *HTT* transcript. Expression of each SNP allele was measured after 72 h by qPCR. No significant differences were seen in the potency or selectivity of any of the siRNA concentrations tested. Data show mean expression of each SNP allele ± SEM (n = 5), statistical analysis carried out using two-way ANOVA with Bonferroni post-hoc testing. Asterisks between bars denote within treatment allele expression differences on post-hoc testing. *P < 0.05.

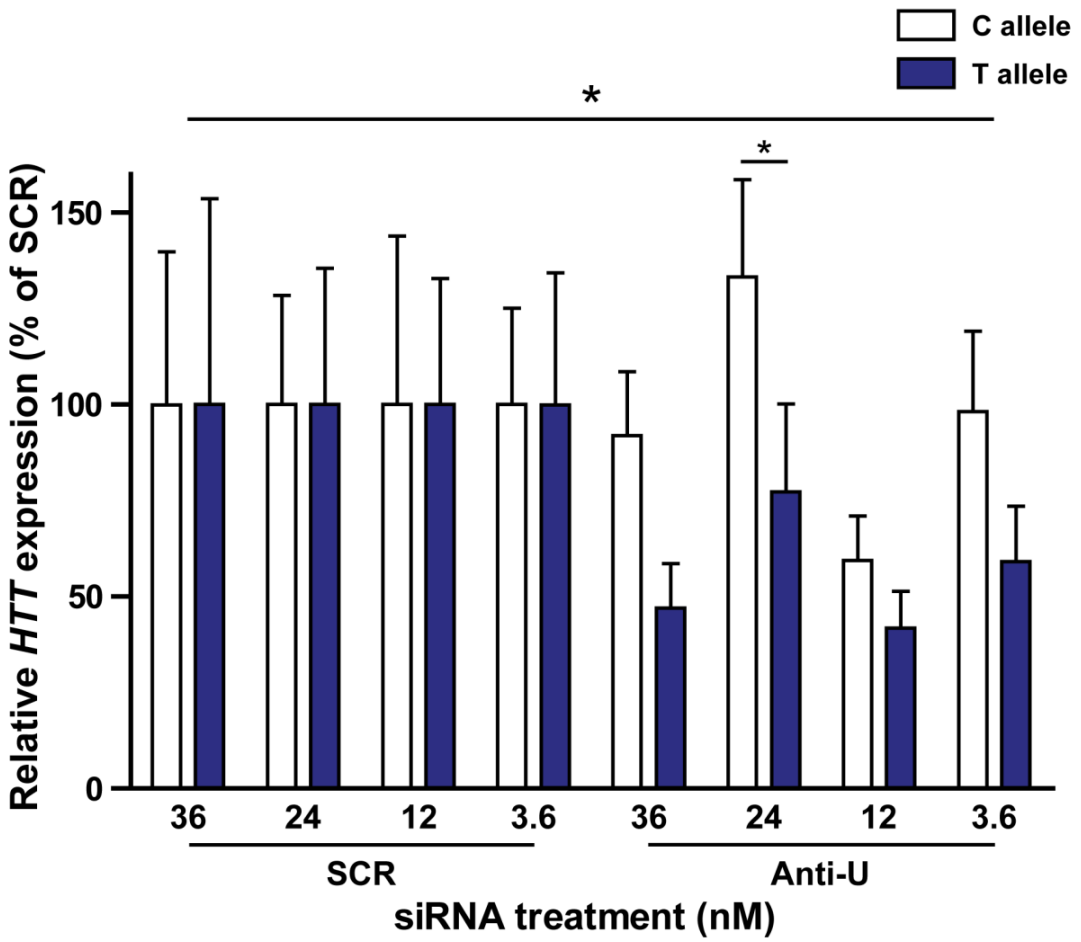

Figure 3.9. Dose-ranging analysis of siRNA targeting the U allele of rs362331. Monocyte-derived macrophages were isolated from SNP-genotyped HD patients and treated with GeRPs containing varying concentrations of siRNA targeted to the U allele of rs362331 in exon 50 of the *HTT* transcript. Expression of each SNP allele was measured after 72 h by qPCR. No significant differences were seen in the potency or selectivity of any of the siRNA concentrations tested. Data show mean expression of each SNP allele ± SEM (n = 5), statistical analysis carried out using two-way ANOVA with Bonferroni post-hoc testing. Asterisks between bars denote within treatment allele expression differences on post-hoc testing. *P < 0.05.

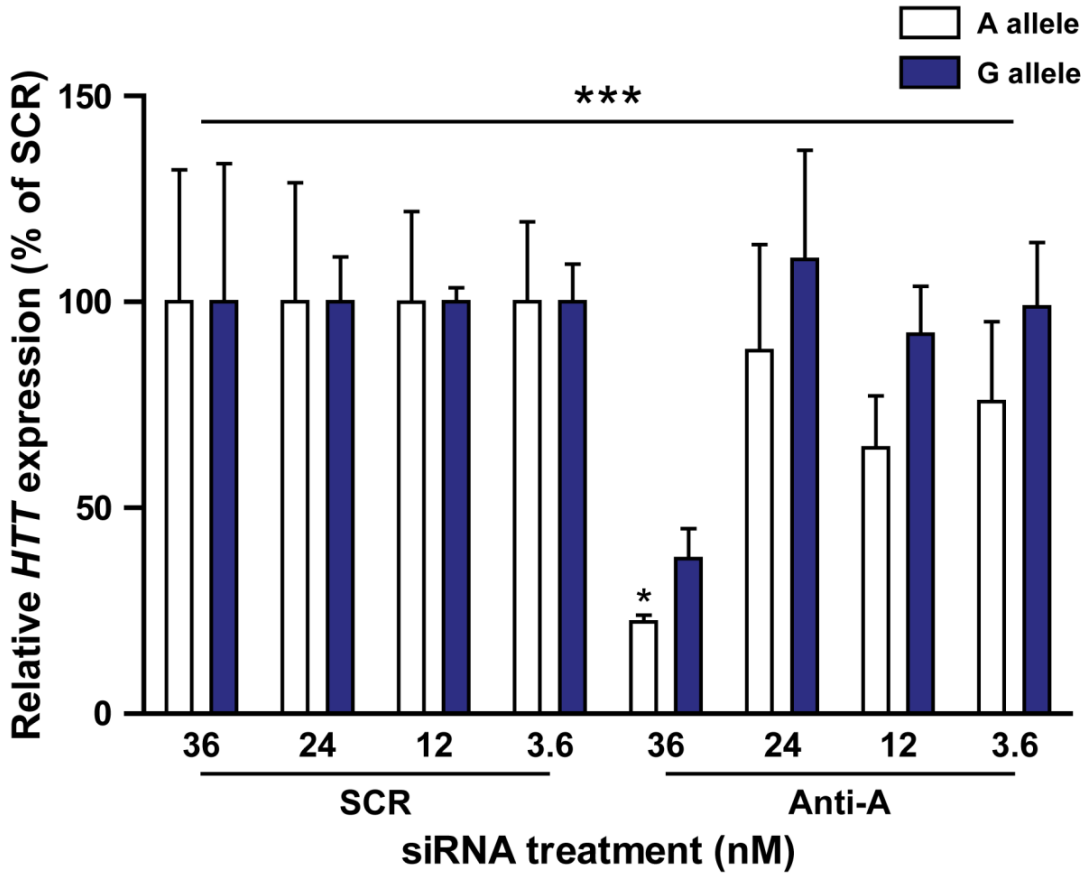

Figure 3.10. Dose-ranging analysis of siRNA targeting the A allele of rs362273. Monocyte-derived macrophages were isolated from SNP-genotyped HD patients and treated with GeRPs containing varying concentrations of siRNA targeted to the A allele of rs362273 in exon 57 of the *HTT* transcript. Expression of each SNP allele was then measured after 72 h by qPCR. No significant differences were seen in the potency or selectivity of any of the siRNA concentrations tested. Data show mean expression of each SNP allele ± SEM (n = 3), statistical analysis carried out using two-way ANOVA with Bonferroni post-hoc testing. Asterisks above bars show post-test significance compared to the same allele in the SCR-treated samples. *P < 0.05, **P < 0.01, ***P < 0.001.

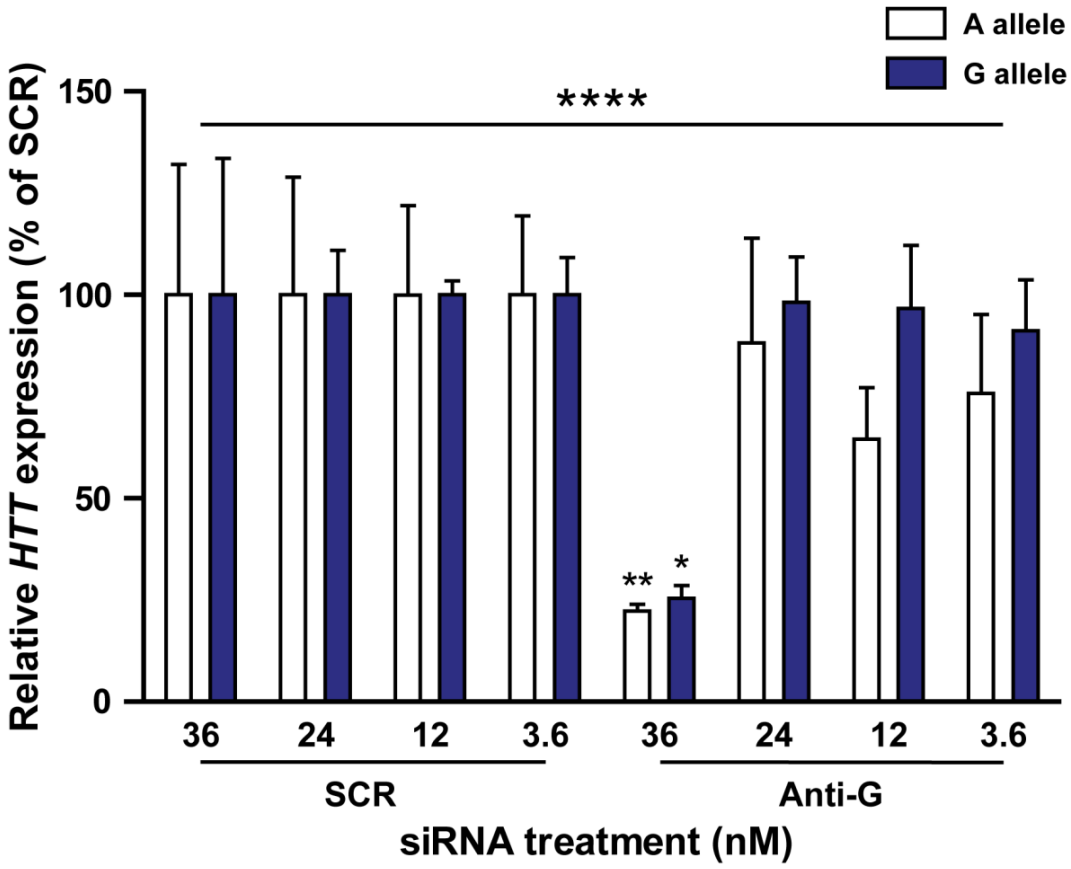

Figure 3.11. Dose-ranging analysis of siRNA targeting the G allele of rs362273. Monocyte-derived macrophages were isolated from SNP-genotyped HD patients and treated with GeRPs containing varying concentrations of siRNA targeted to the G allele of rs362273 in exon 57 of the *HTT* transcript. Expression of each SNP allele was then measured after 72 h by qPCR. No significant differences were seen in the potency or selectivity of any of the siRNA concentrations tested. Data show mean expression of each SNP allele ± SEM (n = 3), statistical analysis carried out using two-way ANOVA with Bonferroni post-hoc testing. Asterisks above bars show post-test significance compared to the same allele in the SCR-treated samples. *P < 0.05, **P < 0.01, ***P < 0.001, ****P < 0.0001.

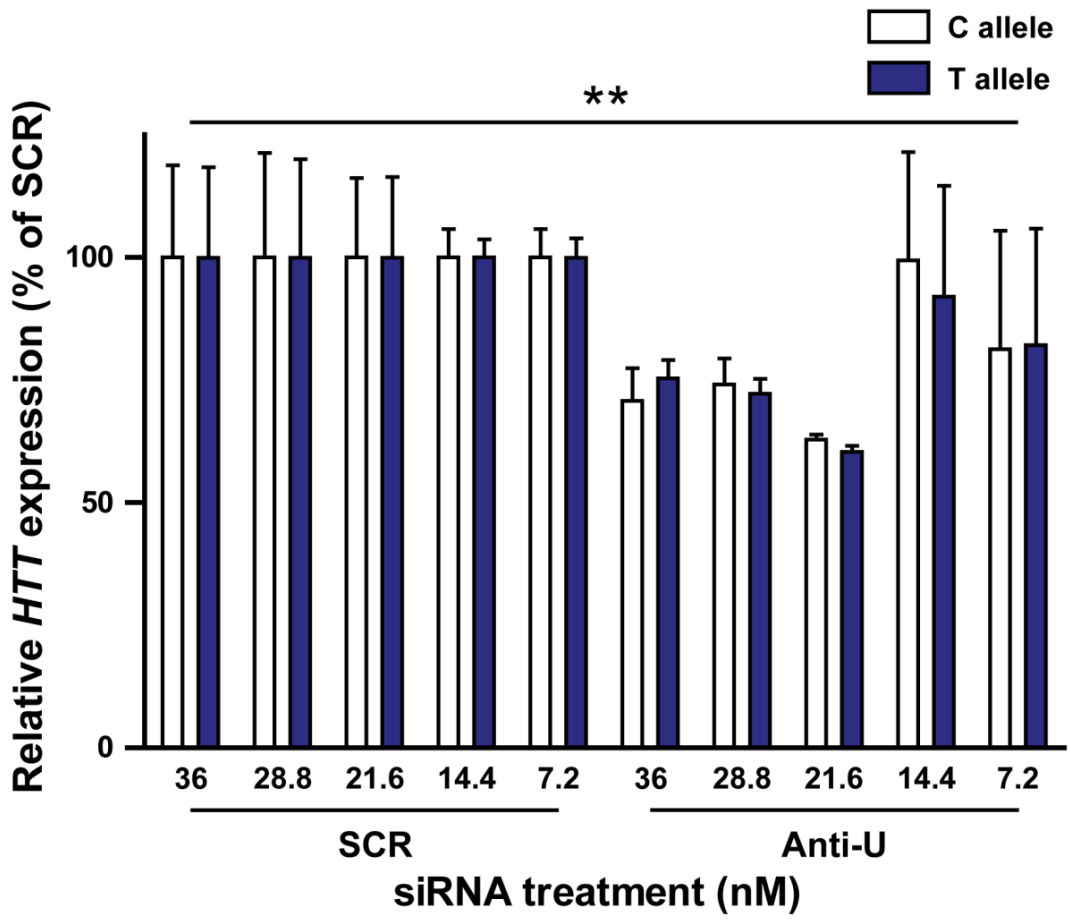

Figure 3.12. Dose-ranging analysis of siRNA targeting the U allele of rs362307. Monocyte-derived macrophages were isolated from SNP-genotyped HD patients and treated with GeRPs containing varying concentrations of siRNA targeted to the U allele of rs362307 in the 3'-UTR of the *HTT* transcript. Expression of each SNP allele was then measured after 72 h by qPCR. No significant differences were seen in the potency or selectivity of any of the siRNA concentrations tested. Data show mean expression of each SNP allele ± SEM (n = 3), statistical analysis carried out using two-way ANOVA with Bonferroni post-hoc testing. *P < 0.05, **P < 0.01.

3.5.5 Protein validation of siRNA allele-selectivity

This project has so far demonstrated highly selective SNP-targeted knockdown of *HTT* mRNA using siRNA targeted to both alleles of rs362331. However, as before it is necessary to validate mRNA readings with protein analysis. Previous work using anti-total *HTT* siRNA has demonstrated approximately 50 % total HTT protein knockdown 72 h after transfection, corresponding to a 70 % reduction in *HTT* mRNA (Träger et al., 2014); this degree of on-target mRNA knockdown was also achieved using siRNA targeted to rs362331.

To address this, siRNA targeting each allele of rs362331 was packaged into GeRPs at a dose of 36 nM, as initial experiments showed this formulation to achieve the optimal combination of potency and selectivity. As the siRNAs targeting rs362273 and rs362307 did not achieve significant selectivity during initial testing by qPCR, it was decided not to advance their use to protein studies. Monocyte-derived macrophages were isolated from peripheral blood samples donated by HD subjects heterozygous for rs362331, before being transfected with GeRPs containing either SCR, anti-total *HTT* or allele-selective siRNA. The cultures were then harvested after 72 h and the levels of both total and mHTT protein were measured by MSD assays. To identify which siRNA was targeting which *HTT* allele, PBMC pellets collected from each subject were further analysed by SLiC in order to link each SNP allele to either wild-type or m*HTT* (Liu et al., 2008). Three of the subjects used for protein analysis had linkage of the C allele of rs362331 to m*HTT* (Fig. 3.13), while five had linkage of the T allele to m*HTT* (Fig. 3.14); samples from these subject groups were analysed separately.

Consistent with previous work, treatment of C-linked subjects with anti-total *HTT* siRNA resulted in an approximately 50 % reduction in both total and mHTT protein levels. Furthermore, treatment with both allele-selective siRNAs resulted in a significant decrease in total HTT protein, the potency of which did not differ between the anti-U and anti-C siRNAs. This is consistent with the qPCR data presented earlier in this chapter. However, preferential suppression of mHTT protein was not seen following treatment with anti-C siRNA compared to anti-U siRNA.

When analysing samples with linkage of the T allele to m*HTT*, significant knockdown of total HTT was again seen following treatment with each allele-selective siRNA. This was equivalent to the HTT knockdown seen in the C-linked samples, demonstrating that the effect of each siRNA on total HTT is independent of which SNP allele is linked to m*HTT*. However, significant knockdown of mHTT was only seen following treatment with the anti-U siRNA, with no significant difference in mHTT levels being seen between the SCR and anti-C treated samples. Furthermore, no difference in mHTT levels was seen between the anti-total *HTT* and anti-U treated samples, while mHTT levels were found to be significantly higher in the anti-C treated samples compared to the anti-total *HTT* treated samples. This demonstrates that preferential suppression of mHTT is achieved in T-linked subjects following treatment with anti-U compared to anti-C siRNA, and shows that the selective knockdown seen with mRNA also translates to protein studies.

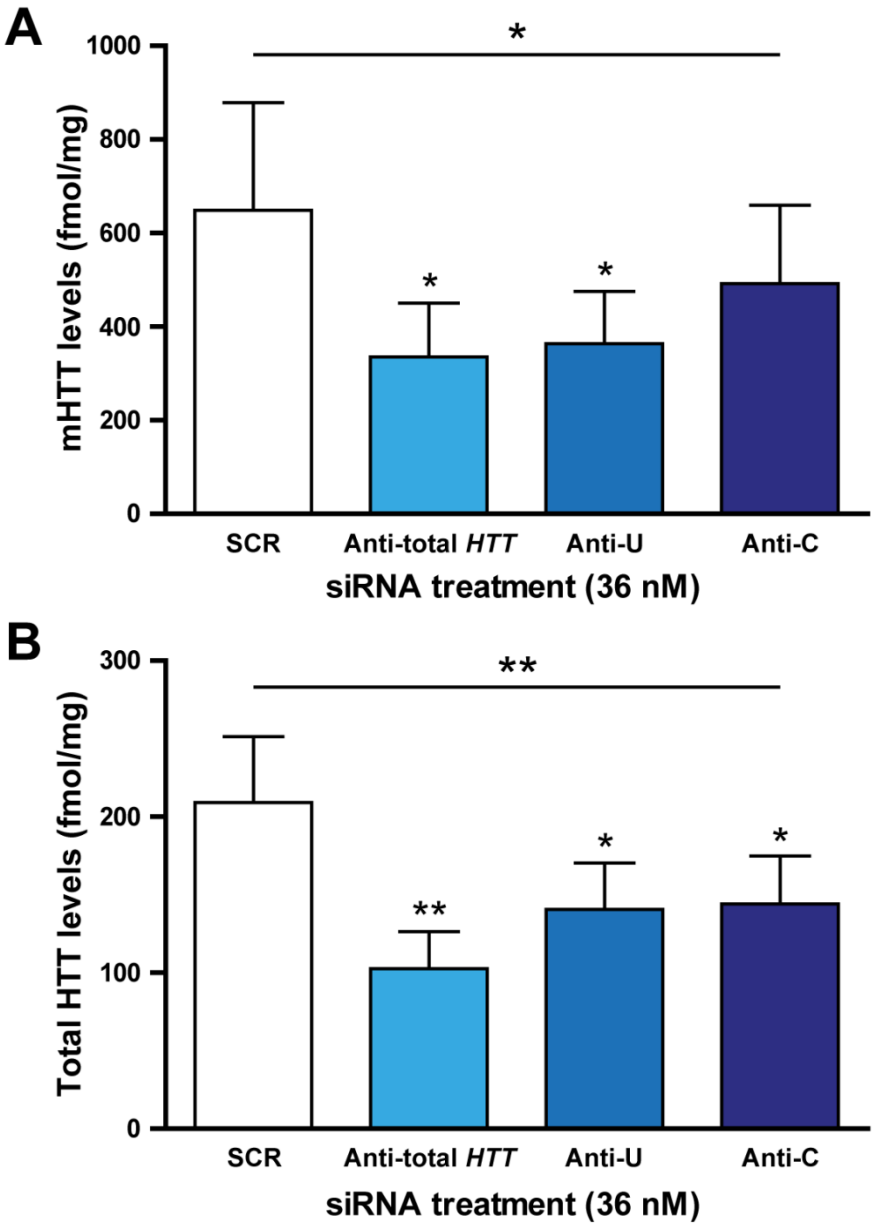

Figure 3.13. Analysis of HTT protein knockdown in HD subjects with the C allele of rs362331 linked to m*HTT*. Monocyte-derived macrophages were isolated from HD patients heterozygous for rs362331 with linkage of the C allele to m*HTT*, before treating with GeRPs containing either SCR, anti-total *HTT* or allele-selective siRNA targeted to each allele of rs362331. Expression of (A) mutant and (B) total HTT protein was measured after 72 h using MSD assays, before normalisation to total protein content as measured by BCA assays. Data show mean protein levels ± SEM (n = 3), statistical analysis carried out using one-way ANOVA with Tukey post-hoc testing. Asterisks above bars show post-test significance compared to the SCR-treated samples. *P < 0.05, **P < 0.01.

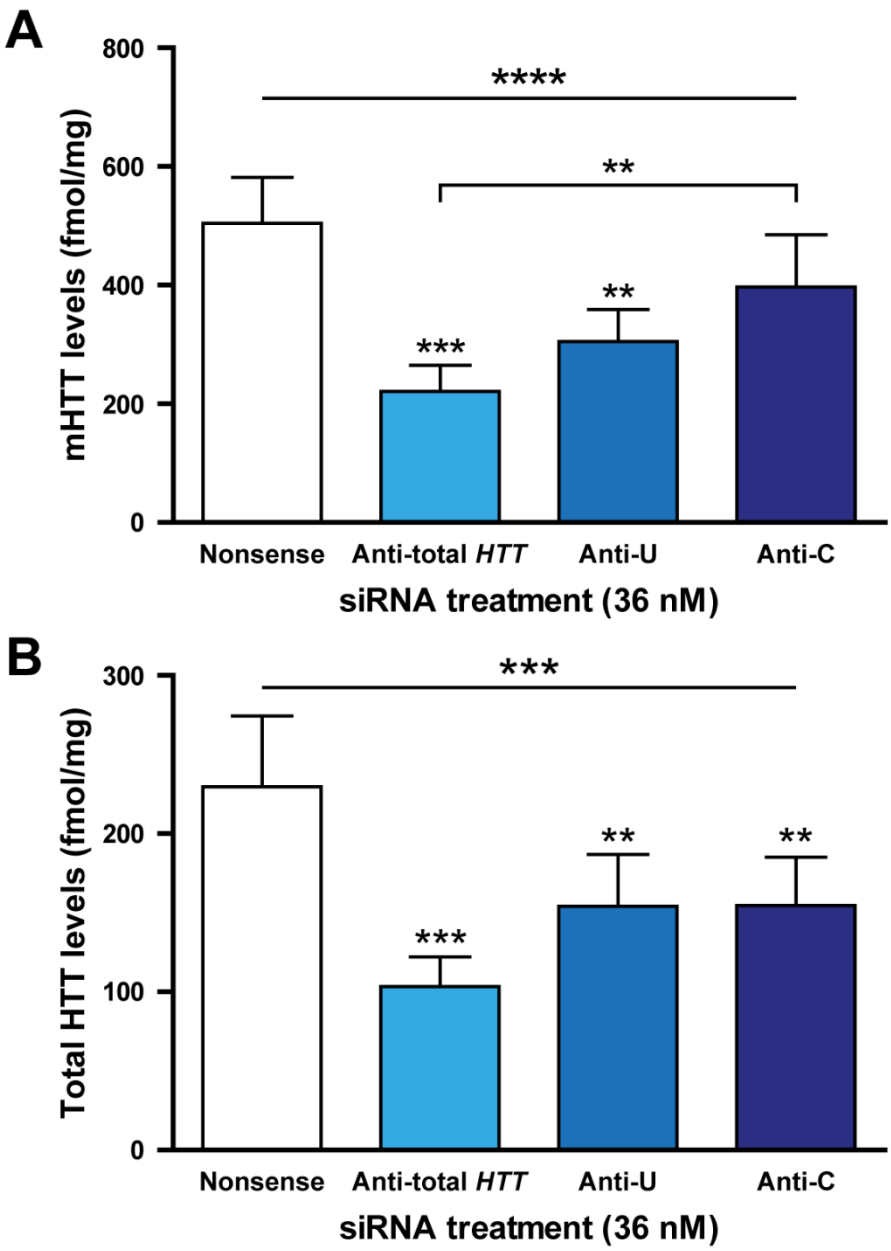

Figure 3.14. Analysis of HTT protein knockdown in HD subjects with the T allele of rs362331 linked to m*HTT*. Monocyte-derived macrophages were isolated from HD patients heterozygous for rs362331 with linkage of the T allele to m*HTT*, before treating with GeRPs containing either SCR, anti-total *HTT* or allele-selective siRNA targeted to each allele of rs362331. Expression of (A) mutant and (B) total HTT protein was measured after 72 h using MSD assays, before normalisation to total protein content as measured by BCA assays. Data show mean protein levels ± SEM (n = 5), statistical analysis carried out using one-way ANOVA with Tukey post-hoc testing. Asterisks above bars show post-test significance compared to the SCR-treated samples. *P < 0.05, **P < 0.01, ***P < 0.001, ****P < 0.0001.

3.5.6 Analysis of HD myeloid cell cytokine production following allele-selective HTT suppression

Previous work has shown that transfection of HD myeloid cells with anti-total *HTT* siRNA results in a significant decrease in the production of IL-6, IL-8 and TNFα following stimulation with LPS and IFN-γ (Träger et al., 2014). To address whether allele-selective suppression of mutant and/or wild-type HTT has similar effects, monocyte-derived macrophages were isolated from HD subjects heterozygous for rs362331, before being transfected with GeRPs containing 36 nM of SCR, anti-total *HTT* or allele-selective siRNA. The cells were stimulated with LPS and IFN-γ 72 h after transfection, before the supernatants were harvested after a further 24 h and analysed using MSD assays. SNP linkage of rs362331 to m*HTT* was again carried out using the SLiC protocol; two were found to have linkage of the C allele to m*HTT*, while three had linkage of the T allele to m*HTT*. As no significant differences were seen in the mRNA knockdown provided by the anti-U and anti-C siRNAs, samples were grouped for analysis into anti-wild-type and anti-mutant *HTT*.

Consistent with previous data, treatment with anti-total *HTT* siRNA produced a significant reduction in cytokine production for all three cytokines that were analysed (Fig. 3.15). Interestingly, targeting of both wild-type and m*HTT* with allele-selective siRNA also produced a significant reduction in the production of all three cytokines. This was the case regardless of whether wild-type or m*HTT* was targeted, and there were no significant differences in the levels of any of the cytokines between the allele-selective treatment groups. This suggests that wild-type HTT may also play a role in immune cell function,

and is consistent with data showing that total HTT-lowering in control cells significantly reduces their cytokine response to LPS (Träger et al., 2014).

While post-hoc testing did not reveal any statistically significant differences in cytokine production between the samples treated with anti-total *HTT* and allele-selective siRNA, the mean levels of both IL-6 and TNFα were more than 50 % lower following total *HTT* knockdown compared to selective knockdown of either wild-type or m*HTT*. The reduction of both of these cytokines was also found to be more significant in the anti-total *HTT* samples compared to SCR control ($p < 0.01$ compared to $p < 0.05$). This suggests that the overall HTT load in a cell may be crucial to determining its cytokine production, as the reduced IL-6 and TNFα suppression seen in the allele-selective siRNA-treated samples may be due to the sparing of one *HTT* allele compared to total *HTT*-lowering. Regardless, these data demonstrate that the allele-selective suppression of both wild-type and mHTT is able to ameliorate the hyper-reactive cytokine phenotype of HD myeloid cells.

Figure 3.15. Analysis of HD myeloid cell cytokine production following allele-selective HTT suppression. Monocyte-derived macrophages were isolated from SNP-genotyped HD patients and treated with GeRPs containing either SCR, anti-total *HTT* or allele-selective siRNA targeted to each allele of rs362331. Linkage of each SNP allele to either wild-type or m*HTT* was determined using the SLiC protocol. After 72 h the macrophages were stimulated with LPS and IFNγ, before the culture supernatants were collected after a further 24 h and analysed using MSD assays. Cytokine values were normalised to total protein content as measured by BCA assays. Data show mean cytokine levels ± SEM ($n = 5$ for IL-6 and TNFα, $n = 4$ for IL-8), statistical analysis carried out using one-way ANOVA with Tukey post-hoc testing. Asterisks above bars show post-test significance compared to the SCR-treated samples. *$P < 0.05$, **$P < 0.01$, ***$P < 0.001$.

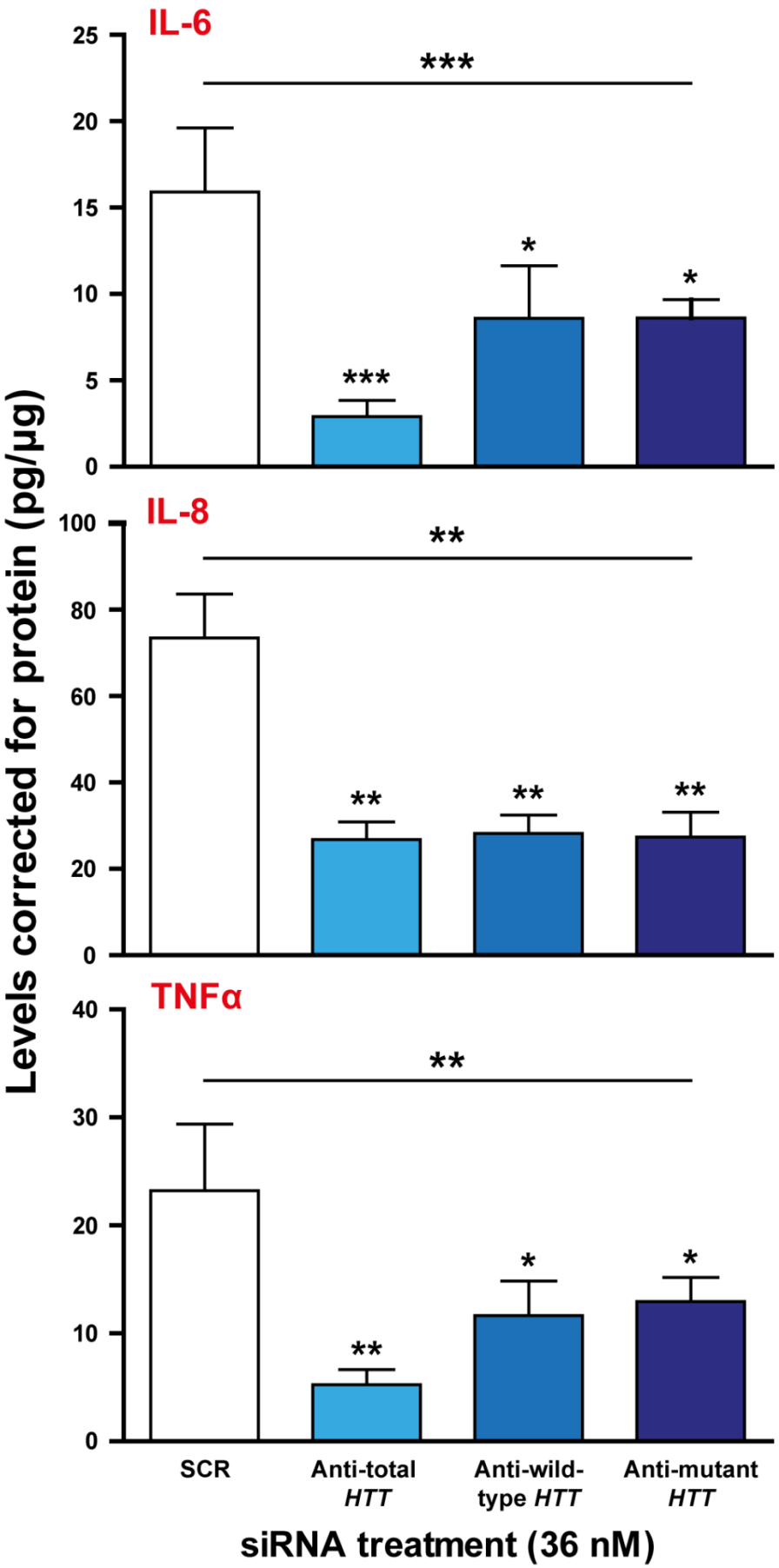
IL-6
IL-8
TNFα
Levels corrected for protein (pg/µg)
SCR
Anti-total HTT
Anti-wild-type HTT
Anti-mutant HTT
siRNA treatment (36 nM)

3.6 Discussion

The monogenic nature of HD makes it an ideal target for treatment by PTGS, with suppression of the mHTT protein being shown to ameliorate pathology and improve the disease course in animal models (Drouet et al., 2009; Kordasiewicz et al., 2012). Indeed, clinical trials are ongoing to carry out non-selective HTT-lowering in human HD patients using intrathecal infusion of ASOs, with the aim of suppressing mHTT by 50 % (Ionis Pharmaceuticals, 2015). Work presented in this chapter demonstrates allele-selective suppression of mHTT in primary *ex vivo* patient cells, using siRNA targeted to rs362331 in exon 50 of the *HTT* transcript. siRNA targeted to the U allele of rs362331 was able to achieve 74 % on-target knockdown with only 17 % suppression of the off-target C allele, while siRNA targeted to the C allele of rs362331 was able to achieve 63 % on-target knockdown with only 30 % off-target suppression of the U allele. This discrimination was found to be highly statistically significant at an siRNA dose of 36 nM. Crucially, the degree of on-target knockdown was equivalent to that provided by the previously used anti-total *HTT* siRNA, while no significant difference was seen between expression of the off-target allele compared to SCR control for either siRNA. Knockdown selectivity was also found to translate to the protein level, with only treatment with anti-U and not anti-C siRNA resulting in a significant decrease in mHTT protein when studying samples with linkage of the T allele of rs362331 to m*HTT*. As expected, the degree of total HTT suppression was independent of which SNP allele was linked to m*HTT*. This is a significant advance in HD therapeutics, as previous work has largely been limited to cell lines and animal models (Carroll et al., 2011; Drouet et al., 2014).

This study also demonstrates the possibility of carrying out a patient-centred workflow comprising SNP genotyping, SNP linkage and allele-selective silencing tailored specifically to an individual's genotype in a small cohort. This is in contrast to previous studies that have largely made use of (often homozygous) pre-genotyped cell lines and animal models, and presents a significant advance in the potential use of personalised genomic medicine. These techniques will form the basis of treatment if allele-selective silencing is to be used in the clinic, and this study demonstrates the first instance of their being used in combination, instead of individually as part of a technical study. While this provides valuable insight into the potential applications of this technology, there are a number of issues that need to be addressed.

Work presented in this chapter reinforces previous studies demonstrating that the potency and selectivity of m*HTT* suppression varies considerably depending on the specific SNP site being targeted (Carroll et al., 2011). Here, highly significant selectivity was achieved using siRNAs targeted to both alleles of rs362331. In contrast, considerable off-target knockdown was seen when targeting both alleles of rs362273, while siRNA targeting the U allele of rs362307 were not found to be selective at all. This variation applies even between SNPs that have an equivalent base mismatch, as both rs362331 and rs362307 are C/T in heterozygous individuals. This is likely due to the nucleotide sequence and tertiary structure of the transcript surrounding the base mismatch (Southwell et al., 2014), and demonstrates that the choice of SNP to target is a crucial issue to address during the preclinical stages of allele-selective drug design. This is particularly relevant given the limited number of potential sequences that may be used to target

each SNP, in contrast to the thousands which are available for the non-selective lowering of both *HTT* alleles (Sah and Aronin, 2011). This problem is exacerbated when using siRNAs instead of ASOs, as over 90 % of *HTT* SNPs are intronic and therefore not targetable by siRNA (Keiser et al., 2016).

A further issue arising from this observation is that it should not be assumed that the SNPs with the highest prevalence of heterozygosity will be targetable with allele-selective therapeutics. The rs362307 SNP in the 3'-UTR of *HTT* is the most prevalent SNP in Caucasian HD patients, with a heterozygosity rate of approximately 48.6 % (Pfister et al., 2009). However, siRNAs targeted to this SNP were unable to achieve selectivity despite carrying out a comprehensive dose-ranging analysis. This suggests that it may be necessary to target less prevalent SNPs in order to improve selectivity. As a result, it may be that predictions about what proportion of HD patients may be treated are overly optimistic, if additional prevalent SNPs are also found to be unsuitable for therapeutic targeting.

Furthermore, this study demonstrates that oligonucleotide therapeutics that have been developed in cell models must be validated in primary human cells to confirm their selectivity. The siRNAs targeting rs362273 and rs362307 were previously shown to be selective when co-transfected into HeLa cells with a luciferase reporter (Pfister et al., 2009), yet did not retain their selectivity when used to transfect HD patient myeloid cells. This may be because the siRNAs were only used to suppress a short construct when they were tested in HeLa cells, instead of the full-length *HTT* mRNA that is present in patient cells. This may be as much a reflection on the limitations of

the luciferase model as it is on the quality of the siRNA; regardless, the point remains that validation in primary cells is vital for therapeutic development.

Indeed, it should perhaps not be surprising that some of the siRNAs tested were unable to achieve selectivity, as they are aiming to discriminate between a single base mismatch with identical nucleotide sequences on either side. The 3'-UTR SNP rs362307 is particularly challenging for allele-selective silencing, as the surrounding sequence is extremely GC rich (Sah and Aronin, 2011), with the SNP itself comprising a pyrimidine (C/T) mismatch (purine (A/G) mismatches typically allow greater selectivity). Nucleotide sequences utilising single base mismatches have been shown to be inadequate when targeting this SNP (Pfister et al., 2009), which has now generated poor discrimination across multiple research groups and studies (Drouet et al., 2014). While previous studies have shown that adding an additional base mismatch is able to improve selectivity for the on-target allele (Pfister et al., 2009), the benefits of this approach are clearly limited. One potential solution may be chemical modification of the siRNAs in question, as chemical modification of ASOs has been shown to improve allele-selectivity (Østergaard et al., 2013). However, it should be noted that some chemical modifications have been found to cause toxicity. This shows that the discrimination achieved by targeting rs362331 should by no means be regarded as trivial, given the significant technical challenges involved.

Perhaps one of the most important insights to be gained from this study relates to the significant practical considerations that will be associated with taking allele-selective silencing to clinical trials. While this study was able to overcome the technical hurdles involved in genotyping a large cohort of HD

patients and individually linking each SNP allele to either wild-type or m*HTT* in a subset of subjects, it remains to be seen whether this will be feasible in a clinical setting. Crucially, it is essential that the genotyping process carried out before dosing HD patients is 100 % specific, as incorrect genotyping will lead to the administration of an siRNA that selectively suppresses wild-type while preserving mHTT. This is a major safety concern, especially given the technical complexity of the SLiC protocol, which is a complicated multi-step procedure carried out over several days (Liu et al., 2008). Such a technique is unlikely to ever be available in a standard clinical laboratory, and would likely be confined to specialist facilities.

Furthermore, the technical challenges associated with allele-selective silencing are compounded by the relatively low prevalence of heterozygous SNPs in the HD patient population. The rs362331 SNP that provided optimal selectivity in this study is only heterozygous in 39.4 % of HD subjects, with no linkage of either allele to m*HTT* (Pfister et al., 2009); this means that two siRNAs would be required to treat every patient heterozygous for this SNP. This still leaves a majority of the patient population who would be unable to be treated by targeting this SNP, with multiple SNPs needing to be utilised to treat a majority of HD patients. Current estimates suggest that 75 % of patients may be treatable by targeting three SNP sites (Pfister et al., 2009), however this does not take into account the fact that some of the most prevalent SNPs (e.g. rs362307) may not be amenable to allele-selective silencing. While the development of siRNAs to target three SNP sites may not appear daunting in a preclinical setting, it must be appreciated that under current legislation each siRNA would need to be licensed as an individual

drug, with no provision available for combined trials of multiple siRNAs. It is therefore questionable whether drug companies are likely to invest the vast resources required to carry out clinical trials for even a single allele-selective siRNA, let alone the multiple trials that would be required to cover a majority of HD patients. It has been suggested that using two therapeutics targeted to each allele of a single SNP would allow treatment of the entire patient population by offering selective knockdown for heterozygous patients and non-selective knockdown for homozygous patients (Skotte et al., 2014). However, this strategy would still require accurate genotyping and twice the resources needed to carry out clinical trials of non-selective HTT-lowering

Although the above issues suggest that allele-selective suppression is unlikely to be used as a therapeutic for HD, there is considerable evidence that suppression of wild-type HTT in the adult brain is well tolerated. While conditional *Htt* knockout has been shown to cause neurodegeneration in mice (Dragatsis et al., 2000), *Htt* depletion at later time points was associated with reduced neuronal pathology. This suggests that, while HTT is essential for neuronal development during embryogenesis (Godin et al., 2010; Tong et al., 2011), its role in later life is less vital. This hypothesis was recently advanced by a study of inducible *Htt* knockout mice showing that, while ubiquitous *Htt* knockout was associated with 95 % death after two months of life, knockout after four months and eight months was associated with 70 % and 95 % survival respectively (Wang et al., 2016). Selective knockout of neuronal *Htt* was then found to have no effect on survival after 4 months of life, while no deficits were found when studying either motor performance or brain volume following knockout at these later time points.

Crucially, death at two months was found to be due to acute pancreatitis caused by degeneration of pancreatic acinar cells, demonstrating that *Htt* knockout in mice causes age-related death that is not due to its depletion in neurons. This suggests that concerns over wild-type HTT suppression may be exaggerated when limited to the adult CNS.

This conclusion is supported by data showing that wild-type suppression is well tolerated in both mice and non-human primates. Three studies of non-selective RNAi injection in the mouse striatum did not find any adverse effects up to either four or five months after treatment (McBride et al., 2008; Boudreau et al., 2009; Stanek et al., 2014). Indeed, a further study demonstrated that transient *Htt*-lowering does not cause any damage up to 9 months after treatment, while a sustained 75 % *Htt* reduction in the normal adult mouse brain does not affect motor performance up to at least four months (Kordasiewicz et al., 2012). This work was expanded to include non-human primates, where infusion of ASOs into the CNS of rhesus monkeys was tolerated for up to eight weeks after the termination of a twenty-one day treatment period. Furthermore, a 45 % reduction of *HTT* expression in the rhesus putamen does not induce motor deficits or neuronal degeneration up to six weeks after the injection of RNAi (McBride et al., 2011); this was later extended to show that partial RNAi-mediated HTT-lowering is well tolerated in the rhesus striatum for at least six months (Grondin et al., 2012).

Indeed, excluding drug-related toxicity there is currently no evidence that siRNA or ASO-medated HTT-lowering is detrimental in any animal model that has been studied to date. This may be due to the fact that siRNAs and ASOs only produce partial HTT-lowering of approximately 50 %, allowing the

remaining wild-type protein to maintain normal cellular function; it may also be due to the age-related development of compensatory mechanisms (Wang et al., 2016). Although it is not possible to accurately scale up animal studies into humans, this work provides support for the use of non-selective HTT-lowering in HD. While the results of the first-into-man HTT-lowering trials will still be needed to draw firm conclusions on what degree of wild-type HTT suppression is tolerated in the human CNS, it may well be that the success of total HTT-lowering eliminates the need for allele-selective silencing.

However, the difficulties associated with using allele-selective silencing in a clinical setting should not be allowed to obscure the very real benefits it offers as a research tool. The majority of previous work has used conditional *HTT* knockout or total-HTT-lowering to examine the effects of suppressing mHTT on cellular function (see Section 1.2.2). While undoubtedly useful, these studies have been unable to definitively distinguish between the roles of wild-type and mHTT, as both are affected by these techniques. An example of this can be seen in the fact that control myeloid cells also exhibit reduced cytokine responses to LPS following HTT-lowering (Träger et al., 2014), and it is therefore uncertain to what degree the reduction in cytokine production by HD myeloid cells is due to either wild-type or mHTT-lowering. Allele-selective silencing may now be used to dissect the specific functions of wild-type and mHTT in a wide range of cell types, providing access to a level of functional insight that was not previously available. The advent of iPSC technology further raises the possibility of creating isogenic cell lines that are heterozygous for specific SNPs (Park et al., 2008), thereby forgoing the genotyping process required when investigating primary human cells.

Work presented in this chapter takes some of the first steps towards the specific investigation of wild-type and mHTT function, using allele-selective suppression to investigate the cytokine response of HD myeloid cells to LPS. If HTT's effects on cytokine production were limited exclusively to the mutant form of the protein, it would be expected that selective mHTT-lowering would produce a significantly greater reduction in cytokine levels compared to selective lowering of the wild-type. However, no significance differences were seen in the levels of any of the three cytokines tested between samples treated with either anti-mutant or anti-wild-type siRNA. This suggests that wild-type HTT may have an as yet undefined role in normal immune cell function, and is consistent with previous work showing that cytokine production by control myeloid cells in response to LPS is also reduced following total HTT-lowering (Träger et al., 2014).

Further insight may be provided by comparing the effects of total to allele-selective HTT-lowering. Although none of the differences reached statistical significance, the mean IL-6 and TNFα levels measured following total HTT-lowering were less than 50 % of those measured following selective lowering of either the mutant or wild-type allele. This suggests that total cellular HTT load may be the key factor influencing cytokine production, as the sparing of one allele by the allele-selective siRNAs will result in less overall knockdown than that achieved by anti-total *HTT* siRNA. However, considerable further work will be required to confirm or reject this hypothesis, the full extent of which is beyond the scope of this thesis. Regardless, these data provide strong evidence that wild-type HTT has a novel immune cell function.

3.7 Summary

Work presented in this chapter demonstrates for the first time the allele-selective suppression of mHTT in primary human *ex vivo* patient cells. Following optimisation of the GeRP transfection protocol, a large cohort of HD patients was genotyped to identify individuals who were heterozygous for three SNPs in the *HTT* gene. A panel of siRNAs targeting each SNP was then screened using monocyte-derived macrophages isolated from genotyped HD patients. While the siRNAs targeting rs362273 in exon 57 and rs362307 in the 3'-UTR were not found to offer adequate selectivity of mRNA knockdown, siRNAs targeting rs362331 in exon 50 produced highly significant selectivity between alleles, with on-target suppression equivalent to that seen using anti-total *HTT* siRNA. Unfortunately, the selectivity offered by each of these siRNAs was not found to be improved by lowering the concentration packaged into each GeRP. The mRNA suppression provided by the anti-rs362331 siRNAs was further validated by analysis of HTT protein expression, with only treatment with anti-U and not anti-C siRNA found to provide significant knockdown of mHTT in patients with linkage of the T allele of rs362331 to m*HTT*. Finally, the effect of allele-selective *HTT*-lowering on the hyper-reactive cytokine phenotype of HD myeloid cells was investigated, with selective suppression of both wild-type and m*HTT* found to produce a significant reduction in IL-6, IL-8 and TNFα levels. Surprisingly, cytokine production following selective m*HTT* suppression was not found to differ from that following selective wild-type suppression, suggesting that wild-type HTT may have a novel role in immune cell function.

4 Whole transcriptome analysis of HD myeloid cells

4.1 Background

Myeloid cells are perhaps the most well characterised of any peripheral immune cell subset in HD, with previous *ex vivo* studies demonstrating that human HD myeloid cells exhibit hyper-reactive cytokine responses to LPS (Träger et al., 2014), in addition to deficits when migrating to chemotactic stimuli and phagocytosing fluorescent beads (Kwan et al., 2012b; Träger et al., 2015). These changes are mirrored in both knock-in cell lines and mouse models of HD, suggesting that they are the result of a cell-intrinsic effect of mHTT expression. This is further supported by the fact that the hyper-reactive phenotype of HD myeloid cells is reversible following HTT-lowering with anti-total *HTT* siRNA (Träger et al., 2014).

However, studies to date have almost exclusively focused on the phenotypic abnormalities that occur in response to stimulation, and very little information is available on whether these cells are also abnormal in their basal, unstimulated state. Indeed, there is currently no evidence that HD myeloid cells have increased resting expression of the proinflammatory cytokines that are upregulated in response to LPS (Träger et al., 2014). This raises uncertainty about whether mHTT only affects HD myeloid cells following stimulation, or if there is an underlying mechanism producing resting dysfunction that is responsible for the changes seen once the cells are

activated. Work on a murine HD microglial line revealed a cell-autonomous priming effect of mHTT, leading to an increase in resting proinflammatory gene expression (Crotti et al., 2014); this was linked to increased levels of the transcription factor PU.1. This raises the possibility that the hyper-reactive LPS response of HD myeloid cells is due to the baseline effects of mHTT expression, although this hypothesis is yet to be investigated. The potential existence of resting dysfunction in HD myeloid cells has important implications for targeting peripheral immunity as a novel HD therapeutic, as intrinsic pathology is more likely to be treatable over long periods without the need to time interventions to coincide with specific inflammatory events.

Furthermore, while the phenotypic effects of mHTT are relatively well characterised, considerably less is known about its effect on the myeloid cell transcriptome. Transcriptional dysregulation is a key feature of HD pathogenesis (Hodges et al., 2006), and occurs via a number of mechanisms including the sequestration of transcription factors, direct binding of mHTT fragments to DNA, and changes in the activity of intracellular signalling pathways responsible for regulating gene expression (Seredenina and Luthi-Carter, 2012). Mutant HTT has been shown to activate the NFκB pathway by directly interacting with the IKK complex (Khoshnan et al., 2004); this is associated with hyper-reactivity in HD myeloid cells, which exhibit an exaggerated NFκB response to LPS, both in the magnitude of the initial response and in the time taken to return to baseline (Träger et al., 2014). However, there is currently no evidence that HD myeloid cells also display increased NFκB activity in the resting state. Furthermore, the complexity of intracellular signalling downstream of TLR4 necessitates the investigation of

additional pathways to build up a complete profile of the likely mechanisms underlying HD myeloid cell dysfunction (Akira and Takeda, 2004).

Numerous transcriptional changes have been demonstrated in previous studies of HD peripheral blood cells (Borovecki et al., 2005; Runne et al., 2007; Mastrokolias et al., 2015); however, these were largely carried out on heterogeneous cell populations and have rarely been validated between studies. Therefore, the study of individual cell populations using modern sequencing technology is required to characterise the specific transcriptional changes associated with mHTT expression, in addition to determining whether HD immune dysfunction also exists in the absence of stimulation.

4.2 Aims

1. To carry out whole transcriptome analysis of unstimulated and stimulated primary human HD and control monocytes using RNA-Seq.

2. To identify functional gene sets that are enriched in unstimulated and stimulated HD monocytes compared to control using GSEA.

3. To identify upstream regulators that may be responsible for mediating the transcriptional changes seen in HD monocytes using IPA®.

4. To functionally investigate potential changes in the activation states of specific intracellular signalling pathways in HD myeloid cells.

5. To characterise the effects of HTT-lowering on the transcriptome of HD myeloid cells.

4.3 Methods

PBMCs were isolated using density centrifugation (Section 2.4.1), before $CD14^+$ monocytes were isolated by magnetic cell sorting (Section 2.4.2). Monocyte stimulation was carried out using 2 µg/ml LPS and 10 ng/ml IFNγ for 4 h, before RNA was extracted using the RNeasy Mini Kit (Section 2.7.1) and its integrity was confirmed using a 2100 Bioanalyzer (Section 2.7.3). RNA samples were analysed by RNA-Seq (Section 2.8), before the raw data files were used for differential expression, splicing, GSEA and IPA® analyses (Section 2.10). Analysis of NFκB, ERK and p38 MAPK signalling activity was carried out by Western blotting (Section 2.11.4). Potential reversal of gene expression changes following HTT-lowering was investigated using SYBR Green qPCR (Section 2.7.5) following transfection with SCR and anti-total *HTT* siRNA-containing GeRPs (Section 2.5.2). Statistical analysis was carried out according to Section 2.14.2.

4.4 Contributions

Work presented in this chapter was carried out in collaboration with UCL Genetics Institute and Cardiff University School of Medicine. Sample collection, myeloid cell culture and RNA isolation were carried out by James Miller, before the samples were shipped to deCODE Genetics, Iceland for analysis by RNA-Seq. Differential expression, splicing and IPA® analyses were then carried out by Dr Kitty Lo, while GSEA was carried out by Professor Peter Holmans. The processed data was then returned to James Miller for biological analysis. Western blotting experiments were carried out by James Miller with assistance from Dr Lucy Carty, while qPCR experiments were carried out by James Miller. Cytoscape figures were generated in collaboration with Dr Timothy Stone. Findings presented in this chapter were published in Human Molecular Genetics (full manuscript included in the Appendices of this thesis):

Miller, J.R., Lo, K.K., Andre, R., Hensman Moss, D.J., Träger, U., Stone, T.C., Jones, L., Holmans, P., Plagnol, V., Tabrizi, S.J. 2016. RNA-Seq of Huntington's disease patient myeloid cells reveals innate transcriptional dysregulation associated with proinflammatory pathway activation. *Hum Mol Genet* [online]. Available from: doi: 10.1093/hmg/ddw142.

4.5 Results

4.5.1 Sample collection and data processing

The lack of existing knowledge regarding transcriptional alterations in HD monocytes necessitates a broad approach to gene expression profiling in these cells. To address this, $CD14^+$ monocytes were isolated from peripheral blood samples donated by thirty manifest HD patients and thirty-three controls. All of the HD patients had early or moderate stage disease to control for the potential effects of disease stage on gene expression (Seredenina and Luthi-Carter, 2012), while all subjects were non-smokers in order to eliminate the myriad effects of smoking on the monocyte transcriptome (Zeller et al., 2010). Following isolation, monocytes were cultured with and without stimulation with LPS and IFNγ for 4 h, as this has previously been shown to be the peak time point for gene expression changes downstream of the LPS receptor TLR4 (Aung et al., 2006; Yamamoto et al., 2004). RNA-Seq of these samples was then carried out to provide a quantitative analysis of the entire HD monocyte transcriptome.

Following sequencing and alignment, data QC was carried out using the RNA-SeQC package; this confirmed that metrics including rRNA rate and exonic rate were within acceptable parameters (Table 4.1). Finally, LPS stimulation was tested by pooling the HD and control monocytes and performing differential expression analysis between the unstimulated and stimulated datasets; 12,599 genes were differentially expressed (FDR < 0.05; data not shown), confirming that successful stimulation took place.

Table 4.1. Summary of RNA-Seq QC statistics. RNA-Seq data files were pooled and analysed using the RNA-SeQC package to determine data quality was within acceptable parameters. One sample did not meet the QC threshold and was removed from further analysis; this sample is not included in this summary.

QC Statistic	Mean ± SD
End 1 mapping rate	1.013 ± 0.009
End 2 mapping rate	0.987 ± 0.009
Estimated library size	1.03E+08 ± 2.85E+07
Exonic rate	0.876 ± 0.024
Genes detected	1.79E+04 ± 7.62E+02
Intergenic rate	0.026 ± 0.005
Intragenic rate	0.974 ± 0.005
Intronic rate	0.098 ± 0.020
Mapped	1.02E+08 ± 2.11E+07
Mean fragment length	183.427 ± 51.374
rRNA rate	0.010 ± 0.006
Transcripts detected	9.97E+04 ± 3.04E+03
Unique rate of mapped	0.757 ± 0.051

4.5.2 HD monocytes exhibit resting proinflammatory transcriptional changes

Following data processing and QC, separate differential expression analyses were carried out on the unstimulated and stimulated datasets, in order to identify transcripts that were significantly altered between HD and control monocytes. Analysis of the unstimulated dataset revealed differential expression of 130 genes (FDR < 0.05) in resting HD monocytes compared to control (Table 4.2; complete list in Appendices); 101 of these genes were found to be significantly upregulated, while 29 were found to be significantly downregulated. Although the differentially expressed genes were associated with a wide range of effector functions, proinflammatory cytokines and chemokines were among the most prominent.

Table 4.2. The top twenty gene expression changes in resting HD monocytes (ranked by FDR).

Gene name	Ensembl ID	RPKM (control)	RPKM (HD)	Log2 fold change	*p*-value	FDR	Protein function
FAM124A	ENSG00000150510	0.242	0.812	2.684	4.61E-08	6.05E-04	Functionally uncharacterised
IL19	ENSG00000142224	0.586	1.473	2.358	1.15E-07	7.57E-04	Proinflammatory cytokine
IL23A	ENSG00000110944	1.914	3.597	1.576	7.84E-07	2.55E-03	Proinflammatory cytokine
FAM213B	ENSG00000157870	7.837	5.201	-0.604	8.99E-07	2.55E-03	Prostaglandin metabolism
TGFA	ENSG00000163235	0.665	1.392	1.550	9.69E-07	2.55E-03	Growth factor
FZD7	ENSG00000155760	0.397	0.246	-0.721	1.39E-06	3.04E-03	Wnt protein receptor
C6orf223	ENSG00000181577	0.063	0.297	2.127	1.92E-06	3.60E-03	Functionally uncharacterised
PROCR	ENSG00000101000	3.695	10.872	1.552	3.61E-06	5.69E-03	Receptor for activated protein C
NT5E	ENSG00000135318	0.210	0.725	2.082	4.24E-06	5.69E-03	Extracellular nucleotide hydrolysis
SMO	ENSG00000128602	0.259	0.124	-1.161	4.33E-06	5.69E-03	G protein-coupled receptor
CISH	ENSG00000114737	2.723	5.161	1.439	5.90E-06	7.04E-03	Negative regulation of JAK/STAT signalling
C6orf165	ENSG00000213204	0.038	0.086	1.205	6.57E-06	7.20E-03	Functionally uncharacterised
CCL19	ENSG00000172724	0.518	1.767	1.763	8.79E-06	8.89E-03	Chemoattraction of T and B lymphocytes
PTGS2	ENSG00000073756	2.319	18.604	1.813	9.52E-06	8.93E-03	Prostaglandin synthesis enzyme
HPSE	ENSG00000173083	11.322	24.941	1.142	1.10E-05	9.68E-03	Extracellular matrix remodelling
VEGFA	ENSG00000112715	5.475	14.251	0.898	1.35E-05	1.11E-02	Angiogenesis and endothelial cell growth
ANXA11	ENSG00000122359	136.875	105.621	-0.374	1.72E-05	1.33E-02	Phospholipid-binding protein
CDK2	ENSG00000123374	5.534	7.186	0.390	1.88E-05	1.39E-02	Cell cycle regulation
R3HCC1	ENSG00000104679	15.225	11.394	-0.421	2.18E-05	1.45E-02	Nucleic acid binding
PGAP3	ENSG00000161395	2.943	2.310	-0.364	2.28E-05	1.45E-02	GPI-specific phospholipase

Resting HD monocytes were found to express significantly increased levels of *IL6*, *IL12B*, *IL19*, *IL23A*, *CCL8*, *CCL19*, *CCL20*, *CXCL6* and *CSF2* gene transcripts (Table 4.3); this is the first time that increased resting expression of proinflammatory cytokines has been demonstrated in HD myeloid cells at either the mRNA or protein level. Each of these genes had a log2 fold change of > 1, corresponding to a > 2-fold increase in mRNA expression.

Analysis of the stimulated dataset revealed a stark contrast in terms of differential expression, as only three genes were found to be significantly altered (FDR < 0.05; Table 4.4). Each of these genes (*DNAJB13*, *STAC* and *RASEF*) were also differentially expressed in the unstimulated dataset (these genes are displayed as red dots in Fig. 4.1). Comparison of the log2 fold changes for the differentially expressed genes revealed a general trend whereby the relative expression differences between HD and control were reduced in the stimulated compared to the unstimulated dataset; this was the case for 116 of the 130 genes (Fig. 4.1). This concentration of transcriptional change in resting HD monocytes is a marked departure from previous functional studies, where stimuli have been required to elicit abnormalities.

Table 4.3. Differentially expressed cytokines and chemokines in resting HD monocytes (ranked by FDR).

Gene name	Ensembl ID	RPKM (control)	RPKM (HD)	Log2 fold change	*p*-value	FDR
IL19	ENSG00000142224	0.586	1.473	2.358	1.15E-07	7.57E-04
IL23A	ENSG00000110944	1.914	3.597	1.576	7.84E-07	2.55E-03
CCL19	ENSG00000172724	0.518	1.767	1.763	8.79E-06	8.89E-03
CSF2	ENSG00000164400	0.680	1.369	2.888	3.00E-05	1.55E-02
IL12B	ENSG00000113302	1.772	6.429	2.531	5.69E-05	2.27E-02
IL6	ENSG00000136244	12.656	97.048	2.678	8.73E-05	2.69E-02
CCL8	ENSG00000108700	41.093	103.771	2.142	1.74E-04	3.54E-02
CCL20	ENSG00000115009	9.411	46.334	2.219	2.42E-04	4.08E-02
CXCL6	ENSG00000124875	12.417	43.757	1.805	4.23E-04	4.96E-02

Table 4.4. The top twenty gene expression changes in stimulated HD monocytes (ranked by FDR).

Gene name	Ensembl ID	RPKM (control)	RPKM (HD)	Log2 fold change	*p*-value	FDR	Protein function
DNAJB13	ENSG00000187726	0.058	0.135	1.251	2.38E-06	2.68E-02	Heat shock protein family member
STAC	ENSG00000144681	0.101	0.203	1.831	5.30E-06	2.68E-02	Neuron-specific signal transduction
RASEF	ENSG00000165105	0.014	0.131	3.297	6.57E-06	2.68E-02	Regulation of membrane traffic
OTOF	ENSG00000115155	0.102	0.409	1.917	2.23E-05	6.09E-02	Calcium ion sensor
SPARC	ENSG00000113140	2.965	1.074	-1.518	2.49E-05	6.09E-02	Regulation of cell growth
SP3	ENSG00000172845	11.178	14.023	0.336	4.69E-05	7.43E-02	Transcription factor
RPS6KA2	ENSG00000071242	0.687	0.402	-0.757	5.33E-05	7.43E-02	Serine/threonine protein kinase
STEAP1	ENSG00000164647	0.369	0.585	2.051	5.84E-05	7.43E-02	Metalloreductase enzyme
CD300E	ENSG00000186407	12.516	37.032	1.427	6.06E-05	7.43E-02	Myeloid cell surface protein
C5	ENSG00000106804	0.289	0.442	0.594	6.07E-05	7.43E-02	Complement system component
NEK11	ENSG00000114670	0.374	0.524	0.490	6.93E-05	7.72E-02	Protein kinase
RAB3D	ENSG00000105514	0.152	0.332	1.072	8.13E-05	8.05E-02	Protein transport
PLEKHN1	ENSG00000187583	1.743	2.573	0.567	8.54E-05	8.05E-02	Functionally uncharacterised
ATXN7L3	ENSG00000087152	23.446	27.121	0.213	1.01E-04	8.34E-02	Component of the histone acetylation complex SAGA
FAM214B	ENSG00000005238	12.457	16.003	0.367	1.08E-04	8.34E-02	Functionally uncharacterised
PTCRA	ENSG00000171611	0.240	0.120	-0.998	1.21E-04	8.34E-02	Pre-T-cell receptor complex component
CTSK	ENSG00000143387	7.331	3.847	-0.964	1.28E-04	8.34E-02	Lysosomal cysteine proteinase
TFAP2E	ENSG00000116819	0.143	0.204	0.555	1.35E-04	8.34E-02	Sequence-specific DNA-binding protein
KLHL6	ENSG00000172578	4.684	3.193	-0.548	1.37E-04	8.34E-02	B lymphocyte antigen receptor signaling
CPED1	ENSG00000106034	0.393	0.235	-0.719	1.38E-04	8.34E-02	Functionally uncharacterised

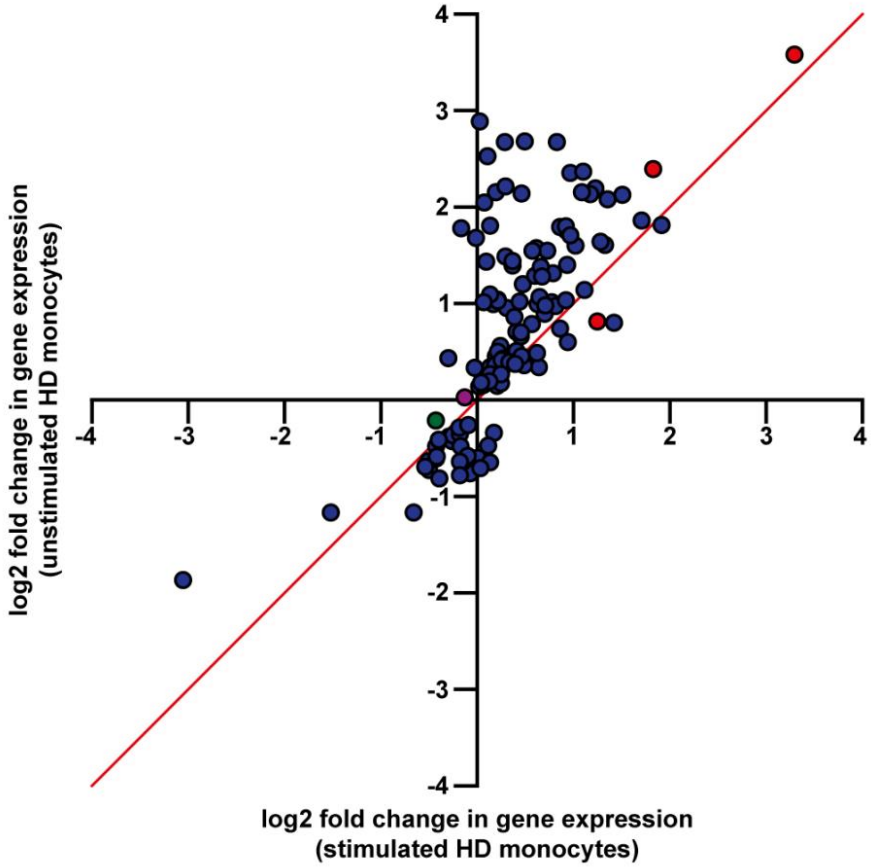

Figure 4.1. Comparison of log2 fold changes in unstimulated and stimulated HD and control monocytes. The log2 fold changes for the 130 differentially expressed genes (FDR < 0.05) were compared between the unstimulated and stimulated datasets. The magnitude of the relative expression difference (whether positive or negative) was greater in the unstimulated samples for 116 of the genes, suggesting that transcriptional differences between HD and control become less pronounced in response to stimulation. Genes that were only differentially expressed in the unstimulated samples are shown in blue, while the three genes that were differentially expressed in both datasets are shown in red. *HTT* is shown in green, while the NFκB transcription family member *RELA* (p65) is shown in purple (however neither of these genes were differentially expressed). The line x = y is also shown.

4.5.3 HD monocytes do not show changes in alternative splicing

While the above data demonstrate that HD monocytes experience transcriptional changes at the whole mRNA level, it is also important to consider the potential impact of variations in alternative splicing on HD myeloid cell function. Alternative splicing has been shown to be an important pathogenic mechanism in tissues from a range of neurodegenerative diseases, including HD brain (Fernández-Nogales et al., 2014). The RNA-Seq expression datasets were therefore subjected to analyses of differential exon, intron and transcript expression using the R package Ballgown. However, no significant differences were detected in either the unstimulated or stimulated datasets for any of these analyses (FDR < 0.05; Tables 4.5-4.10). This suggests that, in contrast to other previously studied tissues, changes in alternative splicing are not a significant factor in mediating HD innate immune dysfunction.

Table 4.5. The top ten exon splicing changes in unstimulated HD monocytes (ranked by FDR).

Gene ID	Feature	Transcript	ID	*p*-value	FDR
WDR20	Exon	11926	202144	1.11E-05	5.53E-01
LOC100288332	Exon	13825	21865	1.39E-05	5.53E-01
LAMB3	Exon	3539	130	1.68E-05	5.53E-01
CCDC88C	Exon	11631	200554	1.81E-05	5.53E-01
CILP	Exon	12758	209927	2.38E-05	5.53E-01
LGR5	Exon	9329	179768	2.45E-05	5.53E-01
LGR5	Exon	9329	179767	2.84E-05	5.53E-01
ZFC3H1	Exon	9330	179770	3.27E-05	5.53E-01
LGR5	Exon	9329	179769	3.45E-05	5.53E-01
LGR5	Exon	9329	179764	4.37E-05	5.53E-01

Table 4.6. The top ten exon splicing changes in stimulated HD monocytes (ranked by FDR).

Gene ID	Feature	Transcript	ID	*p*-value	FDR
RHOT1	Exon	15773	27628	6.89E-06	9.99E-01
ST3GAL4	Exon	7978	16708	9.80E-06	9.99E-01
LGR5	Exon	9329	179769	2.13E-05	9.99E-01
LILRB3	Exon	20082	62341	3.09E-05	9.99E-01
LGR5	Exon	9329	179761	4.15E-05	9.99E-01
LGR5	Exon	9329	179763	4.19E-05	9.99E-01
ZFC3H1	Exon	9330	179774	4.45E-05	9.99E-01
ZFC3H1	Exon	9330	179770	4.80E-05	9.99E-01
LILRA6	Exon	20083	62351	5.17E-05	9.99E-01
TRIM21	Exon	5913	150624	5.96E-05	9.99E-01

Table 4.7. The top ten intron splicing changes in unstimulated HD monocytes (ranked by FDR).

Gene ID	Feature	Transcript	ID	*p*-value	FDR
PIKFYVE	Intron	22445	84654	3.12E-06	3.77E-01
PRMT1	Intron	19727	62638	4.28E-06	3.77E-01
PEX5	Intron	8269	162867	1.41E-05	6.37E-01
CLEC18B	Intron	14702	25072	1.92E-05	6.37E-01
PEX5	Intron	8269	162869	2.27E-05	6.37E-01
ECM1	Intron	2270	117696	2.51E-05	6.37E-01
FAM96A	Intron	12730	19828	2.53E-05	6.37E-01
PEX5	Intron	8269	162866	3.99E-05	6.96E-01
PEX5	Intron	8268	162864	4.43E-05	6.96E-01
PEX5	Intron	8269	162871	5.46E-05	6.96E-01

Table 4.8. The top ten intron splicing changes in stimulated HD monocytes (ranked by FDR).

Gene ID	Feature	Transcript	ID	*p*-value	FDR
MEFV	Intron	13651	204928	6.18E-06	9.93E-01
PEX5	Intron	8269	162869	2.30E-05	9.93E-01
ADAMTS14	Intron	4795	136356	5.57E-05	9.93E-01
KIAA1245	Intron	2187	11729	6.53E-05	9.93E-01
PEX5	Intron	8269	162866	9.07E-05	9.93E-01
PEX5	Intron	8269	162867	9.09E-05	9.93E-01
METTL1	Intron	9212	170447	9.46E-05	9.93E-01
ZNF90	Intron	18758	56593	9.58E-05	9.93E-01
DACH1	Intron	10490	18124	9.70E-05	9.93E-01
PEX5	Intron	8268	162865	9.89E-05	0.99347

Table 4.9. The top ten transcript splicing changes in unstimulated HD monocytes (ranked by FDR).

Gene ID	Feature	ID	*p*-value	FDR
LOC100505813	Transcript	30495	7.44E-06	1.11E-01
FZD7	Transcript	22359	1.48E-05	1.11E-01
PGAP3	Transcript	15961	1.67E-05	1.11E-01
C1orf93	Transcript	135	1.84E-05	1.11E-01
SPARC	Transcript	30494	2.09E-05	1.11E-01
C1orf93	Transcript	138	3.04E-05	1.35E-01
OSGEPL1	Transcript	22222	3.57E-05	1.36E-01
CDK2	Transcript	9078	4.88E-05	1.62E-01
R3HCC1	Transcript	35202	6.16E-05	1.82E-01
BCAP31	Transcript	39617	9.03E-05	2.40E-01

Table 4.10. The top ten transcript splicing changes in stimulated HD monocytes (ranked by FDR).

Gene ID	Feature	ID	*p*-value	FDR
OGG1	Transcript	25522	9.35E-05	8.54E-01
JAG1	Transcript	23106	2.33E-04	8.54E-01
C5orf32	Transcript	30185	2.59E-04	8.54E-01
LRCH1	Transcript	10366	3.02E-04	8.54E-01
P2RY6	Transcript	7304	3.51E-04	8.54E-01
SPARC	Transcript	30494	3.65E-04	8.54E-01
RAPGEF1	Transcript	37646	3.91E-04	8.54E-01
UBTD2	Transcript	30651	3.98E-04	8.54E-01
WDR73	Transcript	13166	4.53E-04	8.54E-01
RPAP3	Transcript	8708	5.35E-04	8.54E-01

Figure 4.2. Functional gene sets associated with innate immunity and inflammation are enriched in resting HD monocytes. GSEA was used to identify biologically relevant gene sets that are enriched in resting HD monocytes compared to control. A network diagram of significant biological themes among the upregulated genes is shown, indicating number of genes (node size), statistical significance (darkest shading = lowest *p*-value) and gene content similarity via the Jaccard coefficient (edge thickness). Nodes with similar gene content cluster more closely due to an edge-weighted layout (modified for readability). An FDR cut-off of < 0.05 was used to determine gene set inclusion in the diagram, before the Jaccard coefficient was used to filter out gene sets with similar gene content. The diagram was rendered in Cytoscape 3.3.0.

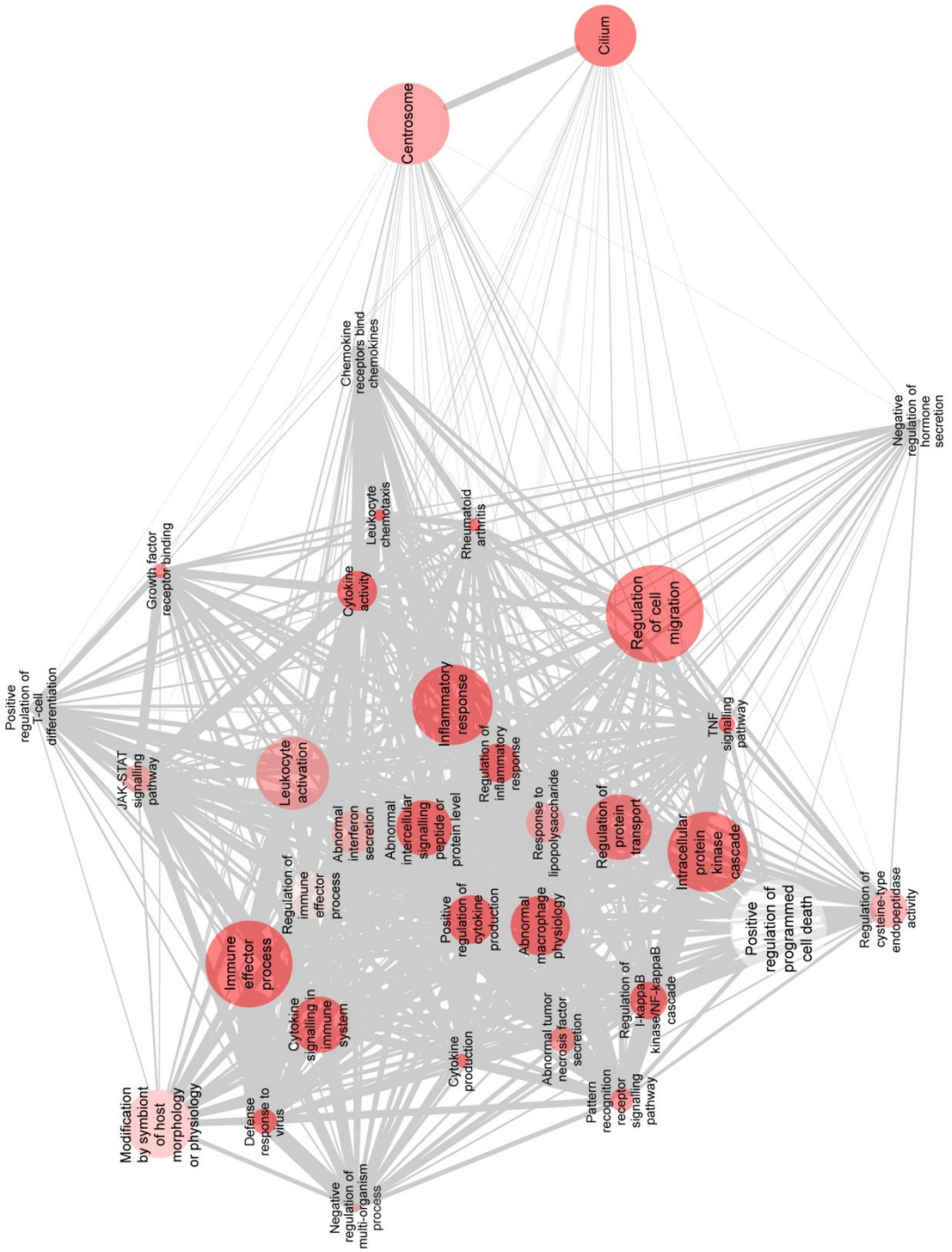
Cilium
Centrosome
Chemokine receptors bind chemokines
Negative regulation of hormone secretion
Growth factor receptor binding
Leukocyte chemotaxis
Rheumatoid arthritis
Cytokine activity
Regulation of cell migration
Positive regulation of T-cell differentiation
Inflammatory response
TNF signalling pathway
JAK-STAT signaling pathway
Leukocyte activation
Regulation of inflammatory response
Abnormal interferon secretion
Abnormal intercellular signalling peptide or protein level
Response to lipopolysaccharide
Regulation of protein transport
Intracellular protein kinase cascade
Regulation of immune effector process
Positive regulation of cytokine production
Abnormal macrophage physiology
Positive regulation of programmed cell death
Regulation of cysteine-type endopeptidase activity
Immune effector process
Cytokine signalling in immune system
Regulation of I-kappaB kinase/NF-kappaB cascade
Cytokine production
Abnormal tumor necrosis factor secretion
Modification by symbiont of host morphology or physiology
Defense response to virus
Pattern recognition receptor signalling pathway
Negative regulation of multi-organism process

4.5.4 Proinflammatory functional gene sets are enriched in resting HD monocytes

While the study of specific transcripts in isolation is a useful tool for investigating monocyte function, it is important to recognise that such a paradigm is open to potential bias, as the investigator will naturally focus on the expression of genes that they personally find the most interesting. Furthermore, it is questionable to what extent broader functional conclusions can be drawn from changes in a relatively small number of arbitrarily significant genes. To address this, a comprehensive GSEA was carried out to assign wider biological relevance to the observed expression changes. GSEA allows for the unbiased identification of gene sets showing evidence of combined differential expression, without relying on the genes being individually significant after correction for multiple testing; this enables relevant biological trends to be uncovered.

Multiple sources were used to compile a list of over 14,000 functional gene sets (Section 2.10.2); each of these was then tested for enrichment, whereby the upregulated and downregulated genes were analysed separately. Analysis of the unstimulated dataset revealed a total of eighty-five significantly enriched gene sets (FDR < 0.05) within the upregulated genes in HD monocytes (Table 4.11; complete list in Appendices). Functional gene sets relating to innate immunity, inflammation and cytokine production were among the most prominently featured (Fig. 4.2); this confirms that the proinflammatory changes seen at the individual transcript level are also present across the broader HD monocyte transcriptome. Additional functional

gene sets including those relating to the NFκB and JAK/STAT intracellular signalling cascades were also found to be significantly enriched. In contrast, only six gene sets relating to vacuole, lysosome and catabolic function were found to be significantly enriched (FDR < 0.05) amongst the downregulated genes in unstimulated HD monocytes (Table 4.12).

4.5.5 Analysis of functional gene set enrichment in stimulated HD monocytes

GSEA of the stimulated dataset did not reveal any significant enrichment (FDR < 0.05) of functional gene sets among the upregulated genes in HD monocytes (Table 4.13); this is consistent with the above loss of significance for individual transcripts. However, analysis of the downregulated genes revealed eighty-three gene sets that were significantly enriched (FDR < 0.05) in stimulated HD monocytes compared to control (Table 4.14; complete list in Appendices). Gene sets relating to translation, protein localisation, cholesterol homeostasis and cellular components including the membrane, mitochondria and lysosome were among the most affected (Fig. 4.3).

Figure 4.3. Analysis of functional gene set enrichment in stimulated HD monocytes. GSEA was used to identify biologically relevant gene sets that are enriched in stimulated HD monocytes compared to control. A network diagram of significant biological themes among the downregulated genes is shown, indicating number of genes (node size), statistical significance (darkest shading = lowest *p*-value) and gene content similarity via the Jaccard coefficient (edge thickness). Nodes with similar gene content cluster more closely due to an edge-weighted layout (modified for readability). An FDR cut-off of < 0.05 was used to determine gene set inclusion in the diagram, before the Jaccard coefficient was used to filter out gene sets with similar gene content. The diagram was rendered in Cytoscape 3.3.0.

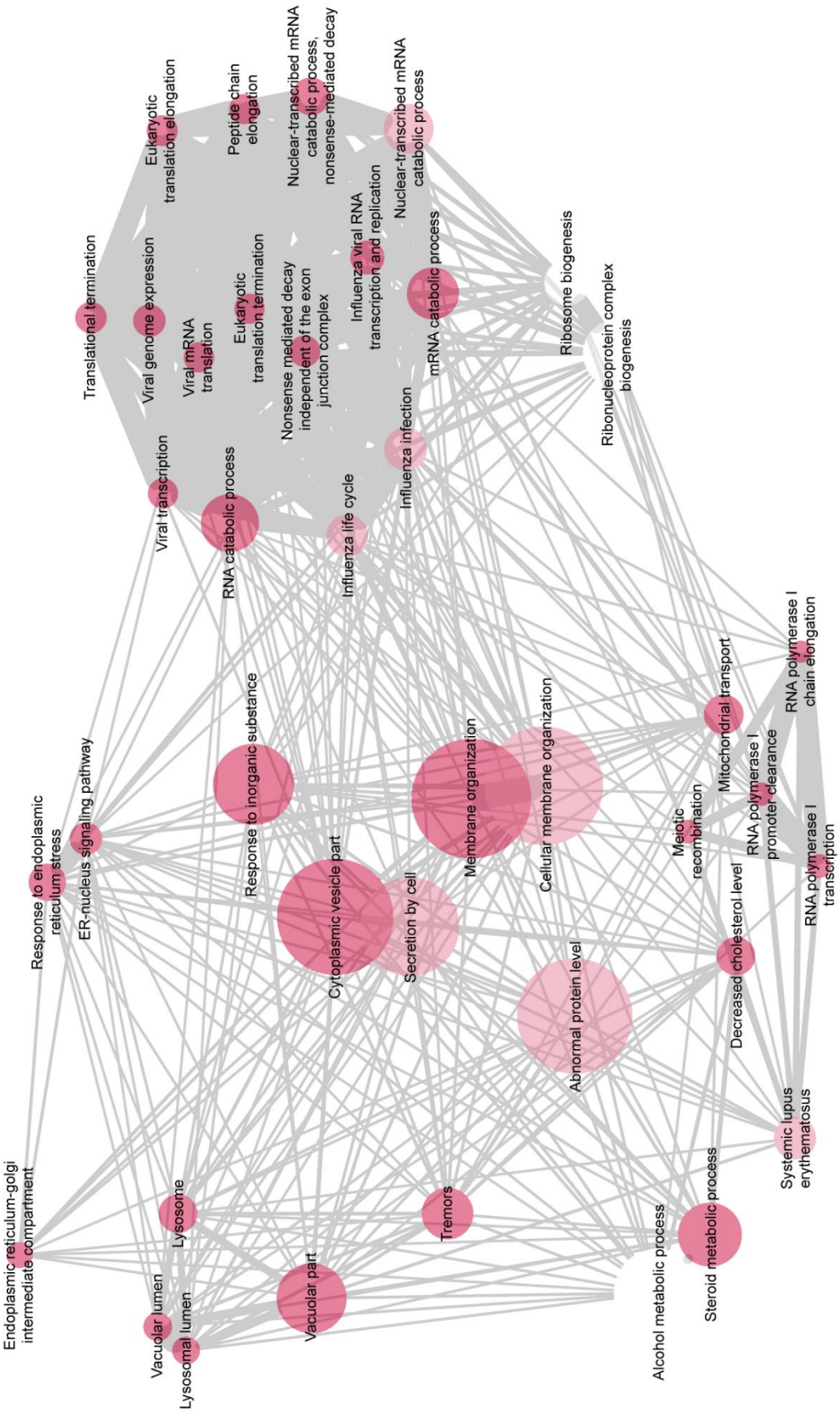
Translational termination
Eukaryotic translation elongation
Peptide chain elongation
Nuclear-transcribed mRNA catabolic process, nonsense-mediated decay
Viral genome expression
Viral mRNA translation
Eukaryotic translation termination
Influenza viral RNA transcription and replication
Nuclear-transcribed mRNA catabolic process
mRNA catabolic process
Ribosome biogenesis
Ribonucleoprotein complex biogenesis
Nonsense mediated decay independent of the exon junction complex
Viral transcription
RNA catabolic process
Influenza life cycle
Influenza infection
Response to endoplasmic reticulum stress
ER-nucleus signaling pathway
Response to inorganic substance
Membrane organization
Cellular membrane organization
Mitochondrial transport
RNA polymerase I chain elongation
Meiotic recombination
RNA polymerase I promoter clearance
Cytoplasmic vesicle part
Secretion by cell
Abnormal protein level
Decreased cholesterol level
RNA polymerase I transcription
Endoplasmic reticulum-golgi intermediate compartment
Lysosome
Tremors
Systemic lupus erythematosus
Vacuolar lumen
Vacuolar part
Steroid metabolic process
Lysosomal lumen
Alcohol metabolic process

Table 4.11. The top twenty enriched gene sets among the upregulated genes in resting HD monocytes (ranked by FDR).

Pathway	Description	Number of genes	NES	*p*-value	FDR
GO: 31347	Regulation of defence response	270	5.631	8.96E-09	1.28E-04
MGI: 2419	Abnormal innate immunity	3	5.378	3.77E-08	2.68E-04
MGI: 8835	Abnormal intercellular signalling peptide or protein level	4	5.077	1.92E-07	6.46E-04
GO: 6954	Inflammatory response	387	5.036	2.38E-07	6.46E-04
GO: 31349	Positive regulation of defence response	352	5.016	2.64E-07	6.46E-04
MGI: 8713	Abnormal cytokine level	4	5.010	2.72E-07	6.46E-04
MGI: 3009	Abnormal cytokine secretion	6	4.923	4.26E-07	8.67E-04
GO: 9615	Response to virus	200	4.760	9.68E-07	1.63E-03
GO: 43900	Regulation of multi-organism process	119	4.727	1.14E-06	1.63E-03
GO: 45088	Regulation of innate immune response	160	4.710	1.24E-06	1.63E-03
MGI: 8469	Abnormal protein level	7	4.677	1.46E-06	1.63E-03
KEGG: 5323	Rheumatoid arthritis	4	4.649	1.67E-06	1.63E-03
GO: 1817	Regulation of cytokine production	151	4.647	1.68E-06	1.63E-03
GO: 5125	Cytokine activity	366	4.643	1.72E-06	1.63E-03
MGI: 2451	Abnormal macrophage physiology	5	4.630	1.83E-06	1.63E-03
KEGG: 4060	Cytokine-cytokine receptor interaction	4	4.624	1.88E-06	1.63E-03
GO: 2252	Immune effector process	92	4.617	1.95E-06	1.63E-03
GO: 9617	Response to bacterium	369	4.590	2.22E-06	1.73E-03
MGI: 1793	Altered susceptibility to infection	4	4.582	2.30E-06	1.73E-03
MGI: 8568	Abnormal interleukin secretion	66	4.509	3.26E-06	2.32E-03

Table 4.12. The top twenty enriched gene sets among the downregulated genes in resting HD monocytes (ranked by FDR).

Pathway	Description	Number of genes	NES	*p*-value	FDR
GO: 5773	Vacuole	310	5.678	6.81E-09	9.71E-05
GO: 44437	Vacuolar part	346	5.317	5.27E-08	2.84E-04
GO: 5764	Lysosome	305	5.241	7.99E-08	2.84E-04
GO: 323	Lytic vacuole	387	5.241	7.99E-08	2.84E-04
GO: 44282	Small molecule catabolic process	373	4.381	5.91E-06	1.40E-02
GO: 44712	Single-organism catabolic process	126	4.381	5.91E-06	1.40E-02
GO: 5759	Mitochondrial matrix	313	3.923	4.37E-05	8.90E-02
MGI: 745	Tremors	5	3.722	9.88E-05	1.57E-01
GO: 19371	Cyclooxygenase pathway	170	3.704	1.06E-04	1.57E-01
MGI: 1541	Abnormal osteoclast physiology	3	3.670	1.21E-04	1.57E-01
GO: 5774	Vacuolar membrane	313	3.661	1.26E-04	1.57E-01
GO: 5775	Vacuolar lumen	186	3.647	1.33E-04	1.57E-01
KEGG: 4142	Lysosome	5	3.609	1.54E-04	1.68E-01
REACTOME: 778	NOD1/2 signalling pathway	13	3.512	2.22E-04	2.24E-01
GO: 43202	Lysosomal lumen	67	3.484	2.47E-04	2.24E-01
GO: 19318	Hexose metabolic process	197	3.446	2.84E-04	2.24E-01
GO: 16054	Organic acid catabolic process	118	3.422	3.11E-04	2.24E-01
GO: 46395	Carboxylic acid catabolic process	64	3.422	3.11E-04	2.24E-01
GO: 5996	Monosaccharide metabolic process	137	3.419	3.14E-04	2.24E-01
MGI: 3106	Abnormal fear-related response	11	3.419	3.14E-04	2.24E-01

Table 4.13. The top twenty enriched gene sets among the upregulated genes in stimulated HD monocytes (ranked by FDR).

Pathway	Description	Number of genes	NES	*p*-value	FDR
GO: 5813	Centrosome	16	4.003	3.13E-05	3.55E-01
GO: 5929	Cilium	393	3.766	8.29E-05	3.55E-01
MGI: 10210	Abnormal circulating cytokine level	63	3.712	1.03E-04	3.55E-01
GO: 7264	Small GTPase mediated signal transduction	86	3.664	1.24E-04	3.55E-01
MGI: 2463	Abnormal neutrophil physiology	53	3.663	1.25E-04	3.55E-01
MGI: 8713	Abnormal cytokine level	4	3.347	4.08E-04	7.68E-01
MGI: 8835	Abnormal intercellular signalling peptide or protein level	4	3.285	5.10E-04	7.68E-01
GO: 60271	Cilium morphogenesis	44	3.267	5.43E-04	7.68E-01
GO: 6954	Inflammatory response	387	3.256	5.65E-04	7.68E-01
GO: 50900	Leukocyte migration	70	3.247	5.83E-04	7.68E-01
REACTOME: 1133	Signalling by Rho GTPases	48	3.174	7.52E-04	7.68E-01
REACTOME: 1031	Rho GTPase cycle	19	3.174	7.52E-04	7.68E-01
MGI: 3037	Increased myocardial infarction size	3	3.167	7.70E-04	7.68E-01
MGI: 8588	Abnormal circulating interleukin level	5	3.119	9.07E-04	7.68E-01
MGI: 8789	Abnormal olfactory epithelium morphology	86	3.110	9.35E-04	7.68E-01
GO: 187	Activation of MAPK activity	17	3.099	9.71E-04	7.68E-01
KEGG: 4062	Chemokine signalling pathway	141	3.080	1.04E-03	7.68E-01
GO: 31514	Motile cilium	178	3.072	1.06E-03	7.68E-01
NCI: 76	Syndecan-1-mediated signalling events	10	3.057	1.12E-03	7.68E-01
MGI: 2462	Abnormal granulocyte physiology	6	3.055	1.13E-03	7.68E-01

Table 4.14. The top twenty enriched gene sets among the downregulated genes in stimulated HD monocytes (ranked by FDR).

Pathway	Description	Number of genes	NES	*p*-value	FDR
GO: 72594	Establishment of protein localization to organelle	124	5.819	2.96E-09	1.88E-05
GO: 6412	Translation	197	5.803	3.26E-09	1.88E-05
GO: 6605	Protein targeting	15	5.443	2.62E-08	1.01E-04
REACTOME: 1287	Translation	8	5.222	8.85E-08	2.55E-04
GO: 22411	Cellular component disassembly	35	5.120	1.53E-07	3.04E-04
GO: 33365	Protein localization to organelle	321	5.113	1.59E-07	3.04E-04
GO: 6612	Protein targeting to membrane	11	5.044	2.28E-07	3.75E-04
GO: 5773	Vacuole	310	4.947	3.77E-07	5.43E-04
GO: 70972	Protein localization to endoplasmic reticulum	9	4.876	5.41E-07	6.93E-04
MGI: 3947	Abnormal cholesterol level	57	4.799	7.97E-07	9.19E-04
GO: 6413	Translational initiation	71	4.693	1.35E-06	1.37E-03
GO: 72599	Establishment of protein localization to endoplasmic reticulum	15	4.677	1.46E-06	1.37E-03
GO: 45047	Protein targeting to endoplasmic reticulum	10	4.665	1.54E-06	1.37E-03
REACTOME: 1165	SRP-dependent co-translational protein targeting to membrane	175	4.646	1.69E-06	1.39E-03
GO: 6613	Co-translational protein targeting to membrane	4	4.623	1.89E-06	1.45E-03
MGI: 5278	Abnormal cholesterol homeostasis	4	4.604	2.07E-06	1.49E-03
GO: 6614	SRP-dependent co-translational protein targeting to membrane	3	4.562	2.53E-06	1.65E-03
GO: 44391	Ribosomal subunit	15	4.547	2.72E-06	1.65E-03
GO: 32984	Macromolecular complex disassembly	15	4.547	2.72E-06	1.65E-03
GO: 44445	Cytosolic part	62	4.522	3.06E-06	1.76E-03

4.5.6 Specific intracellular signalling pathways are predicted to mediate transcriptional changes in HD monocytes

Although patterns of gene expression change provide valuable insight into the functional state of HD monocytes, they do not on their own give any clues as to the cellular mechanisms responsible for mediating this transcriptional dysregulation. Next, upstream regulator analysis was carried out on the unstimulated samples using IPA® software. IPA® compares patterns of gene expression in an experimental dataset with lists of genes that are known to be regulated by specific upstream signalling molecules, in order to infer whether a particular regulatory molecule is likely to be abnormally activated or inhibited. One important caveat with IPA® is that there is a great deal of redundancy in the analysis, due to the considerable overlap in gene sets influenced by specific upstream regulators. This will result in multiple points along an intracellular signalling pathway being suggested as an upstream regulator, even if only one is driving transcriptional change; this means that functional validation of IPA® data is essential to counter this redundancy.

Predicted changes in upstream regulatory molecules are quantified by the activation z-score statistic. This increases or decreases depending on the inferred activation/inhibition state of a particular upstream regulator, with significance in IPA® typically being attributed to regulators that have an overlap *p*-value of < 0.01 and an activation z-score of ≥ 2 or ≤ -2. Analysis of the unstimulated dataset revealed 155 upstream regulators that fulfilled these criteria (Table 4.15; complete list in Appendices); 125 of these were

predicted to be abnormally activated, while thirty were predicted to be abnormally inhibited. Due to the aforementioned redundancy associated with IPA® it is highly unlikely that this many factors are actually affected by mHTT expression, so focus was narrowed to the subset of upstream regulators with the highest activation z-scores, and therefore the strongest evidence for their mediating transcriptional dysregulation in resting HD monocytes.

Crucially, a large number of molecules associated with intracellular signalling pathways downstream of TLR4 were represented in this group (Fig. 4.4). Both RELA and the NFκB complex were featured in the top ten most significant results ranked by activation z-score; this suggests that the NFκB dysfunction previously described in stimulated HD myeloid cells (Träger et al., 2014) may also exist basally. Other notable potential regulators included NFκB1, the ERK and p38 MAPKs and the transcription factor STAT3. These data suggest that the transcriptional changes observed in HD monocytes are related to the abnormal activation of specific upstream signalling molecules that are responsible for driving gene expression in the resting state.

Figure 4.4. Specific intracellular signalling pathways are predicted to be abnormally activated in resting HD monocytes. IPA® software was used to identify numerous signalling pathway components downstream of the TLR4 receptor that are predicted to be abnormally activated in resting HD monocytes compared to control. Upstream regulators with significantly inferred activation are shown in orange (darker colour = higher activation z-score). The activation z-score for each pathway component is also shown (≥ 2 is considered to be significant).

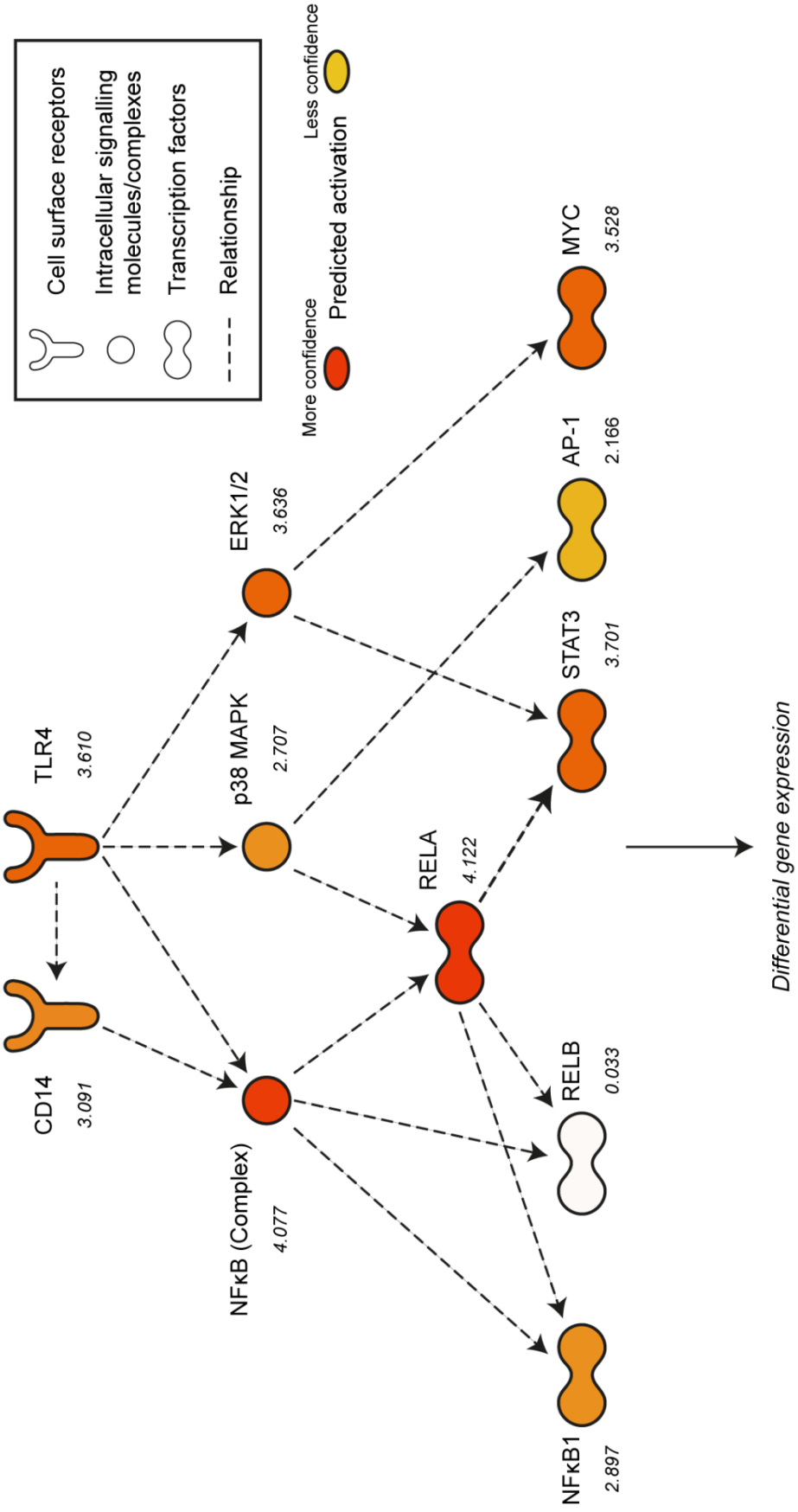
Cell surface receptors
Intracellular signalling molecules/complexes
Transcription factors
Relationship
More confidence
Predicted activation
Less confidence
TLR4
3.610
CD14
3.091
p38 MAPK
2.707
ERK1/2
3.636
NFκB (Complex)
4.077
RELA
4.122
RELB
0.033
NFκB1
2.897
STAT3
3.701
AP-1
2.166
MYC
3.528
Differential gene expression

Table 4.15. Pathway analysis of upstream transcriptional regulators in resting HD monocytes. IPA® was used to identify transcriptional regulators with significant target gene overlap with changes in the resting HD monocyte transcriptome. A *p*-value cut-off of < 0.01 was used to determine which genes were included in the analysis. The upstream regulators were ranked by activation z-score and the fifteen most significant were included in the table.

Upstream regulator	Activation z-score	*p*-value of overlap	Function
TNF	5.764	2.18E-13	Proinflammatory cytokine
IL1B	5.754	8.08E-14	Proinflammatory cytokine
MyD88	4.761	2.92E-12	Cytoplasmic adaptor protein for the TLR family
IFNγ	4.635	3.09E-07	Cytokine involved in mediating the innate immune response
IL1A	4.536	1.69E-11	Proinflammatory cytokine
TLR3	4.323	1.99E-09	Cell surface receptor involved in the activation of the innate immune response
RELA	4.122	5.86E-08	Transcription factor; one of five NFκB family members
NFκB (complex)	4.077	2.63E-08	A family of five transcription factors that mediate the inflammatory response
TLR9	3.773	4.33E-07	Cell surface receptor involved in the activation of the innate immune response
TLR2	3.770	3.94E-09	Cell surface receptor involved in the activation of the innate immune response
STAT3	3.701	2.34E-07	Transcription factor
IL6	3.654	7.39E-06	Proinflammatory cytokine
TICAM1/TRIF	3.651	2.59E-08	TLR cytoplasmic adaptor protein; mediates an alternative pathway to MyD88
ERK1/2	3.636	5.33E-06	Protein kinase intracellular signalling molecules
TLR4	3.610	7.68E-12	Cell surface receptor involved in the activation of the innate immune response

4.5.7 NFκB but not ERK or p38 MAPK signalling is abnormally increased in resting HD myeloid cells

While IPA® is an excellent starting point for identifying the molecular mechanisms responsible for mediating gene expression changes in HD monocytes, its limitations as a purely bioinformatics tool necessitate functional validation of predicted upstream regulators before any firm conclusions can be drawn. Previous work has demonstrated that the NFκB pathway is dysregulated in stimulated HD myeloid cells, with increased initial activation and a prolonged time to return to baseline (Träger et al., 2014). However, there is currently no evidence that this dysfunction also exists when HD myeloid cells are in their basal, resting state. Investigation of NFκB pathway activation in unstimulated HD myeloid cells was next performed to validate the upstream regulator analysis carried out with IPA®.

Monocytes were isolated from peripheral blood samples donated by manifest HD and control subjects and differentiated into macrophages in culture. Western blotting was then carried out to quantify the expression of IκBα, a cytoplasmic inhibitor of the NFκB family of transcription factors. A decrease in IκBα expression is used to demonstrate an increase in NFκB activity, as reduced inhibition will lead to increased translocation of NFκB to the nucleus. Consistent with the upstream regulator analysis, resting HD myeloid cells had significantly reduced IκBα protein levels compared to their healthy counterparts (Fig 4.5). This demonstrates that the NFκB dysregulation previously described in stimulated HD myeloid cells also exists basally.

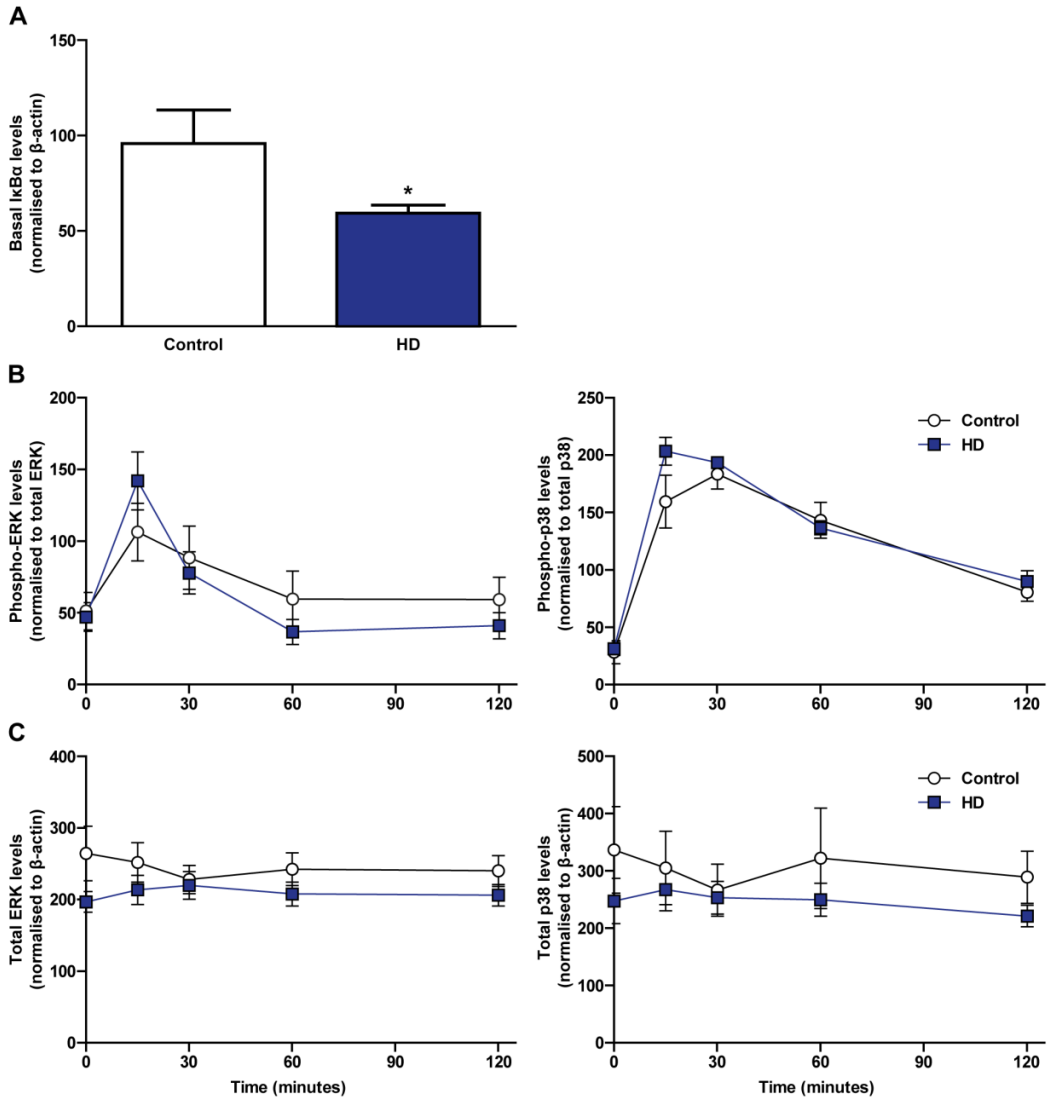

Figure 4.5. NFκB but not ERK or p38 MAPK signalling is abnormally activated in resting HD myeloid cells. Monocyte-derived macrophages were obtained from HD and control peripheral blood samples and pulsed with LPS and IFNγ for 15, 30, 60 and 120 min, or left unstimulated. Western blotting was then carried out on the unstimulated samples to quantify basal levels of IκBα, while additional Western blotting was carried out on all samples to quantify the levels of total and active, phosphorylated ERK and p38 MAPK. (**A**) Resting HD myeloid cells express significantly reduced IκBα protein compared with control (control n = 7, HD n = 9). However, no significant differences were seen in (**B**) the ratio of phosphorylated to total enzyme, or (**C**) the ratio of total enzyme to β-actin for ERK or p38 at any of the time points that were studied (n = 10). IκBα blots were analysed using unpaired two-tailed Student's *t*-tests. MAPK blots were analysed by two-way ANOVAs with Bonferroni post-hoc multiple comparison testing. Error bars represent ± SEM. *p < 0.05

However, signalling downstream of TLR4 is extremely complex, and the contribution of alternative pathways to HD myeloid cell dysfunction is yet to be fully characterised. Next, the ERK and p38 MAPKs were investigated to determine if they are also abnormally activated in HD myeloid cells; these signalling molecules were selected as they both play a major role in immune cell signalling (Akira and Takeda, 2004), and were identified by IPA® as potential regulators of the gene expression changes seen in resting HD monocytes. Both ERK and p38 are activated by phosphorylation; this allows their activation states to be determined by quantifying the ratio of phosphorylated to total protein. Monocytes were again isolated from manifest HD and control peripheral blood samples, before being differentiated into macrophages in culture. Cells from each subject were stimulated with LPS and IFNγ for 15, 30, 60 and 120 min, or left unstimulated, in order to build up a broad profile of the signalling response. However, no significant differences were seen in the activation of ERK or p38 between HD and control, either basally or at any of the time points following LPS stimulation (Fig. 4.5). Furthermore, there was no significant difference in the expression of total ERK or p38 when normalised to the reference protein β-actin. This suggests that, in contrast to NFκB, the ERK and p38 MAPK signalling pathways are not abnormally activated in HD myeloid cells; these signalling pathways are therefore unlikely to mediate the transcriptional changes seen in the unstimulated dataset.

4.5.8 The effects of HTT-lowering on gene expression in HD monocytes

Next, it was investigated whether short term HTT-lowering has a significant effect on the transcriptional changes seen between HD and control monocytes. Monocytes were isolated from peripheral blood samples donated by six manifest HD patients, and treated with GeRPs containing either SCR or anti-total *HTT* siRNA. The cells were cultured for 72 h before either being left unstimulated or stimulated with LPS and IFNγ for 4 h in an identical manner to the main RNA-Seq dataset; this gave a total of four treatment groups. RNA was then harvested and the samples were analysed by RNA-Seq. Differential expression analysis using a likelihood ratios test was carried out to determine whether the expression changes seen in HD monocytes are reversed by treatment with anti-total *HTT* siRNA.

Perhaps surprisingly, none of the expression changes from the unstimulated dataset were found to be significantly reversed following HTT-lowering. While seventy-one genes were found to be significantly altered (FDR < 0.05) between SCR and anti-total *HTT* siRNA-treated monocytes (Table 4.16; complete list in Appendices), none of these genes showed any evidence of differential expression in the original RNA-Seq dataset. This suggests that a short-term reduction in HTT expression may not be sufficient to substantially reverse the transcriptional changes seen in HD monocytes.

Table 4.16. The top twenty gene changes in HD monocytes following HTT-lowering (ranked by FDR).

Gene name	Ensembl ID	RPKM (SCR)	RPKM (α-HTT)	Log2 fold change	p value	FDR	Protein function
COX5A	ENSG00000178741	120.152	41.172	-1.562	4.76E-137	3.98E-133	Mitochondrial electron transport
ECI2	ENSG00000198721	6.403	3.912	-0.737	6.82E-39	2.85E-35	Mitochondrial fatty acid metabolism
HTT	ENSG00000197386	10.218	4.230	-1.280	1.00E-27	2.79E-24	Diverse functions; mutations cause HD
SRPR	ENSG00000182934	62.426	43.624	-0.488	1.05E-20	2.19E-17	ER signal recognition
PPARA	ENSG00000186951	2.051	1.514	-0.471	1.16E-17	1.93E-14	Nuclear receptor transcription factor
VAMP3	ENSG00000049245	52.249	37.049	-0.483	3.43E-17	4.78E-14	Vesicular transport
SPG20	ENSG00000133104	26.372	17.912	-0.512	2.22E-13	2.57E-10	Endosomal trafficking
ACP5	ENSG00000102575	563.842	319.723	-1.050	2.46E-13	2.57E-10	Acid phosphatase enzyme
CAPZA1	ENSG00000116489	107.840	84.262	-0.319	6.40E-13	5.94E-10	Regulates growth of actin filaments
NDUFA8	ENSG00000119421	22.077	17.141	-0.385	2.92E-12	2.44E-09	Mitochondrial NADH dehydrogenase
C8orf33	ENSG00000182307	6.731	4.975	-0.445	3.81E-11	2.80E-08	Functionally uncharacterised
ARHGEF7	ENSG00000102606	6.301	5.296	-0.233	4.02E-11	2.80E-08	Guanine nucleotide exchange factor
HDGF	ENSG00000143321	47.811	35.132	-0.459	1.03E-10	6.64E-08	Mitogenic growth factor
BAG5	ENSG00000166170	4.191	3.719	-0.185	1.37E-10	8.19E-08	Anti-apoptotic protein
TOMM70A	ENSG00000154174	14.166	12.552	-0.152	2.22E-10	1.24E-07	Mitochondrial import receptor
CSE1L	ENSG00000124207	18.510	16.133	-0.215	1.86E-09	9.69E-07	Nuclear export receptor for importin
CNOT11	ENSG00000158435	14.431	11.196	-0.355	2.56E-09	1.26E-06	mRNA deadenylase component
ACTG1	ENSG00000184009	705.135	1031.133	0.582	2.92E-09	1.35E-06	G-actin (globular monomeric form)
UBE2D4	ENSG00000078967	3.913	3.028	-0.399	1.25E-08	5.49E-06	Ubiquitin-conjugating enzyme
HIF1AN	ENSG00000166135	8.113	6.787	-0.241	1.99E-08	8.32E-06	Oxygen sensor

However, it is possible that the lack of any significant reversal is due to the low n number used for the HTT-lowering RNA-Seq experiments, in addition to the rigorous multiple testing corrections inherent in the analysis of such a large dataset. In order to confirm this result, monocytes were isolated from peripheral blood samples donated by manifest HD patients and controls, before being treated with GeRPs containing either SCR or anti-total *HTT* siRNA. After 72 h, the monocytes were harvested unstimulated and RNA was used for qPCR analysis of gene expression. Six differentially expressed genes from the original unstimulated monocyte dataset were selected for investigation based on their biological relevance and the magnitude of their relative expression changes. While a significant 20 % reduction in *CSF2* expression was observed in the anti-total *HTT* treated samples, none of the other transcripts were found to be significantly altered in response to HTT-lowering (Fig. 4.6). This is consistent with the RNA-Seq data described above, and suggests that a more sustained reduction in cellular HTT levels may be required in order to reverse the transcriptional dysregulation associated with mHTT expression in resting HD monocytes.

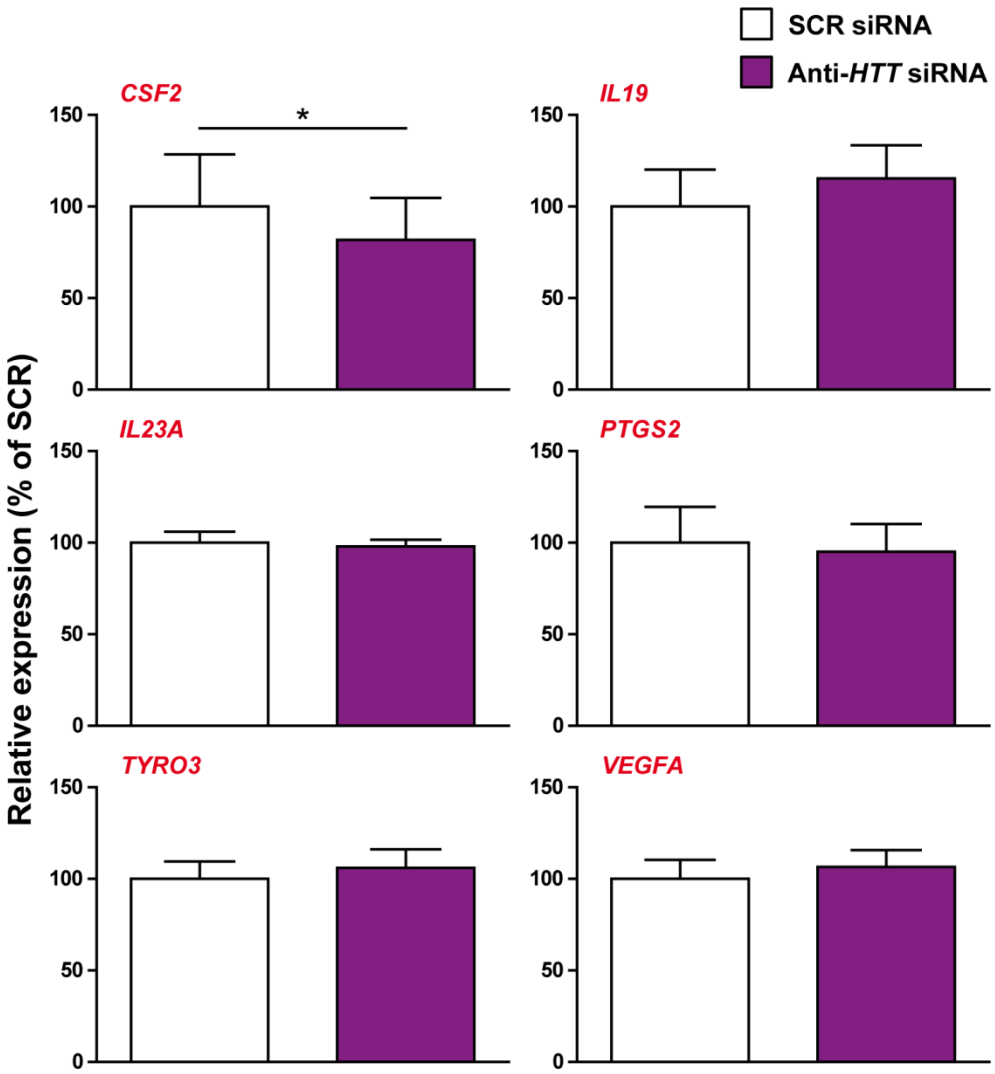

Figure 4.6. Analysis of gene expression changes following HTT-lowering in HD monocytes. Monocytes were isolated from manifest HD patients and transfected with GeRPs containing either SCR or anti-total *HTT* siRNA. RNA was harvested after 72 h and used for gene expression analysis by qPCR. Consistent with the RNA-Seq data, with the exception of *CSF2* no reversal of HD-related gene expression changes was seen in the samples treated with anti-total *HTT* siRNA. Data shown as relative expression ± SEM (*n* = 9), statistical analysis carried out using two-tailed paired Student's t-tests. *P < 0.05.

4.6 Discussion

Previous studies of HD myeloid cells have primarily focused on characterising their responses to stimulation, for example using LPS (Träger et al., 2014). While this has generated a wealth of functional data, notably their hyper-reactive cytokine phenotype, relatively little is known about whether HD myeloid cells are also abnormal in their basal, resting state. Work presented in this chapter makes use of modern RNA-Seq technology to show that HD monocytes have a significantly altered resting transcriptome. This suggests that mHTT has a state-independent effect on HD myeloid cells, likely occurring via a mechanism that is not limited to alterations in intracellular signalling pathways following stimulation. This should perhaps not be surprising, as mHTT has been shown to have state-independent effects on gene expression in a wide range of tissues from HD patients and animal models, including brain, skeletal muscle and whole blood (Seredenina and Luthi-Carter, 2012).

Crucially, analysis of the HD monocyte transcriptome found that proinflammatory cytokines and chemokines are upregulated even in the absence of stimulation, for the first time showing increased resting cytokine expression at either the mRNA or protein level. Profiling of HD patient plasma has demonstrated elevated peripheral levels of proinflammatory cytokines and chemokines (Björkqvist et al., 2008; Wild et al., 2011), with increased IL-6 being detectable up to 16 years before predicted disease onset. While myeloid cells have long been regarded as the likely primary source, this study provides the first direct evidence that their cytokine

expression is increased without artificial experimental stimuli, with *IL6* being among the gene transcripts most affected. The existence of broad proinflammatory changes in the resting HD monocyte transcriptome was confirmed by GSEA, which identified significant enrichment of numerous functional gene sets relating to innate immunity, inflammation and cytokine production. This was vital for assigning wider biological relevance to the RNA-Seq expression changes, in addition to avoiding the potential investigator bias that could result from examining specific genes in isolation. Examination of directionality revealed that the majority of significant expression changes involved upregulation; this is consistent with a previous RNA-Seq study carried out on post-mortem HD brain (Labadorf et al., 2015).

Experiments on human monocyte models have shown that mHTT expression has cell-autonomous effects on immune cell function (Träger et al., 2014), and that the phenotypic changes observed in these cells are not simply a secondary response to CNS pathology. Furthermore, mHTT has been suggested to have a proinflammatory priming effect on a murine HD microglial cell line, with an increase in the resting expression of proinflammatory molecules leading to an exaggerated response once a stimulus is encountered (Crotti et al., 2014). This was found to occur as the result of an enrichment of proinflammatory transcription factors including the myeloid lineage-determining factor PU.1. Data presented in this thesis strongly suggests that mHTT has an equivalent priming effect on primary human myeloid cells; this is likely to contribute to the hyper-reactive cytokine response to LPS stimulation.

Furthermore, the discovery of resting proinflammatory changes in HD monocytes is likely to have significant relevance for the pathobiology of the disease in human patients. Although elevated cytokine levels have been demonstrated in HD plasma (Björkqvist et al., 2008), there is currently no evidence that HD patients have an increased incidence of infectious or inflammatory events compared to control subjects. Indeed, the disease-modifying benefits of modulating the peripheral immune system in animal models of HD are not dependent on the amelioration of artificial inflammatory stimuli (Bouchard et al., 2012; Hsiao et al., 2014; Zwilling et al., 2011). These observations suggest that the *in vivo* proinflammatory changes seen in HD are not dependent on, or primarily caused by, episodic excessive cytokine release from cells undergoing repeated stimulation. Instead, they may be reconciled by a chronic increase in the basal release of proinflammatory mediators from circulating myeloid cells. Further mechanistic rationale for this hypothesis is provided by the fact that several of the upregulated cytokines in HD peripheral blood are pre-synthesised in the resting state. TNFα is synthesised as a membrane-bound precursor that is cleaved in response to stimulation (Black et al., 1997), while IL-8 undergoes vesicular storage prior to release (Lacy and Stow, 2011). Myeloid cell priming by mHTT could therefore result in increased cytokine storage in advance of stimulation, or indeed increased basal release in the absence of stimulation. The elevated cytokine levels seen in HD patient plasma perhaps suggest that the latter effect is more likely.

While time and cost restrictions meant that it was only possible to include manifest HD patients as part of this study, it is likely that the mHTT-priming

phenomenon also exists in pre-manifest subjects. Previous studies have shown that immune alterations are detectable many years before the onset of motor symptoms (Björkqvist et al., 2008); this includes the release of proinflammatory mediators such as IL-6. The transcriptional changes seen in HD monocytes therefore seem unlikely to only appear once a patient has progressed to manifest disease. Crucially, the short lifespan of peripheral blood cells precludes the possibility of a chronic effect built up over many years, as may be the case for long-lived cells such as neurons. This hypothesis is supported by the presence of cell-autonomous dysfunction in HD myeloid cells (Träger et al., 2014), as peripheral immune changes have been shown to occur independently of neurodegeneration; they are therefore unlikely to be closely linked to the symptoms associated with advancing disease in the CNS. The potential disease-modifying role of the peripheral immune system raises the intriguing possibility that HD myeloid cells may even be involved in the modification of disease onset, however this will remain conjecture until further studies are carried out.

Perhaps the most surprising feature of this study was the lack of significant alterations in the transcriptome of stimulated HD monocytes. While the directions of effect between HD and control were largely consistent, comparison of the log2 fold changes for the 130 differentially expressed genes revealed that the relative size of the majority of the fold changes was reduced under stimulated conditions to the point that the expression differences were no longer significant. This may be due to the extremely strong activating response produced by LPS, leading to a plateau in transcriptional activity as the cell reaches the limits of its mRNA synthesis

capacity. This is likely to result in the masking of biological differences, as the proinflammatory transcriptional profile of resting HD monocytes is ablated by the stronger inflammatory stimulus provided by LPS. In view of the lack of differential expression in stimulated HD monocytes, the basal priming effects of mHTT only seem more likely to mediate the hyper-reactive LPS response.

Interestingly, GSEA revealed significant enrichment of a number of gene sets among the downregulated genes in stimulated HD monocytes. Alterations in functional gene sets relating to protein localisation and targeting is consistent with established defects in the HD cytoskeleton (Gunawardena et al., 2003), while further enrichment was observed in gene sets relating to organelles known to be affected by mHTT expression, including mitochondria and the lysosome (Damiano et al., 2010; Turner et al., 2009; Martin et al., 2015). However, while these results show that mHTT has adverse effects on the transcriptome of stimulated HD monocytes, the small number of differentially expressed genes suggests that these enrichments may not have the same biological significance as those seen basally.

Although the expression changes alone provide strong evidence that mHTT expression has a priming effect on the transcriptome of resting HD monocytes, further investigation of intracellular signalling pathways is required to identify the underlying mechanism. Studies in cell lines have revealed an interaction of mHTT with IKK, one of the key components of the NFκB pathway (Khoshnan et al., 2004); this results in increased phosphorylation of the NFκB inhibitor IκB, leading to an increase in the expression of proinflammatory genes as more NFκB molecules are free to translocate to the nucleus. This mechanism has been linked to hyper-

reactivity in HD myeloid cells (Träger et al., 2014), however it was not previously known if it also has an effect in the resting state. Following IPA® identification of RELA, NFκB1 and the NFκB complex as potential regulators of transcriptional dysregulation, functional validation by Western blotting revealed a significant reduction in the expression of IκBα in unstimulated HD myeloid cells; this provides strong evidence that NFκB signalling is also affected basally. These data provide a mechanistic explanation for the priming hypothesis, as this abnormal resting activation of NFκB signalling is likely to play a key role in mediating the proinflammatory transcriptional changes seen in HD monocytes.

This result, coupled with the redundancy inherent in IPA®, means it is highly likely that the activation of a number of other upstream regulators will have been inferred due to their target gene overlap with NFκB, and not because they are also affected by the expression of mHTT. This can be seen in the fact that thirteen of the fifteen upstream regulators with the most significant activation z-scores are known to be involved in NFκB signalling (whether as an activating cytokine, cell surface receptor or downstream transcription factor). The enrichment of a functional gene set relating to the NFκB signalling cascade on GSEA analysis further supports this conclusion. Other notable hits included the ERK and p38 MAPKs, in addition to the transcription factor STAT3. However, JAK/STAT signalling has previously been shown to be unaffected in HD myeloid cells (Träger et al., 2013); STAT3's considerable target gene overlap with NFκB is therefore likely to be responsible for its inferred activation on IPA® (Hoesel and Schmid, 2013). The ERK and p38 MAPKs are vital components of the intracellular signalling

cascade downstream of TLR4 (Akira and Takeda, 2004). However, investigation of their activation states using Western blotting revealed no changes between HD and control myeloid cells, either basally or at any point during the experimental time course. While additional pathogenic interactions of mHTT with the transcriptional machinery cannot be ruled out, taken together these data further suggest that the observed transcriptional changes are likely to be due in large part to resting dysfunction in the NFκB pathway.

However, it should be noted that not all mHTT-related transcriptional changes are pathological, as some may be compensatory or even irrelevant (Seredenina and Luthi-Carter, 2012). Transcriptional dysregulation in HD is the result of a wide range of mechanisms, including but not limited to the sequestration of transcription factors in aggregates and the direct binding of mHTT fragments to DNA (Seredenina and Luthi-Carter, 2012). It should therefore not be expected that alterations in intracellular signalling pathways will account for all of the expression changes seen in HD monocytes, as a number will presumably be due to the alternative effects of mHTT on the cellular transcriptome. Despite this, upstream regulator analysis has been shown to be a useful tool for investigating HD immune cell function, particularly when combined with subsequent functional experiments.

Furthermore, the data presented in this chapter suggest that the pre-eminent pathogenic mechanisms of mHTT are likely to vary depending on the cell type in question. Experiments on a murine HD microglial cell line found that increased expression of the PU.1 transcription factor mediates resting proinflammatory transcriptional activation in this model (Crotti et al., 2014). However, neither that study nor the current study found any increase in PU.1

expression in HD patient monocytes. IPA® of the unstimulated dataset also did not infer any significant activation of PU.1 in resting HD monocytes. Regardless, this study demonstrates that mHTT has a similar priming effect on the transcriptome of HD monocytes to that described in the murine microglial line. The authors of the microglial study suggested that the prominent role for PU.1 is due to the separate developmental origins of microglia (Crotti et al., 2014). However, it is also likely that the relative importance of particular intracellular signalling pathways in specific cell types helps determine their varying contributions to HD pathogenesis. The fact that NFκB binding motifs were also found to be enriched in the microglial line shows that the mechanisms by which mHTT interacts with each signalling pathway are unlikely to be drastically altered between cell types (Crotti et al., 2014). However, as the PU.1 and NFκB pathways are vital for microglial and monocyte/macrophage function respectively, it is not surprising that their dysregulation by mHTT will cause them to have a central role in mediating phenotypic dysfunction in these cell types. Conversely, equivalent dysfunction is unlikely to be displayed by cells where these pathways play less important roles. This can be seen in the results described in Chapter 5.

Surprisingly, both RNA-Seq and qPCR analysis failed to reveal any substantial reversal of the expression changes described in unstimulated monocytes following treatment with anti-total *HTT* siRNA. It is possible that this is due to the cellular kinetics of mHTT, whereby the pathogenic species responsible for transcriptional dysregulation persist longer than the 72 h time point used for these experiments. It may also be that the transcriptional changes associated with mHTT expression take time to normalise following a

reduction in mHTT protein. While it is encouraging that qPCR revealed a significant reduction in *CSF2* expression following anti-total *HTT* siRNA treatment, a longer time course is required to determine if more sustained HTT-lowering results in a similar reversal of additional expression changes. However, this is problematic when studying monocytes, as they are short-lived cells that are ill-suited to lengthy experimental workflows.

Finally, this study demonstrates that the in-depth characterisation of HD-associated transcriptional changes requires the study of specific cell populations from large patient cohorts with modern sequencing techniques. Previous analyses of HD peripheral immune cells have largely been unable to replicate differentially expressed genes between studies (Borovecki et al., 2005; Runne et al., 2007; Mastrokolias et al., 2015); this is likely due to the use of heterogeneous cell populations, in addition to the limitations associated with less advanced analytical techniques. Dramatically improved transcriptomic coverage compared to traditional microarrays has been provided by high-throughput sequencing (Wang et al., 2009), while the study of a specific cell subset allows the noise associated with studying multiple cell populations with varying transcriptional profiles to be eliminated. While the recruitment of such large patient cohorts raises substantial practical considerations, the fact that genomic studies in mice have been found to poorly mimic human inflammatory conditions only underlines the importance of thoroughly investigating primary human tissues (Seok et al., 2013). There is also no guarantee that observations made in one cell type will apply to another, as it has not been possible to establish a consistent transcriptional signature between different HD tissues (Seredenina and Luthi-Carter, 2012).

4.7 Summary

This study used RNA-Seq to carry out whole transcriptome analysis of HD and control monocytes in both the unstimulated and stimulated states. The work presented in this chapter provides the first evidence that HD myeloid cells are basally abnormal, with increased expression of proinflammatory cytokine mRNA even in the absence of stimulation. A comprehensive GSEA further revealed significant enrichment of functional gene sets relating to innate immunity, inflammation and cytokine production. In contrast, the transcriptome of stimulated HD monocytes was comparatively unaffected. These data suggest that mHTT has a cell-autonomous priming effect on resting HD monocytes, leading to an exaggerated proinflammatory response to stimulation. IPA® combined with Western blotting was then used to demonstrate that the NFκB dysregulation previously described in stimulated HD myeloid cells also extends to the resting state; abnormal activation of this pathway is likely to be a key mechanism in mediating the observed transcriptional changes. However, no differences were seen in ERK and p38 MAPK signalling between either unstimulated or stimulated HD and control myeloid cells. Surprisingly, HTT-lowering did not produce a substantial reversal of gene expression changes; this was likely due to the persistence of pathogenic mHTT species beyond the time point used for the experiment. The existence of basal dysfunction is encouraging for the potential use of immunomodulatory drugs to modify HD progression, as the beneficial effects are likely to extend beyond ameliorating the consequences of time-limited infectious or inflammatory events. This only serves to reinforce the importance of systemic immunity in the wider study of neurodegeneration.

5 Adaptive immune biology in HD

5.1 Background

While changes in the immune system are now an established feature of HD pathogenesis (Ellrichmann et al., 2013), it remains unclear if HD immune dysfunction is universal, or is instead restricted to specific cell types. To date, the vast majority of studies have focused on characterising the HD innate immune system, with work presented in Chapter 4 of this thesis demonstrating that HD myeloid cells have an abnormal proinflammatory transcriptional profile even in the absence of stimulation. However, while the phenotypic abnormalities associated with HD innate immune cells are now relatively well understood (Träger et al., 2014; Kwan et al., 2012b), very little is known about the adaptive immune system in HD.

In contrast to the innate immune system, which provides an immediate generic response to a wide range of pathogens, the adaptive immune system generates a highly specific secondary response that is also known as immunological memory. The adaptive immune response is largely mediated by T lymphocytes, that produce cytokines to enhance or suppress the activity of other immune cells, and B lymphocytes, that generate antibodies following exposure to specific pathogens. T lymphocytes may be further categorised into a wide range of subtypes, including $CD4^+$ helper T lymphocytes and $CD8^+$ cytotoxic T lymphocytes. There is much interplay between the innate and adaptive immune systems, for example through the formation of cytokine

feedback loops; such interactions are required for both to function effectively (Iwasaki and Medzhitov, 2015; Shanker, 2010).

Despite the advances made in the study of HD immunity, it is not currently clear whether such interplay is affected in HD, or if the cells of the adaptive immune system even experience comparable dysfunction to their innate immune counterparts. Answering this question is vital to fully understanding the mechanisms behind HD immune dysfunction, as the key role of T lymphocytes in common processes such as cytokine production means it is certainly possible that they contribute to the elevated peripheral levels seen in HD patients. Indeed, there is considerable overlap in the cytokines produced by the innate and adaptive immune systems; this is the case for IL-6, increased levels of which are detectable in HD plasma up to 16 years before the predicted onset of motor symptoms (Björkqvist et al., 2008). It is a further possibility that dysfunction in each arm of the immune system contributes to that of the other; for example, elevated cytokine production by helper T lymphocytes would lead to an enhanced macrophage response that would exacerbate the *ex vivo* dysfunction that has previously been demonstrated in HD myeloid cells. This means it is not possible to conclude that the innate immune system is solely responsible for HD immune dysfunction until adaptive immunity has been comprehensively investigated.

Previous work has shown that HD T lymphocytes express mHTT, the levels of which correlate with disease burden scores in a similar manner to that of HD monocytes (Weiss et al., 2012). Levels of the signature T_h2 cytokine IL-4 are also elevated in the peripheral blood of HD patients with advanced disease, suggesting that mHTT may have an adverse effect on T lymphocyte

function (Björkqvist et al., 2008). However, the same study found that circulating Ig levels are not altered in the plasma of HD patients, perhaps pointing away from widespread changes in HD adaptive immune function. Furthermore, a recent study found that T lymphocytes are not significantly enriched in post-mortem brain tissue from HD patients (Silvestroni et al., 2009). However, this evidence remains largely circumstantial, and the functional properties of HD adaptive immune cells are yet to be directly studied in isolation. In order to answer the question of whether the peripheral adaptive immune system is contributing to HD pathogenesis, a comprehensive, multi-faceted approach to investigating the intrinsic biology of T lymphocytes is required.

5.2 Aims

1. To determine whether the frequencies of circulating immune cells are altered between human HD and control peripheral blood.

2. To characterise the phenotype of human HD T lymphocytes by investigating proliferation and cytokine production.

3. To examine the expression of key T lymphocyte related genes in human HD and control helper T lymphocytes.

4. To determine whether HD peripheral immune dysfunction is universal or restricted to specific immune cell subsets.

5.3 Methods

PBMCs were isolated using density centrifugation (Section 2.4.1), before $CD4^+$ helper T lymphocytes were isolated using magnetic cell sorting (Section 2.4.2). T lymphocytes were stimulated using either anti-human CD3 and anti-human CD28 functional grade antibodies or PHA-P (Section 2.4.4). Flow cytometric analysis of cell surface and intracellular markers was used to quantify peripheral immune subsets (Section 2.13). T lymphocyte proliferation was analysed using CFSE (Section 2.6.4), while T lymphocyte cytokine production was quantified using MSD cytokine assays (Section 2.12.2). Cytokine values were normalised to total protein levels as measured by BCA assays (Section 2.11.2). Transcriptional profiling of $CD4^+$ T lymphocytes was carried out using multiplex PCR arrays (Section 2.9). Statistical analysis was carried out according to Section 2.14.3.

5.4 Contributions

Flow cytometric analysis of immune cell subsets was carried out in collaboration with Dr Ulrike Träger. The remainder of the experiments were performed and analysed in their entirety by James Miller. Findings presented in this chapter were published in PLOS ONE (full manuscript included in the appendices of this thesis):

Miller, J.R., Träger, U., Andre, R., Tabrizi, S.J. 2015. Mutant Huntingtin Does Not Affect the Intrinsic Phenotype of Human Huntington's Disease T Lymphocytes. *PLOS ONE* [online], 10(11), e0141793. Available from: doi: 10.1371/journal.pone.0141793.

5.5 Results

5.5.1 The circulating monocyte balance is altered between HD and control peripheral blood

HD patients of all disease stages have been shown to have elevated levels of circulating proinflammatory cytokines and chemokines compared to controls (Björkqvist et al., 2008; Wild et al., 2011). While this is likely to be primarily due to transcriptional and functional alterations in HD myeloid cells (Träger et al., 2014), a potential contributing factor is a shift in the relative frequencies of immune cell subtypes in HD peripheral blood, leading to a change in the cytokine environment being produced. In order to address this, PBMCs were isolated from peripheral blood samples donated by HD and control subjects. The PBMCs were then then stained with antibodies to a wide range of cellular markers, before being analysed by flow cytometry.

While the focus of this chapter is primarily on the cells of the adaptive immune system, innate immune cell subsets were also included in the antibody panels as their relative prevalence in HD peripheral blood has not been previously studied. This is especially important as primed circulating monocytes are likely to be a key source of the elevated peripheral cytokine levels seen in HD (see Chapter 4). Flow cytometric analysis revealed a significant ($p < 0.01$) increase in the frequency of classical ($CD14^{++}$ $CD16^{-}$) monocytes in HD compared to control PBMCs (Fig. 5.1; gating in Fig. 5.2). This raises the possibility that alterations in the circulating monocyte balance contribute to peripheral cytokine upregulation in HD. However, the frequency of alternative ($CD14^{+}$ $CD16^{++}$) monocytes was not found to be affected.

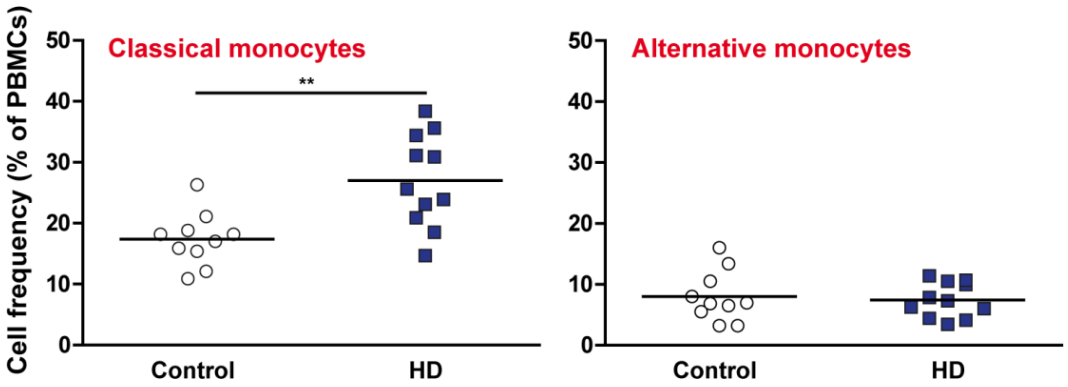

Figure 5.1. The circulating monocyte balance is altered between HD and control peripheral blood. PBMCs were isolated from HD and control peripheral blood, before the frequencies of classical ($CD14^{++}$ $CD16^{-}$) and alternative ($CD14^{+}$ $CD16^{++}$) monocytes were measured by flow cytometry. The frequency of classical monocytes was found to be significantly increased in HD peripheral blood compared to control, while the frequency of alternative monocytes was unaffected. Statistical analysis was carried out using two-tailed unpaired Student's *t*-tests. **P < 0.01.

5.5.2 The frequencies of additional immune cell subsets are not altered between HD and control peripheral blood

Concurrently, the same PBMC samples were used to analyse the frequencies of additional key cell types in the peripheral immune system (Table 5.1). In contrast to the changes seen in classical monocytes, no significant differences were seen in the frequencies of any of the major T lymphocyte subsets that were investigated (Fig. 5.3; gating in Fig. 5.4). This is consistent with a recent study showing that the frequency of $CD3^{+}$ T lymphocytes is not altered between the spleen and bone marrow of R6/2 and wild-type mice (Träger et al., 2015). The activation levels of these T lymphocyte subsets were further assessed by $CD62L^{low}$ expression; again, no differences were seen between the HD and control PBMCs (Fig. 5.5).

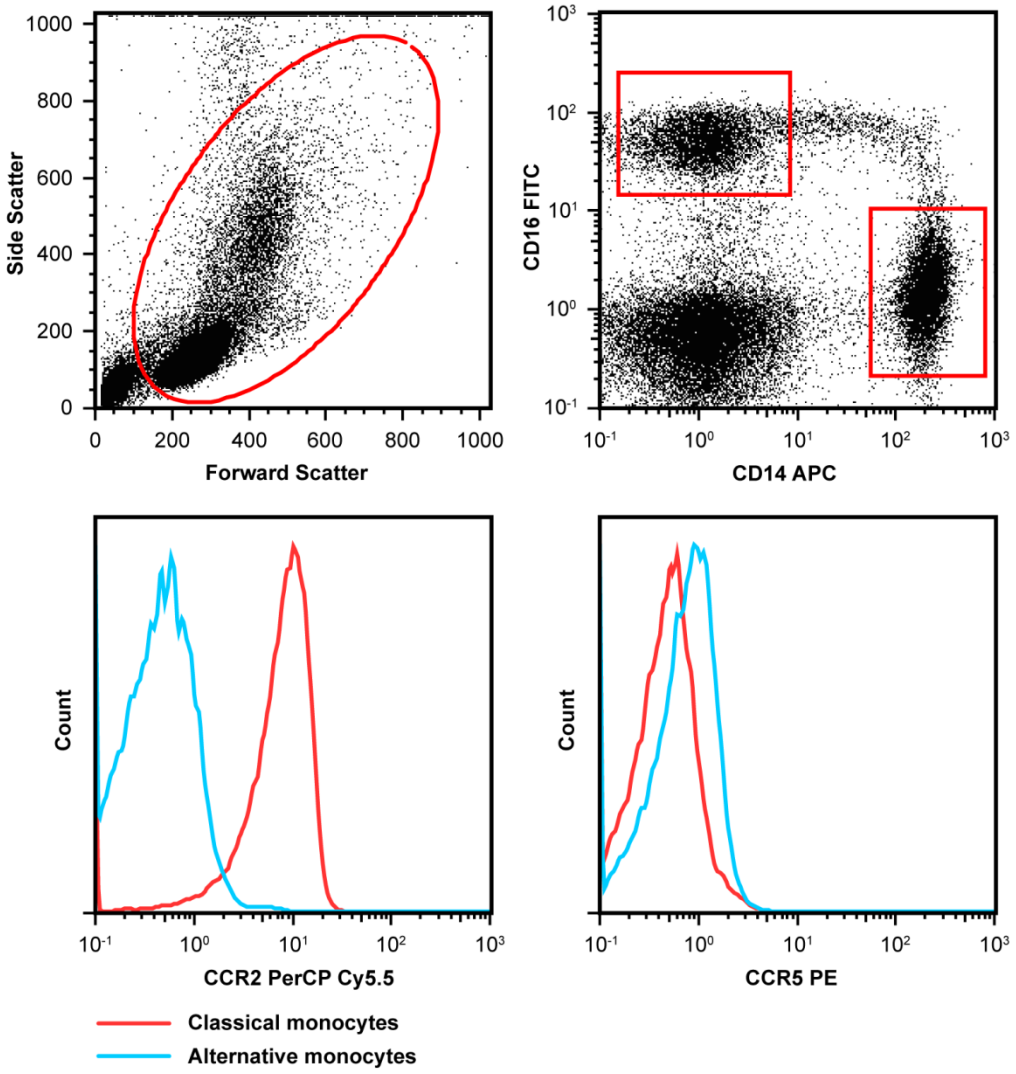

Figure 5.2. Gating strategy for analysis of monocyte subsets. After gating on live cells using a FSC/SSC gate, a CD14 vs. CD16 plot was used to determine the percentages of classical ($CD14^{++}$ $CD16^{-}$) and alternative ($CD14^{+}$ $CD16^{++}$) monocytes. These populations were then confirmed using histograms for CCR2 (classical monocytes) and CCR5 (alternative monocytes).

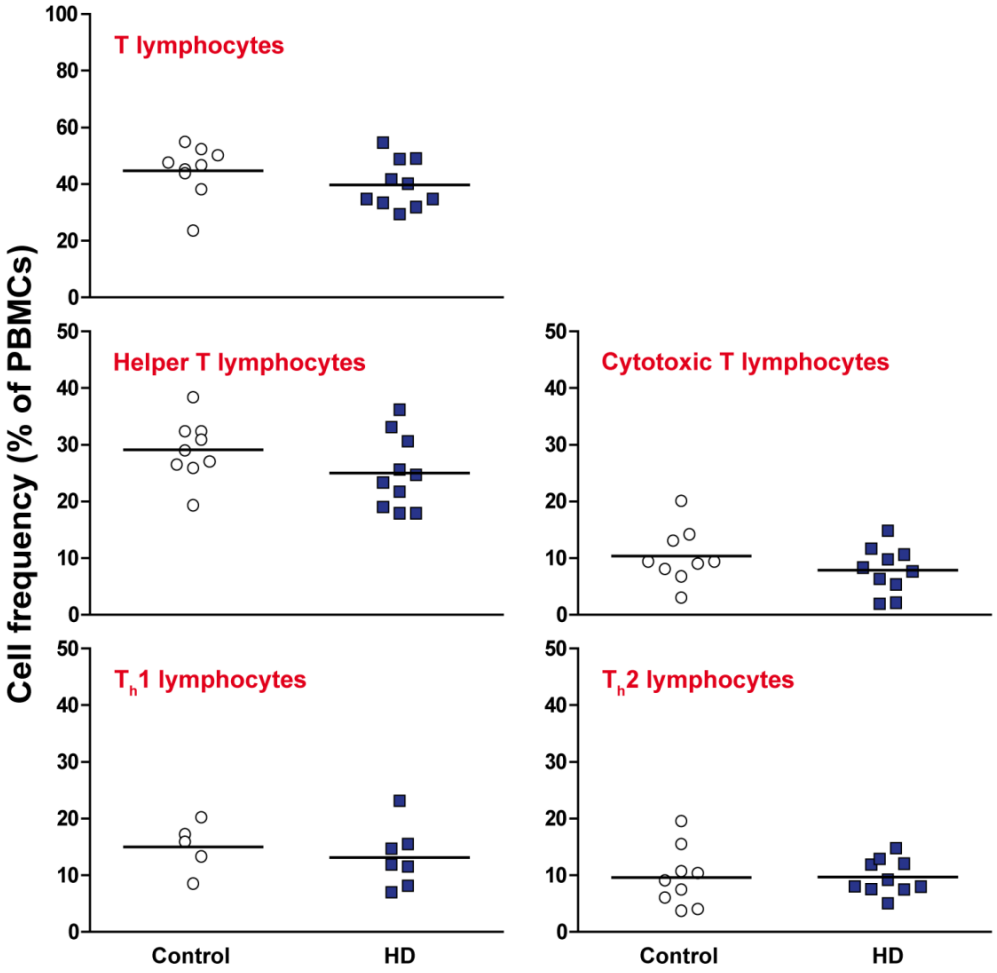

Figure 5.3. The frequencies of CD3⁺ T lymphocyte subsets do not differ between HD and control peripheral blood. PBMCs were isolated from HD and control peripheral blood samples and the frequencies of a range of T lymphocyte populations were measured by flow cytometry using antibodies to T lymphocytes ($CD3^+$), helper T lymphocytes ($CD3^+$ $CD4^+$) and cytotoxic T lymphocytes ($CD3^+$ $CD8^+$). Within the helper T lymphocyte population, the T_h1 and T_h2 subtypes were analysed using antibodies to CXCR3 and CCR4 respectively. No significant differences were seen between HD and control for any of the cell subsets. Statistical analysis was carried out using two-tailed unpaired Student's *t*-tests.

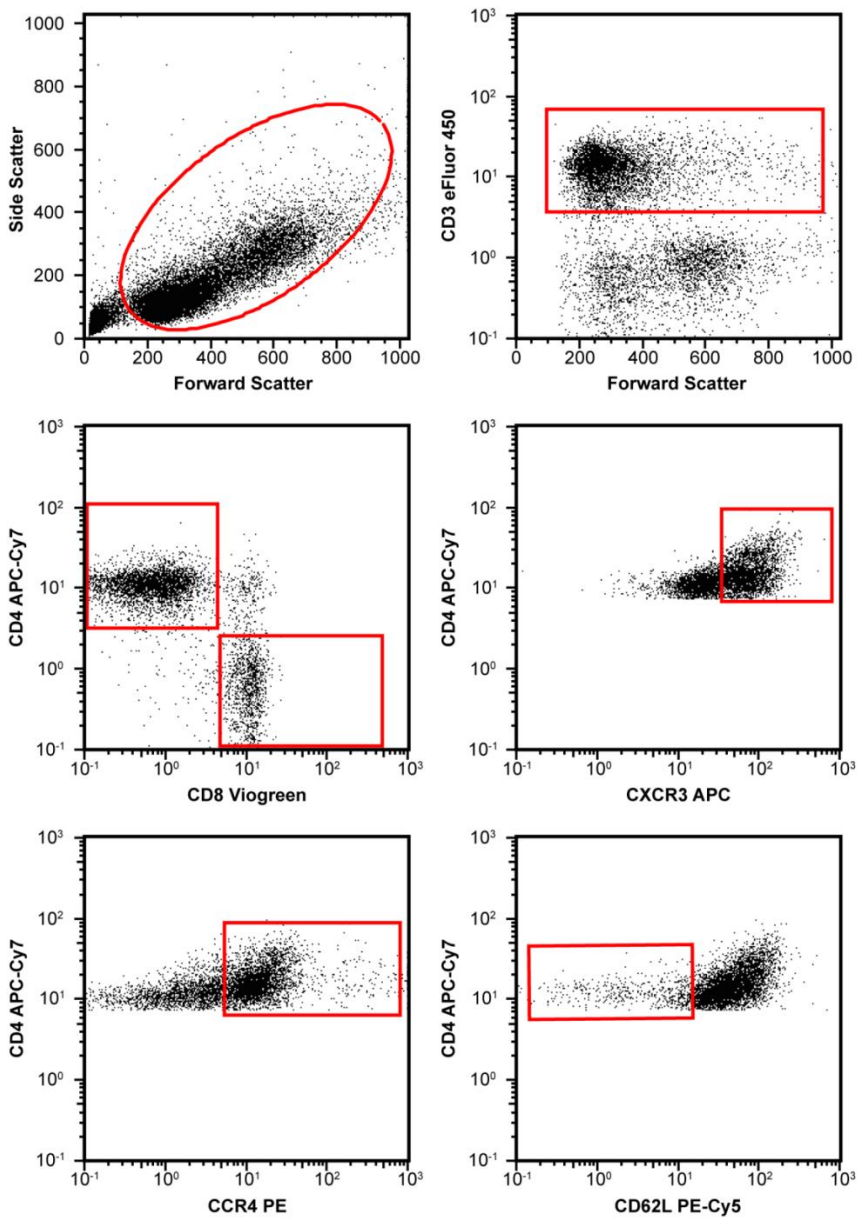

Figure 5.4. Gating strategy for CD3⁺ T lymphocyte subset analysis. After gating on live cells using a FSC/SSC gate, a FSC vs. CD3 plot was used to determine the frequency of $CD3^+$ T lymphocytes. Within the $CD3^+$ population, the frequencies of $CD4^+$ helper T lymphocytes and $CD8^+$ cytotoxic T lymphocytes were determined, before the frequencies of $CXCR3^+$ T_h1 and $CCR4^+$ T_h2 lymphocytes within the $CD4^+$ helper T lymphocyte population were determined. Activation levels of T lymphocytes were also determined based on $CD62L^{low}$ expression.

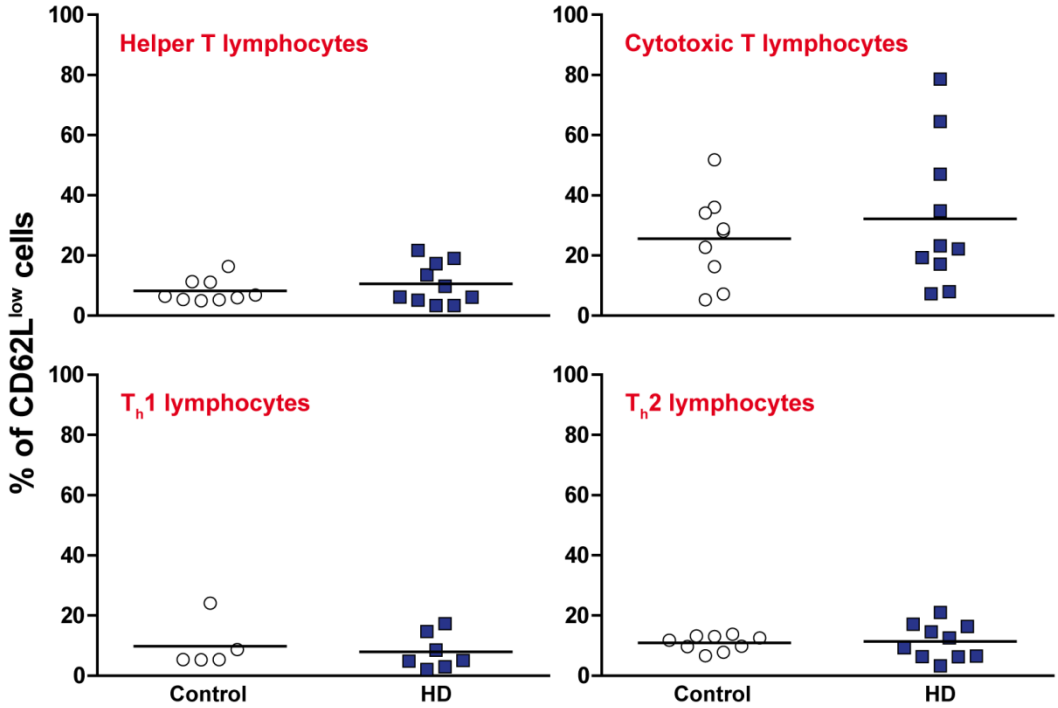

Figure 5.5. Activation levels of CD3⁺ T lymphocyte subsets are not altered between HD and control peripheral blood. Within the previously analysed T lymphocyte populations (Fig. 5.3.), the activation levels of each were measured using $CD62L^{low}$ expression. No significant differences were seen in the activation of any of the HD cell subsets compared to control. Statistical analysis was carried out using two-tailed unpaired Student's *t*-tests.

An additional antibody panel was used to analyse the frequencies of T_h17 lymphocytes, T_{reg} lymphocytes, NK cells and NKT cells. As with the above $CD3^+$ T lymphocyte subsets, no significant differences were seen between HD and control for any of the cell subsets that were investigated (Fig. 5.6; gating in Fig. 5.7).

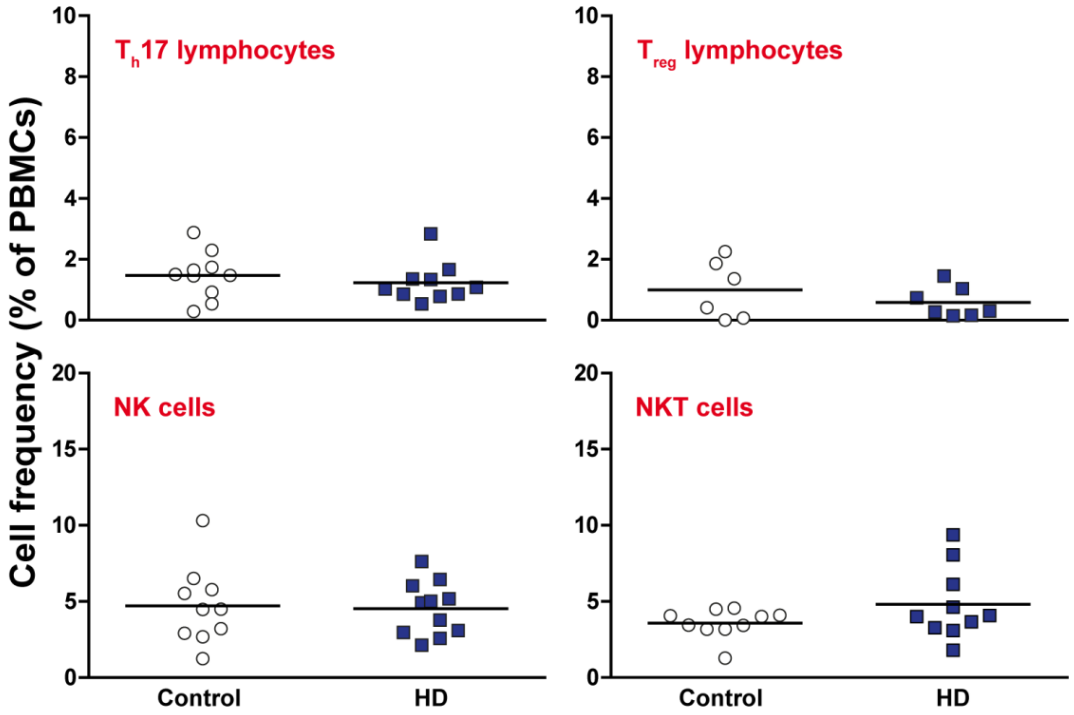

Figure 5.6. The frequencies of additional immune cell subsets are not altered between HD and control peripheral blood. The frequencies of additional immune cell subsets in HD and control peripheral blood were measured using antibodies to T_h17 lymphocytes ($IL\text{-}17^+$), T_{reg} lymphocytes ($CD25^+$ $FOXP3^+$), NK cells ($CD3^-$ $CD56^+$) and NKT cells ($CD3^+$ $CD56^+$). No significant differences were seen between HD and control for any of the cell types that were analysed. Statistical analysis was carried out using two-tailed unpaired Student's *t*-tests.

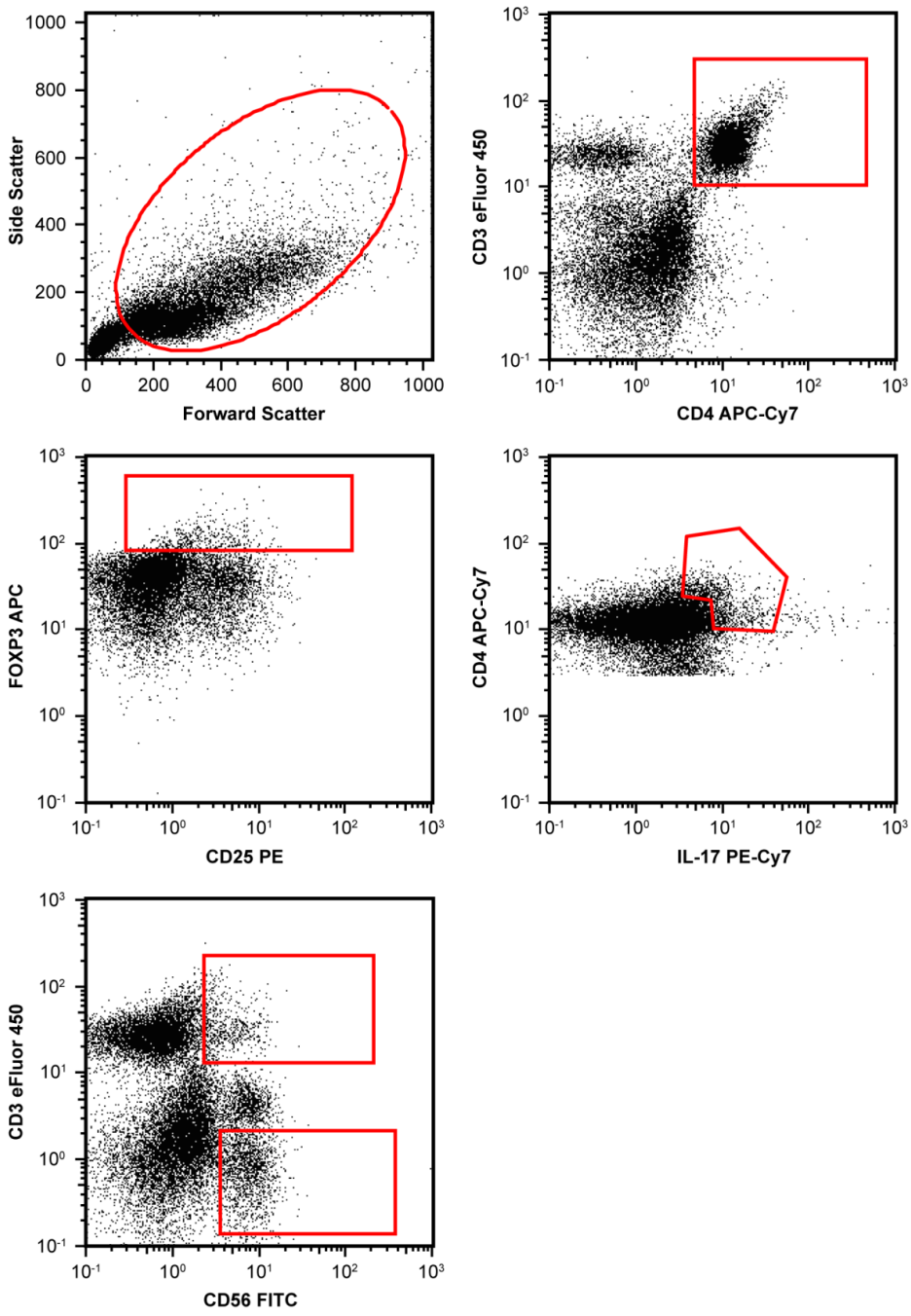

Figure 5.7. Gating schematic for T_h17 lymphocyte, T_{reg} lymphocyte, NK cell and NKT cell analysis. After gating on live cells using a FSC/SSC gate, a CD3 vs. CD56 plot was used to determine the frequencies of NK cells ($CD3^-$ $CD56^+$) and NKT cells ($CD3^+$ $CD56^+$). Within the $CD3^+$ $CD4^+$ T lymphocyte population, the frequencies of the T_{reg} ($CD25^+$ $FOXP3^+$) and T_h17 ($IL\text{-}17^+$) lymphocyte subsets were also determined.

Finally, the frequencies of the main cell types involved in humoral immunity were measured using antibodies to B lymphocytes and plasma cells. Once more, no significant differences in their frequencies were detected between the HD and control PBMC populations (Fig. 5.8; gating in Fig. 5.9). This is consistent with a previous study showing that B lymphocyte frequencies are not altered in the spleens of R6/2 and wild-type mice (Träger et al., 2015). These data suggest that, with the exception of classical monocytes, there are no substantial alterations in the relative frequencies of the major immune cell subsets in HD and control peripheral blood.

Table 5.1. Summary of immune cell subset analysis.

Immune cell subset	Cellular markers	Altered in HD?
Classical monocytes	$CD14^{++}$ $CD16^{-}$	Yes (increased)
Alternative monocytes	$CD14^{+}$ $CD16^{++}$	No
T lymphocytes	$CD3^{+}$	No
Helper T lymphocytes	$CD3^{+}$ $CD4^{+}$	No
T_h1 lymphocytes	$CD3^{+}$ $CD4^{+}$ $CXCR3^{+}$	No
T_h2 lymphocytes	$CD3^{+}$ $CD4^{+}$ $CCR4^{+}$	No
Cytotoxic T lymphocytes	$CD3^{+}$ $CD8^{+}$	No
T_h17 lymphocytes	$CD3^{+}$ $CD4^{+}$ $IL\text{-}17^{+}$	No
T_{reg} lymphocytes	$CD3^{+}$ $CD4^{+}$ $CD25^{+}$ $FOXP3^{+}$	No
NK cells	$CD3^{-}$ $CD56^{+}$	No
NKT cells	$CD3^{+}$ $CD56^{+}$	No
B lymphocytes	$CD19^{++}$	No
Plasma cells	$CD19^{+}$ $CD138^{+}$	No

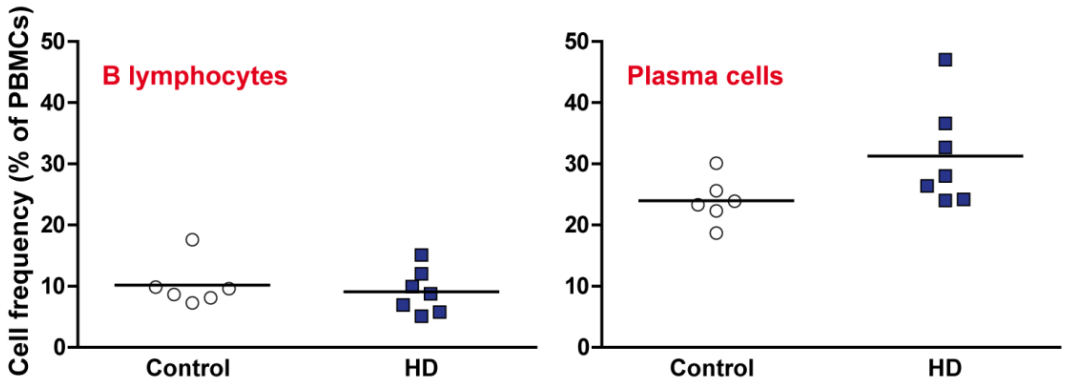

Figure 5.8. The frequencies of humoral immune cell subsets are not altered between HD and control peripheral blood. PBMCs were isolated from HD and control peripheral blood samples and the frequencies of B lymphocytes ($CD19^{++}$) and plasma cells ($CD19^{+}$ $CD138^{+}$) were measured by flow cytometry. No significant differences were seen between HD and control for either cell subset. Statistical analysis was carried out using two-tailed unpaired Student's *t*-tests.

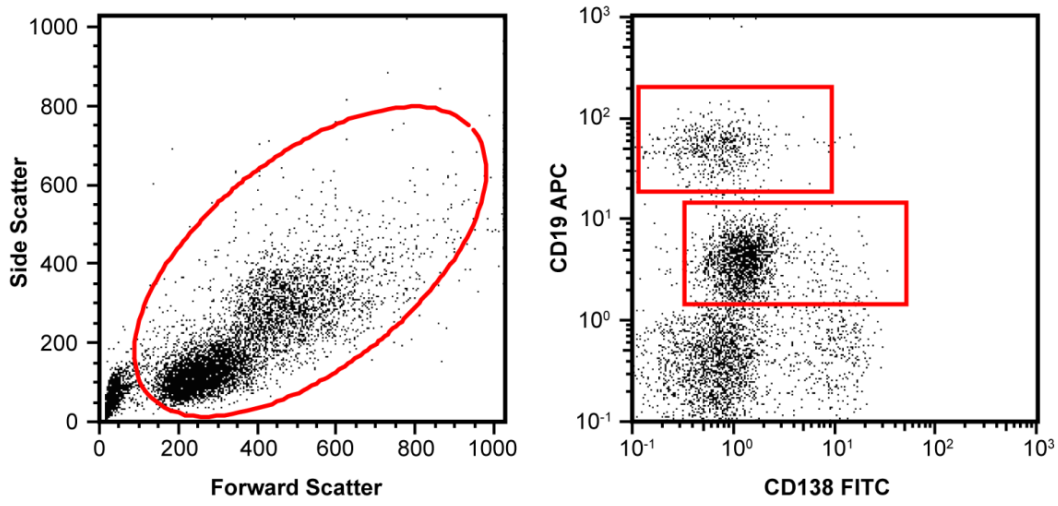

Figure 5.9. Gating schematic for humoral cell analysis. After gating on live cells using a FSC/SSC gate, a CD19 vs. CD138 plot was used to determine the frequencies of B lymphocytes ($CD19^{++}$) and plasma cells ($CD19^{+}$ $CD138^{+}$).

5.5.3 T lymphocyte proliferation is not impaired in HD

While the above data demonstrate that there are no changes in the frequencies of key adaptive immune cell subsets in HD peripheral blood, investigating the phenotype of these cells remains vital for determining whether the adaptive immune system is functionally affected by the expression of mHTT. Myeloid cells from HD patients display functional deficits when migrating to chemotactic stimuli and phagocytosing fluorescent beads (Kwan et al., 2012b; Träger et al., 2015). Here, HD T lymphocytes were investigated to identify comparable functional abnormalities.

The ability of lymphocytes to rapidly proliferate in response to a stimulus is a key feature of adaptive immunity. PBMCs were isolated from peripheral blood samples donated by manifest HD and control subjects, before being stained with the intracellular dye CFSE. CFSE is a highly stable fluorescent dye that is evenly distributed between the two daughter cells produced when a cell divides. This allows the tracking of multiple cell divisions *in vitro* as a sequential halving of fluorescence intensity on flow cytometry (Quah et al., 2007; Hawkins et al., 2007). After staining, the PBMCs were either left unstimulated, stimulated with anti-CD3 and anti-CD28 antibodies, or stimulated with PHA-P. This enabled testing of the cells' responses to antigenic and mitogenic stimuli, respectively. Cultures were harvested after 72, 96 and 120 h to build up a broad profile of the proliferative response. Additional flow cytometry antibodies were used to independently investigate proliferation in the T lymphocyte, helper T lymphocyte and cytotoxic T

lymphocyte populations (gating schematic in Fig. 5.10); these data were then analysed using a range of statistics outlined by Roederer (Roederer, 2011).

The most common statistic used to analyse lymphocyte proliferation data is 'fraction diluted', which uses a univariate CFSE gate to determine the percentage of cells in the final culture that have divided at least once. However, this is a somewhat simplistic assessment of the data, as it provides no information on the proportion of cells from the initial population that entered division, or indeed the number of divisions those cells have undergone. This information is provided by the 'percentage divided', 'proliferation index' and 'division index' statistics (Table 5.2). The proliferative response of HD and control $CD3^+$ lymphocytes was analysed using all four of the above statistics. However, no significant differences were seen for any of the experimental conditions at any of the time points that were studied (Figs. 5.11-5.14). Similar results were obtained for the helper T lymphocyte and cytotoxic T lymphocyte subsets, with no significant differences observed for any of the experimental conditions or time points investigated (complete data in Appendices). These results demonstrate that proliferation in response to stimuli is not impaired in the major T lymphocyte populations in HD.

Table 5.2. Statistical parameters used for T lymphocyte proliferation assays.

Statistic	Description
Fraction diluted	The percentage of cells in the final culture that divided at least once.
Percentage divided	The percentage of cells from the initial culture that divided at least once.
Proliferation index	The average number of divisions undergone by the dividing cells only.
Division index	The average number of divisions undergone by all cells in culture.

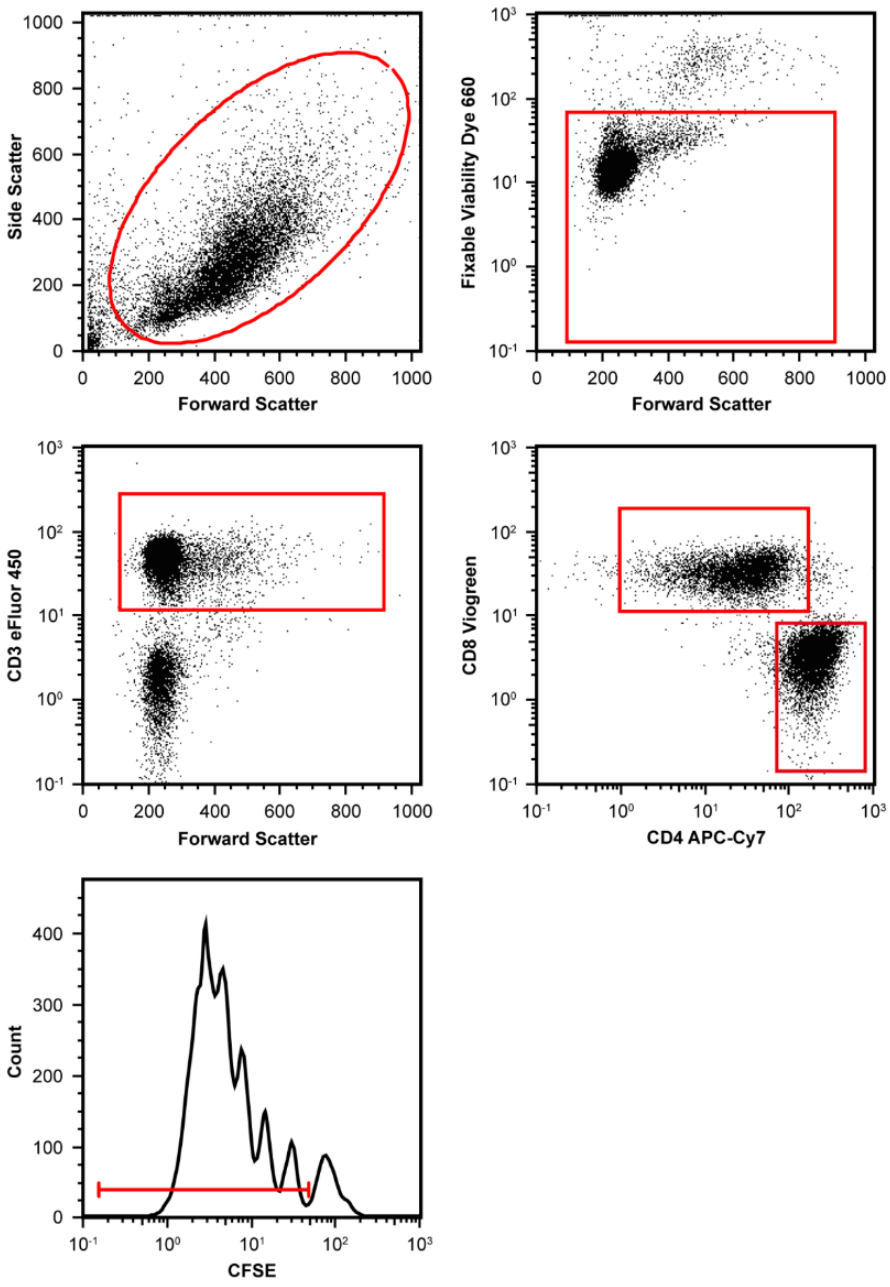

Figure 5.10. Gating strategy for T lymphocyte proliferation analysis. After gating on live cells using a FSC/SSC gate, non-viable cells were excluded using Fixable Viability Dye 660. A FSC vs. CD3 plot was then used to identify the $CD3^+$ T lymphocyte population, within which a CD4 vs. CD8 plot was used to identify the helper ($CD3^+$ $CD4^+$) and cytotoxic ($CD3^+$ $CD8^+$) T lymphocyte populations. A histogram was then used to analyse the CFSE fluorescence profile of each cell subset. The fraction diluted statistic was calculated by creating a univariate gate below the undivided peak, while all other proliferation statistics were calculated using the proliferation analysis tool included in the FlowJo software.

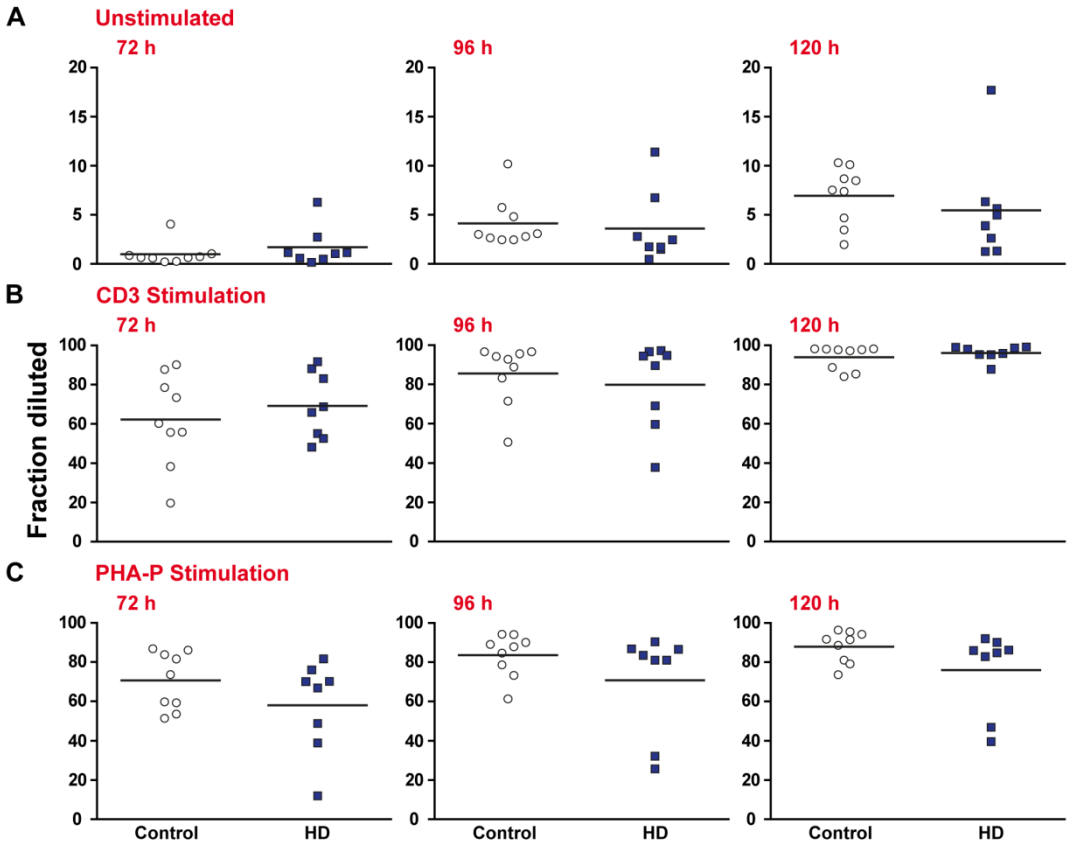

Figure 5.11. Fraction diluted analysis of T lymphocytes. PBMCs were isolated from HD and control peripheral blood samples and stained with CFSE. The percentage of $CD3^+$ T lymphocytes in the final culture that divided at least once (A) in the absence of stimulation, (B) with 5 µg/ml anti-CD3 and 2 µg/ml anti-CD28 antibody stimulation, and (C) with 10 µg/ml PHA-P stimulation was then measured after 72, 96 and 120 h by flow cytometry. No significant differences were seen between HD and control for any of the experimental time points or conditions. Statistical analysis was carried out using two-tailed unpaired Student's *t*-tests with a Holm-Šidak correction (alpha = 0.05) for multiple comparisons.

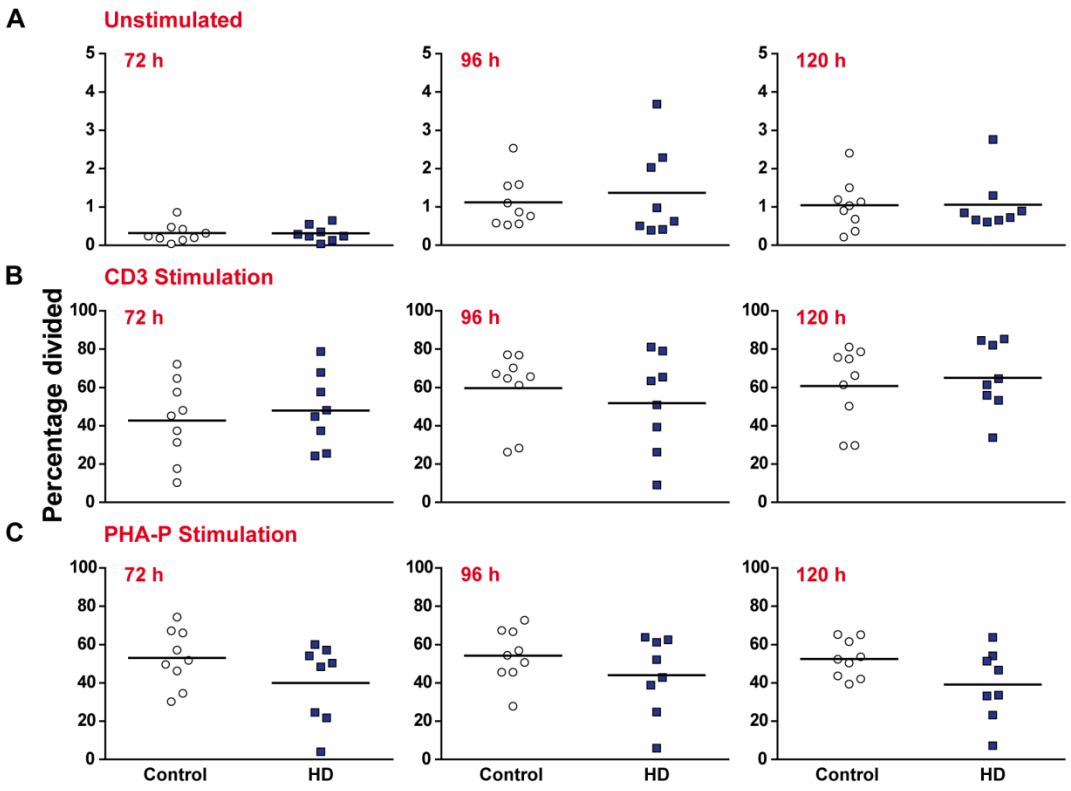

Figure 5.12. Percentage divided analysis of T lymphocytes. PBMCs were isolated from HD and control peripheral blood samples and stained with CFSE. The percentage of $CD3^+$ T lymphocytes from the initial culture that divided (A) in the absence of stimulation, (B) with 5 µg/ml anti-CD3 and 2 µg/ml anti-CD28 antibody stimulation, and (C) with 10 µg/ml PHA-P stimulation was then measured after 72, 96 and 120 h by flow cytometry. No significant differences were seen between HD and control for any of the experimental time points or conditions. Statistical analysis was carried out using two-tailed unpaired Student's *t*-tests with a Holm-Šidak correction (alpha = 0.05) for multiple comparisons.

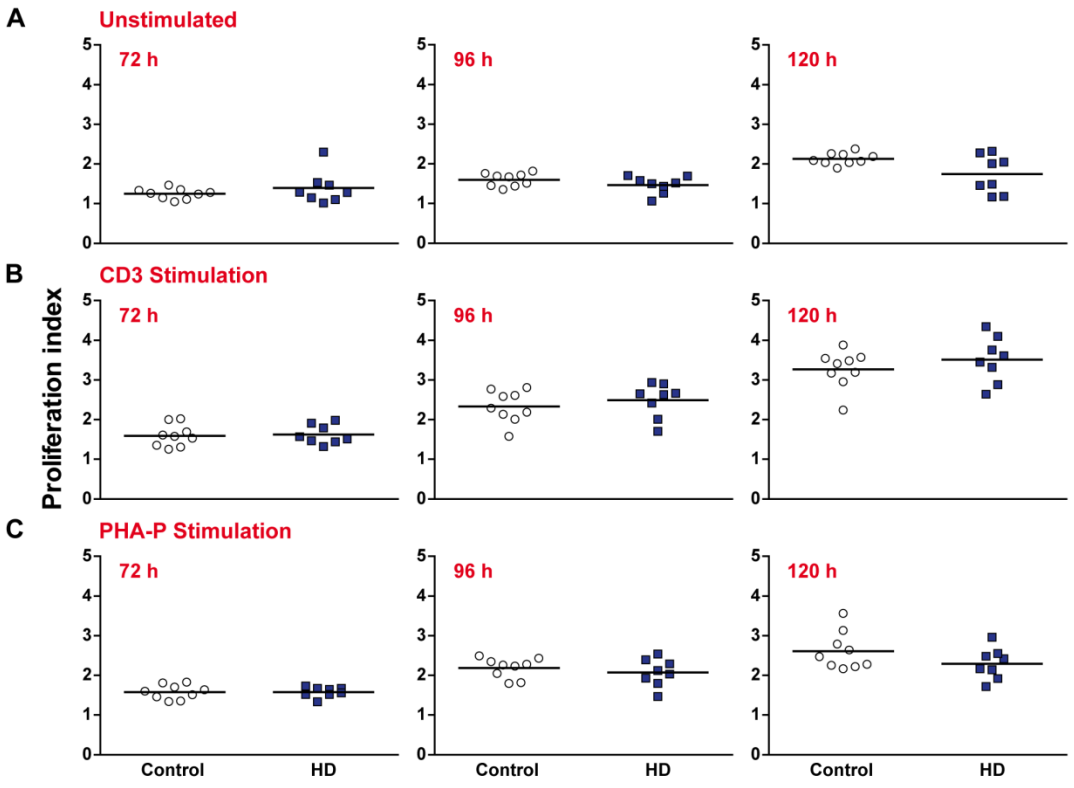

Figure 5.13. Proliferation index analysis of T lymphocytes. PBMCs were isolated from HD and control peripheral blood samples and stained with CFSE. The number of divisions that proliferating $CD3^+$ T lymphocytes underwent (A) in the absence of stimulation, (B) with 5 µg/ml anti-CD3 and 2 µg/ml anti-CD28 antibody stimulation, and (C) with 10 µg/ml PHA-P stimulation was then measured after 72, 96 and 120 h by flow cytometry. No significant differences were seen between HD and control for any of the experimental time points or conditions. Statistical analysis was carried out using two-tailed unpaired Student's *t*-tests with a Holm-Šidak correction (alpha = 0.05) for multiple comparisons.

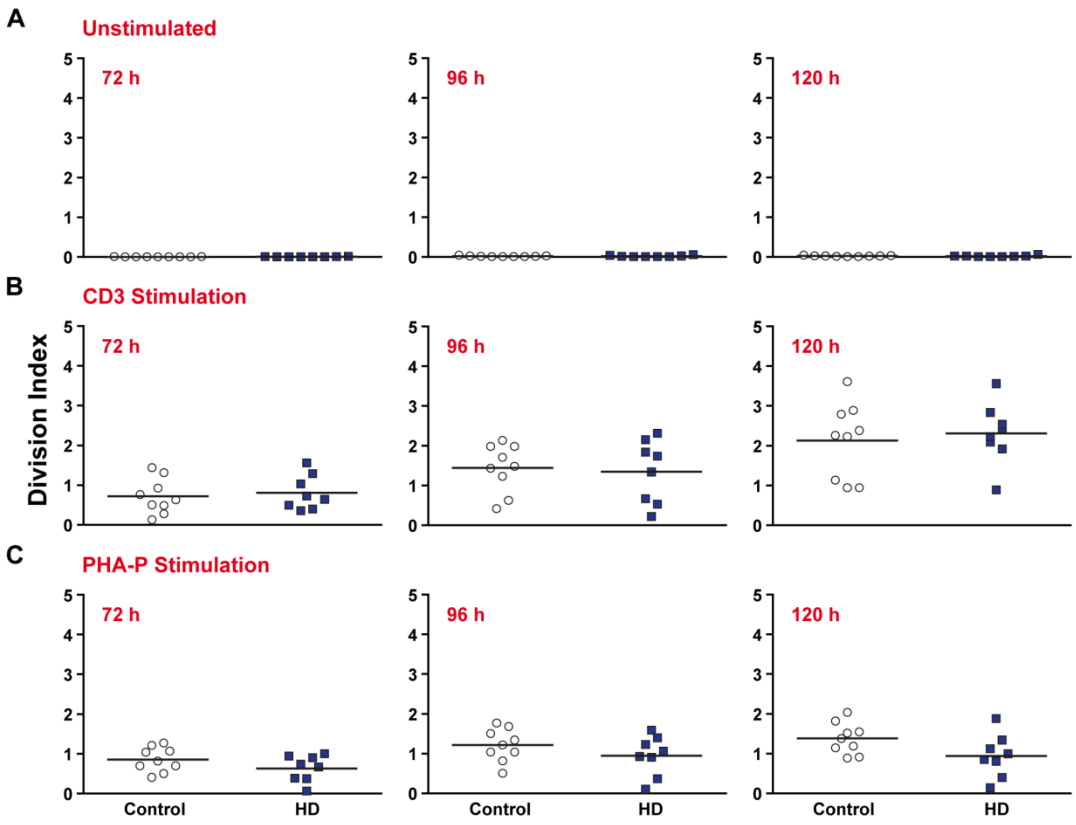

Figure 5.14. Division index analysis of T lymphocytes. PBMCs were isolated from HD and control peripheral blood samples and stained with CFSE. The number of divisions that all $CD3^+$ T lymphocytes underwent (A) in the absence of stimulation, (B) with 5 µg/ml anti-CD3 and 2 µg/ml anti-CD28 antibody stimulation, and (C) with 10 µg/ml PHA-P stimulation was then measured after 72, 96 and 120 h by flow cytometry. No significant differences were seen between HD and control for any of the experimental time points or conditions. Statistical analysis was carried out using two-tailed unpaired Student's *t*-tests with a Holm-Šidak correction (alpha = 0.05) for multiple comparisons.

5.5.4 Cytokine production by *ex vivo* helper T lymphocytes is not altered in HD compared to control

While these data demonstrate that T lymphocyte proliferation in response to a stimulus is not impaired in HD, perhaps the most important function of these cells is to produce a wide range of effector cytokines that are involved in directing the immune response. While HD patients have significantly elevated plasma levels of proinflammatory cytokines (Björkqvist et al., 2008), it is not currently clear what proportion of these excess cytokines are produced by the cells of either the innate or adaptive immune systems. While evidence to date strongly suggests that myeloid cells are the primary source, it is highly possible that T lymphocytes also contribute; indeed, there is overlap in the HD upregulated cytokines produced by these cell types, for example IL-6 and IL-8. Investigation of potential hyper-reactivity in HD T lymphocytes must therefore be carried out to form a more complete picture of the cell subsets responsible.

To address this, helper T lymphocytes were isolated from peripheral blood samples donated by manifest HD and control subjects. Helper T lymphocytes were selected for investigation as they are one of the most important effector cell types in the adaptive immune system, and are involved in directing the vast majority of adaptive immune responses via the production of a wide range of cytokines. Following isolation, the helper T lymphocytes were stimulated with 5 µg/ml anti-CD3 and 2 µg/ml anti-CD28 antibodies, or left unstimulated. The cell culture supernatants were harvested after 48 h and analysed using a multiplex MSD assay for IFNγ, IL-1β, IL-2, IL-4, IL-6, IL-8,

IL-10, IL-12p70, IL-13 and TNFα. An additional singleplex assay was used to measure levels of IL-5. In contrast to the hyper-reactivity displayed by HD myeloid cells to LPS, no significant differences were seen in the levels of any of the eleven cytokines that were measured in the stimulated HD and control samples following normalisation to total protein levels (Fig. 5.15). Furthermore, while several of the cytokines were below the detection limits of the assay in the unstimulated samples, those that were measurable also showed no significant differences between HD and control (Fig. 5.16). These results demonstrate that cytokine production by helper T lymphocytes is not significantly affected by mHTT expression, and that these cells do not display a similar hyper-reactive response to immune stimuli as that seen in HD myeloid cells (Träger et al., 2014).

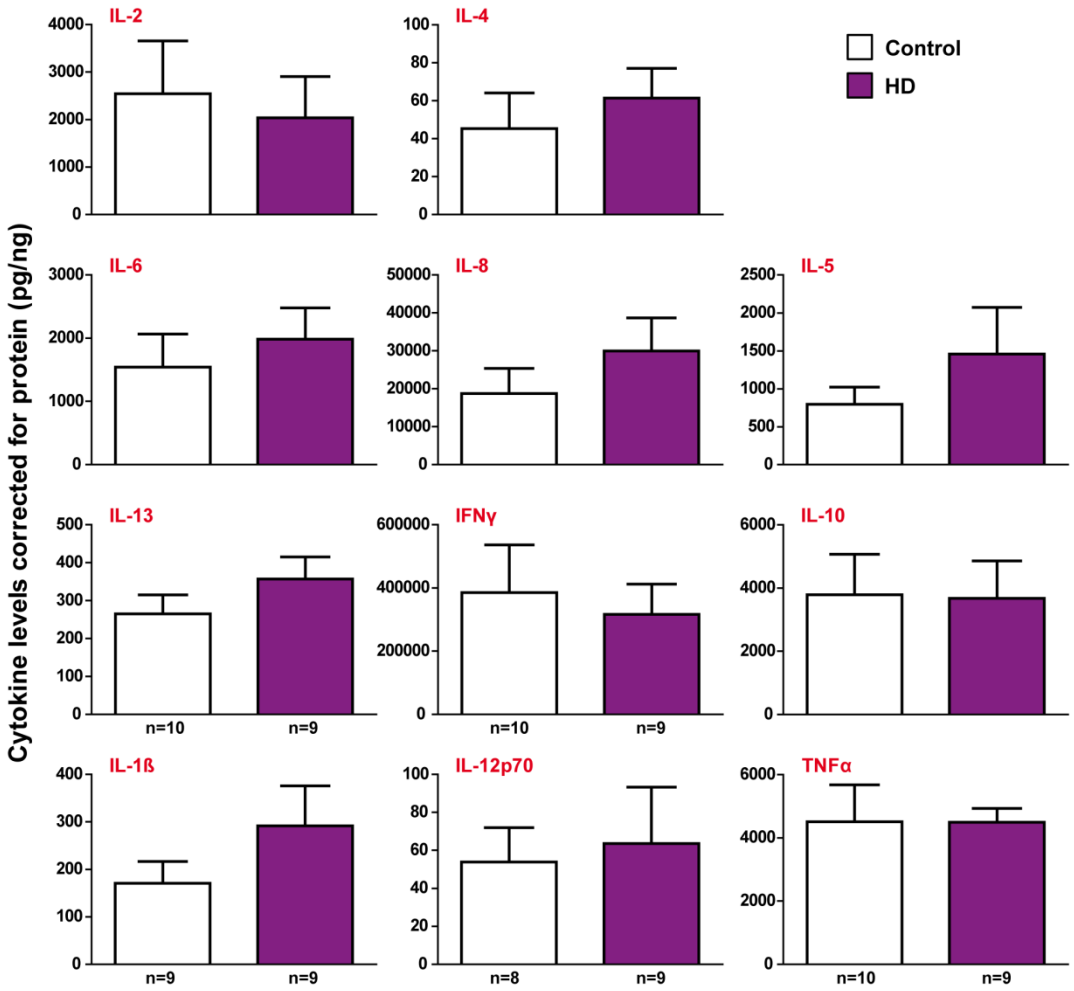

Figure 5.15. Cytokine production by stimulated helper T lymphocytes is not altered in HD compared to control. $CD4^+$ helper T lymphocytes were isolated from HD and control peripheral blood samples and stimulated with 5 µg/ml anti-CD3 and 2 µg/ml anti-CD28 antibodies. Supernatants were collected after 48 h and cytokine profiling was carried out using MSD assays. No significant differences were seen in the levels of any of the cytokines produced by HD and control $CD4^+$ helper T lymphocytes after normalisation to total protein levels. Statistical analysis was carried out using two-tailed unpaired Student's *t*-tests. Data show mean concentrations ± SEM.

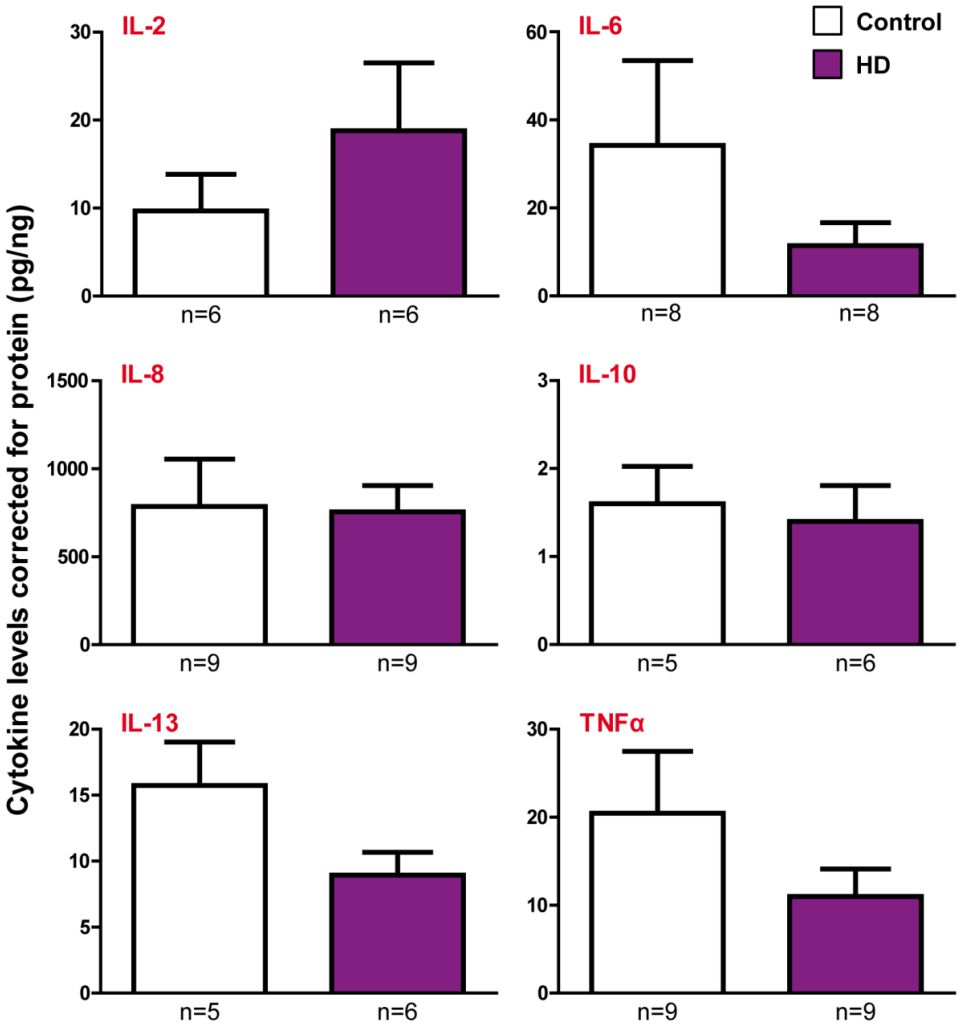

Figure 5.16. Cytokine production by unstimulated helper T lymphocytes is not altered in HD compared to control. $CD4^+$ helper T lymphocytes were isolated from HD and control peripheral blood samples and seeded without stimulation. Supernatants were collected after 48 h and cytokine profiling was carried out using MSD assays. No significant differences were seen in the levels of any of the detectable cytokines produced by HD and control $CD4^+$ helper T lymphocytes after normalisation to total protein levels. Statistical analysis was carried out using two-tailed unpaired Student's *t*-tests. Data show mean concentrations ± SEM.

5.5.5 The transcriptional profile of helper T lymphocytes is not dysregulated in HD compared to control

While these experiments have suggested that the intrinsic phenotype of T lymphocytes is not affected by mHTT expression, it is still possible that there are transcriptional changes that do not have a detectable functional effect in an *ex vivo* setting. Data presented in Chapter 4 of this thesis demonstrates that mHTT has a substantial 'priming' effect on the transcriptome of HD monocytes; this is likely to be responsible for their hyper-reactive response to immune stimuli. While comparable phenotypic dysfunction has not been identified in HD T lymphocytes, assessment of their transcriptional profile is necessary for a more complete understanding of adaptive immunity in HD. Helper T lymphocytes were isolated from peripheral blood samples donated by manifest HD and control subjects and either left unstimulated or stimulated with 5 µg/ml anti-CD3 and 2 µg/ml antibodies for 8 h. The mRNA expression of eighty-four key T lymphocyte genes was then analysed using Human T_h1 and T_h2 Responses RT^2 Profiler PCR Arrays.

Analysis of the PCR array data revealed two genes that were significantly upregulated ($p < 0.05$) in the unstimulated HD samples compared to control (*TNFSF4*, *PTGDR2*; Table 5.3), and three genes that were significantly upregulated in the stimulated HD samples compared to control (*TYK2*, *TNFRSF8*, *STAT6*; Table 5.4). No genes were found to be significantly downregulated in either the unstimulated or stimulated HD samples compared to control. However, none of the upregulated genes had a fold change of > 1.8 between HD and control, and only two (*PTGDR2* and

TNFRSF8) had a fold change of > 1.5. Furthermore, the expression of key signalling molecules such as *MAPK8* (*JNK1*) and *JAK1/2* was not altered in either the unstimulated or stimulated HD samples compared to control (complete list in Appendices).

Consistent with the cytokine profiling data, the mRNA levels of *IFNG*, *IL2*, *IL5*, *IL6*, *IL10*, *IL13* and *TNF* were not altered between HD and control in either the unstimulated or stimulated samples. Transcript levels of *IL4* and *IL12B* were not detectable in the unstimulated samples, but were similarly unaffected in the stimulated samples. Unfortunately, *IL1B* and *IL8* were not included in the genes covered by the PCR arrays. The lack of any change in *IL6*, *IL10* and *IL12B* is a further contrast with HD myeloid cells, as previous studies and the work presented in Chapter 4 have shown that HD monocytes express significantly more mRNA for each of these cytokines than control cells (Träger et al., 2014). Taken together, these results demonstrate that sub-phenotypic transcriptional dysregulation is not a significant phenomenon in HD helper T lymphocytes.

Table 5.3. The top twenty gene expression changes in unstimulated HD helper T lymphocytes. Data presented as fold change in the HD samples calculated from ΔΔ-CT values. Statistical analysis was carried out using two-tailed unpaired Student's *t*-tests (control *n* = 12, HD *n* = 11); expression changes are ranked by *p*-value.

Gene name	Fold change	*p*-value
TNFSF4	1.471	0.008
PTGDR2	1.788	0.014
GATA3	1.177	0.056
IL18R1	1.336	0.058
IL5	2.245	0.063
LAT	0.893	0.101
IL2RA	1.154	0.102
CSF2	0.490	0.124
JAK1	1.108	0.137
CCR4	1.258	0.183
TLR6	1.497	0.198
TNFRSF9	0.564	0.227
IL13	0.689	0.227
IL12RB2	0.789	0.255
CD86	0.681	0.270
IL10	1.580	0.271
BCL6	0.737	0.276
IL2	1.297	0.281
IL15	0.858	0.296
LTA	0.905	0.299

Table 5.4. The top twenty gene expression changes in stimulated HD helper T lymphocytes. Data presented as fold change in the HD samples calculated from ΔΔ-CT values. Statistical analysis was carried out using two-tailed unpaired Student's *t*-tests (control *n* = 12, HD *n* = 11); expression changes are ranked by *p*-value.

Gene name	Fold change	*p*-value
TYK2	1.176	0.002
TNFRSF8	1.702	0.013
STAT6	1.231	0.035
TNFSF4	1.756	0.066
JAK1	1.169	0.072
CCR4	1.191	0.118
IL18R1	1.129	0.149
CD27	1.261	0.152
STAT1	0.844	0.162
IL15	0.800	0.184
IL5	0.724	0.197
TGFB3	1.536	0.211
MAPK8	1.082	0.215
CD28	1.104	0.237
YY1	1.052	0.272
GATA3	1.817	0.300
IL9	0.704	0.308
IL6R	1.174	0.319
FASLG	1.320	0.319
CCR5	1.194	0.327

5.6 Discussion

Altered peripheral immunity is an established feature of HD pathogenesis, with increases in proinflammatory cytokine levels being detectable in circulating plasma up to sixteen years before the predicted onset of motor symptoms (Björkqvist et al., 2008). The majority of previous studies have focused on the intrinsic functional differences between HD and control immune cells, with HD myeloid cells being found to display a hyper-reactive cytokine response to LPS stimulation (Träger et al., 2014). While the functional changes in these cell types likely play a central role in mediating HD peripheral immune dysfunction, it is important to consider that changes in the circulating immune cell population may have a knock-on effect on the peripheral cytokine and chemokine environment. For example, an increase in the frequency of T_h2 lymphocytes in HD blood would likely contribute to the upregulation of the signature T_h2 cytokine IL-4 seen in advanced HD plasma (Björkqvist et al., 2008).

This thesis demonstrates that HD patients have a significantly increased frequency of classical monocytes in their PBMC populations compared to controls. While there is considerable debate regarding the exact function of individual monocyte populations, classical monocytes are thought to form the majority of the total monocyte population and primarily circulate in the blood responding to inflammatory stimuli (Ziegler-Heitbrock, 2007). In contrast, alternative monocytes are believed to primarily localise to specific tissues in order to produce high levels of proinflammatory mediators. This suggests that the altered monocyte balance is unlikely to play a significant role in

mediating the cytokine increases seen in HD peripheral blood, as classical monocytes are thought to be primarily phagocytic in function with few inflammatory attributes (Mukherjee et al., 2015). In contrast, the frequency of the proinflammatory alternative monocyte population was not found to be significantly affected. While it is possible that the increase in classical monocyte frequency makes a minor contribution to peripheral cytokine levels, the wealth of functional data on HD monocytes provides a much more convincing explanation.

Furthermore, data presented in this chapter show that the frequencies of a wide range of additional immune cells are not altered between HD and peripheral blood. This is consistent with a previous study which found that the frequencies of T and B lymphocytes are not altered in the spleen and bone marrow of R6/2 mice (Träger et al., 2015). Taken together, these results disprove the hypothesis that widespread changes in HD immune cell frequencies could be contributing to the altered cytokine environment seen in HD peripheral blood. These immune alterations are therefore likely to be almost exclusively the result of functional differences arising from the expression of mHTT, and not a shift in the relative prevalence of cell types producing specific cytokines.

Data presented in Chapter 4 of this thesis suggest that basal proinflammatory priming in HD myeloid cells is likely to be a key mechanism in mediating peripheral immune dysfunction. However, this does not preclude other cell subsets from playing a contributory role. T lymphocytes are vital to adaptive immune function, and a comprehensive investigation of their function is needed to determine whether HD immune dysfunction is universal

or restricted to specific cell types. Indeed, the close interplay between T lymphocytes and myeloid cells, in the form of cell-cell interactions and cytokine feedback loops, means that T lymphocytes could even contribute to HD myeloid cell dysfunction via excessive stimulatory input (Shanker, 2010).

Mutant HTT protein levels in human HD T lymphocytes have been found to correlate with disease burden scores in HD patients in a similar manner to mHTT levels in HD monocytes (Weiss et al., 2012). While mHTT expression should not be taken as a guarantee of phenotypic dysfunction, profiling of HD plasma found that levels of the signature T_h2 cytokine IL-4 are increased in patients with advanced disease (Björkqvist et al., 2008). While largely circumstantial in isolation, the potential significance of these results necessitates a comprehensive investigation of the intrinsic biology of T lymphocytes in HD.

HD myeloid cells have been shown to exhibit numerous functional deficits, including in migration and phagocytosis (Kwan et al., 2012b; Träger et al., 2015). The results presented in this chapter demonstrate that HD T lymphocytes do not exhibit comparable abnormalities when proliferating in response to a stimulus. This was the case at all of the time points that were studied, and applied to both the percentage of cells that entered division and the number of divisions those cells underwent. More specific analysis of helper and cytotoxic T lymphocyte subsets similarly failed to yield any significant differences between HD and control.

In addition to the resting proinflammatory transcriptional profile described in Chapter 4, HD myeloid cells display a hyper-reactive cytokine response to

LPS stimulation (Träger et al., 2014). However, no such increase in cytokine release was seen in HD helper T lymphocytes, both basally and in response to antigenic stimulation. This lack of functional distinction is supported by the flow cytometry data, as activation levels of T lymphocytes as measured by $CD62L^{low}$ expression were not found to be altered between HD and control. These data suggest that, in contrast to myeloid cells, HD T lymphocytes do not suffer from any intrinsic functional impairment in response to mHTT expression. One explanation for this may be in the relative contributions of different intracellular signalling pathways to the function of each cell type.

Previous work using cell lines and HD mouse models has shown that mHTT has a direct interaction with IKK, a key kinase in the NFκB pathway (Khoshnan et al., 2004). This leads to increased nuclear translocation of NFκB and an increase in the transcription of NFκB-regulated genes. In myeloid cells the NFκB pathway is vital for the production of proinflammatory cytokines such as IL-6 and TNFα (Hayden and Ghosh, 2011), and work presented in Chapter 4 of this thesis has shown that increased basal NFκB activity is likely to play a key role in mediating resting transcriptional dysregulation in HD monocytes. While the NFκB pathway is also involved in T lymphocyte signalling, additional transcription factors such as the NFAT and MAPK families are heavily involved in key processes such as cytokine production (Macian, 2005; Dodeller and Schulze-Koops, 2006). It is therefore possible that while similar NFκB dysfunction may exist in HD T lymphocytes, the reduced relative importance of the pathway means that compensatory mechanisms are in place to prevent phenotypic dysfunction. Furthermore, NFκB is known to be activated by different mechanisms in each cell type.

Myeloid cell NFκB signalling is typically activated via stimulation of the LPS receptor TLR4 (Okun et al., 2009), whereas T lymphocytes are classically stimulated through the TCR (Brownlie and Zamoyska, 2013). While TLR4 is expressed by helper T lymphocytes, its exact function remains unclear, and it has even been suggested to have a repressive effect on T lymphocyte activation (González-Navajas et al., 2010). There is also evidence that NFκB has anti-inflammatory functions in naïve CD4+ T lymphocytes, with overexpression of the NFκB family member NFκB1 (p50) leading to reduced transcription of IL-2 (Kang et al., 1992). Taken together, these data suggest that the lack of phenotypic abnormalities in HD T lymphocytes may be due to the altered and reduced role of NFκB signalling in T lymphocytes compared to myeloid cells.

Mutant HTT has diverse effects on transcription, including the sequestration of transcription factors in aggregates and the direct binding of mHTT fragments to DNA (Chen-Plotkin et al., 2006; Benn et al., 2008), and transcriptional dysregulation has been consistently demonstrated in a wide range of HD tissues (Seredenina and Luthi-Carter, 2012). However, the degree to which individual signalling pathways are affected by mHTT expression is likely to vary considerably. PCR array analysis of helper T lymphocytes was used to show that widespread changes in key T lymphocyte related genes are lacking in HD compared to control in both the unstimulated and stimulated states. This is in marked contrast to the widespread resting enrichment of proinflammatory functional gene sets in HD myeloid cells described in Chapter 4. The expression of key signalling molecules such as *MAPK8* (*JNK1*) and *JAK1/2* was unaffected in HD T

lymphocytes, supporting the hypothesis that the normal function of alternative signalling pathways is able to compensate for potential NFκB pathway dysregulation. While the key T_h2 transcription factor *STAT6* was found to have increased expression in stimulated HD cells, no additional changes were seen in any related transcripts. Furthermore, it has been shown that JAK/STAT signalling is not significantly affected in HD myeloid cells (Träger et al., 2013), making it likely that the small increase in expression (fold change 1.23) observed in our dataset does not have a great deal of functional significance. Increased resting expression of proinflammatory cytokines such as *IL6*, *IL10* and *IL12B* was also lacking in HD helper T lymphocytes, drawing a further contrast with the basal changes described in the transcriptome of HD myeloid cells. When combined with the functional data described above, these results lead to the conclusion that the intrinsic function of HD T lymphocytes is not significantly affected by the expression of mHTT.

However, it is important to note that these results do not exclude the possibility of *in vivo* differences in T lymphocyte function, as excessive stimulation from hyper-reactive myeloid cells could provoke an increased T lymphocyte response independent of any intrinsic cellular dysfunction. This is one potential explanation for the increased IL-4 levels seen in the plasma of HD patients (Björkqvist et al., 2008), although it has also been suggested that increased secretion of this anti-inflammatory cytokine may be a compensatory response to the chronic increase in inflammatory mediators seen in HD plasma (Ellrichmann et al., 2013). This conclusion is supported by the increased IL-4 levels only being seen in the later stages of the

disease. Regardless, determining whether the *in vivo* activity of T lymphocytes is altered in response to excessive innate immune activation would require a series of complicated functional experiments, the scope of which is beyond the remit of this thesis.

The results presented in this chapter have shown that the intrinsic phenotype of T lymphocytes is not significantly affected by the expression of mHTT. These findings advance our understanding of HD as a disease of the whole body, and support the work presented in Chapter 4 suggesting that abnormal myeloid cells are the most likely source of peripheral immune dysfunction in HD. This has important implications for potential novel therapies that aim to treat HD by modulating the peripheral immune system, as it shows that benefits are only likely to be achieved when targeting specific cell types. Furthermore, this chapter demonstrates the value of taking a systematic approach to investigating the function of individual cell types in HD, as the phenotypic effects of mHTT expression are clearly dependent on the cellular environment and the relative contributions of the signalling pathways the mutant protein interacts with.

5.7 Summary

Work presented in this chapter investigated the frequencies of a wide range of immune cell subsets in HD and control peripheral blood, in order to determine whether a shift in the relative proportions of specific cell subsets could be a contributing factor in the elevated levels of proinflammatory cytokines seen in HD plasma. However, while HD PBMCs were found to contain a significantly higher proportion of classical monocytes than control PBMCs, the frequencies of all of the other major immune cell subsets that were investigated were found to be unchanged. Furthermore, this chapter investigated whether HD T lymphocytes exhibit similar phenotypic abnormalities to those displayed by HD myeloid cells. However, no significant differences were found between HD and control in tests of both proliferation and cytokine production, while PCR arrays were used to determine that the expression of key T lymphocyte related genes is not substantially affected in either unstimulated or stimulated HD helper T lymphocytes. These findings demonstrate that HD peripheral immune dysfunction is not universal, but is instead restricted to specific cell types that are primarily part of the innate immune system.

6 Conclusions and future work

6.1 Allele-selective silencing as a therapeutic for HD

Work presented in this thesis demonstrates for the first time the allele-selective suppression of mHTT in primary human *ex vivo* patient cells. This was achieved using siRNA targeted to each allele of rs362331 in exon 50 of the *HTT* transcript. While previous studies have successfully shown selectivity using HD cell lines or animal models (Østergaard et al., 2013; Drouet et al., 2014), this study is the first to establish the feasibility of carrying out an experimental workflow comprising SNP genotyping, SNP linkage and targeted knockdown of the mutant allele in human HD patients. This is an important advance as it provides insight into the likely clinical application of this technology, with the added technical considerations associated with personalised genomic medicine.

From a purely technical standpoint, this study shows that the potency and selectivity achieved using allele-specific siRNAs varies depending on the SNP in question, even when considering heterozygous SNPs with an equivalent base mismatch. This is consistent with previous studies using ASOs (Carroll et al., 2011), and can be seen in the greatly increased allele-selectivity achieved when targeting rs362331 compared to rs362273 and rs362307. Extensive preclinical validation of potential SNP targets will therefore be crucial for the development of any allele-selective therapeutic, with a failure to achieve selectivity at the most prevalent SNP sites (e.g. rs362307) limiting the HD patients who would benefit from such an approach.

While this study has established the feasibility of individually treating patients based on their SNP genotype, it remains to be seen whether such an approach will ever be suitable for widespread clinical use. With even the most prevalent SNPs being heterozygous in less than 50 % of patients, a combined approach comprising individual clinical trials of multiple SNP-targeted therapeutics would be required to cover even a majority of HD patients. The cost implications of such a strategy, not to mention the logistical difficulties associated with recruiting large cohorts of genotyped patients for clinical trials, are likely to prove prohibitive. This is compounded by the high level of technical difficulty associated with the SLiC technique required to link SNP alleles to m*HTT* (Liu et al., 2008), with widespread introduction into clinical laboratories seeming an unlikely proposition. Indeed, barring the development of straightforward genotyping techniques such personalised medical jiggery-pokery is likely to become the future preserve of the limited few wealthy enough to afford it.

Furthermore, there are significant ethical issues associated with developing therapeutics to treat a minority of Caucasian patients when the majority of HD occurs in the developing world (Warby et al., 2011). The prevalence of SNP heterozygosities has been shown to vary widely between populations of different ethnic groups (Lombardi et al., 2009; Warby et al., 2009; Pfister et al., 2009), so it is likely that any drugs developed for Caucasian populations would not be widely usable elsewhere. Indeed, it is almost inconceivable that the sophisticated genotyping techniques required to use allele-selective therapeutics will be widely available in developing nations in the near future; even if a heterozygous SNP was applicable worldwide, the technology to

make use of it is not. There is therefore a convincing argument to be made that the resources required to develop these treatments would be better spent on therapeutics with universal applicability to HD patients. These are likely to focus on total HTT-lowering, with numerous animal studies offering encouraging data to suggest that partial suppression of wild-type HTT is tolerated in the mammalian brain (McBride et al., 2008; Grondin et al., 2012). If initial human trials provide similar results, it may be that allele-selective suppression is not required for the safe and effective treatment of HD.

However, the leviathan practical considerations associated with taking allele-selective silencing to clinical trials by no means diminish its vast potential as a research tool for dissecting the specific cellular roles of wild-type and mHTT. For example, work presented in this thesis has demonstrated that selectively lowering both wild-type and mHTT has equivalent effects on HD myeloid cell cytokine production. It is likely that the coming years will yield numerous studies in this vein, providing sophisticated data beyond what was previously available with total HTT-lowering or conditional *HTT* knockout.

6.2 Myeloid cell function in HD

Work presented in Chapter 4 of this thesis used modern RNA-Seq technology to characterise the entire HD myeloid cell transcriptome. This showed that mHTT-related dysfunction is not limited to the stimulated state, with HD monocytes demonstrating significant basal transcriptional changes. Pathway analysis of the dataset revealed that these transcriptional changes were largely proinflammatory in nature, including the first ever demonstration of increased resting cytokine expression in HD myeloid cells at either the

mRNA or protein level. Functional follow up revealed that increased basal NFκB activity is involved in mediating these changes, suggesting that mHTT has a priming effect on HD myeloid cells similar to that described in a murine HD microglial line (Crotti et al., 2014). This resting proinflammatory profile is likely to play a role in the hyper-reactive LPS response seen in HD myeloid cells (Träger et al., 2014). The discovery of resting dysfunction in HD myeloid cells provides valuable new insight into the peripheral pathogenesis of HD, as primed myeloid cells are likely to make a significant contribution to the elevated cytokine levels seen in HD plasma (Björkqvist et al., 2008).

Interestingly, the selective lowering of wild-type and mHTT was not found to produce differential effects on cytokine production by HD myeloid cells in response to LPS. This suggests that wild-type HTT may have a novel role in immune cell function, and is consistent with previous data showing that total HTT-lowering in control cells also inhibits cytokine production (Träger et al., 2014). As a greater reduction in IL-6 and TNFα levels was seen using anti-total *HTT* siRNA compared to either allele-selective siRNA, it may well be that the total cellular HTT load is the key factor in determining cytokine production. However, this observation must be reconciled with the hyper-reactive cytokine profile of HD myeloid cells, as this is presumably due to a mHTT-specific effect. Future work should therefore focus on dissecting the specific roles of wild-type and mHTT in myeloid cells, in addition to their relative contributions to cytokine production.

Further investigation is also required to determine why HTT-lowering was unable to reverse the transcriptional changes seen in resting HD monocytes, as measured by both RNA-Seq and PCR. The most likely hypothesis is that

transcriptional changes take time to normalise following a reduction in cellular HTT levels, however the short-lived nature of monocytes *ex vivo* means this is challenging to investigate. It may be possible to overcome this using a monocyte cell line, although it remains to be seen whether such models recapitulate the transcriptional changes seen in primary human cells. It may also be valuable to investigate whether individual monocyte populations are differentially affected by mHTT expression, as this could lend additional relevance to the shift in monocyte frequencies seen in HD peripheral blood. However, the lack of inflammatory functions of the affected classical monocyte population still suggests that a major role for altered cell frequencies in HD immune dysfunction is unlikely (Mukherjee et al., 2015).

6.3 Adaptive immune function in HD

It was previously unknown whether HD peripheral immune dysfunction was universal or limited to specific cell types. Work presented in Chapter 5 of this thesis demonstrates that the intrinsic phenotype of T lymphocytes is not affected by mHTT expression, suggesting that the pathogenic effects of mHTT vary considerably from cell to cell. This is likely to be due to variations in the relative contributions of affected intracellular signalling pathways. However, the *ex vivo* data presented in this thesis does not rule out the possibility that the function of HD T lymphocytes is altered *in vivo*, as the formation of feedback loops with the innate immune system could result in an exaggeration of T lymphocyte function in response to excessive stimulation from myeloid cells. This is one potential explanation for the increase in IL-4 levels seen in HD plasma (Björkqvist et al., 2008), and future work could

utilise co-culture experiments to determine whether interactions between innate and adaptive immune cells are affected in HD.

These results demonstrate the need for the detailed investigation of individual cell types in order to determine their relative contributions to HD peripheral immune dysfunction. However, it will be important to direct the limited time and resources available for such studies to cell types for which there are convincing rationales. For example, while the effects of mHTT expression on B lymphocytes are yet to be analysed in depth, the lack of any change in circulating Ig levels in HD plasma casts serious doubt on the existence of any potential abnormalities (Björkqvist et al., 2008). Indeed, it could be argued that the lack of any *in vivo* change renders such investigation irrelevant in disease terms. As with so many things, it will be important to strike a balance between being comprehensive and practical when studying the function of further immune cell subsets in HD.

6.4 The peripheral immune system as a therapeutic target in HD

These results further raise the possibility that the peripheral immune system could be utilised as a novel therapeutic target for HD. It has already been shown that dampening the peripheral immune system has beneficial effects on disease progression in HD mouse models (Bouchard et al., 2012; Zwilling et al., 2011), and the basal myeloid cell dysfunction outlined in Chapter 4 suggests the existence of a chronic problem that may be amenable to long-term treatment with immunomodulatory drugs. This discovery also makes the dosing schedule of any potential intervention significantly easier, as it will not

need to be timed to coincide with specific infective events and is likely to be beneficial even in the absence of any inflammatory stimuli.

Promisingly, the drugs to do this already exist to treat conditions such as rheumatoid arthritis, for which TNFα inhibition has been a therapeutic staple for many years. TNF inhibition has already been shown to provide therapeutic benefit in preclinical studies (Hsiao et al., 2014), and it should be relatively straightforward to extend this approach to patients. However, the degree to which this may provide long-term benefits remains to be seen, and must be weighed against the side effects associated with any drug which is taken to clinical trial. Alternative approaches may include targeting specific mechanisms associated with HD immune dysfunction, for example the NFκB pathway. However, the selectivity of drugs designed to do this remains questionable, and the multitude of cellular functions associated with NFκB raises serious questions about the potential for off-target toxic effects.

One outstanding question relates to the ceiling of therapeutic benefit available from targeting the peripheral immune system. While mouse studies have suggested that neurological phenotypes may be improved by peripheral immune suppression, a similar effect is yet to be shown in humans or even primates. An ideal strategy would make use of an immunomodulatory drug that is able to cross the blood-brain barrier, as neuroinflammation has also been shown to be a key component of HD pathogenesis (Björkqvist et al., 2009); this would allow two potential mechanisms to be treated with a single drug. Furthermore, agonising over the potential limitations of immunomodulation in HD is to a large extent disputing semantics. While even the most optimistic investigator would struggle to argue that this

approach will provide a complete cure for HD, the current lack of any medications that are able to slow HD progression makes this an avenue worth investigating, as even a modest symptomatic improvement would be invaluable in the wider patient context.

This thesis therefore demonstrates the feasibility of tailoring therapeutic interventions to an individual's genotype, and introduces this approach as a highly promising method for investigating the specific cellular functions of wild-type and mHTT. It further establishes that HD myeloid cells are basally abnormal as the result of a mHTT/NFκB-mediated priming effect, and shows that phenotypic dysfunction previously described in HD innate immune cells does not extend to the cells of the adaptive immune system. These findings advance our understanding of HD as a disease of the whole body, support the targeting of peripheral immunity as a therapeutic for HD, and reinforce the importance of peripheral immunity in the study of neurodegeneration.

Appendices

A.1 RPMI 1640 media formulation

Table A.1. RPMI 1640 media formulation. Ingredients of RPMI 1640 media used for all cell culture experiments (Thermo Fisher Scientific catalogue number 31870-074).

Components	Molecular weight	Concentration (mg/L)	mM
Amino acids			
Glycine	75.0	10.0	0.133
L-Arginine	174.0	200.0	1.149
L-Asparagine	132.0	50.0	0.379
L-Aspartic acid	133.0	20.0	0.150
L-Cystine	240.0	50.0	0.208
L-Glutamic acid	147.0	20.0	0.136
L-Histidine	155.0	15.0	0.097
L-Hydroxyproline	131.0	20.0	0.153
L-Isoleucine	131.0	50.0	0.382
L-Leucine	131.0	50.0	0.382
L-Lysine hydrochloride	146.0	40.0	0.274
L-Methionine	149.0	15.0	0.101
L-Phenylalanine	165.0	15.0	0.091
L-Proline	115.0	20.0	0.174
L-Serine	105.0	30.0	0.286
L-Threonine	119.0	20.0	0.168
L-Tryptophan	204.0	5.0	0.025
L-Tyrosine	181.0	20.0	0.110
L-Valine	117.0	20.0	0.171

Vitamins			
Biotin	244.0	0.2	8.197E-04
Choline chloride	140.0	3.0	0.021
D-Calcium pantothenate	477.0	0.25	5.241E-04
Folic acid	441.0	1.0	0.002
Niacinamide	122.0	1.0	0.008
Para-aminobenzoic acid	137.0	1.0	0.007
Pyridoxine hydrochloride	206.0	1.0	0.005
Riboflavin	376.0	0.2	5.319E-04
Thiamine hydrochloride	337.0	1.0	0.003
Vitamin B12	1355.0	0.005	3.690E-06
i-Inositol	180.0	35.0	0.194
Inorganic salts			
Calcium nitrate ($Ca(NO_3)_2$-$4H_2O$)	236.0	100.0	0.424
Magnesium sulphate ($MgSO_4$-$7H_2O$)	246.0	100.0	0.407
Potassium chloride (KCl)	75.0	400.0	5.333
Sodium bicarbonate ($NaHCO_3$)	84.0	2000.0	23.810
Sodium chloride (NaCl)	58.0	6000.0	103.448
Sodium phosphate dibasic (Na_2HPO_4)	142.0	800.0	5.634
Other components			
D-Glucose (dextrose)	180.0	2000.0	11.111
Glutathione (reduced)	307.0	1.0	0.003
Phenol red	376.4	5.0	0.013

A.2 Patient details

Table A.2. Age and *HTT* CAG repeat length for all subjects who donated samples for the study presented in Chapter 3. Cohorts listed separately for each experiment.

Experiment	Subject group	*n*	Age (mean ± SD)	CAG (mean ± SD)
ATP assay analysis of lower EP GeRPs	Control	2	52.3 ± 19.5	-
	HD	5	52.2 ± 10.9	43.2 ± 0.7
qPCR analysis of lower EP GeRPS	HD	5	60.1 ± 5.6	43.0 ± 0.6
TR-FRET analysis of lower EP GeRPs	HD	3	38.2 ± 11.8	51.3 ± 6.1
Allele-selective suppression targeting rs362331	HD	3	50.1 ± 10.3	44.0 ± 2.2
Allele-selective suppression targeting rs362273	HD	4	51.2 ± 13.3	42.8 ± 0.8
Allele-selective suppression targeting rs362307	HD	4	55.9 ± 10.2	43.3 ± 1.5
siRNA dose-ranging targeting rs362331	HD	5	57.2 ± 6.9	41.8 ± 0.7
siRNA dose-ranging targeting rs362273	HD	3	60.0 ± 4.8	42.3 ± 0.5
siRNA dose-ranging targeting rs362307	HD	3	61.3 ± 12.1	41.0 ± 0.8
Protein analysis of anti-rs362331 siRNA (C linked to m*HTT*)	HD	3	43.4 ± 5.1	45.3 ± 2.6
Protein analysis of anti-rs362331 siRNA (T linked to m*HTT*)	HD	5	51.1 ± 16.3	44.6 ± 2.7
Cytokine analysis of anti-rs362331 siRNA (IL-6 and TNFα)	HD	5	49.9 ± 11.1	45.2 ± 2.6
Cytokine analysis of anti-rs362331 siRNA (IL-8)	HD	4	46.2 ± 9.3	46.0 ± 2.2

Table A.3. Age and *HTT* CAG repeat length for all subjects who donated samples for the study presented in Chapter 4. Cohorts listed separately for each experiment.

Experiment	Subject group	*n*	Age (mean ± SD)	CAG (mean ± SD)
RNA-Seq analysis of the monocyte transcriptome	Control	33	48.9 ± 13.2	-
	HD	30	51.3 ± 11.0	44.4 ± 2.8
IκBα Western blotting	Control	7	52.9 ± 16.2	-
	HD	9	62.1 ± 6.0	42.4 ± 2.6
ERK and p38 Western blotting	Control	10	55.3 ± 10.9	-
	HD	10	61.8 ± 5.8	42.4 ± 2.4
RNA-Seq analysis of gene expression following HTT-lowering	HD	6	50.8 ± 8.2	45.0 ± 1.8
qPCR analysis of gene expression following HTT-lowering	HD	9	52.3 ± 10.2	45.3 ± 1.7

Table A.4. Age and *HTT* CAG repeat length for all subjects who donated samples for the study presented in Chapter 5. Cohorts listed separately for each experiment.

Experiment	Subject group	*n*	Age (mean ± SD)	CAG (mean ± SD)
Monocyte and NK cell subset analysis	Control	10	46.8 ± 10.9	-
	HD	11	57.0 ± 9.9	41.9 ± 1.5
$CD3^+$ T lymphocyte subset analysis – T_h1 cells	Control	5	44.9 ± 9.4	-
	HD	7	52.2 ± 10.0	42.3 ± 1.0
$CD3^+$ T lymphocyte subset analysis – all other cell types	Control	9	46.2 ± 12.1	-
	HD	10	55.6 ± 9.9	42.0 ± 1.6
NKT cell subset analysis	Control	10	46.8 ± 10.9	-
	HD	10	56.2 ± 10.1	41.8 ± 1.5
T_h17 lymphocyte subset analysis	Control	10	46.8 ± 10.9	-
	HD	10	55.6 ± 9.9	42.0 ± 1.6
T_{reg} lymphocyte, B lymphocyte and plasma cell subset analysis	Control	6	46.1 ± 8.2	-
	HD	7	52.2 ± 9.2	42.3 ± 0.9

T lymphocyte proliferation assays	Control	9	54.8 ± 7.4	-
	HD	8	56.2 ± 8.6	43.0 ± 2.4
Stimulated T lymphocyte cytokine profiling – IL-1β	Control	9	55.4 ± 12.6	-
	HD	9	57.4 ± 11.4	43.2 ± 1.9
Stimulated T lymphocyte cytokine profiling – IL-12p70	Control	8	56.1 ± 13.3	-
	HD	9	57.4 ± 11.4	43.2 ± 1.9
Stimulated T lymphocyte cytokine profiling – all other cytokines	Control	10	56.4 ± 12.3	-
	HD	9	57.4 ± 11.4	43.2 ± 1.9
Unstimulated T lymphocyte cytokine profiling – IL-2	Control	6	53.9 ± 15.3	-
	HD	6	52.4 ± 10.2	44.0 ± 1.8
Unstimulated T lymphocyte cytokine profiling – IL-6	Control	8	57.1 ± 12.4	-
	HD	8	57.8 ± 12.1	43.0 ± 1.93
Unstimulated T lymphocyte cytokine profiling – IL-8	Control	9	55.1 ± 12.3	-
	HD	9	57.4 ± 11.4	43.2 ± 1.9
Unstimulated T lymphocyte cytokine profiling – IL-10	Control	5	57.7 ± 15.4	-
	HD	6	54.7 ± 11.9	43.5 ± 2.0
Unstimulated T lymphocyte cytokine profiling – IL-13	Control	5	57.1 ± 15.5	-
	HD	6	56.9 ± 14.2	43.5 ± 2.0
Unstimulated T lymphocyte cytokine profiling – TNFα	Control	9	55.4 ± 12.6	-
	HD	9	57.4 ± 11.4	43.2 ± 1.9
PCR arrays	Control	12	49.3 ± 15.3	-
	HD	11	58.7 ± 5.7	42.6 ± 1.4

A.3 Monocyte RNA-Seq results

Table A.5. Complete list of differentially expressed genes in unstimulated HD monocytes (FDR < 0.05).

Gene ID	Ensembl ID	RPKM (Control)	RPKM (HD)	log2 fold change	*p*-value	FDR
FAM124A	ENSG00000150510	0.242	0.812	2.684	4.61E-08	6.05E-04
IL19	ENSG00000142224	0.586	1.473	2.358	1.15E-07	7.57E-04
IL23A	ENSG00000110944	1.914	3.597	1.576	7.84E-07	2.55E-03
FAM213B	ENSG00000157870	7.837	5.201	-0.604	8.99E-07	2.55E-03
TGFA	ENSG00000163235	0.665	1.392	1.550	9.69E-07	2.55E-03
FZD7	ENSG00000155760	0.397	0.246	-0.721	1.39E-06	3.04E-03
C6orf223	ENSG00000181577	0.063	0.297	2.127	1.92E-06	3.60E-03
PROCR	ENSG00000101000	3.695	10.872	1.552	3.61E-06	5.69E-03
NT5E	ENSG00000135318	0.210	0.725	2.082	4.24E-06	5.69E-03
SMO	ENSG00000128602	0.259	0.124	-1.161	4.33E-06	5.69E-03
CISH	ENSG00000114737	2.723	5.161	1.439	5.90E-06	7.04E-03
C6orf165	ENSG00000213204	0.038	0.086	1.205	6.57E-06	7.20E-03
CCL19	ENSG00000172724	0.518	1.767	1.763	8.79E-06	8.89E-03
PTGS2	ENSG00000073756	2.319	18.604	1.813	9.52E-06	8.93E-03
HPSE	ENSG00000173083	11.322	24.941	1.142	1.10E-05	9.68E-03
VEGFA	ENSG00000112715	5.475	14.251	0.898	1.35E-05	1.11E-02
ANXA11	ENSG00000122359	136.875	105.621	-0.374	1.72E-05	1.33E-02
CDK2	ENSG00000123374	5.534	7.186	0.390	1.88E-05	1.37E-02
R3HCC1	ENSG00000104679	15.225	11.394	-0.421	2.18E-05	1.45E-02
PGAP3	ENSG00000161395	2.943	2.310	-0.364	2.28E-05	1.45E-02
TTLL7	ENSG00000137941	0.135	0.219	0.712	2.31E-05	1.45E-02
NKX3-1	ENSG00000167034	0.025	0.195	2.157	2.44E-05	1.46E-02
PLEKHN1	ENSG00000187583	0.858	1.466	0.793	2.57E-05	1.47E-02
CSF2	ENSG00000164400	0.680	1.369	2.888	3.00E-05	1.55E-02
SLC25A37	ENSG00000147454	8.575	22.865	1.291	3.03E-05	1.55E-02
RASEF	ENSG00000165105	0.003	0.041	3.580	3.16E-05	1.55E-02
DNAJB13	ENSG00000187726	0.095	0.168	0.818	3.19E-05	1.55E-02
FAM126A	ENSG00000122591	2.424	3.294	0.457	3.51E-05	1.65E-02
SERPINA9	ENSG00000170054	0.159	0.503	2.196	4.00E-05	1.81E-02
CHORDC1	ENSG00000110172	16.382	20.651	0.346	4.38E-05	1.89E-02
IL2RA	ENSG00000134460	0.945	4.621	2.047	4.45E-05	1.89E-02
CD300E	ENSG00000186407	92.872	161.854	0.801	4.67E-05	1.92E-02
IL12B	ENSG00000113302	1.772	6.429	2.531	5.69E-05	2.27E-02
BBS12	ENSG00000181004	0.641	0.810	0.345	6.02E-05	2.28E-02
LEPREL1	ENSG00000090530	0.140	0.366	1.400	6.08E-05	2.28E-02
PLXNB1	ENSG00000164050	0.649	0.917	0.507	6.41E-05	2.29E-02
KANSL1L	ENSG00000144445	2.326	2.828	0.293	6.64E-05	2.29E-02
STAC	ENSG00000144681	0.947	2.009	2.399	6.66E-05	2.29E-02

BBS7	ENSG00000138686	2.337	2.817	0.289	6.79E-05	2.29E-02
MPND	ENSG00000008382	7.750	5.647	-0.480	8.65E-05	2.69E-02
STX1A	ENSG00000106089	2.160	5.172	1.319	8.70E-05	2.69E-02
IL6	ENSG00000136244	12.656	97.048	2.678	8.73E-05	2.69E-02
SPARC	ENSG00000113140	8.356	3.885	-1.161	9.11E-05	2.69E-02
PTGES	ENSG00000148344	0.767	3.161	1.797	9.18E-05	2.69E-02
WASF1	ENSG00000112290	0.345	0.532	0.666	9.22E-05	2.69E-02
NAGLU	ENSG00000108784	8.155	6.428	-0.349	9.67E-05	2.76E-02
GK5	ENSG00000175066	0.881	1.880	1.014	9.89E-05	2.77E-02
ZNF414	ENSG00000133250	4.682	3.857	-0.284	1.10E-04	3.00E-02
SERPINB7	ENSG00000166396	0.360	1.802	2.677	1.13E-04	3.03E-02
NAT8L	ENSG00000185818	0.052	0.032	-0.760	1.19E-04	3.12E-02
ZDHHC13	ENSG00000177054	5.097	6.295	0.317	1.24E-04	3.18E-02
FGF2	ENSG00000138685	0.013	0.081	2.371	1.26E-04	3.18E-02
DLL4	ENSG00000128917	0.022	0.119	2.135	1.33E-04	3.29E-02
HECW2	ENSG00000138411	0.142	0.278	0.955	1.38E-04	3.35E-02
PVALB	ENSG00000100362	0.457	0.122	-1.862	1.44E-04	3.43E-02
TEFM	ENSG00000172171	4.705	5.690	0.285	1.49E-04	3.43E-02
MIR1249	ENSG00000221598	5.001	3.261	-0.636	1.49E-04	3.43E-02
RETN	ENSG00000104918	3.527	8.346	1.382	1.54E-04	3.46E-02
INHBA	ENSG00000122641	4.711	7.527	1.781	1.56E-04	3.46E-02
PF4	ENSG00000163737	0.627	1.888	1.606	1.60E-04	3.50E-02
EVC2	ENSG00000173040	0.096	0.194	0.999	1.67E-04	3.50E-02
KCNJ15	ENSG00000157551	2.191	4.176	0.996	1.68E-04	3.50E-02
TMEM54	ENSG00000121900	0.272	0.560	1.041	1.68E-04	3.50E-02
CCL8	ENSG00000108700	41.093	103.771	2.142	1.74E-04	3.54E-02
HHLA2	ENSG00000114455	0.092	0.194	1.492	1.75E-04	3.54E-02
TYRO3	ENSG00000092445	0.160	0.233	0.566	1.81E-04	3.61E-02
VCAN	ENSG00000038427	9.829	19.306	0.975	1.85E-04	3.62E-02
SOX5	ENSG00000134532	0.324	0.957	1.609	1.96E-04	3.70E-02
SMPDL3A	ENSG00000172594	12.351	25.672	1.036	1.99E-04	3.70E-02
TIA1	ENSG00000116001	10.715	12.290	0.207	2.02E-04	3.70E-02
ACOT2	ENSG00000119673	2.488	1.809	-0.475	2.04E-04	3.70E-02
TSPAN33	ENSG00000158457	30.848	20.432	-0.630	2.05E-04	3.70E-02
JRKL	ENSG00000183340	1.980	2.281	0.225	2.06E-04	3.70E-02
SCARF2	ENSG00000244486	0.183	0.126	-0.597	2.11E-04	3.75E-02
CECR5	ENSG00000069998	16.022	12.869	-0.336	2.15E-04	3.77E-02
PRDM8	ENSG00000152784	0.443	1.038	1.070	2.21E-04	3.81E-02
CEP152	ENSG00000103995	1.331	1.645	0.3194	2.41E-04	4.08E-02
CCL20	ENSG00000115009	9.411	46.334	2.219	2.42E-04	4.08E-02
CHIT1	ENSG00000133063	0.406	0.327	-0.642	2.47E-04	4.10E-02
DDX52	ENSG00000141141	8.645	9.481	0.143	2.50E-04	4.10E-02
CASP5	ENSG00000137757	4.235	8.799	1.030	2.55E-04	4.13E-02
MCTP2	ENSG00000140563	0.434	0.840	1.023	2.64E-04	4.20E-02
SLC45A1	ENSG00000162426	0.093	0.062	-0.576	2.69E-04	4.20E-02
RYR1	ENSG00000196218	0.463	0.296	-0.635	2.70E-04	4.20E-02

PPBP	ENSG00000163736	104.558	372.454	1.865	2.76E-04	4.20E-02
NOD2	ENSG00000167207	7.769	10.937	0.501	2.77E-04	4.20E-02
LOXL2	ENSG00000134013	1.409	0.785	-0.811	2.80E-04	4.20E-02
IFT81	ENSG00000122970	1.069	1.477	0.489	2.82E-04	4.20E-02
PHTF1	ENSG00000116793	5.744	6.854	0.263	2.88E-04	4.20E-02
KIAA0226L	ENSG00000102445	6.743	11.080	0.743	2.88E-04	4.20E-02
SDCCAG8	ENSG00000054282	12.135	15.482	0.366	3.11E-04	4.44E-02
VWCE	ENSG00000167992	0.390	0.229	-0.777	3.13E-04	4.44E-02
CLDN1	ENSG00000163347	0.021	0.088	2.154	3.16E-04	4.44E-02
PID1	ENSG00000153823	66.894	99.415	0.600	3.18E-04	4.44E-02
SNX25	ENSG00000109762	1.150	1.816	0.700	3.33E-04	4.61E-02
ATXN7L3	ENSG00000087152	24.959	27.604	0.153	3.40E-04	4.63E-02
EDN1	ENSG00000078401	1.426	3.003	1.09	3.42E-04	4.63E-02
KTN1	ENSG00000126777	47.133	53.741	0.201	3.54E-04	4.70E-02
NEK11	ENSG00000114670	0.434	0.558	0.365	3.59E-04	4.70E-02
KLC2	ENSG00000174996	1.256	1.676	0.431	3.60E-04	4.70E-02
MCFD2	ENSG00000180398	8.660	9.670	0.175	3.64E-04	4.70E-02
S100A12	ENSG00000163221	181.237	250.205	0.457	3.65E-04	4.70E-02
ACSF3	ENSG00000176715	5.405	4.522	-0.260	3.69E-04	4.70E-02
PPM1H	ENSG00000111110	1.782	1.281	-0.472	3.72E-04	4.70E-02
ZDHHC2	ENSG00000104219	6.655	8.800	0.414	3.82E-04	4.78E-02
NAMPT	ENSG00000105835	216.560	399.133	0.860	3.86E-04	4.78E-02
OSM	ENSG00000099985	4.084	12.513	1.443	4.02E-04	4.93E-02
MAPRE3	ENSG00000084764	7.512	9.857	0.397	4.15E-04	4.96E-02
TMPRSS9	ENSG00000178297	0.126	0.085	-0.605	4.19E-04	4.96E-02
CXCL6	ENSG00000124875	12.417	43.757	1.805	4.23E-04	4.96E-02
MMP8	ENSG00000118113	0.138	0.366	1.406	4.27E-04	4.96E-02
GM2A	ENSG00000196743	50.440	33.690	-0.585	4.36E-04	4.96E-02
C3orf80	ENSG00000180044	0.026	0.083	1.643	4.38E-04	4.96E-02
FAM177A1	ENSG00000151327	4.933	6.168	0.334	4.46E-04	4.96E-02
C1orf233	ENSG00000228594	1.109	0.704	-0.703	4.59E-04	4.96E-02
FGFR1OP2	ENSG00000111790	14.595	16.204	0.160	4.60E-04	4.96E-02
SOX13	ENSG00000143842	0.258	0.158	-0.687	4.63E-04	4.96E-02
CA13	ENSG00000185015	0.265	0.356	0.435	4.74E-04	4.96E-02
SGK1	ENSG00000118515	80.937	59.608	-0.410	4.75E-04	4.96E-02
PLCB4	ENSG00000101333	0.015	0.032	1.682	4.76E-04	4.96E-02
MYEOV	ENSG00000172927	0.122	0.282	1.281	4.76E-04	4.96E-02
SERPINB9	ENSG00000170542	18.758	39.539	1.017	4.77E-04	4.96E-02
ZNF654	ENSG00000175105	1.979	2.362	0.267	4.80E-04	4.96E-02
C1orf115	ENSG00000162817	0.072	0.147	0.985	4.82E-04	4.96E-02
NME7	ENSG00000143156	3.380	4.323	0.375	4.84E-04	4.96E-02
FAM111A	ENSG00000166801	7.942	9.530	0.273	4.84E-04	4.96E-02
KRCC1	ENSG00000172086	17.549	19.998	0.196	4.84E-04	4.96E-02
OTOF	ENSG00000115155	0.165	0.598	1.814	4.86E-04	4.96E-02
IGFN1	ENSG00000163395	0.090	0.509	1.710	4.88E-04	4.96E-02
GTF2E2	ENSG00000197265	17.947	20.273	0.181	4.91E-04	4.96E-02

Table A.6. Complete list of differentially expressed genes in HD monocytes following HTT-lowering (FDR < 0.05).

Gene ID	Ensembl ID	RPKM (SCR siRNA)	RPKM (Anti-*HTT* siRNA)	log2 fold change	*p*-value	FDR
COX5A	ENSG00000178741	120.152	41.172	-1.562	4.76E-137	3.98E-133
ECI2	ENSG00000198721	6.403	3.912	-0.737	6.82E-39	2.85E-35
HTT	ENSG00000197386	10.218	4.300	-1.280	1.00E-27	2.79E-24
SRPR	ENSG00000182934	62.426	43.624	-0.488	1.05E-20	2.19E-17
PPARA	ENSG00000186951	2.051	1.514	-0.471	1.16E-17	1.93E-14
VAMP3	ENSG00000049245	52.249	37.049	-0.483	3.43E-17	4.78E-14
SPG20	ENSG00000133104	26.372	17.912	-0.512	2.22E-13	2.57E-10
ACP5	ENSG00000102575	563.842	319.723	-1.050	2.46E-13	2.57E-10
CAPZA1	ENSG00000116489	107.840	84.262	-0.319	6.40E-13	5.94E-10
NDUFA8	ENSG00000119421	22.077	17.142	-0.385	2.92E-12	2.44E-09
C8orf33	ENSG00000182307	6.731	4.975	-0.445	3.81E-11	2.80E-08
ARHGEF7	ENSG00000102606	6.301	5.296	-0.233	4.02E-11	2.80E-08
HDGF	ENSG00000143321	47.811	35.132	-0.459	1.03E-10	6.64E-08
BAG5	ENSG00000166170	4.191	3.719	-0.185	1.37E-10	8.19E-08
TOMM70A	ENSG00000154174	14.166	12.552	-0.152	2.22E-10	1.24E-07
CSE1L	ENSG00000124207	18.510	16.133	-0.215	1.86E-09	9.69E-07
CNOT11	ENSG00000158435	14.431	11.196	-0.355	2.56E-09	1.26E-06
ACTG1	ENSG00000184009	705.135	1031.133	0.582	2.92E-09	1.35E-06
UBE2D4	ENSG00000078967	3.913	3.028	-0.399	1.25E-08	5.49E-06
HIF1AN	ENSG00000166135	8.113	6.787	-0.241	1.99E-08	8.32E-06
PAFAH1B1	ENSG00000007168	22.116	19.385	-0.178	2.42E-08	9.61E-06
NLK	ENSG00000087095	3.617	2.945	-0.280	4.29E-08	1.63E-05
UBE3C	ENSG00000009335	24.640	21.733	-0.151	5.04E-08	1.83E-05
VTI1B	ENSG00000100568	26.175	32.030	0.277	6.15E-08	2.14E-05
MCFD2	ENSG00000180398	8.048	6.365	-0.358	6.78E-08	2.26E-05
SUMO3	ENSG00000184900	45.921	36.797	-0.374	1.02E-07	3.27E-05
CTNND1	ENSG00000198561	31.248	24.832	-0.313	1.93E-07	5.98E-05
TMEM192	ENSG00000170088	7.396	6.356	-0.258	2.18E-07	6.51E-05
HAT1	ENSG00000128708	38.753	29.463	-0.324	3.19E-07	9.19E-05
NSUN2	ENSG00000037474	30.837	23.487	-0.357	3.61E-07	1.01E-04
GTF3C4	ENSG00000125484	3.678	3.153	-0.218	4.15E-07	1.12E-04
ACADS	ENSG00000122971	8.727	6.559	-0.414	6.35E-07	1.66E-04
ITGB1	ENSG00000150093	111.194	95.289	-0.205	9.19E-07	2.32E-04
TALDO1	ENSG00000177156	417.422	334.931	-0.351	1.09E-06	2.61E-04
GNS	ENSG00000135677	166.870	120.949	-0.444	1.10E-06	2.61E-04
ZNF720	ENSG00000197302	2.215	2.869	0.450	3.11E-06	7.20E-04
SOAT1	ENSG00000057252	63.227	82.848	0.351	5.72E-06	1.29E-03
GSS	ENSG00000100983	25.511	29.332	0.212	7.56E-06	1.66E-03
RNF214	ENSG00000167257	5.657	4.963	-0.224	8.68E-06	1.86E-03
MRPL45	ENSG00000174100	9.426	8.063	-0.223	9.36E-06	1.95E-03

UQCR10	ENSG00000184076	23.029	28.690	0.310	2.02E-05	4.11E-03
STX6	ENSG00000135823	12.326	8.202	-0.578	2.07E-05	4.11E-03
SLC25A44	ENSG00000160785	7.604	6.485	-0.193	2.13E-05	4.14E-03
PPT1	ENSG00000131238	331.211	231.084	-0.550	3.35E-05	6.36E-03
SF3B2	ENSG00000087365	77.738	68.950	-0.144	3.52E-05	6.52E-03
FURIN	ENSG00000140564	34.831	25.430	-0.441	3.64E-05	6.61E-03
CHSY1	ENSG00000131873	6.061	4.914	-0.243	5.35E-05	9.49E-03
ZNF622	ENSG00000173545	18.959	16.352	-0.199	5.51E-05	9.58E-03
SET	ENSG00000119335	47.605	41.599	-0.210	6.62E-05	1.13E-02
ABCC3	ENSG00000108846	17.374	12.400	-0.636	7.87E-05	1.31E-02
ANKRD13C	ENSG00000118454	3.369	2.863	-0.236	8.18E-05	1.34E-02
PRR13	ENSG00000205352	82.505	73.800	-0.156	8.97E-05	1.44E-02
RAB12	ENSG00000206418	29.276	21.229	-0.410	9.53E-05	1.50E-02
GALNT2	ENSG00000143641	15.788	18.803	0.277	9.75E-05	1.51E-02
TMEM184C	ENSG00000164168	11.178	9.845	-0.182	1.04E-04	1.57E-02
PANX1	ENSG00000110218	13.388	10.930	-0.257	1.24E-04	1.85E-02
LEO1	ENSG00000166477	11.405	9.251	-0.267	1.47E-04	2.14E-02
RECQL	ENSG00000004700	24.388	20.266	-0.22568	1.51E-04	2.14E-02
ZNF776	ENSG00000152443	1.778	1.451	-0.277	1.53E-04	2.14E-02
SLC25A32	ENSG00000164933	6.041	6.816	0.247	1.56E-04	2.14E-02
MPI	ENSG00000178802	5.981	5.281	-0.263	1.56E-04	2.14E-02
NBR1	ENSG00000188554	22.278	18.719	-0.251	1.70E-04	2.29E-02
STRN	ENSG00000115808	3.473	3.041	-0.214	1.77E-04	2.34E-02
MIPEP	ENSG00000027001	3.888	5.631	0.509	1.92E-04	2.47E-02
TGOLN2	ENSG00000152291	37.632	33.288	-0.200	1.93E-04	2.47E-02
SARS	ENSG00000031698	56.071	47.449	-0.237	1.99E-04	2.52E-02
FUBP1	ENSG00000162613	40.255	34.989	-0.140	2.20E-04	2.71E-02
PSMA1	ENSG00000129084	110.274	94.206	-0.160	2.21E-04	2.71E-02
DHRS7B	ENSG00000109016	7.729	9.004	0.214	2.96E-04	3.57E-02
MFSD10	ENSG00000109736	25.456	20.818	-0.290	2.99E-04	3.57E-02
ANKRD40	ENSG00000154945	7.278	6.578	-0.158	4.11E-04	4.84E-02

A.4 Monocyte GSEA results

Table A.7. Complete list of enriched gene sets among the upregulated genes in unstimulated HD monocytes (FDR < 0.05).

Pathway	NES	*p*-value	FDR	Description
GO: 31347	5.631	8.96E-09	1.28E-04	Regulation of defence response
MGI: 2419	5.378	3.77E-08	2.68E-04	Abnormal innate immunity
MGI: 8835	5.077	1.92E-07	6.46E-04	Abnormal intercellular signalling peptide or protein level
GO: 6954	5.036	2.38E-07	6.46E-04	Inflammatory response
GO: 31349	5.016	2.64E-07	6.46E-04	Positive regulation of defence response
MGI: 8713	5.010	2.72E-07	6.46E-04	Abnormal cytokine level
MGI: 3009	4.923	4.26E-07	8.67E-04	Abnormal cytokine secretion
GO: 9615	4.760	9.68E-07	1.63E-03	Response to virus
GO: 43900	4.727	1.14E-06	1.63E-03	Regulation of multi-organism process
GO: 45088	4.710	1.24E-06	1.63E-03	Regulation of innate immune response
MGI: 8469	4.677	1.46E-06	1.63E-03	Abnormal protein level
KEGG: 5323	4.649	1.67E-06	1.63E-03	Rheumatoid arthritis
GO: 1817	4.647	1.68E-06	1.63E-03	Regulation of cytokine production
GO: 5125	4.643	1.72E-06	1.63E-03	Cytokine activity
MGI: 2451	4.630	1.83E-06	1.63E-03	Abnormal macrophage physiology
KEGG: 4060	4.624	1.88E-06	1.63E-03	Cytokine-cytokine receptor interaction
GO: 2252	4.617	1.95E-06	1.63E-03	Immune effector process
GO: 9617	4.590	2.22E-06	1.73E-03	Response to bacterium
MGI: 1793	4.582	2.30E-06	1.73E-03	Altered susceptibility to infection
MGI: 8568	4.509	3.26E-06	2.32E-03	Abnormal interleukin secretion
GO: 5126	4.488	3.59E-06	2.44E-03	Cytokine receptor binding
MGI: 5025	4.444	4.42E-06	2.82E-03	Abnormal response to infection
GO: 46888	4.437	4.56E-06	2.82E-03	Negative regulation of hormone secretion
GO: 45089	4.427	4.78E-06	2.84E-03	Positive regulation of innate immune response
MGI: 2444	4.410	5.17E-06	2.94E-03	Abnormal T cell physiology

REACTOME: 287	4.358	6.56E-06	3.60E-03	Cytokine signalling in immune system
KEGG: 4668	4.277	9.47E-06	5.00E-03	TNF signalling pathway
GO: 70201	4.255	1.05E-05	5.32E-03	Regulation of establishment of protein localization
MGI: 2406	4.208	1.29E-05	6.16E-03	Increased susceptibility to infection
REACTOME: 218	4.205	1.31E-05	6.16E-03	Chemokine receptors bind chemokines
GO: 51607	4.199	1.34E-05	6.16E-03	Defence response to virus
GO: 1819	4.188	1.41E-05	6.26E-03	Positive regulation of cytokine production
GO: 71345	4.151	1.66E-05	7.14E-03	Cellular response to cytokine stimulus
MGI: 10210	4.144	1.71E-05	7.15E-03	Abnormal circulating cytokine level
GO: 35821	4.113	1.95E-05	7.83E-03	Modification of morphology or physiology of other organism
GO: 2218	4.110	1.98E-05	7.83E-03	Activation of innate immune response
MGI: 8751	4.090	2.16E-05	8.30E-03	Abnormal interleukin level
GO: 43122	4.073	2.32E-05	8.70E-03	Regulation of I-kappaB kinase/NF-kappaB cascade
GO: 30595	4.024	2.86E-05	1.02E-02	Leukocyte chemotaxis
GO: 72527	4.022	2.89E-05	1.02E-02	Pyrimidine-containing compound metabolic process
GO: 50727	4.018	2.93E-05	1.02E-02	Regulation of inflammatory response
GO: 5929	3.996	3.22E-05	1.09E-02	Cilium
GO: 2696	3.972	3.56E-05	1.18E-02	Positive regulation of leukocyte activation
GO: 7243	3.960	3.75E-05	1.21E-02	Intracellular protein kinase cascade
GO: 30334	3.940	4.07E-05	1.29E-02	Regulation of cell migration
GO: 50900	3.928	4.28E-05	1.33E-02	Leukocyte migration
GO: 51251	3.916	4.50E-05	1.36E-02	Positive regulation of lymphocyte activation
GO: 51817	3.912	4.58E-05	1.36E-02	Modification of morphology or physiology of other organism involved in symbiotic interaction
GO: 2758	3.900	4.81E-05	1.40E-02	Innate immune response-activating signal transduction
GO: 2694	3.891	4.99E-05	1.42E-02	Regulation of leukocyte activation
GO: 51223	3.870	5.44E-05	1.52E-02	Regulation of protein transport
MGI: 5416	3.854	5.81E-05	1.59E-02	Abnormal circulating protein level
GO: 1816	3.849	5.93E-05	1.59E-02	Cytokine production
GO: 70851	3.832	6.36E-05	1.68E-02	Growth factor receptor binding
GO: 2237	3.819	6.70E-05	1.73E-02	Response to molecule of bacterial origin

GO: 45580	3.799	7.26E-05	1.80E-02	Regulation of T cell differentiation
GO: 2000145	3.799	7.26E-05	1.80E-02	Regulation of cell motility
GO: 60326	3.796	7.35E-05	1.80E-02	Cell chemotaxis
GO: 32880	3.793	7.44E-05	1.80E-02	Regulation of protein localization
MGI: 8556	3.769	8.20E-05	1.95E-02	Abnormal tumour necrosis factor secretion
GO: 2221	3.762	8.43E-05	1.97E-02	Pattern recognition receptor signalling pathway
GO: 32101	3.758	8.56E-05	1.97E-02	Regulation of response to external stimulus
GO: 19221	3.727	9.69E-05	2.14E-02	Cytokine-mediated signalling pathway
GO: 43903	3.726	9.73E-05	2.14E-02	Regulation of symbiosis, encompassing mutualism through parasitism
GO: 50778	3.725	9.77E-05	2.14E-02	Positive regulation of immune response
GO: 5813	3.702	1.07E-04	2.31E-02	Centrosome
GO: 51249	3.691	1.12E-04	2.37E-02	Regulation of lymphocyte activation
GO: 45321	3.683	1.15E-04	2.41E-02	Leukocyte activation
GO: 72528	3.679	1.17E-04	2.42E-02	Pyrimidine-containing compound biosynthetic process
GO: 45619	3.673	1.20E-04	2.44E-02	Regulation of lymphocyte differentiation
GO: 2000116	3.646	1.33E-04	2.65E-02	Regulation of cysteine-type endopeptidase activity
KEGG: 4630	3.643	1.35E-04	2.65E-02	JAK-STAT signalling pathway
GO: 32496	3.640	1.36E-04	2.65E-02	Response to lipopolysaccharide
GO: 50867	3.637	1.38E-04	2.65E-02	Positive regulation of cell activation
GO: 43901	3.633	1.40E-04	2.66E-02	Negative regulation of multi-organism process
GO: 10942	3.617	1.49E-04	2.79E-02	Positive regulation of cell death
MGI: 8555	3.602	1.58E-04	2.92E-02	Abnormal interferon secretion
MGI: 8588	3.599	1.60E-04	2.92E-02	Abnormal circulating interleukin level
GO: 45621	3.583	1.70E-04	3.06E-02	Positive regulation of lymphocyte differentiation
GO: 44003	3.569	1.79E-04	3.19E-02	Modification by symbiont of host morphology or physiology
GO: 45582	3.502	2.31E-04	4.06E-02	Positive regulation of T cell differentiation
GO: 2697	3.496	2.36E-04	4.10E-02	Regulation of immune effector process
GO: 50870	3.458	2.72E-04	4.67E-02	Positive regulation of T cell activation
GO: 43068	3.439	2.92E-04	4.95E-02	Positive regulation of programmed cell death
GO: 2757	3.434	2.97E-04	4.98E-02	Immune response-activating signal transduction

Table A.8. Complete list of enriched gene sets among the downregulated genes in stimulated HD monocytes (FDR < 0.05).

Pathway	NES	*p*-value	FDR	Description
GO: 72594	5.819	2.96E-09	1.88E-05	Establishment of protein localization to organelle
GO: 6412	5.803	3.26E-09	1.88E-05	Translation
GO: 6605	5.443	2.62E-08	1.01E-04	Protein targeting
REACTOME: 1287	5.222	8.85E-08	2.55E-04	Translation
GO: 22411	5.120	1.53E-07	3.04E-04	Cellular component disassembly
GO: 33365	5.113	1.59E-07	3.04E-04	Protein localization to organelle
GO: 6612	5.044	2.28E-07	3.75E-04	Protein targeting to membrane
GO: 5773	4.947	3.77E-07	5.43E-04	Vacuole
GO: 70972	4.876	5.41E-07	6.93E-04	Protein localization to endoplasmic reticulum
MGI: 3947	4.799	7.97E-07	9.19E-04	Abnormal cholesterol level
GO: 6413	4.693	1.35E-06	1.37E-03	Translational initiation
GO: 72599	4.677	1.46E-06	1.37E-03	Establishment of protein localization to endoplasmic reticulum
GO: 45047	4.665	1.54E-06	1.37E-03	Protein targeting to ER
REACTOME: 1165	4.646	1.69E-06	1.39E-03	SRP-dependent co-translational protein targeting to membrane
GO: 6613	4.623	1.89E-06	1.45E-03	Co-translational protein targeting to membrane
MGI: 5278	4.604	2.07E-06	1.49E-03	Abnormal cholesterol homeostasis
GO: 6614	4.562	2.53E-06	1.65E-03	SRP-dependent co-translational protein targeting to membrane
GO: 44391	4.547	2.72E-06	1.65E-03	Ribosomal subunit
GO: 32984	4.547	2.72E-06	1.65E-03	Macromolecular complex disassembly
GO: 44445	4.522	3.06E-06	1.76E-03	Cytosolic part
KEGG: 3010	4.509	3.26E-06	1.79E-03	Ribosome
REACTOME: 190	4.473	3.86E-06	1.93E-03	CAP-dependent translation initiation
REACTOME: 383	4.473	3.86E-06	1.93E-03	Eukaryotic translation initiation
MGI: 3949	4.459	4.12E-06	1.98E-03	Abnormal circulating lipid level
GO: 6414	4.415	5.05E-06	2.33E-03	Translational elongation
GO: 43241	4.373	6.13E-06	2.69E-03	Protein complex disassembly
GO: 3735	4.367	6.30E-06	2.69E-03	Structural constituent of ribosome

GO: 43624	4.348	6.87E-06	2.83E-03	Cellular protein complex disassembly
GO: 5764	4.330	7.46E-06	2.83E-03	Lysosome
GO: 323	4.330	7.46E-06	2.83E-03	Lytic vacuole
MGI: 180	4.325	7.63E-06	2.83E-03	Abnormal circulating cholesterol level
MGI: 3982	4.308	8.24E-06	2.97E-03	Increased cholesterol level
GO: 5840	4.299	8.58E-06	3.00E-03	Ribosome
GO: 19058	4.278	9.43E-06	3.20E-03	Viral infectious cycle
REACTOME: 2	4.240	1.12E-05	3.53E-03	3'-UTR-mediated translational regulation
REACTOME: 621	4.240	1.12E-05	3.53E-03	L13A-mediated translational silencing of caeruloplasmin expression
REACTOME: 512	4.237	1.13E-05	3.53E-03	GTP hydrolysis and joining of the 60S ribosomal subunit
REACTOME: 415	4.229	1.17E-05	3.56E-03	Formation of a pool of free 40S subunits
GO: 22626	4.220	1.22E-05	3.61E-03	Cytosolic ribosome
MGI: 5178	4.201	1.33E-05	3.83E-03	Increased circulating cholesterol level
GO: 7005	4.185	1.43E-05	4.01E-03	Mitochondrion organization
REACTOME: 782	4.173	1.50E-05	4.03E-03	Nonsense-mediated decay
REACTOME: 780	4.173	1.50E-05	4.03E-03	Nonsense-mediated decay enhanced by the exon junction complex
REACTOME: 556	4.164	1.56E-05	4.06E-03	Influenza viral RNA transcription and replication
GO: 6401	4.161	1.58E-05	4.06E-03	RNA catabolic process
GO: 184	4.152	1.65E-05	4.13E-03	Nuclear-transcribed mRNA catabolic process, nonsense-mediated decay
KEGG: 4142	4.130	1.81E-05	4.45E-03	Lysosome
REACTOME: 382	4.116	1.93E-05	4.63E-03	Eukaryotic translation elongation
GO: 19080	4.102	2.05E-05	4.80E-03	Viral genome expression
GO: 5775	4.098	2.08E-05	4.80E-03	Vacuolar lumen
GO: 6415	4.091	2.15E-05	4.85E-03	Translational termination
GO: 956	4.075	2.30E-05	5.10E-03	Nuclear-transcribed mRNA catabolic process
REACTOME: 1349	4.032	2.77E-05	6.01E-03	Viral mRNA translation
GO: 6402	4.025	2.85E-05	6.05E-03	mRNA catabolic process
MGI: 745	4.022	2.89E-05	6.05E-03	Tremors
REACTOME: 839	3.992	3.28E-05	6.74E-03	Peptide chain elongation
GO: 19083	3.978	3.47E-05	7.02E-03	Viral transcription

REACTOME: 384	3.967	3.64E-05	7.23E-03	Eukaryotic translation termination
REACTOME: 554	3.963	3.70E-05	7.23E-03	Influenza infection
REACTOME: 555	3.936	4.14E-05	7.96E-03	Influenza life cycle
GO: 43202	3.926	4.32E-05	8.00E-03	Lysosomal lumen
REACTOME: 1041	3.925	4.34E-05	8.00E-03	RNA polymerase I transcription
REACTOME: 781	3.923	4.37E-05	8.00E-03	Nonsense-mediated decay independent of the exon junction complex
GO: 6839	3.916	4.50E-05	8.10E-03	Mitochondrial transport
GO: 44437	3.906	4.69E-05	8.32E-03	Vacuolar part
GO: 5793	3.854	5.81E-05	1.01E-02	Endoplasmic reticulum-Golgi intermediate compartment
REACTOME: 1038	3.848	5.95E-05	1.02E-02	RNA polymerase I promoter clearance
GO: 8202	3.777	7.94E-05	1.34E-02	Steroid metabolic process
GO: 10035	3.773	8.06E-05	1.35E-02	Response to inorganic substance
GO: 44433	3.725	9.77E-05	1.61E-02	Cytoplasmic vesicle part
GO: 34976	3.710	1.04E-04	1.68E-02	Response to endoplasmic reticulum stress
MGI: 8469	3.689	1.13E-04	1.80E-02	Abnormal protein level
MGI: 3983	3.660	1.26E-04	1.99E-02	Decreased cholesterol level
GO: 61024	3.656	1.28E-04	1.99E-02	Membrane organization
GO: 6066	3.640	1.36E-04	2.09E-02	Alcohol metabolic process
GO: 16044	3.593	1.63E-04	2.48E-02	Cellular membrane organization
REACTOME: 1037	3.588	1.67E-04	2.49E-02	RNA polymerase I chain elongation
GO: 6984	3.554	1.90E-04	2.80E-02	ER-nucleus signalling pathway
KEGG: 5322	3.460	2.70E-04	3.94E-02	Systemic lupus erythematosus
GO: 32940	3.455	2.75E-04	3.96E-02	Secretion by cell
GO: 22613	3.442	2.89E-04	4.11E-02	Ribonucleoprotein complex biogenesis
GO: 42254	3.404	3.32E-04	4.67E-02	Ribosome biogenesis
REACTOME: 647	3.389	3.51E-04	4.87E-02	Meiotic recombination

A.5 Monocyte IPA® results

Table A.9. Complete list of upstream regulators inferred to be significantly activated in unstimulated HD monocytes. Significance defined as activation z-score ≥ 2, *p*-value of overlap < 0.01.

Upstream regulator	Molecule type	Activation z-score	*p*-value of overlap
TNF	Cytokine	5.764	2.18E-13
IL1B	Cytokine	5.754	8.08E-14
MYD88	Other	4.761	2.92E-12
IFNG	Cytokine	4.635	3.09E-07
IL1A	Cytokine	4.536	1.69E-11
TLR3	Transmembrane receptor	4.323	1.99E-09
RELA	Transcription regulator	4.122	5.86E-08
NFκB (complex)	Complex	4.077	2.63E-08
TLR9	Transmembrane receptor	3.773	4.33E-07
TLR2	Transmembrane receptor	3.77	3.94E-09
STAT3	Transcription regulator	3.701	2.34E-07
IL6	Cytokine	3.654	7.39E-06
TICAM1	Other	3.651	2.59E-08
ERK1/2	Group	3.636	5.33E-06
TLR4	Transmembrane receptor	3.61	7.68E-12
SMARCA4	Transcription regulator	3.584	1.83E-04
MYC	Transcription regulator	3.528	1.54E-03
CSF2	Cytokine	3.435	4.46E-03
ERK	Group	3.381	2.58E-07
TLR7	Transmembrane receptor	3.368	2.61E-04
PDGF BB	Complex	3.35	1.83E-07
SAMSN1	Other	3.317	1.51E-04
TNFSF12	Cytokine	3.265	1.52E-05
Jnk	Group	3.255	3.83E-06
LCN2	Transporter	3.221	3.54E-07
IL17A	Cytokine	3.213	7.05E-05
IL2	Cytokine	3.12	1.39E-04
CD14	Transmembrane receptor	3.091	6.84E-09
IL18	Cytokine	3.081	6.29E-05
EZH2	Transcription regulator	3.074	3.96E-03
TBK1	Kinase	3.053	5.03E-07
EGFR	Kinase	2.991	1.83E-07
HIF1A	Transcription regulator	2.979	8.80E-06
NOD2	Other	2.952	3.94E-05
Akt	Group	2.949	3.15E-03
IRF1	Transcription regulator	2.925	2.48E-04

TLR	Group	2.904	7.53E-06
NFKB1	Transcription regulator	2.897	6.74E-10
PPIF	Enzyme	2.887	6.92E-05
PTGS2	Enzyme	2.849	3.03E-04
DOCK8	Other	2.828	1.94E-03
SASH1	Other	2.828	2.33E-03
ERBB2	Kinase	2.814	1.63E-03
RNASE1	Enzyme	2.8	1.91E-07
RNASE2	Enzyme	2.76	2.37E-06
MET	Kinase	2.759	7.28E-04
MAPK8	Kinase	2.72	2.25E-05
P38 MAPK	Group	2.707	1.40E-07
ETS1	Transcription regulator	2.693	4.97E-03
PTPRJ	Phosphatase	2.646	1.08E-03
IL15	Cytokine	2.611	1.39E-03
PRKCE	Kinase	2.6	6.37E-04
TLR5	Transmembrane receptor	2.595	1.20E-05
F7	Peptidase	2.592	1.59E-05
PARP1	Enzyme	2.589	1.94E-03
NAMPT	Cytokine	2.58	1.49E-06
TRAF3IP2	Other	2.575	1.52E-04
AHR	Nuclear receptor	2.566	6.70E-04
TGFA	Growth factor	2.564	1.26E-04
TP63	Transcription regulator	2.505	5.46E-03
OSM	Cytokine	2.503	6.63E-05
KRT17	Other	2.449	3.85E-04
KLK5	Peptidase	2.449	1.69E-05
TMEM173	Other	2.433	1.07E-03
F2	Peptidase	2.425	1.32E-04
TRPV4	Ion channel	2.425	1.03E-04
PRKCA	Kinase	2.423	7.67E-03
LDL	Complex	2.421	6.87E-04
TIRAP	Other	2.418	9.71E-07
IL17C	Cytokine	2.412	4.96E-06
AGER	Transmembrane receptor	2.41	5.41E-05
SRC	Kinase	2.407	4.33E-03
PPRC1	Transcription regulator	2.401	3.47E-03
IL33	Cytokine	2.397	1.88E-03
FCGR2A	Transmembrane receptor	2.395	1.69E-05
CLEC7A	Transmembrane receptor	2.395	1.69E-05
CEBPB	Transcription regulator	2.391	3.32E-04
MAP2K1/2	Group	2.386	4.81E-03
GM-CSF	Group	2.385	3.02E-04
IRF5	Transcription regulator	2.354	1.88E-03
XBP1	Transcription regulator	2.351	3.48E-03

NFATC2	Transcription regulator	2.325	7.12E-03
Cg	Complex	2.294	2.70E-04
MAPK9	Kinase	2.274	4.97E-03
Mek	Group	2.271	1.73E-03
Lymphotoxin-α1-β2	Complex	2.236	4.02E-05
JAK2	Kinase	2.236	9.62E-03
C5	Other	2.224	1.26E-04
CD40LG	Cytokine	2.223	9.37E-06
PADI2	Enzyme	2.219	8.87E-05
IL6R	Transmembrane receptor	2.219	1.72E-03
BCL2	Transporter	2.219	1.24E-03
IL23A	Cytokine	2.213	3.99E-04
TLR1	Transmembrane receptor	2.213	1.26E-04
RET	Kinase	2.213	2.56E-04
NFKBIA	Transcription regulator	2.213	2.60E-08
PF4	Cytokine	2.213	6.08E-05
RETN	Other	2.204	8.87E-05
IRAK4	Kinase	2.193	5.74E-08
ICAM1	Transmembrane receptor	2.19	9.81E-04
P2RX7	Ion channel	2.19	1.73E-04
CCL5	Cytokine	2.188	1.61E-04
FN1	Enzyme	2.183	2.79E-03
TXNIP	Other	2.183	7.07E-03
MAVS	Other	2.17	1.38E-04
Ap1	Complex	2.166	5.42E-04
HSPD1	Enzyme	2.158	1.26E-04
LEPR	Transmembrane receptor	2.157	5.21E-03
HSP90B1	Other	2.152	5.10E-04
KITLG	Growth factor	2.15	8.58E-03
TRAF6	Enzyme	2.142	1.72E-03
IL12B	Cytokine	2.138	1.65E-05
TNFRSF1A	Transmembrane receptor	2.122	1.76E-07
EGF	Growth factor	2.121	2.00E-04
IFNA2	Cytokine	2.046	5.39E-04
Ige	Complex	2.025	2.16E-04
CAMP	Other	2.024	1.88E-03
TANK	Other	2.018	4.39E-05
BCR (complex)	Complex	2.013	6.58E-03
IL32	Cytokine	2.012	8.88E-06
EGR1	Transcription regulator	2.011	6.55E-04
MIF	Cytokine	2.01	1.52E-04
TGIF1	Transcription regulator	2	2.12E-04
NLRC4	Other	2	7.46E-05
NEK6	Kinase	2	1.31E-04

Table A.10. Complete list of upstream regulators inferred to be significantly inhibited in unstimulated HD monocytes. Significance defined as activation z-score ≤ -2, *p*-value of overlap < 0.01.

Upstream regulator	Molecule type	Activation z-score	*p*-value of overlap
miR-155-5p	Mature microRNA	-3.39	1.92E-09
HMOX1	Enzyme	-3.088	1.14E-05
COL18A1	Other	-2.975	4.32E-04
IL10RA	Transmembrane receptor	-2.879	1.92E-05
THRA	Nuclear receptor	-2.828	5.36E-04
FBXO32	Enzyme	-2.646	1.18E-07
DUSP1	Phosphatase	-2.606	2.05E-08
IL37	Cytokine	-2.605	6.05E-08
PROC	Peptidase	-2.6	9.71E-07
IgG	Complex	-2.523	1.65E-06
TAB1	Enzyme	-2.433	7.97E-05
NLRP12	Other	-2.372	1.67-04
INSIG1	Other	-2.309	5.60E-05
Alpha catenin	Group	-2.282	5.01E-04
BPIFA1	Other	-2.216	1.52E-05
SOCS1	Other	-2.213	2.50E-03
ZFP36	Transcription regulator	-2.207	9.43E-10
CD3	Complex	-2.198	6.91E-04
TRAIP	Enzyme	-2.176	3.08E-04
CD28	Transmembrane receptor	-2.158	4.97E-03
ITGB2	Transmembrane receptor	-2.157	2.79E-05
RPSA	Translation regulator	-2.156	3.18E-06
ARRB2	Other	-2.144	1.59E-05
Nr1h	Group	-2.103	5.85E-04
ABCA1	Transporter	-2.08	1.52E-04
PTGER4	G-protein coupled receptor	-2.019	1.77E-03
TRAF3	Other	-2.019	8.60E-04
SERPINE1	Other	-2	1.44E-03
USP18	Peptidase	-2	2.50E-03
Cdc42	Enzyme	-2	1.21E-03

A.6 T lymphocyte proliferation assay results

Table A.11. Analysis of T lymphocyte proliferation data using the fraction diluted statistic. Fraction diluted is calculated as the percentage of cells in the final culture that have divided at least once. Control *n* = 9, HD *n* = 8. Data shown as mean ± SEM.

Cell type	Treatment	Time point	Fraction diluted	
			Control	HD
T lymphocytes ($CD3^+$)	Unstimulated	72 h	1.00 ± 0.39	1.69 ± 0.71
	Unstimulated	96 h	4.13 ± 0.85	3.59 ± 1.30
	Unstimulated	120 h	6.95 ± 0.98	5.46 ± 1.87
	Anti-CD3 + CD28	72 h	62.17 ± 7.73	69.19 ± 5.96
	Anti-CD3 + CD28	96 h	85.56 ± 5.14	79.91 ± 7.81
	Anti-CD3 + CD28	120 h	93.92 ± 2.02	96.15 ± 1.33
	PHA-P	72 h	70.68 ± 4.89	58.05 ± 8.28
	PHA-P	96 h	83.71 ± 3.62	70.90 ± 9.25
	PHA-P	120 h	87.97 ± 2.70	76.05 ± 7.27
Helper T lymphocytes ($CD3^+$ $CD4^+$)	Unstimulated	72 h	0.82 ± 0.35	1.26 ± 0.44
	Unstimulated	96 h	3.18 ± 0.52	3.26 ± 1.35
	Unstimulated	120 h	6.29 ± 1.24	5.24 ± 1.98
	Anti-CD3 + CD28	72 h	66.54 ± 6.57	75.51 ± 4.64
	Anti-CD3 + CD28	96 h	88.42 ± 3.99	83.13 ± 6.83
	Anti-CD3 + CD28	120 h	95.83 ± 1.03	97.69 ± 1.00
	PHA-P	72 h	68.29 ± 6.20	65.89 ± 4.57
	PHA-P	96 h	84.99 ± 2.04	79.98 ± 3.65
	PHA-P	120 h	87.89 ± 1.86	84.41 ± 1.94
Cytotoxic T lymphocytes ($CD3^+$ $CD8^+$)	Unstimulated	72 h	1.09 ± 0.43	4.36 ± 2.83
	Unstimulated	96 h	7.06 ± 2.17	4.82 ± 1.88
	Unstimulated	120 h	11.15 ± 2.44	8.29 ± 3.61
	Anti-CD3 + CD28	72 h	73.59 ± 7.51	73.20 ± 6.03
	Anti-CD3 + CD28	96 h	87.48 ± 5.56	85.24 ± 6.62
	Anti-CD3 + CD28	120 h	93.57 ± 3.21	96.54 ± 1.52
	PHA-P	72 h	72.32 ± 7.99	63.76 ± 10.91
	PHA-P	96 h	85.54 ± 5.14	71.91 ± 12.91
	PHA-P	120 h	90.14 ± 3.69	75.46 ± 12.02

Table A.12. Analysis of T lymphocyte proliferation data using the percentage divided statistic. Percentage divided is calculated as the percentage of cells from the initial culture that divided at least once. Control *n* = 9, HD *n* = 8. Data shown as mean ± SEM.

Cell type	Treatment	Time point	Percentage divided	
			Control	HD
T lymphocytes ($CD3^+$)	Unstimulated	72 h	0.32 ± 0.08	0.31 ± 0.07
	Unstimulated	96 h	1.12 ± 0.22	1.36 ± 0.42
	Unstimulated	120 h	1.05 ± 0.22	1.06 ± 0.26
	Anti-CD3 + CD28	72 h	42.68 ± 6.91	48.01 ± 6.84
	Anti-CD3 + CD28	96 h	59.73 ± 6.37	51.78 ± 9.02
	Anti-CD3 + CD28	120 h	60.80 ± 6.70	65.09 ± 6.39
	PHA-P	72 h	53.01 ± 4.95	40.02 ± 7.24
	PHA-P	96 h	54.17 ± 4.63	43.98 ± 7.26
	PHA-P	120 h	52.58 ± 3.27	39.11 ± 6.51
Helper T lymphocytes ($CD3^+$ $CD4^+$)	Unstimulated	72 h	0.20 ± 0.08	0.28 ± 0.08
	Unstimulated	96 h	0.96 ± 0.18	1.11 ± 0.49
	Unstimulated	120 h	1.11 ± 0.31	1.18 ± 0.49
	Anti-CD3 + CD28	72 h	46.24 ± 5.56	54.71 ± 5.85
	Anti-CD3 + CD28	96 h	64.98 ± 5.03	58.96 ± 9.53
	Anti-CD3 + CD28	120 h	67.44 ± 4.04	79.15 ± 5.27
	PHA-P	72 h	52.19 ± 5.59	47.95 ± 4.21
	PHA-P	96 h	58.91 ± 2.91	53.95 ± 3.72
	PHA-P	120 h	58.90 ± 2.21	50.10 ± 2.84
Cytotoxic T lymphocytes ($CD3^+$ $CD8^+$)	Unstimulated	72 h	0.78 ± 0.32	0.61 ± 0.17
	Unstimulated	96 h	1.51 ± 0.40	1.55 ± 0.51
	Unstimulated	120 h	1.29 ± 0.19	1.58 ± 0.47
	Anti-CD3 + CD28	72 h	52.86 ± 7.61	49.65 ± 7.10
	Anti-CD3 + CD28	96 h	63.10 ± 8.72	57.48 ± 9.04
	Anti-CD3 + CD28	120 h	63.90 ± 9.16	67.33 ± 8.27
	PHA-P	72 h	53.14 ± 9.93	44.92 ± 9.07
	PHA-P	96 h	56.00 ± 8.66	47.10 ± 10.22
	PHA-P	120 h	52.66 ± 7.94	44.17 ± 9.67

Table A.13. Analysis of T lymphocyte proliferation data using the proliferation index statistic. Proliferation index is calculated as the average number of divisions undergone by the dividing cells only. Control *n* = 9, HD *n* = 8. Data shown as mean ± SEM.

Cell type	Treatment	Time point	Proliferation index	
			Control	HD
T lymphocytes ($CD3^+$)	Unstimulated	72 h	1.25 ± 0.04	1.39 ± 0.14
	Unstimulated	96 h	1.60 ± 0.06	1.47 ± 0.08
	Unstimulated	120 h	2.13 ± 0.05	1.75 ± 0.17
	Anti-CD3 + CD28	72 h	1.59 ± 0.09	1.62 ± 0.08
	Anti-CD3 + CD28	96 h	2.33 ± 0.13	2.49 ± 0.15
	Anti-CD3 + CD28	120 h	3.27 ± 0.16	3.51 ± 0.20
	PHA-P	72 h	1.58 ± 0.06	1.58 ± 0.05
	PHA-P	96 h	2.19 ± 0.08	2.07 ± 0.12
	PHA-P	120 h	2.61 ± 0.16	2.30 ± 0.14
Helper T lymphocytes ($CD3^+$ $CD4^+$)	Unstimulated	72 h	1.22 ± 0.04	1.42 ± 0.15
	Unstimulated	96 h	1.49 ± 0.05	1.48 ± 0.07
	Unstimulated	120 h	2.04 ± 0.06	1.76 ± 0.13
	Anti-CD3 + CD28	72 h	1.49 ± 0.07	1.61 ± 0.07
	Anti-CD3 + CD28	96 h	2.09 ± 0.12	2.43 ± 0.16
	Anti-CD3 + CD28	120 h	3.05 ± 0.15	3.33 ± 0.23
	PHA-P	72 h	1.42 ± 0.04	1.45 ± 0.05
	PHA-P	96 h	1.94 ± 0.05	1.88 ± 0.11
	PHA-P	120 h	2.22 ± 0.15	2.06 ± 0.11
Cytotoxic T lymphocytes ($CD3^+$ $CD8^+$)	Unstimulated	72 h	1.49 ± 0.24	1.99 ± 0.55
	Unstimulated	96 h	1.94 ± 0.11	1.69 ± 0.13
	Unstimulated	120 h	2.31 ± 0.24	1.86 ± 0.23
	Anti-CD3 + CD28	72 h	1.88 ± 0.13	1.81 ± 0.18
	Anti-CD3 + CD28	96 h	2.80 ± 0.17	3.00 ± 0.27
	Anti-CD3 + CD28	120 h	3.88 ± 0.19	3.65 ± 0.27
	PHA-P	72 h	2.04 ± 0.11	1.79 ± 0.13
	PHA-P	96 h	2.84 ± 0.15	2.44 ± 0.22
	PHA-P	120 h	3.32 ± 0.22	2.76 ± 0.30

Table A.14. Analysis of T lymphocyte proliferation data using the division index statistic. Division index is calculated as the average number of divisions undergone by all cells in culture. Control *n* = 9, HD *n* = 8. Data shown as mean ± SEM.

Cell type	Treatment	Time point	Division index	
			Control	HD
T lymphocytes ($CD3^+$)	Unstimulated	72 h	0.004 ± 0.001	0.005 ± 0.001
	Unstimulated	96 h	0.018 ± 0.004	0.020 ± 0.006
	Unstimulated	120 h	0.022 ± 0.004	0.020 ± 0.006
	Anti-CD3 + CD28	72 h	0.72 ± 0.15	0.81 ± 0.16
	Anti-CD3 + CD28	96 h	1.44 ± 0.20	1.35 ± 0.28
	Anti-CD3 + CD28	120 h	2.13 ± 0.31	2.31 ± 0.27
	PHA-P	72 h	0.86 ± 0.10	0.63 ± 0.12
	PHA-P	96 h	1.21 ± 0.14	0.95 ± 0.18
	PHA-P	120 h	1.38 ± 0.13	0.94 ± 0.19
Helper T lymphocytes ($CD3^+$ $CD4^+$)	Unstimulated	72 h	0.003 ± 0.001	0.004 ± 0.001
	Unstimulated	96 h	0.014 ± 0.003	0.016 ± 0.006
	Unstimulated	120 h	0.022 ± 0.006	0.021 ± 0.010
	Anti-CD3 + CD28	72 h	0.71 ± 0.11	0.90 ± 0.13
	Anti-CD3 + CD28	96 h	1.46 ± 0.16	1.49 ± 0.29
	Anti-CD3 + CD28	120 h	2.06 ± 0.17	2.66 ± 0.26
	PHA-P	72 h	0.75 ± 0.09	0.69 ± 0.06
	PHA-P	96 h	1.15 ± 0.07	1.03 ± 0.11
	PHA-P	120 h	1.32 ± 0.12	1.04 ± 0.09
Cytotoxic T lymphocytes ($CD3^+$ $CD8^+$)	Unstimulated	72 h	0.009 ± 0.003	0.011 ± 0.005
	Unstimulated	96 h	0.031 ± 0.010	0.025 ± 0.009
	Unstimulated	120 h	0.032 ± 0.007	0.032 ± 0.014
	Anti-CD3 + CD28	72 h	1.06 ± 0.21	0.98 ± 0.23
	Anti-CD3 + CD28	96 h	1.88 ± 0.33	1.78 ± 0.39
	Anti-CD3 + CD28	120 h	2.57 ± 0.42	2.49 ± 0.38
	PHA-P	72 h	1.15 ± 0.25	0.87 ± 0.19
	PHA-P	96 h	1.66 ± 0.30	1.29 ± 0.30
	PHA-P	120 h	1.79 ± 0.33	1.37 ± 0.33

A.7 T lymphocyte PCR array results

Table A.15. Complete list of expression changes observed in unstimulated HD helper T lymphocytes (ranked by *p*-value). Data presented as fold change calculated from ΔΔ-CT values, statistical analysis carried out using unpaired two-tailed Student's *t*-tests.

Gene name	Fold change	*p*-value
TNFSF4	1.471	0.008
PTGDR2	1.788	0.014
GATA3	1.177	0.056
IL18R1	1.336	0.058
IL5	2.245	0.063
LAT	0.893	0.101
IL2RA	1.154	0.102
CSF2	0.490	0.124
JAK1	1.108	0.137
CCR4	1.258	0.183
TLR6	1.497	0.198
TNFRSF9	0.564	0.227
IL13	0.689	0.227
IL12RB2	0.789	0.255
CD86	0.681	0.270
IL10	1.580	0.271
BCL6	0.737	0.276
IL2	1.297	0.281
IL15	0.858	0.296
LTA	0.905	0.299
STAT6	2.548	0.307
CREBBP	1.089	0.318
IL6	0.309	0.319
SPP1	0.317	0.322
CTLA4	1.082	0.335
EBI3	0.409	0.348
IL4R	1.080	0.352
CD40LG	1.090	0.354
CD28	1.067	0.369
GFI1	1.167	0.370
MAPK8	1.055	0.372
IL18	0.684	0.375
IRF1	0.897	0.388
CCL7	0.608	0.391
TBX21	1.203	0.400

TNF	0.856	0.417
IFNG	0.780	0.422
CD4	1.051	0.452
IL6R	1.054	0.459
LAG3	1.043	0.459
FASLG	1.106	0.464
NFATC2	1.089	0.474
NFATC1	0.955	0.512
CD27	0.942	0.522
IL1R1	1.114	0.527
IRF4	0.977	0.537
IL24	1.049	0.587
SLC11A1	0.994	0.603
PTPRC	0.964	0.616
IL7	1.078	0.671
HAVCR2	0.839	0.672
CCR2	1.116	0.677
YY1	1.029	0.682
IL7R	0.956	0.710
CXCR3	1.166	0.711
IL27RA	0.969	0.741
IL13RA1	0.675	0.743
JAK2	1.083	0.749
CD80	0.899	0.763
CCR5	1.031	0.775
ICOS	0.962	0.777
STAT1	0.972	0.787
STAT4	1.007	0.808
TGFB3	1.137	0.811
TYK2	1.013	0.825
PCGF2	0.985	0.831
VEGFA	0.661	0.898
SOCS1	0.983	0.911
MAF	1.052	0.919
TLR4	0.855	0.937
CCL5	1.146	0.956
CCR3	0.961	0.956
SOCS5	0.992	0.969
CEBPB	0.947	0.971

Table A.16. Complete list of expression changes observed in stimulated HD helper T lymphocytes (ranked by *p*-value). Data presented as fold change calculated from ΔΔ-CT values, statistical analysis carried out using unpaired two-tailed Student's *t*-tests.

Gene name	Fold change	*p*-value
TYK2	1.176	0.002
TNFRSF8	1.702	0.013
STAT6	1.231	0.035
TNFSF4	1.756	0.066
JAK1	1.169	0.072
CCR4	1.191	0.118
IL18R1	1.129	0.149
CD27	1.261	0.152
STAT1	0.844	0.162
IL15	0.800	0.184
IL5	0.724	0.197
TGFB3	1.536	0.211
MAPK8	1.082	0.215
CD28	1.104	0.237
YY1	1.052	0.272
GATA3	1.817	0.300
IL9	0.704	0.308
IL6R	1.174	0.319
FASLG	1.320	0.319
CCR5	1.194	0.327
CD40LG	1.119	0.336
VEGFA	1.126	0.348
IL2RA	1.036	0.350
IL12RB2	0.712	0.351
NFATC2	1.088	0.360
TLR6	0.848	0.361
EBI3	0.848	0.366
SPP1	0.949	0.367
IL18	0.539	0.370
IL27	0.747	0.376
PTGDR2	1.122	0.381
IL4	0.743	0.383
BCL6	1.080	0.411
IL10	0.932	0.446
IL27RA	1.040	0.452
CTLA4	1.082	0.452
SLC11A1	0.820	0.458
NFATC1	1.055	0.468

PCGF2	0.899	0.470
GFI1	1.095	0.474
LAT	0.838	0.500
HAVCR2	1.040	0.503
IL12B	1.018	0.504
TNFRSF9	1.162	0.506
IL4R	0.920	0.507
CSF2	1.173	0.511
IRF4	1.024	0.517
CEBPB	1.117	0.532
IL2	0.858	0.574
SOCS5	1.036	0.585
STAT4	1.046	0.590
CCR3	0.773	0.593
JAK2	1.025	0.595
IL1R1	0.990	0.626
TNF	0.987	0.626
IL7	1.079	0.646
CCR2	1.181	0.647
CREBBP	1.027	0.648
IL6	0.672	0.666
CD4	1.115	0.697
LTA	1.071	0.704
CCL7	0.396	0.721
IL1RL1	1.578	0.738
CXCR3	0.965	0.738
SOCS1	0.941	0.739
LAG3	1.033	0.760
TLR4	0.935	0.774
TBX21	0.926	0.783
IL3	0.777	0.783
CD86	0.904	0.806
IL24	0.959	0.825
PTPRC	1.003	0.826
CD80	0.982	0.884
IL13	0.955	0.920
IFNG	0.808	0.929
IL13RA1	0.949	0.938
CCL5	1.059	0.947
ICOS	1.002	0.953
IRF1	0.999	0.976
IL7R	1.006	0.979
MAF	0.924	0.987

References

Ajami, B., Bennett, J. L., Krieger, C., Tetzlaff, W. and Rossi, F. M. 2007. Local self-renewal can sustain CNS microglia maintenance and function throughout adult life. *Nat Neurosci,* 10(12)**,** pp. 1538-1543.

Akira, S. and Takeda, K. 2004. Toll-like receptor signalling. *Nat Rev Immunol,* 4(7)**,** pp. 499-511.

Andre, R., Scahill, R. I., Haider, S. and Tabrizi, S. J. 2014. Biomarker development for Huntington's disease. *Drug Discov Today,* 19(7)**,** pp. 972-979.

Aouadi, M., Tesz, G. J., Nicoloro, S. M., Wang, M., Chouinard, M., Soto, E., Ostroff, G. R. and Czech, M. P. 2009. Orally delivered siRNA targeting macrophage Map4k4 suppresses systemic inflammation. *Nature,* 458(7242)**,** pp. 1180-1184.

Apostol, B. L., Illes, K., Pallos, J., Bodai, L., Wu, J., Strand, A., Schweitzer, E. S., Olson, J. M., Kazantsev, A., Marsh, J. L. and Thompson, L. M. 2006. Mutant huntingtin alters MAPK signaling pathways in PC12 and striatal cells: ERK1/2 protects against mutant huntingtin-associated toxicity. *Hum Mol Genet,* 15(2)**,** pp. 273-285.

Arrasate, M., Mitra, S., Schweitzer, E. S., Segal, M. R. and Finkbeiner, S. 2004. Inclusion body formation reduces levels of mutant huntingtin and the risk of neuronal death. *Nature,* 431(7010)**,** pp. 805-810.

Auffray, C., Sieweke, M. H. and Geissmann, F. 2009. Blood monocytes: development, heterogeneity, and relationship with dendritic cells. *Annu Rev Immunol,* 27, pp. 669-692.

Aung, H. T., Schroder, K., Himes, S. R., Brion, K., van Zuylen, W., Trieu, A., Suzuki, H., Hayashizaki, Y., Hume, D. A., Sweet, M. J. and Ravasi, T. 2006. LPS regulates proinflammatory gene expression in macrophages by altering histone deacetylase expression. *FASEB J,* 20(9)**,** pp. 1315-1327.

Barton, G. M. and Medzhitov, R. 2003. Toll-like receptor signaling pathways. *Science,* 300(5625)**,** pp. 1524-1525.

Bates, G. P., Dorsey, R., Gusella, J. F., Hayden, M. R., Kay, C., Leavitt, B. R., Nance, M., Ross, C. A., Scahill, R. I., Wetzel, R., Wild, E. J. and Tabrizi, S. J. 2015. Huntington disease. *Nat Rev Dis Primers* [online]*,* 1:15005. Available from: doi: 10.1038/nrdp.2015.5.

Bates, G. P., Tabrizi, S. J. and Jones, L. 2014. *Huntington's Disease*. 4th ed. Oxford: Oxford University Press.

Beal, M. F., Ferrante, R. J., Swartz, K. J. and Kowall, N. W. 1991. Chronic quinolinic acid lesions in rats closely resemble Huntington's disease. *J Neurosci,* 11(6)**,** pp. 1649-1659.

Benn, C. L., Sun, T., Sadri-Vakili, G., McFarland, K. N., DiRocco, D. P., Yohrling, G. J., Clark, T. W., Bouzou, B. and Cha, J. H. 2008. Huntingtin modulates transcription, occupies gene promoters in vivo, and binds directly to DNA in a polyglutamine-dependent manner. *J Neurosci,* 28(42)**,** pp. 10720-10733.

Bennett, C. F. and Swayze, E. E. 2010. RNA targeting therapeutics: molecular mechanisms of antisense oligonucleotides as a therapeutic platform. *Annu Rev Pharmacol Toxicol,* 50, pp. 259-293.

Bennett, E. J., Shaler, T. A., Woodman, B., Ryu, K. Y., Zaitseva, T. S., Becker, C. H., Bates, G. P., Schulman, H. and Kopito, R. R. 2007. Global changes to the ubiquitin system in Huntington's disease. *Nature,* 448(7154)**,** pp. 704-708.

Benraiss, A. and Goldman, S. A. 2011. Cellular therapy and induced neuronal replacement for Huntington's disease. *Neurotherapeutics,* 8(4)**,** pp. 577-590.

Bettencourt, C., Hensman Moss, D. J., Flower, M., Wiethoff, S., Brice, A., Goizet, C., Stevanin, G., Koutsis, G., Karadima, G., Panas, M., Yescas-Gómez, P., García-Velázquez, L. E., Alonso-Vilatela, M. E., Lima, M., Raposo, M., Traynor, B., Sweeney, M., Wood, N., Giunti, P., Durr, A., Holmans, P., Houlden, H., Tabrizi, S. J., Jones, L. and network, S. 2016. DNA repair pathways underlie a common genetic mechanism modulating onset in polyglutamine diseases. *Ann Neurol*, 79(6), pp. 983-990.

Bečanović, K., Nørremølle, A., Neal, S. J., Kay, C., Collins, J. A., Arenillas, D., Lilja, T., Gaudenzi, G., Manoharan, S., Doty, C. N., Beck, J., Lahiri, N., Portales-Casamar, E., Warby, S. C., Connolly, C., De Souza, R. A., Tabrizi, S. J., Hermanson, O., Langbehn, D. R., Hayden, M. R., Wasserman, W. W., Leavitt, B. R. and Network, R. I. o. t. E. H. s. D. 2015. A SNP in the HTT promoter alters NF-κB binding and is a bidirectional genetic modifier of Huntington disease. *Nat Neurosci,* 18(6)**,** pp. 807-816.

Björkqvist, M., Wild, E. J. and Tabrizi, S. J. 2009. Harnessing immune alterations in neurodegenerative diseases. *Neuron,* 64(1)**,** pp. 21-24.

Björkqvist, M., Wild, E. J., Thiele, J., Silvestroni, A., Andre, R., Lahiri, N., Raibon, E., Lee, R. V., Benn, C. L., Soulet, D., Magnusson, A., Woodman, B., Landles, C., Pouladi, M. A., Hayden, M. R., Khalili-Shirazi, A., Lowdell, M. W., Brundin, P., Bates, G. P., Leavitt, B. R., Möller, T. and Tabrizi, S. J. 2008. A novel pathogenic pathway of immune activation detectable before clinical onset in Huntington's disease. *J Exp Med,* 205(8)**,** pp. 1869-1877.

Black, R. A., Rauch, C. T., Kozlosky, C. J., Peschon, J. J., Slack, J. L., Wolfson, M. F., Castner, B. J., Stocking, K. L., Reddy, P., Srinivasan, S., Nelson, N., Boiani, N., Schooley, K. A., Gerhart, M., Davis, R., Fitzner, J. N., Johnson, R. S., Paxton, R. J., March, C. J. and Cerretti, D. P. 1997. A metalloproteinase disintegrin that releases tumour-necrosis factor-alpha from cells. *Nature,* 385(6618)**,** pp. 729-733.

Borovecki, F., Lovrecic, L., Zhou, J., Jeong, H., Then, F., Rosas, H. D., Hersch, S. M., Hogarth, P., Bouzou, B., Jensen, R. V. and Krainc, D. 2005. Genome-wide expression profiling of human blood reveals biomarkers for Huntington's disease. *Proc Natl Acad Sci U S A,* 102(31)**,** pp. 11023-11028.

Bouchard, J., Truong, J., Bouchard, K., Dunkelberger, D., Desrayaud, S., Moussaoui, S., Tabrizi, S. J., Stella, N. and Muchowski, P. J. 2012. Cannabinoid Receptor 2 Signaling in Peripheral Immune Cells Modulates Disease Onset and Severity in Mouse Models of Huntington's Disease. *J Neurosci,* 32(50)**,** pp. 18259-18268.

Boudreau, R. L., McBride, J. L., Martins, I., Shen, S., Xing, Y., Carter, B. J. and Davidson, B. L. 2009. Nonallele-specific silencing of mutant and wild-type huntingtin demonstrates therapeutic efficacy in Huntington's disease mice. *Mol Ther,* 17(6)**,** pp. 1053-1063.

Bradford, J., Shin, J. Y., Roberts, M., Wang, C. E., Li, X. J. and Li, S. 2009. Expression of mutant huntingtin in mouse brain astrocytes causes age-dependent neurological symptoms. *Proc Natl Acad Sci U S A,* 106(52)**,** pp. 22480-22485.

Bradford, J., Shin, J. Y., Roberts, M., Wang, C. E., Sheng, G., Li, S. and Li, X. J. 2010. Mutant huntingtin in glial cells exacerbates neurological symptoms of Huntington disease mice. *J Biol Chem,* 285(14)**,** pp. 10653-10661.

Brown, G. C. and Neher, J. J. 2010. Inflammatory neurodegeneration and mechanisms of microglial killing of neurons. *Mol Neurobiol,* 41(2-3)**,** pp. 242-247.

Brownlie, R. J. and Zamoyska, R. 2013. T cell receptor signalling networks: branched, diversified and bounded. *Nat Rev Immunol,* 13(4)**,** pp. 257-269.

Brundin, P., Melki, R. and Kopito, R. 2010. Prion-like transmission of protein aggregates in neurodegenerative diseases. *Nat Rev Mol Cell Biol,* 11(4)**,** pp. 301-307.

Bult, C. J., Eppig, J. T., Kadin, J. A., Richardson, J. E., Blake, J. A. and Group, M. G. D. 2008. The Mouse Genome Database (MGD): mouse biology and model systems. *Nucleic Acids Res,* 36(Database issue)**,** pp. D724-8.

Carroll, J. B., Warby, S. C., Southwell, A. L., Doty, C. N., Greenlee, S., Skotte, N., Hung, G., Bennett, C. F., Freier, S. M. and Hayden, M. R. 2011. Potent and selective antisense oligonucleotides targeting single-nucleotide polymorphisms in the Huntington disease gene / allele-specific silencing of mutant huntingtin. *Mol Ther,* 19(12)**,** pp. 2178-2185.

Chang, D. T., Rintoul, G. L., Pandipati, S. and Reynolds, I. J. 2006. Mutant huntingtin aggregates impair mitochondrial movement and trafficking in cortical neurons. *Neurobiol Dis,* 22(2)**,** pp. 388-400.

Chen, S., Berthelier, V., Yang, W. and Wetzel, R. 2001. Polyglutamine aggregation behavior in vitro supports a recruitment mechanism of cytotoxicity. *J Mol Biol,* 311(1)**,** pp. 173-182.

Chen-Plotkin, A. S., Sadri-Vakili, G., Yohrling, G. J., Braveman, M. W., Benn, C. L., Glajch, K. E., DiRocco, D. P., Farrell, L. A., Krainc, D., Gines, S., MacDonald, M. E. and Cha, J. H. 2006. Decreased association of the transcription factor Sp1 with genes downregulated in Huntington's disease. *Neurobiol Dis,* 22(2)**,** pp. 233-241.

Choo, Y. S., Johnson, G. V., MacDonald, M., Detloff, P. J. and Lesort, M. 2004. Mutant huntingtin directly increases susceptibility of mitochondria to the calcium-induced permeability transition and cytochrome c release. *Hum Mol Genet,* 13(14)**,** pp. 1407-1420.

Chopra, V., Fox, J. H., Lieberman, G., Dorsey, K., Matson, W., Waldmeier, P., Housman, D. E., Kazantsev, A., Young, A. B. and Hersch, S. 2007. A small-molecule therapeutic lead for Huntington's disease: preclinical pharmacology and efficacy of C2-8 in the R6/2 transgenic mouse. *Proc Natl Acad Sci U S A,* 104(42)**,** pp. 16685-16689.

Ciammola, A., Sassone, J., Alberti, L., Meola, G., Mancinelli, E., Russo, M. A., Squitieri, F. and Silani, V. 2006. Increased apoptosis, Huntingtin inclusions and altered differentiation in muscle cell cultures from Huntington's disease subjects. *Cell Death Differ,* 13(12)**,** pp. 2068-2078.

Cicchetti, F., Lacroix, S., Cisbani, G., Vallières, N., Saint-Pierre, M., St-Amour, I., Tolouei, R., Skepper, J. N., Hauser, R. A., Mantovani, D., Barker, R. A. and Freeman, T. B. 2014.

Mutant huntingtin is present in neuronal grafts in Huntington disease patients. *Ann Neurol,* 76(1)**,** pp. 31-42.

Cong, X., Held, J. M., DeGiacomo, F., Bonner, A., Chen, J. M., Schilling, B., Czerwieniec, G. A., Gibson, B. W. and Ellerby, L. M. 2011. Mass spectrometric identification of novel lysine acetylation sites in huntingtin. *Mol Cell Proteomics,* 10(10)**,** M111.009829.

Croft, D., Mundo, A. F., Haw, R., Milacic, M., Weiser, J., Wu, G., Caudy, M., Garapati, P., Gillespie, M., Kamdar, M. R., Jassal, B., Jupe, S., Matthews, L., May, B., Palatnik, S., Rothfels, K., Shamovsky, V., Song, H., Williams, M., Birney, E., Hermjakob, H., Stein, L. and D'Eustachio, P. 2014. The Reactome pathway knowledgebase. *Nucleic Acids Res,* 42(Database issue)**,** pp. D472-7.

Crotti, A., Benner, C., Kerman, B. E., Gosselin, D., Lagier-Tourenne, C., Zuccato, C., Cattaneo, E., Gage, F. H., Cleveland, D. W. and Glass, C. K. 2014. Mutant Huntingtin promotes autonomous microglia activation via myeloid lineage-determining factors. *Nat Neurosci,* 17(4)**,** pp. 513-521.

Dalrymple, A., Wild, E. J., Joubert, R., Sathasivam, K., Björkqvist, M., Petersén, A., Jackson, G. S., Isaacs, J. D., Kristiansen, M., Bates, G. P., Leavitt, B. R., Keir, G., Ward, M. and Tabrizi, S. J. 2007. Proteomic profiling of plasma in Huntington's disease reveals neuroinflammatory activation and biomarker candidates. *J Proteome Res,* 6(7)**,** pp. 2833-2840.

Damiano, M., Galvan, L., Déglon, N. and Brouillet, E. 2010. Mitochondria in Huntington's disease. *Biochim Biophys Acta,* 1802(1)**,** pp. 52-61.

DeLuca, D. S., Levin, J. Z., Sivachenko, A., Fennell, T., Nazaire, M. D., Williams, C., Reich, M., Winckler, W. and Getz, G. 2012. RNA-SeQC: RNA-seq metrics for quality control and process optimization. *Bioinformatics,* 28(11)**,** pp. 1530-1532.

Deshmane, S. L., Kremlev, S., Amini, S. and Sawaya, B. E. 2009. Monocyte chemoattractant protein-1 (MCP-1): an overview. *J Interferon Cytokine Res,* 29(6)**,** pp. 313-326.

DiFiglia, M., Sapp, E., Chase, K. O., Davies, S. W., Bates, G. P., Vonsattel, J. P. and Aronin, N. 1997. Aggregation of huntingtin in neuronal intranuclear inclusions and dystrophic neurites in brain. *Science,* 277(5334)**,** pp. 1990-1993.

Dodeller, F. and Schulze-Koops, H. 2006. The p38 mitogen-activated protein kinase signaling cascade in CD4 T cells. *Arthritis Res Ther,* 8(2)**,** pp. 205.

Dragatsis, I., Levine, M. S. and Zeitlin, S. 2000. Inactivation of Hdh in the brain and testis results in progressive neurodegeneration and sterility in mice. *Nat Genet,* 26(3)**,** pp. 300-306.

Drouet, V., Perrin, V., Hassig, R., Dufour, N., Auregan, G., Alves, S., Bonvento, G., Brouillet, E., Luthi-Carter, R., Hantraye, P. and Déglon, N. 2009. Sustained effects of nonallele-specific Huntingtin silencing. *Ann Neurol,* 65(3)**,** pp. 276-285.

Drouet, V., Ruiz, M., Zala, D., Feyeux, M., Auregan, G., Cambon, K., Troquier, L., Carpentier, J., Aubert, S., Merienne, N., Bourgois-Rocha, F., Hassig, R., Rey, M., Dufour, N., Saudou, F., Perrier, A. L., Hantraye, P. and Déglon, N. 2014. Allele-specific silencing of mutant huntingtin in rodent brain and human stem cells. *PLOS One* [online]*,* 9(6)**,** e99341. Available from: doi: 10.1371/journal.pone.0099341.

Eder, C. 2009. Mechanisms of interleukin-1beta release. *Immunobiology,* 214(7)**,** pp. 543-553.

Ellrichmann, G., Reick, C., Saft, C. and Linker, R. A. 2013. The role of the immune system in Huntington's disease. *Clin Dev Immunol,* 2013:541259.

Farrer, L. A. 1986. Suicide and attempted suicide in Huntington disease: implications for preclinical testing of persons at risk. *Am J Med Genet,* 24(2)**,** pp. 305-311.

Fernández-Nogales, M., Cabrera, J. R., Santos-Galindo, M., Hoozemans, J. J., Ferrer, I., Rozemuller, A. J., Hernández, F., Avila, J. and Lucas, J. J. 2014. Huntington's disease is a four-repeat tauopathy with tau nuclear rods. *Nat Med,* 20(8)**,** pp. 881-885.

Fiszer, A., Olejniczak, M., Galka-Marciniak, P., Mykowska, A. and Krzyzosiak, W. J. 2013. Self-duplexing CUG repeats selectively inhibit mutant huntingtin expression. *Nucleic Acids Res,* 41(22)**,** pp. 10426-10437.

Frazee, A. C., Pertea, G., Jaffe, A. E., Langmead, B., Salzberg, S. L. and Leek, J. T. 2015. Ballgown bridges the gap between transcriptome assembly and expression analysis. *Nat Biotechnol,* 33(3)**,** pp. 243-246.

Gagnon, K. T., Pendergraff, H. M., Deleavey, G. F., Swayze, E. E., Potier, P., Randolph, J., Roesch, E. B., Chattopadhyaya, J., Damha, M. J., Bennett, C. F., Montaillier, C., Lemaitre,

M. and Corey, D. R. 2010. Allele-selective inhibition of mutant huntingtin expression with antisense oligonucleotides targeting the expanded CAG repeat. *Biochemistry,* 49(47)**,** pp. 10166-10178.

Gambazzi, L., Gokce, O., Seredenina, T., Katsyuba, E., Runne, H., Markram, H., Giugliano, M. and Luthi-Carter, R. 2010. Diminished activity-dependent brain-derived neurotrophic factor expression underlies cortical neuron microcircuit hypoconnectivity resulting from exposure to mutant huntingtin fragments. *J Pharmacol Exp Ther,* 335(1)**,** pp. 13-22.

Gauthier, L. R., Charrin, B. C., Borrell-Pagès, M., Dompierre, J. P., Rangone, H., Cordelières, F. P., De Mey, J., MacDonald, M. E., Lessmann, V., Humbert, S. and Saudou, F. 2004. Huntingtin controls neurotrophic support and survival of neurons by enhancing BDNF vesicular transport along microtubules. *Cell,* 118(1)**,** pp. 127-138.

Geissmann, F., Manz, M. G., Jung, S., Sieweke, M. H., Merad, M. and Ley, K. 2010. Development of monocytes, macrophages, and dendritic cells. *Science,* 327(5966)**,** pp. 656-661.

Genetic Modifiers of Huntington's Disease (GeM-HD) Consortium. 2015. Identification of Genetic Factors that Modify Clinical Onset of Huntington's Disease. *Cell,* 162(3)**,** pp. 516-526.

Gharami, K., Xie, Y., An, J. J., Tonegawa, S. and Xu, B. 2008. Brain-derived neurotrophic factor over-expression in the forebrain ameliorates Huntington's disease phenotypes in mice. *J Neurochem,* 105(2)**,** pp. 369-379.

Godin, J. D., Colombo, K., Molina-Calavita, M., Keryer, G., Zala, D., Charrin, B. C., Dietrich, P., Volvert, M. L., Guillemot, F., Dragatsis, I., Bellaiche, Y., Saudou, F., Nguyen, L. and Humbert, S. 2010. Huntingtin is required for mitotic spindle orientation and mammalian neurogenesis. *Neuron,* 67(3)**,** pp. 392-406.

Goemans, N. M., Tulinius, M., van den Akker, J. T., Burm, B. E., Ekhart, P. F., Heuvelmans, N., Holling, T., Janson, A. A., Platenburg, G. J., Sipkens, J. A., Sitsen, J. M., Aartsma-Rus, A., van Ommen, G. J., Buyse, G., Darin, N., Verschuuren, J. J., Campion, G. V., de Kimpe, S. J. and van Deutekom, J. C. 2011. Systemic administration of PRO051 in Duchenne's muscular dystrophy. *N Engl J Med,* 364(16)**,** pp. 1513-1522.

González-Navajas, J. M., Fine, S., Law, J., Datta, S. K., Nguyen, K. P., Yu, M., Corr, M., Katakura, K., Eckman, L., Lee, J. and Raz, E. 2010. TLR4 signaling in effector CD4+ T cells regulates TCR activation and experimental colitis in mice. *J Clin Invest,* 120(2)**,** pp. 570-581.

Goodman, A. O., Murgatroyd, P. R., Medina-Gomez, G., Wood, N. I., Finer, N., Vidal-Puig, A. J., Morton, A. J. and Barker, R. A. 2008. The metabolic profile of early Huntington's disease--a combined human and transgenic mouse study. *Exp Neurol,* 210(2)**,** pp. 691-698.

Graham, R. K., Deng, Y., Slow, E. J., Haigh, B., Bissada, N., Lu, G., Pearson, J., Shehadeh, J., Bertram, L., Murphy, Z., Warby, S. C., Doty, C. N., Roy, S., Wellington, C. L., Leavitt, B. R., Raymond, L. A., Nicholson, D. W. and Hayden, M. R. 2006. Cleavage at the caspase-6 site is required for neuronal dysfunction and degeneration due to mutant huntingtin. *Cell,* 125(6)**,** pp. 1179-1191.

Grondin, R., Kaytor, M. D., Ai, Y., Nelson, P. T., Thakker, D. R., Heisel, J., Weatherspoon, M. R., Blum, J. L., Burright, E. N., Zhang, Z. and Kaemmerer, W. F. 2012. Six-month partial suppression of Huntingtin is well tolerated in the adult rhesus striatum. *Brain,* 135(4)**,** pp. 1197-1209.

Gu, X., André, V. M., Cepeda, C., Li, S. H., Li, X. J., Levine, M. S. and Yang, X. W. 2007. Pathological cell-cell interactions are necessary for striatal pathogenesis in a conditional mouse model of Huntington's disease. *Mol Neurodegener* [online]*,* 2:8. Available from: doi: 10.1186/1750-1326-2-8.

Gu, X., Li, C., Wei, W., Lo, V., Gong, S., Li, S. H., Iwasato, T., Itohara, S., Li, X. J., Mody, I., Heintz, N. and Yang, X. W. 2005. Pathological cell-cell interactions elicited by a neuropathogenic form of mutant Huntingtin contribute to cortical pathogenesis in HD mice. *Neuron,* 46(3)**,** pp. 433-444.

Guidetti, P., Bates, G. P., Graham, R. K., Hayden, M. R., Leavitt, B. R., MacDonald, M. E., Slow, E. J., Wheeler, V. C., Woodman, B. and Schwarcz, R. 2006. Elevated brain 3-hydroxykynurenine and quinolinate levels in Huntington disease mice. *Neurobiol Dis,* 23(1)**,** pp. 190-197.

Gunawardena, S., Her, L. S., Brusch, R. G., Laymon, R. A., Niesman, I. R., Gordesky-Gold, B., Sintasath, L., Bonini, N. M. and Goldstein, L. S. 2003. Disruption of axonal transport by loss of huntingtin or expression of pathogenic polyQ proteins in Drosophila. *Neuron,* 40(1)**,** pp. 25-40.

Guo, Z., Rudow, G., Pletnikova, O., Codispoti, K. E., Orr, B. A., Crain, B. J., Duan, W., Margolis, R. L., Rosenblatt, A., Ross, C. A. and Troncoso, J. C. 2012. Striatal neuronal loss correlates with clinical motor impairment in Huntington's disease. *Mov Disord,* 27(11)**,** pp. 1379-1386.

Gusella, J. F., MacDonald, M. E. and Lee, J. M. 2014. Genetic modifiers of Huntington's disease. *Mov Disord,* 29(11)**,** pp. 1359-1365.

Gusella, J. F., Wexler, N. S., Conneally, P. M., Naylor, S. L., Anderson, M. A., Tanzi, R. E., Watkins, P. C., Ottina, K., Wallace, M. R. and Sakaguchi, A. Y. 1983. A polymorphic DNA marker genetically linked to Huntington's disease. *Nature,* 306(5940)**,** pp. 234-238.

Halliday, G. M., McRitchie, D. A., Macdonald, V., Double, K. L., Trent, R. J. and McCusker, E. 1998. Regional specificity of brain atrophy in Huntington's disease. *Exp Neurol,* 154(2)**,** pp. 663-672.

Hamer, M. and Chida, Y. 2009. Physical activity and risk of neurodegenerative disease: a systematic review of prospective evidence. *Psychol Med,* 39(1)**,** pp. 3-11.

Harris, M. A., Clark, J., Ireland, A., Lomax, J., Ashburner, M., Foulger, R., Eilbeck, K., Lewis, S., Marshall, B., Mungall, C., Richter, J., Rubin, G. M., Blake, J. A., Bult, C., Dolan, M., Drabkin, H., Eppig, J. T., Hill, D. P., Ni, L., Ringwald, M., Balakrishnan, R., Cherry, J. M., Christie, K. R., Costanzo, M. C., Dwight, S. S., Engel, S., Fisk, D. G., Hirschman, J. E., Hong, E. L., Nash, R. S., Sethuraman, A., Theesfeld, C. L., Botstein, D., Dolinski, K., Feierbach, B., Berardini, T., Mundodi, S., Rhee, S. Y., Apweiler, R., Barrell, D., Camon, E., Dimmer, E., Lee, V., Chisholm, R., Gaudet, P., Kibbe, W., Kishore, R., Schwarz, E. M., Sternberg, P., Gwinn, M., Hannick, L., Wortman, J., Berriman, M., Wood, V., de la Cruz, N., Tonellato, P., Jaiswal, P., Seigfried, T., White, R. and Consortium, G. O. 2004. The Gene Ontology (GO) database and informatics resource. *Nucleic Acids Res,* 32(Database issue)**,** pp. D258-61.

Hawkins, E. D., Hommel, M., Turner, M. L., Battye, F. L., Markham, J. F. and Hodgkin, P. D. 2007. Measuring lymphocyte proliferation, survival and differentiation using CFSE time-series data. *Nat Protoc,* 2(9)**,** pp. 2057-2067.

Hay, D. G., Sathasivam, K., Tobaben, S., Stahl, B., Marber, M., Mestril, R., Mahal, A., Smith, D. L., Woodman, B. and Bates, G. P. 2004. Progressive decrease in chaperone protein levels in a mouse model of Huntington's disease and induction of stress proteins as a therapeutic approach. *Hum Mol Genet,* 13(13)**,** pp. 1389-1405.

Hayden, M. S. and Ghosh, S. 2011. NF-κB in immunobiology. *Cell Res,* 21(2)**,** pp. 223-244.

Hodges, A., Strand, A. D., Aragaki, A. K., Kuhn, A., Sengstag, T., Hughes, G., Elliston, L. A., Hartog, C., Goldstein, D. R., Thu, D., Hollingsworth, Z. R., Collin, F., Synek, B., Holmans, P. A., Young, A. B., Wexler, N. S., Delorenzi, M., Kooperberg, C., Augood, S. J., Faull, R. L.,

Olson, J. M., Jones, L. and Luthi-Carter, R. 2006. Regional and cellular gene expression changes in human Huntington's disease brain. *Hum Mol Genet,* 15(6)**,** pp. 965-977.

Hoek, R. M., Ruuls, S. R., Murphy, C. A., Wright, G. J., Goddard, R., Zurawski, S. M., Blom, B., Homola, M. E., Streit, W. J., Brown, M. H., Barclay, A. N. and Sedgwick, J. D. 2000. Down-regulation of the macrophage lineage through interaction with OX2 (CD200). *Science,* 290(5497)**,** pp. 1768-1771.

Hoesel, B. and Schmid, J. A. 2013. The complexity of NF-κB signaling in inflammation and cancer. *Mol Cancer* [online]*,* 12:86. Available from: doi: 10.1186/1476-4598-12-86.

Hsiao, H. Y., Chiu, F. L., Chen, C. M., Wu, Y. R., Chen, H. M., Chen, Y. C., Kuo, H. C. and Chern, Y. 2014. Inhibition of soluble tumor necrosis factor is therapeutic in Huntington's disease. *Hum Mol Genet,* 23(16)**,** pp. 4328-4344.

Huntington, G. 1872. On Chorea. *The Medical and Surgical Reporter,* 26, pp. 317-321.

Huntington Study Group. 1996. Unified Huntington's Disease Rating Scale: reliability and consistency. Huntington Study Group. *Mov Disord,* 11(2)**,** pp. 136-142.

Hurelbrink, C. B., Armstrong, R. J., Dunnett, S. B., Rosser, A. E. and Barker, R. A. 2002. Neural cells from primary human striatal xenografts migrate extensively in the adult rat CNS. *Eur J Neurosci,* 15(7)**,** pp. 1255-1266.

Iwasaki, A. and Medzhitov, R. 2015. Control of adaptive immunity by the innate immune system. *Nat Immunol,* 16(4)**,** pp. 343-353.

Kanehisa, M., Goto, S., Sato, Y., Furumichi, M. and Tanabe, M. 2012. KEGG for integration and interpretation of large-scale molecular data sets. *Nucleic Acids Res,* 40(Database issue)**,** pp. D109-14.

Kang, S. M., Tran, A. C., Grilli, M. and Lenardo, M. J. 1992. NF-kappa B subunit regulation in nontransformed CD4+ T lymphocytes. *Science,* 256(5062)**,** pp. 1452-1456.

Kay, C., Skotte, N. H., Southwell, A. L. and Hayden, M. R. 2014. Personalized gene silencing therapeutics for Huntington disease. *Clin Genet,* 86(1)**,** pp. 29-36.

Keiser, M. S., Kordasiewicz, H. B. and McBride, J. L. 2016. Gene suppression strategies for dominantly inherited neurodegenerative diseases: lessons from Huntington's disease and spinocerebellar ataxia. *Hum Mol Genet,* 25(R1)**,** pp. R53-64.

Khoshnan, A., Ko, J., Watkin, E. E., Paige, L. A., Reinhart, P. H. and Patterson, P. H. 2004. Activation of the IkappaB kinase complex and nuclear factor-kappaB contributes to mutant huntingtin neurotoxicity. *J Neurosci,* 24(37)**,** pp. 7999-8008.

Kierdorf, K., Erny, D., Goldmann, T., Sander, V., Schulz, C., Perdiguero, E. G., Wieghofer, P., Heinrich, A., Riemke, P., Hölscher, C., Müller, D. N., Luckow, B., Brocker, T., Debowski, K., Fritz, G., Opdenakker, G., Diefenbach, A., Biber, K., Heikenwalder, M., Geissmann, F., Rosenbauer, F. and Prinz, M. 2013. Microglia emerge from erythromyeloid precursors via Pu.1- and Irf8-dependent pathways. *Nat Neurosci,* 16(3)**,** pp. 273-280.

Kim, D., Pertea, G., Trapnell, C., Pimentel, H., Kelley, R. and Salzberg, S. L. 2013. TopHat2: accurate alignment of transcriptomes in the presence of insertions, deletions and gene fusions. *Genome Biol* [online]*,* 14(4)**:** R36. Available from: doi: 10.1186/gb-2013-14-4-r36.

Kim, M. W., Chelliah, Y., Kim, S. W., Otwinowski, Z. and Bezprozvanny, I. 2009. Secondary structure of Huntingtin amino-terminal region. *Structure,* 17(9)**,** pp. 1205-1212.

Kordasiewicz, H. B., Stanek, L. M., Wancewicz, E. V., Mazur, C., McAlonis, M. M., Pytel, K. A., Artates, J. W., Weiss, A., Cheng, S. H., Shihabuddin, L. S., Hung, G., Bennett, C. F. and Cleveland, D. W. 2012. Sustained therapeutic reversal of Huntington's disease by transient repression of huntingtin synthesis. *Neuron,* 74(6)**,** pp. 1031-1044.

Kumar, H., Kawai, T. and Akira, S. 2009. Toll-like receptors and innate immunity. *Biochem Biophys Res Commun,* 388(4)**,** pp. 621-625.

Kwan, W., Magnusson, A., Chou, A., Adame, A., Carson, M. J., Kohsaka, S., Masliah, E., Möller, T., Ransohoff, R., Tabrizi, S. J., Björkqvist, M. and Muchowski, P. J. 2012a. Bone marrow transplantation confers modest benefits in mouse models of Huntington's disease. *J Neurosci,* 32(1)**,** pp. 133-142.

Kwan, W., Träger, U., Davalos, D., Chou, A., Bouchard, J., Andre, R., Miller, A., Weiss, A., Giorgini, F., Cheah, C., Möller, T., Stella, N., Akassoglou, K., Tabrizi, S. J. and Muchowski, P. J. 2012b. Mutant huntingtin impairs immune cell migration in Huntington disease. *J Clin Invest,* 122(12)**,** pp. 4737-4747.

Labadorf, A., Hoss, A. G., Lagomarsino, V., Latourelle, J. C., Hadzi, T. C., Bregu, J., MacDonald, M. E., Gusella, J. F., Chen, J. F., Akbarian, S., Weng, Z. and Myers, R. H. 2015. RNA Sequence Analysis of Human Huntington Disease Brain Reveals an Extensive Increase in Inflammatory and Developmental Gene Expression. *PLOS One* [online]*,* 10(12)**,** e0143563. Available from: doi: 10.1371/journal.pone.0143563.

Labbadia, J., Cunliffe, H., Weiss, A., Katsyuba, E., Sathasivam, K., Seredenina, T., Woodman, B., Moussaoui, S., Frentzel, S., Luthi-Carter, R., Paganetti, P. and Bates, G. P. 2011. Altered chromatin architecture underlies progressive impairment of the heat shock response in mouse models of Huntington disease. *J Clin Invest,* 121(8)**,** pp. 3306-3319.

Lacy, P. and Stow, J. L. 2011. Cytokine release from innate immune cells: association with diverse membrane trafficking pathways. *Blood,* 118(1)**,** pp. 9-18.

Landwehrmeyer, G. B., Dubois, B., de Yébenes, J. G., Kremer, B., Gaus, W., Kraus, P. H., Przuntek, H., Dib, M., Doble, A., Fischer, W., Ludolph, A. C. and Group, E. H. s. D. I. S. 2007. Riluzole in Huntington's disease: a 3-year, randomized controlled study. *Ann Neurol,* 62(3)**,** pp. 262-272.

Langbehn, D. R., Hayden, M. R., Paulsen, J. S. and Group, P.-H. I. o. t. H. S. 2010. CAG-repeat length and the age of onset in Huntington disease (HD): a review and validation study of statistical approaches. *Am J Med Genet B Neuropsychiatr Genet,* 153B(2)**,** pp. 397-408.

Lanska, D. J., Lanska, M. J., Lavine, L. and Schoenberg, B. S. 1988. Conditions associated with Huntington's disease at death. A case-control study. *Arch Neurol,* 45(8)**,** pp. 878-880.

Leavitt, B. R., van Raamsdonk, J. M., Shehadeh, J., Fernandes, H., Murphy, Z., Graham, R. K., Wellington, C. L., Raymond, L. A. and Hayden, M. R. 2006. Wild-type huntingtin protects neurons from excitotoxicity. *J Neurochem,* 96(4)**,** pp. 1121-1129.

Lee, J. M., Ramos, E. M., Lee, J. H., Gillis, T., Mysore, J. S., Hayden, M. R., Warby, S. C., Morrison, P., Nance, M., Ross, C. A., Margolis, R. L., Squitieri, F., Orobello, S., Di Donato, S., Gomez-Tortosa, E., Ayuso, C., Suchowersky, O., Trent, R. J., McCusker, E., Novelletto, A., Frontali, M., Jones, R., Ashizawa, T., Frank, S., Saint-Hilaire, M. H., Hersch, S. M., Rosas, H. D., Lucente, D., Harrison, M. B., Zanko, A., Abramson, R. K., Marder, K., Sequeiros, J., Paulsen, J. S., Landwehrmeyer, G. B., Myers, R. H., MacDonald, M. E., Gusella, J. F., (HSG), P.-H. s. o. t. H. S. G., Network, R. s. o. t. E. H. s. D., Group, H.-M. S. and HSG, C. s. o. t. 2012. CAG repeat expansion in Huntington disease determines age at onset in a fully dominant fashion. *Neurology,* 78(10)**,** pp. 690-695.

Li, S. H., Schilling, G., Young, W. S., Li, X. J., Margolis, R. L., Stine, O. C., Wagster, M. V., Abbott, M. H., Franz, M. L. and Ranen, N. G. 1993. Huntington's disease gene (IT15) is widely expressed in human and rat tissues. *Neuron,* 11(5)**,** pp. 985-993.

Li, W., Serpell, L. C., Carter, W. J., Rubinsztein, D. C. and Huntington, J. A. 2006. Expression and characterization of full-length human huntingtin, an elongated HEAT repeat protein. *J Biol Chem,* 281(23)**,** pp. 15916-15922.

Lin, C. H., Tallaksen-Greene, S., Chien, W. M., Cearley, J. A., Jackson, W. S., Crouse, A. B., Ren, S., Li, X. J., Albin, R. L. and Detloff, P. J. 2001. Neurological abnormalities in a knock-in mouse model of Huntington's disease. *Hum Mol Genet,* 10(2)**,** pp. 137-144.

Liu, W., Kennington, L. A., Rosas, H. D., Hersch, S., Cha, J. H., Zamore, P. D. and Aronin, N. 2008. Linking SNPs to CAG repeat length in Huntington's disease patients. *Nat Methods,* 5(11)**,** pp. 951-953.

Liévens, J. C., Woodman, B., Mahal, A., Spasic-Boscovic, O., Samuel, D., Kerkerian-Le Goff, L. and Bates, G. P. 2001. Impaired glutamate uptake in the R6 Huntington's disease transgenic mice. *Neurobiol Dis,* 8(5)**,** pp. 807-821.

Lombardi, M. S., Jaspers, L., Spronkmans, C., Gellera, C., Taroni, F., Di Maria, E., Donato, S. D. and Kaemmerer, W. F. 2009. A majority of Huntington's disease patients may be treatable by individualized allele-specific RNA interference. *Exp Neurol,* 217(2)**,** pp. 312-319.

Love, M. I., Huber, W. and Anders, S. 2014. Moderated estimation of fold change and dispersion for RNA-seq data with DESeq2. *Genome Biol* [online]*,* 15(12): 550. Available from: doi: 10.1186/s13059-014-0550-8.

Macian, F. 2005. NFAT proteins: key regulators of T-cell development and function. *Nat Rev Immunol,* 5(6)**,** pp. 472-484.

Mangiarini, L., Sathasivam, K., Seller, M., Cozens, B., Harper, A., Hetherington, C., Lawton, M., Trottier, Y., Lehrach, H., Davies, S. W. and Bates, G. P. 1996. Exon 1 of the HD gene with an expanded CAG repeat is sufficient to cause a progressive neurological phenotype in transgenic mice. *Cell,* 87(3)**,** pp. 493-506.

Martin, D. D., Ladha, S., Ehrnhoefer, D. E. and Hayden, M. R. 2015. Autophagy in Huntington disease and huntingtin in autophagy. *Trends Neurosci,* 38(1)**,** pp. 26-35.

Martinez, F. O. and Gordon, S. 2014. The M1 and M2 paradigm of macrophage activation: time for reassessment. *F1000Prime Rep* [online]*,* 6:13. Available from: doi: 10.12703/P6-13..

Martinez-Vicente, M., Talloczy, Z., Wong, E., Tang, G., Koga, H., Kaushik, S., de Vries, R., Arias, E., Harris, S., Sulzer, D. and Cuervo, A. M. 2010. Cargo recognition failure is

responsible for inefficient autophagy in Huntington's disease. *Nat Neurosci,* 13(5)**,** pp. 567-576.

Mastrokolias, A., Ariyurek, Y., Goeman, J. J., van Duijn, E., Roos, R. A., van der Mast, R. C., van Ommen, G. B., den Dunnen, J. T., 't Hoen, P. A. and van Roon-Mom, W. M. 2015. Huntington's disease biomarker progression profile identified by transcriptome sequencing in peripheral blood. *Eur J Hum Genet,* 23(10)**,** pp. 1349-1356.

McBride, J. L., Boudreau, R. L., Harper, S. Q., Staber, P. D., Monteys, A. M., Martins, I., Gilmore, B. L., Burstein, H., Peluso, R. W., Polisky, B., Carter, B. J. and Davidson, B. L. 2008. Artificial miRNAs mitigate shRNA-mediated toxicity in the brain: implications for the therapeutic development of RNAi. *Proc Natl Acad Sci U S A,* 105(15)**,** pp. 5868-5873.

McBride, J. L., Pitzer, M. R., Boudreau, R. L., Dufour, B., Hobbs, T., Ojeda, S. R. and Davidson, B. L. 2011. Preclinical safety of RNAi-mediated HTT suppression in the rhesus macaque as a potential therapy for Huntington's disease. *Mol Ther,* 19(12)**,** pp. 2152-2162.

Mi, H., Muruganujan, A. and Thomas, P. D. 2013. PANTHER in 2013: modeling the evolution of gene function, and other gene attributes, in the context of phylogenetic trees. *Nucleic Acids Res,* 41(Database issue)**,** pp. D377-86.

Mielcarek, M., Benn, C. L., Franklin, S. A., Smith, D. L., Woodman, B., Marks, P. A. and Bates, G. P. 2011. SAHA decreases HDAC 2 and 4 levels in vivo and improves molecular phenotypes in the R6/2 mouse model of Huntington's disease. *PLOS One* [online]*,* 6(11)**,** e27746. Available from: doi: 10.1371/journal.pone.0027746.

Mihm, M. J., Amann, D. M., Schanbacher, B. L., Altschuld, R. A., Bauer, J. A. and Hoyt, K. R. 2007. Cardiac dysfunction in the R6/2 mouse model of Huntington's disease. *Neurobiol Dis,* 25(2)**,** pp. 297-308.

Miller, J., Arrasate, M., Brooks, E., Libeu, C. P., Legleiter, J., Hatters, D., Curtis, J., Cheung, K., Krishnan, P., Mitra, S., Widjaja, K., Shaby, B. A., Lotz, G. P., Newhouse, Y., Mitchell, E. J., Osmand, A., Gray, M., Thulasiramin, V., Saudou, F., Segal, M., Yang, X. W., Masliah, E., Thompson, L. M., Muchowski, P. J., Weisgraber, K. H. and Finkbeiner, S. 2011. Identifying polyglutamine protein species in situ that best predict neurodegeneration. *Nat Chem Biol,* 7(12)**,** pp. 925-934.

Mukherjee, R., Kanti Barman, P., Kumar Thatoi, P., Tripathy, R., Kumar Das, B. and Ravindran, B. 2015. Non-Classical monocytes display inflammatory features: Validation in

Sepsis and Systemic Lupus Erythematous. *Sci Rep* [online], 5:13886. Available from: doi: 10.1038/srep13886.

Nasir, J., Floresco, S. B., O'Kusky, J. R., Diewert, V. M., Richman, J. M., Zeisler, J., Borowski, A., Marth, J. D., Phillips, A. G. and Hayden, M. R. 1995. Targeted disruption of the Huntington's disease gene results in embryonic lethality and behavioral and morphological changes in heterozygotes. *Cell,* 81(5)**,** pp. 811-823.

Nicholls, D. G. 2009. Spare respiratory capacity, oxidative stress and excitotoxicity. *Biochem Soc Trans,* 37(6)**,** pp. 1385-1388.

Novak, M. J. and Tabrizi, S. J. 2010. Huntington's disease. *BMJ* [online], 340:c3109. Available from: doi: 10.1136/bmj.c3109.

Okun, E., Griffioen, K. J., Lathia, J. D., Tang, S. C., Mattson, M. P. and Arumugam, T. V. 2009. Toll-like receptors in neurodegeneration. *Brain Res Rev,* 59(2)**,** pp. 278-292.

Ortega, Z. and Lucas, J. J. 2014. Ubiquitin-proteasome system involvement in Huntington's disease. *Front Mol Neurosci* [online], 7:77. Available from: doi: 10.3389/fnmol.2014.00077.

Østergaard, M. E., Southwell, A. L., Kordasiewicz, H., Watt, A. T., Skotte, N. H., Doty, C. N., Vaid, K., Villanueva, E. B., Swayze, E. E., Bennett, C. F., Hayden, M. R. and Seth, P. P. 2013. Rational design of antisense oligonucleotides targeting single nucleotide polymorphisms for potent and allele selective suppression of mutant Huntingtin in the CNS. *Nucleic Acids Res,* 41(21)**,** pp. 9634-9650.

Owen, J. A., Punt, J. and Stranford, S. A. 2013. *Kuby Immunology*. 7th ed. Macmillan Higher Education.

Palazuelos, J., Aguado, T., Pazos, M. R., Julien, B., Carrasco, C., Resel, E., Sagredo, O., Benito, C., Romero, J., Azcoitia, I., Fernández-Ruiz, J., Guzmán, M. and Galve-Roperh, I. 2009. Microglial CB2 cannabinoid receptors are neuroprotective in Huntington's disease excitotoxicity. *Brain,* 132(11)**,** pp. 3152-3164.

Palfi, S., Condé, F., Riche, D., Brouillet, E., Dautry, C., Mittoux, V., Chibois, A., Peschanski, M. and Hantraye, P. 1998. Fetal striatal allografts reverse cognitive deficits in a primate model of Huntington disease. *Nat Med,* 4(8)**,** pp. 963-966.

Park, I. H., Arora, N., Huo, H., Maherali, N., Ahfeldt, T., Shimamura, A., Lensch, M. W., Cowan, C., Hochedlinger, K. and Daley, G. Q. 2008. Disease-specific induced pluripotent stem cells. *Cell,* 134(5)**,** pp. 877-886.

Passlick, B., Flieger, D. and Ziegler-Heitbrock, H. W. 1989. Identification and characterization of a novel monocyte subpopulation in human peripheral blood. *Blood,* 74(7)**,** pp. 2527-2534.

Paulsen, J. S., Langbehn, D. R., Stout, J. C., Aylward, E., Ross, C. A., Nance, M., Guttman, M., Johnson, S., MacDonald, M., Beglinger, L. J., Duff, K., Kayson, E., Biglan, K., Shoulson, I., Oakes, D., Hayden, M. and Group, P.-H. I. a. C. o. t. H. S. 2008. Detection of Huntington's disease decades before diagnosis: the Predict-HD study. *J Neurol Neurosurg Psychiatry,* 79(8)**,** pp. 874-880.

Paulsen, J. S., Nehl, C., Hoth, K. F., Kanz, J. E., Benjamin, M., Conybeare, R., McDowell, B. and Turner, B. 2005. Depression and stages of Huntington's disease. *J Neuropsychiatry Clin Neurosci,* 17(4)**,** pp. 496-502.

Pavese, N., Gerhard, A., Tai, Y. F., Ho, A. K., Turkheimer, F., Barker, R. A., Brooks, D. J. and Piccini, P. 2006. Microglial activation correlates with severity in Huntington disease: a clinical and PET study. *Neurology,* 66(11)**,** pp. 1638-1643.

Pfister, E. L., Kennington, L., Straubhaar, J., Wagh, S., Liu, W., DiFiglia, M., Landwehrmeyer, B., Vonsattel, J. P., Zamore, P. D. and Aronin, N. 2009. Five siRNAs targeting three SNPs may provide therapy for three-quarters of Huntington's disease patients. *Curr Biol,* 19(9)**,** pp. 774-778.

Ionis Pharmaceuticals. 2015. *Isis Pharmaceuticals Initiates Clinical Study of ISIS-HTT Rx in Patients With Huntington's Disease.* [online]. Available from: http://ir.isispharm.com/phoenix.zhtml?c=222170&p=irol-newsArticle&ID=2069397. [Accessed 14 August 2016].

Politis, M., Lahiri, N., Niccolini, F., Su, P., Wu, K., Giannetti, P., Scahill, R. I., Turkheimer, F. E., Tabrizi, S. J. and Piccini, P. 2015. Increased central microglial activation associated with peripheral cytokine levels in premanifest Huntington's disease gene carriers. *Neurobiol Dis,* 83, pp. 115-121.

Politis, M., Pavese, N., Tai, Y. F., Tabrizi, S. J., Barker, R. A. and Piccini, P. 2008. Hypothalamic involvement in Huntington's disease: an in vivo PET study. *Brain,* 131(11)**,** pp. 2860-2869.

Pouladi, M. A., Morton, A. J. and Hayden, M. R. 2013. Choosing an animal model for the study of Huntington's disease. *Nat Rev Neurosci,* 14(10)**,** pp. 708-721.

Quah, B. J., Warren, H. S. and Parish, C. R. 2007. Monitoring lymphocyte proliferation in vitro and in vivo with the intracellular fluorescent dye carboxyfluorescein diacetate succinimidyl ester. *Nat Protoc,* 2(9)**,** pp. 2049-2056.

Rand, T. A., Petersen, S., Du, F. and Wang, X. 2005. Argonaute2 cleaves the anti-guide strand of siRNA during RISC activation. *Cell,* 123(4)**,** pp. 621-629.

Ransohoff, R. M. and Perry, V. H. 2009. Microglial physiology: unique stimuli, specialized responses. *Annu Rev Immunol,* 27, pp. 119-145.

Roederer, M. 2011. Interpretation of cellular proliferation data: avoid the panglossian. *Cytometry A,* 79(2)**,** pp. 95-101.

Rosas, H. D., Goodman, J., Chen, Y. I., Jenkins, B. G., Kennedy, D. N., Makris, N., Patti, M., Seidman, L. J., Beal, M. F. and Koroshetz, W. J. 2001. Striatal volume loss in HD as measured by MRI and the influence of CAG repeat. *Neurology,* 57(6)**,** pp. 1025-1028.

Rosas, H. D., Hevelone, N. D., Zaleta, A. K., Greve, D. N., Salat, D. H. and Fischl, B. 2005. Regional cortical thinning in preclinical Huntington disease and its relationship to cognition. *Neurology,* 65(5)**,** pp. 745-747.

Rosenblatt, A., Brinkman, R. R., Liang, K. Y., Almqvist, E. W., Margolis, R. L., Huang, C. Y., Sherr, M., Franz, M. L., Abbott, M. H., Hayden, M. R. and Ross, C. A. 2001. Familial influence on age of onset among siblings with Huntington disease. *Am J Med Genet,* 105(5)**,** pp. 399-403.

Rosenblatt, A., Liang, K. Y., Zhou, H., Abbott, M. H., Gourley, L. M., Margolis, R. L., Brandt, J. and Ross, C. A. 2006. The association of CAG repeat length with clinical progression in Huntington disease. *Neurology,* 66(7)**,** pp. 1016-1020.

Ross, C. A., Aylward, E. H., Wild, E. J., Langbehn, D. R., Long, J. D., Warner, J. H., Scahill, R. I., Leavitt, B. R., Stout, J. C., Paulsen, J. S., Reilmann, R., Unschuld, P. G., Wexler, A., Margolis, R. L. and Tabrizi, S. J. 2014. Huntington disease: natural history, biomarkers and prospects for therapeutics. *Nat Rev Neurol,* 10(4)**,** pp. 204-216.

Ross, C. A. and Tabrizi, S. J. 2011. Huntington's disease: from molecular pathogenesis to clinical treatment. *Lancet Neurol,* 10(1)**,** pp. 83-98.

Runne, H., Kuhn, A., Wild, E. J., Pratyaksha, W., Kristiansen, M., Isaacs, J. D., Régulier, E., Delorenzi, M., Tabrizi, S. J. and Luthi-Carter, R. 2007. Analysis of potential transcriptomic biomarkers for Huntington's disease in peripheral blood. *Proc Natl Acad Sci U S A,* 104(36)**,** pp. 14424-14429.

Runne, H., Régulier, E., Kuhn, A., Zala, D., Gokce, O., Perrin, V., Sick, B., Aebischer, P., Déglon, N. and Luthi-Carter, R. 2008. Dysregulation of gene expression in primary neuron models of Huntington's disease shows that polyglutamine-related effects on the striatal transcriptome may not be dependent on brain circuitry. *J Neurosci,* 28(39)**,** pp. 9723-9731.

Ryu, H., Lee, J., Hagerty, S. W., Soh, B. Y., McAlpin, S. E., Cormier, K. A., Smith, K. M. and Ferrante, R. J. 2006. ESET/SETDB1 gene expression and histone H3 (K9) trimethylation in Huntington's disease. *Proc Natl Acad Sci U S A,* 103(50)**,** pp. 19176-19181.

Sadri-Vakili, G., Bouzou, B., Benn, C. L., Kim, M. O., Chawla, P., Overland, R. P., Glajch, K. E., Xia, E., Qiu, Z., Hersch, S. M., Clark, T. W., Yohrling, G. J. and Cha, J. H. 2007. Histones associated with downregulated genes are hypo-acetylated in Huntington's disease models. *Hum Mol Genet,* 16(11)**,** pp. 1293-1306.

Sah, D. W. and Aronin, N. 2011. Oligonucleotide therapeutic approaches for Huntington disease. *J Clin Invest,* 121(2)**,** pp. 500-507.

Sapp, E., Kegel, K. B., Aronin, N., Hashikawa, T., Uchiyama, Y., Tohyama, K., Bhide, P. G., Vonsattel, J. P. and DiFiglia, M. 2001. Early and progressive accumulation of reactive microglia in the Huntington disease brain. *J Neuropathol Exp Neurol,* 60(2)**,** pp. 161-172.

Sapp, E., Schwarz, C., Chase, K., Bhide, P. G., Young, A. B., Penney, J., Vonsattel, J. P., Aronin, N. and DiFiglia, M. 1997. Huntingtin localization in brains of normal and Huntington's disease patients. *Ann Neurol,* 42(4)**,** pp. 604-612.

Sathasivam, K., Neueder, A., Gipson, T. A., Landles, C., Benjamin, A. C., Bondulich, M. K., Smith, D.L., Faull, R.L., Roos, R.A., Howland, D., Detloff, P. J., Housman, D. E. and Bates, G. P. 2013. Aberrant splicing of HTT generates the pathogenic exon 1 protein in Huntington disease. *Proc Natl Acad Sci U S A*, 110(6), pp. 2366-2370.

Schaefer, C. F., Anthony, K., Krupa, S., Buchoff, J., Day, M., Hannay, T. and Buetow, K. H. 2009. PID: the Pathway Interaction Database. *Nucleic Acids Res,* 37(Database issue)**,** pp. D674-9.

Seok, J., Warren, H. S., Cuenca, A. G., Mindrinos, M. N., Baker, H. V., Xu, W., Richards, D. R., McDonald-Smith, G. P., Gao, H., Hennessy, L., Finnerty, C. C., López, C. M., Honari, S., Moore, E. E., Minei, J. P., Cuschieri, J., Bankey, P. E., Johnson, J. L., Sperry, J., Nathens, A. B., Billiar, T. R., West, M. A., Jeschke, M. G., Klein, M. B., Gamelli, R. L., Gibran, N. S., Brownstein, B. H., Miller-Graziano, C., Calvano, S. E., Mason, P. H., Cobb, J. P., Rahme, L. G., Lowry, S. F., Maier, R. V., Moldawer, L. L., Herndon, D. N., Davis, R. W., Xiao, W., Tompkins, R. G. and Inflammation and Host Response to Injury, L. r. S. C. R. P. 2013. Genomic responses in mouse models poorly mimic human inflammatory diseases. *Proc Natl Acad Sci U S A,* 110(9)**,** pp. 3507-3512.

Seredenina, T. and Luthi-Carter, R. 2012. What have we learned from gene expression profiles in Huntington's disease? *Neurobiol Dis,* 45(1)**,** pp. 83-98.

Shanker, A. 2010. Adaptive control of innate immunity. *Immunol Lett,* 131(2)**,** pp. 107-112.

Shin, J. Y., Fang, Z. H., Yu, Z. X., Wang, C. E., Li, S. H. and Li, X. J. 2005. Expression of mutant huntingtin in glial cells contributes to neuronal excitotoxicity. *J Cell Biol,* 171(6)**,** pp. 1001-1012.

Shoulson, I. 1981. Huntington disease: functional capacities in patients treated with neuroleptic and antidepressant drugs. *Neurology,* 31(10)**,** pp. 1333-1335.

Silvestroni, A., Faull, R. L., Strand, A. D. and Möller, T. 2009. Distinct neuroinflammatory profile in post-mortem human Huntington's disease. *Neuroreport,* 20(12)**,** pp. 1098-1103.

Simmons, D. A., Casale, M., Alcon, B., Pham, N., Narayan, N. and Lynch, G. 2007. Ferritin accumulation in dystrophic microglia is an early event in the development of Huntington's disease. *Glia,* 55(10)**,** pp. 1074-1084.

Simmons, D. A., Rex, C. S., Palmer, L., Pandyarajan, V., Fedulov, V., Gall, C. M. and Lynch, G. 2009. Up-regulating BDNF with an ampakine rescues synaptic plasticity and memory in Huntington's disease knockin mice. *Proc Natl Acad Sci U S A,* 106(12)**,** pp. 4906-4911.

Singhrao, S. K., Neal, J. W., Morgan, B. P. and Gasque, P. 1999. Increased complement biosynthesis by microglia and complement activation on neurons in Huntington's disease. *Exp Neurol,* 159(2)**,** pp. 362-376.

Skotte, N. H., Southwell, A. L., Østergaard, M. E., Carroll, J. B., Warby, S. C., Doty, C. N., Petoukhov, E., Vaid, K., Kordasiewicz, H., Watt, A. T., Freier, S. M., Hung, G., Seth, P. P., Bennett, C. F., Swayze, E. E. and Hayden, M. R. 2014. Allele-specific suppression of mutant

huntingtin using antisense oligonucleotides: providing a therapeutic option for all Huntington disease patients. *PLOS One* [online]*,* 9(9)**,** e107434. Available from: doi: 10.1371/journal.pone.0107434.

Slow, E. J., van Raamsdonk, J., Rogers, D., Coleman, S. H., Graham, R. K., Deng, Y., Oh, R., Bissada, N., Hossain, S. M., Yang, Y. Z., Li, X. J., Simpson, E. M., Gutekunst, C. A., Leavitt, B. R. and Hayden, M. R. 2003. Selective striatal neuronal loss in a YAC128 mouse model of Huntington disease. *Hum Mol Genet,* 12(13)**,** pp. 1555-1567.

Soto, E. R., Caras, A. C., Kut, L. C., Castle, M. K. and Ostroff, G. R. 2012. Glucan particles for macrophage targeted delivery of nanoparticles. *J Drug Deliv* [online]*,* 2012:143524. Available from: doi: 10.1155/2012/143524.

Southwell, A. L., Skotte, N. H., Kordasiewicz, H. B., Østergaard, M. E., Watt, A. T., Carroll, J. B., Doty, C. N., Villanueva, E. B., Petoukhov, E., Vaid, K., Xie, Y., Freier, S. M., Swayze, E. E., Seth, P. P., Bennett, C. F. and Hayden, M. R. 2014. In vivo evaluation of candidate allele-specific mutant huntingtin gene silencing antisense oligonucleotides. *Mol Ther,* 22(12)**,** pp. 2093-2106.

Squitieri, F., Frati, L., Ciarmiello, A., Lastoria, S. and Quarrell, O. 2006. Juvenile Huntington's disease: does a dosage-effect pathogenic mechanism differ from the classical adult disease? *Mech Ageing Dev,* 127(2)**,** pp. 208-212.

Squitieri, F. and Jankovic, J. 2012. Huntington's disease: how intermediate are intermediate repeat lengths? *Mov Disord,* 27(14)**,** pp. 1714-1717.

Stanek, L. M., Sardi, S. P., Mastis, B., Richards, A. R., Treleaven, C. M., Taksir, T., Misra, K., Cheng, S. H. and Shihabuddin, L. S. 2014. Silencing mutant huntingtin by adeno-associated virus-mediated RNA interference ameliorates disease manifestations in the YAC128 mouse model of Huntington's disease. *Hum Gene Ther,* 25(5)**,** pp. 461-474.

Steffan, J. S., Agrawal, N., Pallos, J., Rockabrand, E., Trotman, L. C., Slepko, N., Illes, K., Lukacsovich, T., Zhu, Y. Z., Cattaneo, E., Pandolfi, P. P., Thompson, L. M. and Marsh, J. L. 2004. SUMO modification of Huntingtin and Huntington's disease pathology. *Science,* 304(5667)**,** pp. 100-104.

Steffan, J. S., Kazantsev, A., Spasic-Boskovic, O., Greenwald, M., Zhu, Y. Z., Gohler, H., Wanker, E. E., Bates, G. P., Housman, D. E. and Thompson, L. M. 2000. The Huntington's disease protein interacts with p53 and CREB-binding protein and represses transcription. *Proc Natl Acad Sci U S A,* 97(12)**,** pp. 6763-6768.

Storey, J. D. and Tibshirani, R. 2003. Statistical significance for genomewide studies. *Proc Natl Acad Sci U S A,* 100(16)**,** pp. 9440-9445.

Subramanian, A., Tamayo, P., Mootha, V. K., Mukherjee, S., Ebert, B. L., Gillette, M. A., Paulovich, A., Pomeroy, S. L., Golub, T. R., Lander, E. S. and Mesirov, J. P. 2005. Gene set enrichment analysis: a knowledge-based approach for interpreting genome-wide expression profiles. *Proc Natl Acad Sci U S A,* 102(43)**,** pp. 15545-15550.

Summerton, J. E. 2005. Endo-Porter: a novel reagent for safe, effective delivery of substances into cells. *Ann N Y Acad Sci,* 1058, pp. 62-75.

Swami, M., Hendricks, A. E., Gillis, T., Massood, T., Mysore, J., Myers, R. H. and Wheeler, V. C. 2009. Somatic expansion of the Huntington's disease CAG repeat in the brain is associated with an earlier age of disease onset. *Hum Mol Genet,* 18(16)**,** pp. 3039-3047.

Tabrizi, S. J., Langbehn, D. R., Leavitt, B. R., Roos, R. A., Durr, A., Craufurd, D., Kennard, C., Hicks, S. L., Fox, N. C., Scahill, R. I., Borowsky, B., Tobin, A. J., Rosas, H. D., Johnson, H., Reilmann, R., Landwehrmeyer, B., Stout, J. C. and investigators, T.-H. 2009. Biological and clinical manifestations of Huntington's disease in the longitudinal TRACK-HD study: cross-sectional analysis of baseline data. *Lancet Neurol,* 8(9)**,** pp. 791-801.

Tabrizi, S. J., Scahill, R. I., Owen, G., Durr, A., Leavitt, B. R., Roos, R. A., Borowsky, B., Landwehrmeyer, B., Frost, C., Johnson, H., Craufurd, D., Reilmann, R., Stout, J. C., Langbehn, D. R. and Investigators, T.-H. 2013. Predictors of phenotypic progression and disease onset in premanifest and early-stage Huntington's disease in the TRACK-HD study: analysis of 36-month observational data. *Lancet Neurol,* 12(7)**,** pp. 637-649.

Tai, Y. F., Pavese, N., Gerhard, A., Tabrizi, S. J., Barker, R. A., Brooks, D. J. and Piccini, P. 2007. Microglial activation in presymptomatic Huntington's disease gene carriers. *Brain,* 130(7)**,** pp. 1759-1766.

Tesz, G. J., Aouadi, M., Prot, M., Nicoloro, S. M., Boutet, E., Amano, S. U., Goller, A., Wang, M., Guo, C. A., Salomon, W. E., Virbasius, J. V., Baum, R. A., O'Connor, M. J., Soto, E., Ostroff, G. R. and Czech, M. P. 2011. Glucan particles for selective delivery of siRNA to phagocytic cells in mice. *Biochem J,* 436(2)**,** pp. 351-362.

The Huntington's Disease Collaborative Research Group. 1993. A novel gene containing a trinucleotide repeat that is expanded and unstable on Huntington's disease chromosomes. The Huntington's Disease Collaborative Research Group. *Cell,* 72(6)**,** pp. 971-983.

Thompson, L. M., Aiken, C. T., Kaltenbach, L. S., Agrawal, N., Illes, K., Khoshnan, A., Martinez-Vincente, M., Arrasate, M., O'Rourke, J. G., Khashwji, H., Lukacsovich, T., Zhu, Y. Z., Lau, A. L., Massey, A., Hayden, M. R., Zeitlin, S. O., Finkbeiner, S., Green, K. N., LaFerla, F. M., Bates, G., Huang, L., Patterson, P. H., Lo, D. C., Cuervo, A. M., Marsh, J. L. and Steffan, J. S. 2009. IKK phosphorylates Huntingtin and targets it for degradation by the proteasome and lysosome. *J Cell Biol,* 187(7)**,** pp. 1083-1099.

Tong, Y., Ha, T. J., Liu, L., Nishimoto, A., Reiner, A. and Goldowitz, D. 2011. Spatial and temporal requirements for huntingtin (Htt) in neuronal migration and survival during brain development. *J Neurosci,* 31(41)**,** pp. 14794-14799.

Trembath, M. K., Horton, Z. A., Tippett, L., Hogg, V., Collins, V. R., Churchyard, A., Velakoulis, D., Roxburgh, R. and Delatycki, M. B. 2010. A retrospective study of the impact of lifestyle on age at onset of Huntington disease. *Mov Disord,* 25(10)**,** pp. 1444-1450.

Trottier, Y., Biancalana, V. and Mandel, J. L. 1994. Instability of CAG repeats in Huntington's disease: relation to parental transmission and age of onset. *J Med Genet,* 31(5)**,** pp. 377-382.

Träger, U., Andre, R., Lahiri, N., Magnusson-Lind, A., Weiss, A., Grueninger, S., McKinnon, C., Sirinathsinghji, E., Kahlon, S., Pfister, E. L., Moser, R., Hummerich, H., Antoniou, M., Bates, G. P., Luthi-Carter, R., Lowdell, M. W., Björkqvist, M., Ostroff, G. R., Aronin, N. and Tabrizi, S. J. 2014. HTT-lowering reverses Huntington's disease immune dysfunction caused by NFκB pathway dysregulation. *Brain,* 137(3)**,** pp. 819-833.

Träger, U., Andre, R., Magnusson-Lind, A., Miller, J. R., Connolly, C., Weiss, A., Grueninger, S., Silajdžić, E., Smith, D. L., Leavitt, B. R., Bates, G. P., Björkqvist, M. and Tabrizi, S. J. 2015. Characterisation of immune cell function in fragment and full-length Huntington's disease mouse models. *Neurobiol Dis,* 73, pp. 388-398.

Träger, U., Magnusson, A., Lahiri Swales, N., Wild, E., North, J., Lowdell, M. and Björkqvist, M. 2013. JAK/STAT Signalling in Huntington's Disease Immune Cells. *PLOS Curr* [online]*,* 5. Available from: doi: 10.1371/currents.hd.5791c897b5c3bebeed93b1d1da0c0648.

Turner, M. R., Kiernan, M. C., Leigh, P. N. and Talbot, K. 2009. Biomarkers in amyotrophic lateral sclerosis. *Lancet Neurol,* 8(1)**,** pp. 94-109.

Vacher, C., Garcia-Oroz, L. and Rubinsztein, D. C. 2005. Overexpression of yeast hsp104 reduces polyglutamine aggregation and prolongs survival of a transgenic mouse model of Huntington's disease. *Hum Mol Genet,* 14(22)**,** pp. 3425-3433.

van Bilsen, P. H., Jaspers, L., Lombardi, M. S., Odekerken, J. C., Burright, E. N. and Kaemmerer, W. F. 2008. Identification and allele-specific silencing of the mutant huntingtin allele in Huntington's disease patient-derived fibroblasts. *Hum Gene Ther,* 19(7)**,** pp. 710-719.

van der Burg, J. M., Björkqvist, M. and Brundin, P. 2009. Beyond the brain: widespread pathology in Huntington's disease. *Lancet Neurol,* 8(8)**,** pp. 765-774.

Velier, J., Kim, M., Schwarz, C., Kim, T. W., Sapp, E., Chase, K., Aronin, N. and DiFiglia, M. 1998. Wild-type and mutant huntingtins function in vesicle trafficking in the secretory and endocytic pathways. *Exp Neurol,* 152(1)**,** pp. 34-40.

Vonsattel, J. P. 2008. Huntington disease models and human neuropathology: similarities and differences. *Acta Neuropathol,* 115(1)**,** pp. 55-69.

Vonsattel, J. P. and DiFiglia, M. 1998. Huntington disease. *J Neuropathol Exp Neurol,* 57(5)**,** pp. 369-384.

Vonsattel, J. P., Myers, R. H., Stevens, T. J., Ferrante, R. J., Bird, E. D. and Richardson, E. P. 1985. Neuropathological classification of Huntington's disease. *J Neuropathol Exp Neurol,* 44(6)**,** pp. 559-577.

Wang, G., Liu, X., Gaertig, M. A., Li, S. and Li, X. J. 2016. Ablation of huntingtin in adult neurons is nondeleterious but its depletion in young mice causes acute pancreatitis. *Proc Natl Acad Sci U S A,* 113(12)**,** pp. 3359-3364.

Wang, Z., Gerstein, M. and Snyder, M. 2009. RNA-Seq: a revolutionary tool for transcriptomics. *Nat Rev Genet,* 10(1)**,** pp. 57-63.

Warby, S. C., Montpetit, A., Hayden, A. R., Carroll, J. B., Butland, S. L., Visscher, H., Collins, J. A., Semaka, A., Hudson, T. J. and Hayden, M. R. 2009. CAG expansion in the Huntington disease gene is associated with a specific and targetable predisposing haplogroup. *Am J Hum Genet,* 84(3)**,** pp. 351-366.

Warby, S. C., Visscher, H., Collins, J. A., Doty, C. N., Carter, C., Butland, S. L., Hayden, A. R., Kanazawa, I., Ross, C. J. and Hayden, M. R. 2011. HTT haplotypes contribute to differences in Huntington disease prevalence between Europe and East Asia. *Eur J Hum Genet,* 19(5)**,** pp. 561-566.

Watts, J. K. and Corey, D. R. 2012. Silencing disease genes in the laboratory and the clinic. *J Pathol,* 226(2)**,** pp. 365-379.

Weir, D. W., Sturrock, A. and Leavitt, B. R. 2011. Development of biomarkers for Huntington's disease. *Lancet Neurol,* 10(6)**,** pp. 573-590.

Weiss, A., Träger, U., Wild, E. J., Grueninger, S., Farmer, R., Landles, C., Scahill, R. I., Lahiri, N., Haider, S., Macdonald, D., Frost, C., Bates, G. P., Bilbe, G., Kuhn, R., Andre, R. and Tabrizi, S. J. 2012. Mutant huntingtin fragmentation in immune cells tracks Huntington's disease progression. *J Clin Invest,* 122(10)**,** pp. 3731-3736.

Wexler, N. S., Lorimer, J., Porter, J., Gomez, F., Moskowitz, C., Shackell, E., Marder, K., Penchaszadeh, G., Roberts, S. A., Gayán, J., Brocklebank, D., Cherny, S. S., Cardon, L. R., Gray, J., Dlouhy, S. R., Wiktorski, S., Hodes, M. E., Conneally, P. M., Penney, J. B., Gusella, J., Cha, J. H., Irizarry, M., Rosas, D., Hersch, S., Hollingsworth, Z., MacDonald, M., Young, A. B., Andresen, J. M., Housman, D. E., De Young, M. M., Bonilla, E., Stillings, T., Negrette, A., Snodgrass, S. R., Martinez-Jaurrieta, M. D., Ramos-Arroyo, M. A., Bickham, J., Ramos, J. S., Marshall, F., Shoulson, I., Rey, G. J., Feigin, A., Arnheim, N., Acevedo-Cruz, A., Acosta, L., Alvir, J., Fischbeck, K., Thompson, L. M., Young, A., Dure, L., O'Brien, C. J., Paulsen, J., Brickman, A., Krch, D., Peery, S., Hogarth, P., Higgins, D. S., Landwehrmeyer, B. and Project, U. S.-V. C. R. 2004. Venezuelan kindreds reveal that genetic and environmental factors modulate Huntington's disease age of onset. *Proc Natl Acad Sci U S A,* 101(10)**,** pp. 3498-3503.

Wexler, N. S., Young, A. B., Tanzi, R. E., Travers, H., Starosta-Rubinstein, S., Penney, J. B., Snodgrass, S. R., Shoulson, I., Gomez, F. and Ramos Arroyo, M. A. 1987. Homozygotes for Huntington's disease. *Nature,* 326(6109)**,** pp. 194-197.

Wild, E., Magnusson, A., Lahiri, N., Krus, U., Orth, M., Tabrizi, S. J. and Björkqvist, M. 2011. Abnormal peripheral chemokine profile in Huntington's disease. *PLOS Curr* [online]*,* 3:RRN1231. Available from: doi: 10.1371/currents.RRN1231.

Wild, E. J., Boggio, R., Langbehn, D., Robertson, N., Haider, S., Miller, J. R., Zetterberg, H., Leavitt, B. R., Kuhn, R., Tabrizi, S. J., Macdonald, D. and Weiss, A. 2015. Quantification of mutant huntingtin protein in cerebrospinal fluid from Huntington's disease patients. *J Clin Invest,* 125(5)**,** pp. 1979-1986.

Wild, E. J. and Tabrizi, S. J. 2007. The differential diagnosis of chorea. *Pract Neurol,* 7(6)**,** pp. 360-373.

Yamamoto, A., Lucas, J. J. and Hen, R. 2000. Reversal of neuropathology and motor dysfunction in a conditional model of Huntington's disease. *Cell,* 101(1)**,** pp. 57-66.

Yamamoto, M., Sato, S., Hemmi, H., Hoshino, K., Kaisho, T., Sanjo, H., Takeuchi, O., Sugiyama, M., Okabe, M., Takeda, K. and Akira, S. 2003. Role of adaptor TRIF in the MyD88-independent toll-like receptor signaling pathway. *Science,* 301(5633)**,** pp. 640-643.

Yamamoto, M., Yamazaki, S., Uematsu, S., Sato, S., Hemmi, H., Hoshino, K., Kaisho, T., Kuwata, H., Takeuchi, O., Takeshige, K., Saitoh, T., Yamaoka, S., Yamamoto, N., Yamamoto, S., Muta, T., Takeda, K. and Akira, S. 2004. Regulation of Toll/IL-1-receptor-mediated gene expression by the inducible nuclear protein IkappaBzeta. *Nature,* 430(6996)**,** pp. 218-222.

Yanai, A., Huang, K., Kang, R., Singaraja, R. R., Arstikaitis, P., Gan, L., Orban, P. C., Mullard, A., Cowan, C. M., Raymond, L. A., Drisdel, R. C., Green, W. N., Ravikumar, B., Rubinsztein, D. C., El-Husseini, A. and Hayden, M. R. 2006. Palmitoylation of huntingtin by HIP14 is essential for its trafficking and function. *Nat Neurosci,* 9(6)**,** pp. 824-831.

Yu, D., Pendergraff, H., Liu, J., Kordasiewicz, H. B., Cleveland, D. W., Swayze, E. E., Lima, W. F., Crooke, S. T., Prakash, T. P. and Corey, D. R. 2012. Single-stranded RNAs use RNAi to potently and allele-selectively inhibit mutant huntingtin expression. *Cell,* 150**,** pp. 895-908.

Zeitlin, S., Liu, J. P., Chapman, D. L., Papaioannou, V. E. and Efstratiadis, A. 1995. Increased apoptosis and early embryonic lethality in mice nullizygous for the Huntington's disease gene homologue. *Nat Genet,* 11(2)**,** pp. 155-163.

Zeller, T., Wild, P., Szymczak, S., Rotival, M., Schillert, A., Castagne, R., Maouche, S., Germain, M., Lackner, K., Rossmann, H., Eleftheriadis, M., Sinning, C. R., Schnabel, R. B., Lubos, E., Mennerich, D., Rust, W., Perret, C., Proust, C., Nicaud, V., Loscalzo, J., Hübner, N., Tregouet, D., Münzel, T., Ziegler, A., Tiret, L., Blankenberg, S. and Cambien, F. 2010. Genetics and beyond--the transcriptome of human monocytes and disease susceptibility. *PLOS One* [online]*,* 5(5)**,** e10693. Available from: doi: 10.1371/journal.pone.0010693.

Ziegler-Heitbrock, L. 2007. The CD14+ CD16+ blood monocytes: their role in infection and inflammation. *J Leukoc Biol,* 81(3)**,** pp. 584-592.

Zuccato, C., Tartari, M., Crotti, A., Goffredo, D., Valenza, M., Conti, L., Cataudella, T., Leavitt, B. R., Hayden, M. R., Timmusk, T., Rigamonti, D. and Cattaneo, E. 2003. Huntingtin interacts with REST/NRSF to modulate the transcription of NRSE-controlled neuronal genes. *Nat Genet,* 35(1)**,** pp. 76-83.

Zwilling, D., Huang, S. Y., Sathyasaikumar, K. V., Notarangelo, F. M., Guidetti, P., Wu, H. Q., Lee, J., Truong, J., Andrews-Zwilling, Y., Hsieh, E. W., Louie, J. Y., Wu, T., Scearce-Levie, K., Patrick, C., Adame, A., Giorgini, F., Moussaoui, S., Laue, G., Rassoulpour, A., Flik, G., Huang, Y., Muchowski, J. M., Masliah, E., Schwarcz, R. and Muchowski, P. J. 2011. Kynurenine 3-monooxygenase inhibition in blood ameliorates neurodegeneration. *Cell,* 145(6)**,** pp. 863-874.

Publications relating to this thesis

Miller, J.R., Lo, K.K., Andre, R., Hensman Moss, D.J., Träger, U., Stone, T.C., Jones, L., Holmans, P., Plagnol, V., Tabrizi, S.J. 2016. RNA-Seq of Huntington's disease patient myeloid cells reveals innate transcriptional dysregulation associated with proinflammatory pathway activation. *Hum Mol Genet* [online]. Available from: doi: 10.1093/hmg/ddw142.

Miller, J.R., Träger, U., Andre, R., Tabrizi, S.J. 2015. Mutant Huntingtin Does Not Affect the Intrinsic Phenotype of Human Huntington's Disease T Lymphocytes. *PLOS ONE* [online], 10(11), e0141793. Available from: doi: 10.1371/journal.pone.0141793.